LIGAND FIELD SPECTROSCOPY OF GROUP VIII ELEMENTS IN FUSED SALTS

A Thesis

Submitted to the Faculty of Graduate Studies

In Partial Fulfilment of the Requirements

For the Degree of

Doctor of Philosophy

in Chemistry

Division of Natural Sciences

University of Saskatchewan, Regina Campus

by

John Robert Dickinson

Regina, Saskatchewan

January, 1969

ProQuest Information and Learning Company
300 North Zeeb Road
P.O. Box 1346
Ann Arbor, MI 48106-1346

PERMISSION TO USE POSTGRADUATE THESES

Title of thesis ...Ligand Field Spectroscopy of Group VIII.....
Elements in Fused Salts
.....

.....

Name of Author .....John Robert Dickinson.....

Division or College .....Chemistry, Division of Natural Sciences and Mathematics.....

Degree .....Doctor of Philosophy in Chemistry.....

In presenting this thesis in partial fulfillment of the requirements for a postgraduate degree from the University of Saskatchewan, I agree that the Libraries of this University shall make it freely available for inspection. I further agree that permission for extensive copying of this thesis for scholarly purposes may be granted by the professor or professors who supervised my thesis work or, in their absence, by the Chairman of the Division, the Head of the Department or the Dean of the College in which my thesis work was done. It is understood that any copying or publication or use of this thesis or parts thereof for financial gain shall not be allowed without my written permission. It is also understood that due recognition shall be given to me and to the University of Saskatchewan, Regina Campus, in any scholarly use which may be made of any material in my thesis.

Signature .....J. R. Dickinson.....

Date .....March 17, 1969.....

27/9/66
100 c.

UNIVERSITY OF SASKATCHEWAN, REGINA CAMPUS

SCHOOL OF GRADUATE STUDIES

CERTIFICATION OF THESIS WORK

We, the undersigned, certify that John Robert Dickinson

candidate for the Degree of Doctor of Philosophy in Chemistry

has presented his thesis on the subject, Ligand Field Spectroscopy of Group VIII Elements in Fused Salts

that the thesis is acceptable in form and content, and that the student demonstrated a satisfactory knowledge of the field covered by his thesis in an oral examination held on March 17, 1969

External Examiner G. Peter Smith

Professor of Chemistry

Internal Examiners

ABSTRACT

A spectral investigation of complexes of Group VIII elements in fused salts has been carried out using a modified Beckmann DK2A spectrophotometer. Spectra were obtained at 450° C using the LiCl - KCl eutectic melt and at 550° C with the Li_2SO_4 - Na_2SO_4 - K_2SO_4 melt. In the chloride melt, the stable species were found to be $RuCl_6^{3-}$, $RhCl_6^{3-}$, $IrCl_6^{3-}$, $PdCl_4^{2-}$, and $PtCl_4^{2-}$, the first three being octahedral and the last two square planar. The occurrence of trans ligands on the z axis of the square planar compounds was considered, but definite proof was not obtained. Osmium exists in concentrated solutions in the chloride melt as octahedral $OsCl_6^{2-}$. In dilute solutions, on the other hand, the $OsCl_6^{2-}$ species is unstable and gives rise to a species with a lower oxidation state, which has not been identified conclusively, but might be an Os(II) complex.

In the sulphate melt, Co(II) and Ni(II) have been re-examined and the previous assignments confirmed. Spectra of Co(II) in a range of sulphuric acid solutions, some as a function of temperature, have been recorded and interpreted in terms of a distorted octahedral species at the higher temperatures. These results were also used to show that the variation of band intensity as a function of temperature could not be described by either of the two treatments at present available. The spectra of Pd(II) and Rh(III) in the sulphate melt were found to be quite similar to the corresponding chloride melt spectra.

ACKNOWLEDGEMENTS

The author would like to thank the following people: Mr. D. W. Wilson for providing research facilities at Sir John Cass College; Professor W. B. McConnell for the same facilities at Regina Campus; Mr. L. G. Boxall for the computer programmes; Mr. K. F. Denning and Dr. M. Collins for discussions; Mr. R. Cameron for technical assistance; Mr. P. F. Wells; and finally, Dr. K. E. Johnson for suggesting the problem and encouragement during its execution.

Thanks are extended to the following organisations for providing financial assistance: the Science Research Council of Great Britain for awarding a Research Studentship for the academic year 1965 - 66; the University of Saskatchewan, Regina Campus, Chemistry Department for a Teaching Assistantship 1966 - 67; and the National Research Council of Canada for a Postgraduate Scholarship for the period 1967 - 69.

TABLE OF CONTENTS

LIST OF TABLES

LIST OF FIGURES

CHAPTER 1

INTRODUCTION

The application of spectroscopic techniques to solutions of fused salts containing transition metal ions has only recently gained much momentum. Undoubtedly, the initiation of the Molten Salt Reactor Experiment at the Oak Ridge National Laboratory of the U. S. Atomic Energy Commission has been the main impetus behind such studies. Investigations designed to evaluate both the physical and chemical properties of fused salts were an essential preliminary to this experiment. Such investigations covered an extremely wide field encompassing density, viscosity, melt stability, corrosion characteristics, etc. The problem of corrosion of the container material by the fused salt was particularly important in view of the radiation hazard involved. It was obviously necessary to devise a means by which the extent of corrosion could be evaluated. Towards this end, the feasibility of uv - visible spectroscopy as a means of monitoring the concentration of transition metal ions in the fused salt medium was investigated. Since that time, however, this particular area of spectroscopy has provided information of a much wider nature. The main areas of interest within this field can be classified as follows:

A. Analytical applications.

B. Characteristics of the transition metal species present in fused salt solutions.

C. Structural studies of the fused salts.

A. Analytical Applications. Although the original intention was to use ligand field spectroscopy as an analytical tool, it has not been adopted as a general method. The reason for this is that methods capable of detecting much lower concentrations would be preferred. That the method would indeed work has been shown by the work of Boston and Smith (1) on the Ni(II) in LiCl - KCl eutectic melt system. These authors showed that Beers law was accurately obeyed over the concentration range 0.01M - 0.4M. As a quantitative tool, however, the method is limited by the values of the extinction coefficients and whilst these are often higher than in aqueous solution, they are still too small to allow measurements at very low concentrations. (A maximum concentration of ~0.001M in the case of Ni(II) in the LiCl - KCl melt.)

B. Characterisation of the Transition Metal Species. Studies of this nature have undoubtedly constituted the largest proportion of the published results for these systems. Such studies can be regarded as consisting of the determination of two components: the oxidation state of the metal and the geometry of the species. In the majority of cases, this represents the order in which a particular spectrum is interpreted. Oxidation state studies are not very important in their own right since more definitive methods are available for determining the oxidation state present in a melt, namely electrode potential measurements, and the corresponding Nernst plots. Nevertheless, identification of the oxidation state present by spectral means has been reported in the literature. Thus Bailey and McIntyre (2) reported that the spectrum of a LiCl - KCl eutectic to which Re_3Cl_9 had been added was identical to the spectrum of $ReCl_6^{2-}$. In this case the Re(III) disproportionated to Re(IV) and Re metal.

Prior to the commencement of the work reported in this thesis, fused salt spectroscopy had been restricted to the first row transition elements with the exception of the lanthanides and the actinides. During the course of the present investigations, work on the second and third row elements has been published. Ogilvie and Holmes (3) reported the results of their work on Rh(III) in the fused LiCl - KCl and $NaNO_3$ - KNO_3 eutectics, whilst Bailey and McIntyre (4) published the spectra of Pd(II) and Pt(II) in the same chloride solvent. Since both these investigations were part of the original research programme on which this thesis was based, their results will be discussed at some length in the appropriate chapters.

The spectra of all the first row transition elements in the LiCl - KCl eutectic have been reported and the results reviewed by several authors (5, 6, 7). The LiCl - KCl eutectic has undoubtedly been the most popular solvent although other solvents, e.g. the $LiNO_3$ - KNO_3 eutectic, the LiF - NaF - KF eutectic, etc., have been used. Gruen and McBeth (5) have developed a general theory to explain why some first row elements give rise to octahedral species, others to tetrahedral species, and some to an octahedral-tetrahedral equilibrium, in the LiCl - KCl eutectic melt. Their treatment, which was based on corrected ligand field stabilisation energies, is very similar to that of Orgel and McClure (see Reference 8 for further discussion and literature references) which had been criticised in great detail by Katzin (8). Orgel and McClure had attempted to correlate the relative stabilities of octahedral and tetrahedral complexes in terms of the ligand field stabilisation energy only. Katzin pointed out that such an approach oversimplified the problem to such an extent that the results should be treated with extreme caution. In particular, the differences in

bond strength of the M - L bond in octahedral and tetrahedral complexes was shown to be quite an important factor. In all fairness, it must be pointed out that all the information which would be required to carry out an analysis along the lines suggested by Katzin is simply not available. This is not an excuse, however, to accept the results of the Orgel-McClure type approximation without reserve.

Although the Gruen-McBeth theory was reported after Katzin's critique had been published, much of the criticism is still applicable. This later theory attempted to take the effect of electrostatic differences as well as ligand field stabilisation energies into account. Thus, the basis of the theory involved estimation of the free energy change for the reaction:

$$ML_6 \rightleftharpoons ML_4 + 2L$$

This was written as follows:

$$\Delta G = O.S.S.E. + E^{n+} \qquad (1.1)$$

where O.S.S.E. is the octahedral site stabilisation energy, which is the difference between the ligand field octahedral and tetrahedral stabilisation energies assuming that $\Delta_T = \Delta_O \times 4/9$. For example, consider a d^3 system, the ground term of which is split as shown in Figure 1.1:

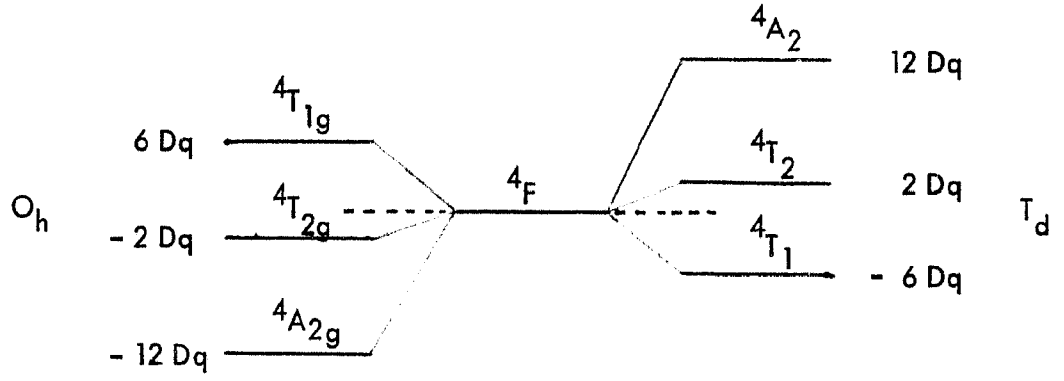

Figure 1.1 Splitting of the ^4F state in O_h and T_d ligand fields

The O.S.S.E. is then given by $\left[-12 - (-6.4/9)\right] Dq = 9.3\ Dq$.

The E^{n+} term in equation 1.1 is supposed to represent the difference in electrostatic energies between the two symmetries. Gruen and McBeth did point out that despite this correction term, contributions such as covalent bonding terms, entropy differences, spin-orbital coupling effects, etc., were neglected. Furthermore, it was suggested that the E^{n+} term was independent of the metal and depended only on the oxidation state. By using the spectral data available for the V(II) and V(III) ions, they were able to calculate the corresponding values of E^{n+}. These were found to be:

$$E^{2+} = -30 \text{ kcal}$$

$$E^{3+} = -10 \text{ kcal}$$

The octahedral site stabilisation energies were converted into kcal/mole by using the value of Dq obtained from spectral data on either melts or crystals, and the appropriate conversion factor. In this way, both terms on the right hand side of equation 1.1 were thus obtained, thereby allowing evaluation of ΔG. That species which gave a large positive ΔG value Cr(III), (+24 kcal/mole), occurs only in the octahedral form, whilst those with large negative values, Fe(II), (-27), Co(II), (-29), Mn(II), (-30), are present only in the tetrahedral form. The remaining species with small negative values occurred as distorted tetrahedral, Ni(II), (-14), Cu(II), (-15) and Cr(II), (-18), or as an octahedral-tetrahedral equilibrium mixture: Ti(III), (-6), V(III), (-8), V(II), (-11 kcal/mole).

The theory is, therefore, consistent with the interpretations of the individual spectra, although the dividing line between the distorted tetrahedral group and the equilibrium group is not very clear cut.

Since this early work, which was of an exploratory nature, was reported, the main investigators in the field, namely D. M. Gruen and G. P. Smith, and their respective collaborators, have apparently concentrated their main efforts on a single element; Gruen on Co(II), and Smith on Ni(II). The results of these investigations will be discussed in Chapters IV and VI respectively.

C. Structural Aspects of Fused Salts. Fused salts occupy a rather unusual position in the liquid state. On the one hand they may be regarded as a large section of the general area of non-aqueous solvents; on the other hand, they may be classified as electrolyte solutions with very high ionic strengths. It has been argued (9) that the second view would constitute the best approach. However, the range of fused salts extends from ionic liquids such as fused KCl, to liquids which are highly covalent, i.e. which may be classified as molecular liquids, such as $AlCl_3$. Such an extensive class of liquids cannot, of course, be described in terms of a single unifying theory of liquid structure. Indeed, it seems that no theory at present available is completely successful even for the relatively simple group of alkali halide melts. Since the pure halides themselves are not very well understood, it is not surprising that mixtures of fused salts are even less well understood. This is particularly unfortunate for the reason that a large proportion of the physical measurements, e.g. spectral and electrochemical studies, etc., which are available for fused salt systems have utilised eutectic mixtures. This particular choice was usually made to alleviate handling difficulties involved with the higher melting points of the pure fused salts.

Although only eutectics were used in the work reported later, a brief review, following that of Bloom and Bockris (10), (to which reference should be made for

original literature references), of the various models which have been applied to the alkali halides in particular is presented. Several models have been suggested as a starting point for predicting properties of fused salts, among which are the following:

(i) Quasi-lattice or vacancy model.

(ii) Hole model.

(iii) Crystallite model.

(iv) Polyhedral hole model.

(v) Liquid free volume model.

(vi) Significant structures model.

The method of approach has been to use a particular model to calculate various parameters which are then compared with the experimental values. Obviously those theories which rely on experimental calibration of parameters in the theoretical expressions are less rigorous than calculations from first principles. However, as Stillinger (11) has shown, such calculations are almost impossible to carry out completely rigorously. The physical properties which have been used to determine the usefulness of the above theories are the following: the entropy and volume change on fusion, the compressibility and the self-diffusion coefficient. A very brief discussion of each of the models listed above, in terms of these properties, is now given.

(i) Quasi-Lattice Model In this model it is assumed that on melting the crystal lattice does not change appreciably, except that vacancies, usually in the form of Schottky defects, occur in such numbers that the volume expansion on fusion is explained. Calculations of the entropy change on fusion and the self-diffusion paramaters are very satisfactory.

(ii) Hole Model In essentials this model is very similar to the quasi-lattice model except that the holes are not Schottky defects on crystal sites, but are randomly distributed throughout the liquid. The holes are envisaged as arising from spontaneous density fluctuations in the melt. The comparison with experiment for all the parameters listed above varies from fair to very good.

(iii) Crystallite Model This can be regarded as an extension of the theory of microdefects, in crystals, to the liquid state. The liquid is regarded as consisting of areas of more or less perfect crystal with the separation between them constituting dislocations. A comparison of the calculated and experimental parameters does not show good agreement. It would appear, however, that this particular model is useful when dealing with highly condensed melts such as borates, silicates, etc.

(iv) Polyhedral Hole The observation that melts which apparently did not contain complex ions could be supercooled led to the suggestion that the ions were ordered in the melt in such a way that they did not pack well and thus did not crystallise on cooling. The model was envisaged as containing holes, dislocations and crystallitesso that it may be regarded as a hybrid of the three previous models. Whilst it may be a reasonable model from an intellectual point of view, it apparently has not been subjected to a quantitative analysis.

(v) Liquid Free Volume Model The starting point for this particular model is a crystal where the particles are contained in cells. Within each cell in the crystal there is a certain free volume in which the particle is free to move. In the liquid it has been suggested that each cell free volume is available to all the particles. However, it was shown that this particular concept led to the occurrence

of cells containing two particles, a result which cannot give rise to the correct entropy of fusion. Instead of cell free volume, the idea of liquid free volume was introduced where the liquid free volume v is defined as follows:

$$v = \bar{v} - v_o$$

where $\bar{v}$ = average volume per molecule

v_o = volume per molecule when the cells correspond to those in which the molecule would be, in a hypothetical solid at the same temperature.

This liquid free volume is envisaged as being distributed thermally over all the cells. The introduction of random free space within the liquid leads to a model which has similarities with both the quasi-lattice and the hole models. A comparison of the calculated and experimental parameters is not very satisfactory.

(vi) Significant Structures Model Two significant structures are thought to be the most important in this particular model. On the one hand there is a pseudo-crystalline structure containing both Schottky and Frenkel defects, (cf. the quasi-lattice model) whilst on the other hand there are gas-like particles in the areas between the crystal (cf. the crystallite model). Bloom and Bockris (10) criticised the model on the grounds that its prediction of physical properties is good only because of its hybrid character. Certainly the predicted properties are in very good agreement with the measured physical properties.

Of the various models discussed above, it would appear that the hole and the significant structures models give the best fit. However, it must be borne in mind that even if a particular model were to predict all the physical properties of a fused

salt, the actual structure of the melt need not be identical in every respect to that of the model.

The application of uv - visible spectroscopy of fused salts containing transition metal ions to the study of the actual structure of the melt has been hinted at by several authors, e.g. Sundheim and Kukk (12), and Øye and Gruen (13). Thus far no detailed correlation between spectra and thermodynamic properties of such solutions has been presented. The method has been used, however, to identify the species in the melt. Thus, Juaz et al. (14) observed the spectral changes in a boric oxide glass containing varying amounts of alkali oxide. At low alkali oxide contents the spectral evidence indicated that both Co(II) and Ni(II) existed within the BO_3 network as MO_6 species. As the alkali oxide content was increased, BO_3 pyramids were converted into BO_4 tetrahedra until the latter were present in the ratio of ~1 in 10. At still higher concentrations the network was disrupted and non-bridging oxygen sites were present; the spectra were now indicative of tetrahedral MO_4 species. The change in spectra was thus used to detect the breakdown of the network structure.

The work reported in this thesis has been concerned almost exclusively with the problem of species identification. Whilst the suitability of the analytical application was not a prime purpose of this work, in order to determine molar extinction coefficients with any degree of confidence, several solutions for each element were used. In this way the applicability of Beer's law for some of the elements was checked. No attempt has been made to correlate the spectra obtained with the structural models of fused salts.

CHAPTER II

THEORY OF LIGAND FIELD SPECTRA

Transition metal compounds show an extremely wide range of colours, both in the solid state and in solution, which result from the presence of absorption bands in the 13 to 25 kK region of the spectrum. An attempt to explain these bands in terms of transitions between the atomic energy levels, assuming that the ligands had little effect on the metal ion, was unsuccessful in view of the fact that different ligands gave rise to different spectra. It can be concluded that the ligands were affecting the atomic energy levels. In order to rationalise this effect, it was suggested that the interactions between the metal ion and the ligands were purely electrostatic in nature and that the ligands should be regarded as point charges, (or as point dipoles in the case of neutral ligands). Calculations of the crystal field splitting 10 Dq using this crystal field model were fairly satisfactory (15). However, when allowance was made for the finite size of the ligand electron cloud, the calculations gave rise to values of 10 Dq having the wrong sign (see reference 16).

The crystal field theory is based on the assumption that there is no covalent contribution to the metal-ligand bond in which case the d orbitals of the free metal ion remain unchanged on forming a complex. There are several different experimental results which suggest that overlap of the metal d orbitals with ligand orbitals is of some importance. Those results which are obtained from spectral measurements are considered below, whilst the others are discussed in some detail by Gray (17).

In the first instance, it is found that the separations between the Russell-Saunders states decrease on going from the free ion to the complex. These separations can be explained in terms of interelectronic repulsions. In the complex then, these repulsions are reduced; an effect which can be visualised as arising from orbital expansion such that the d electrons have more space available to them. This result can be achieved by overlap of the d orbital and a ligand orbital, the d electrons thereby being delocalised onto ligand orbitals. Such an orbital expansion is known as the nephelauxetic effect and will be discussed later (P. 26). A strict application of Laporte's rule, which states that g - g transitions should be forbidden, results in the conclusion that the absorption bands for octahedral complexes should have zero intensity. Since, in fact, the bands are observed they cannot be due to simple d - d transitions. The bands can gain intensity by several mechanisms, (see P. 39), one of which is thought to be mixing of the metal d orbitals with ligand p orbitals.

The existence of such evidence would seem to suggest that the best method of approach would be from the molecular orbital point of view. Unfortunately, a detailed molecular orbital treatment is extremely difficult. However, much work has been reported recently using this technique (18, 19, 20, 21). Nevertheless, the majority of spectral investigations have been discussed in terms of crystal field theory which has been modified such that orbital overlap is taken into account. With these modifications the theory is known as ligand field theory. The term ligand field spectroscopy then refers to spectral investigations which are concerned primarily with d - d transitions.

The absorption spectrum of a transition metal compound is characterised by

four features:

1. The number of bands.
2. The positions of the bands.
3. The shape of the bands.
4. The intensities of the bands.

These features will be discussed in some detail. Since both the number of bands and their positions can be obtained from considerations of the energy level diagrams of the complexes, these two features will be discussed together.

2.1 Energy Level Diagrams. Energy level calculations for complexes constitute a fairly wide field in themselves and the details of such calculations will not be discussed in great detail. In order to discuss energy level diagrams for transition metal complexes, it is necessary first of all to consider the free ion case. Whilst only a very brief discussion of the energy level calculations is presented here, an explicit account is available in the standard texts (22, 23).

For the sake of simplicity it will be assumed that the ions of interest can be described within the L - S coupling scheme. Although this particular coupling scheme is reasonably adequate for the first row transition elements, it is not really applicable to the second or third row elements. In these latter cases, the coupling is more accurately described in terms of 'intermediate coupling'; intermediate, that is between L - S coupling and j - j coupling.

In the L - S, or Russell-Saunders, as it sometimes is called, coupling scheme the individual spin quantum numbers s of the electrons are coupled to give an atomic quantum number S. Similarly, the individual orbital quantum numbers l are coupled

to give the corresponding atomic quantum number L. It is assumed, as a first approximation, that there is no interaction between the orbital and spin wavefunctions, i.e. spin-orbital coupling is neglected. Only certain combinations of the L and S values are allowed by the Pauli exclusion principle. In this context the exclusion principle can be reformulated as follows: 'for equivalent electrons the value of L + S must be even' (23). The allowed combinations of L and S are written in the term symbolism: ^{2S+1}X in which $2S + 1$ is known as the spin multiplicity of the term (values of $2S + 1 = 1, 2, 3, \ldots$ being known as singlet, doublet, triplet, etc., terms), and X is the symbol corresponding to the value of L as follows:

$$L = 0\ 1\ 2\ 3\ \ldots$$

$$X = S\ P\ D\ F\ \ldots$$

The actual method of determining the number and identity of the terms of a particular configuration is fairly straightforward, it merely becomes extremely tedious for d^n configurations with $n > 2$. However, since the box diagram which results will make later discussion clearer, a brief summary of this method is given. (See reference 23 for more details). Consider the $3d^2$ system. The inner shells are completely filled and need not be considered. The first step is to tabulate all the possible combinations of m_l and m_s in groups according to their values of $M_L = \Sigma m_l$ and $M_S = \Sigma m_s$. For the d^2 case, the possible values of M_L are $+4 \rightarrow -4$, and for M_S are $1, 0, -1$. The combinations of the individual m_l and m_s are then written in the following box diagram:

M_S	1	0	-1
M_L			
4		$(2^+, 2^-)$	
3	$(2^+, 1^+)$	$(2^+, 1^-), (2^-, 1^+)$	$(2^-, 1^-)$
2	$(2^+, 0^+)$	$(1^+, 1^-), (2^+, 0^-),$ $(2^-, 0^+)$	$(2^-, 0^-)$
1	$(1^+, 0^+), (2^+, -1^+)$	$(1^+, 0^-), (2^+, -1^-),$ $(1^-, 0^+), (2^-, -1^+)$	$(1^-, 0^-), (2^-, -1^-)$
0	$(2^+, -2^+), (1^+, -1^+)$	$(2^+, -2^-), (1^+, -1^-),$ $(2^-, -2^+), (1^-, -1^+),$ $(0^+, 0^-)$	$(2^-, -2^-), (1^-, -1^-)$

The boxes for negative M_L values are not included since the diagram just repeats itself except for a change in sign. Within the d orbitals there are 10 sites for the two electrons, so there must be a total of 45 micro states in the complete diagram. The next step is to take the micro state with the highest M_L value and the highest M_S value consistent with this, in this case $(2^+, 2^-)$ which corresponds to $M_L = 4$ and $M_S = 0$. Since $M_L = 4$, then the value of L must be 4 and the micro state must, therefore, come from a G term. Furthermore, since $M_S = 0$, then S also must be zero and, therefore, the spin multiplicity is 1. The term is, therefore, a ^1G. Now for $L = 4$, M_L can take all values between +4 and -4, so that each

of the boxes in the $M_S = 0$ column contains a micro state of the ^1G term. In general, terms consist of $(2L + 1)(2S + 1)$ micro states. After all the micro states of the ^1G term have been eliminated, the state with the highest M_S and M_L values is considered. In this case, it is the $(2^+, 1^+)$ state. This corresponds to $M_L = 3$ and $M_S = 1$ which, as before, leads to a ^3F term. In this state M_S can take the values $-1, 0, +1$ with an M_L value in the range -3 to $+3$. In all, there are a total of 21 micro states arising from the ^3F term. Once these have been eliminated, the micro state with the largest M_L and M_S is again chosen and the whole procedure repeated. This is continued until all the micro states have been used up. For the d^2 system, it is found that the following terms arise: ^1G, ^3F, ^1D, ^3P and ^1S.

Once the identity of the terms which arise from the d^n configurations have been obtained, the next question concerns their position on the energy scale. The ground term can be identified relatively easily by applying Hund's rule, viz: for equivalent electrons, the terms(s) with the greatest multiplicity have the lowest energy, and of these the lowest has the largest L value. This rule is, however, only applicable to a determination of the ground state. For example, using Hund's rule, the order for the terms of d^2 would be ^3F, ^3P, with the singlet terms ^1D, ^1G and ^1S lying at higher energy. Experimentally, however, it is found that the ^1D lies below the ^3P. Whilst the identity of the ground term is useful, energy expressions for all the terms of a configuration are still required for the present purposes. The method of calculation is discussed by Ballhausen (23) but the main result is that the sum of the energies of the micro states in each of the boxes corresponds to the sum of the energies of the parent terms. Thus, the box $M_L = 4$, $M_S = 0$ contains the single

micro state $(2^+, 2^-)$ which arises from the ^1G state and therefore:

$$E(^1G) = E(2^+, 2^-).$$

For the box $M_L = 3$, $M_S = 0$, the micro states $(2^+, 1^-)$ and $(2^-, 1^+)$ correspond to terms ^1G and ^3F and thus:

$$E(^1G) + E(^3F) = E(2^+, 1^-) + E(2^-, 1^+)$$

In this way, a set of linear equations for each box can be set up and from these, the term energies, as a combination of micro state energies, can be derived. The energies of the micro states can be written in terms of the Coulomb and exchange integrals J and K respectively, as shown by Ballhausen (23). For equivalent electrons it is found that:

$$J(a, b) = \sum_k a^k F^k$$

$$K(a, b) = \sum_k b^k F^k$$

Tables of the a^k and b^k coefficients have been derived and are listed by Ballhausen (23). Thus it is found that the term energies can be expressed as a linear combination of F^k integrals. For d electrons, it is found that only three integrals corresponding to values of k of 0, 2 and 4 are required. In the d^2 case, the expressions for the term energies are as follows:

$$E(^1G) = F_0 + 4F_2 + F_4$$

$$E(^3F) = F_0 - 8F_2 - 9F_4$$

$$E(^1D) = F_0 - 3F_2 + 36F_4$$

$$E(^3P) = F_0 + 7F_2 - 84F_4$$

$$E(^1S) = F_0 + 14F_2 + 126F_4$$

It is usual, for the sake of convenience, to write F_k rather than F^k, since the latter integrals contain a numerator. They are related as follows:

$$F_k = \frac{F^k}{D^k}$$

where D^k has the values 1, 49 and 441 for k values of 0, 2 and 4 respectively.

From a spectroscopic point of view, it is even more convenient to use Racah parameters rather than the F_k integrals. The Racah parameters are defined as follows:

$$A = F_0 - 49F_4$$

$$B = F_2 - 5F_4$$

$$C = 35F_4$$

In this way, separations between terms of the same multiplicity are a function of B only, e.g. $^3P - {}^3F$ for d^2 is 15B, whilst for terms of different multiplicity the energy difference involves both B and C.

The method outlined above can be applied to all the d^n configurations, although actual calculations are only necessary for $n = 2, 3, 4$, and 5, because of the equivalence of the electrons and 'holes.' In other words, the expressions for the term energies of $d^7 (\equiv d^{10-3})$ are the same as for d^3. The expressions for the term energies of all the d^n configurations have been tabulated (23).

Once the expressions for the term energies of the free ions have been obtained, the next step is to determine the effect of complex formation on these energy levels. The method of approach is to examine the system qualitatively in the first instance, and then this rough picture is clarified by a quantitative treatment. In the following arguments, an octahedral model will be used to indicate the general line of attack.

As shown earlier, the $3d^2$ configuration gives rise to the following terms: ^3P, ^3F, ^1G, ^1D, ^1S. The effects of an octahedral ligand field, as in VCl_6^{3-} for example, are required. These are most easily obtained by the application of group theoretical arguments.

The first point to be made is that the symmetry characteristics of terms are identical in every way to those of the corresponding one-electron orbitals, e.g. a D term has the same properties as a d orbital. That this is so, can be seen if it is recalled that the M_L values of the D term range from +2 to -2. Consequently, it will be sufficient to consider the effects of the ligand field on s, p, d, f, ... orbitals. Cotton (24) discusses the methods and results of group theoretical treatments of this problem in some detail and the discussion which follows approaches the problem from the same point of view. The method involves the determination of the transformation matrices for the orbitals under consideration for each of the symmetry elements in the octahedral point group. The sums of the diagonal elements constitute a reducible representation of the octahedral group which can be reduced, by methods discussed by Cotton, to a sum of the irreducible representations in the group. In this way, it can be shown that a d orbital, and therefore, a D term, splits into T_{2g} and E_g states. The method is quite general and can be applied to all terms in ligand fields of any symmetry. For the d^2 case in octahedral symmetry, the following results are obtained:

Free Ion Term	State In O_h Symmetry
^1S	$^1A_{1g}$
^1D	$^1T_{2g} + {}^1E_g$
^1G	$^1A_{1g} + {}^1T_{2g} + {}^1T_{1g} + {}^1E_g$
^3F	$^3A_{2g} + {}^3T_{1g} + {}^3T_{2g}$
^3P	$^3T_{1g}$

The previous discussion was concerned with the weak field case, i.e., the situation in which the ligands give rise to a small ligand field, which is considered to perturb the free ion levels, but not cause any interaction between them. Now the other limiting case which is normally considered is the strong field case. Here the ligand field is larger than the interelectronic repulsions in the free ion and the energy levels in the complex are determined by the symmetry it possesses. Thus, for an octahedral d^{n+m} complex, the energy levels in the strong field approximation are given by $t_{2g}^n e_g^m$, $t_{2g}^{n-1} e_g^{m+1}$, $t_{2g}^{n-2} e_g^{m+2}$ ... . Now just as the free ion terms are split by considering the perturbing effects of interelectronic repulsions, so the strong field configurations are also split by the same effects. The identity of the states obtained from these configurations are obtained from group theory as indicated by Cotton. In this case, the method is to take the direct products of the representations of the single electrons, e.g., $t_{2g} \times t_{2g}$ for t_{2g}^2, and obtain by the usual methods the irreducible representations in the octahedral group, $A_{1g} + E_g + T_{1g} + T_{2g}$ for the above example. For a particular d^n configuration, it is found that the number of states and their symmetry types are equal in both the weak and strong field cases and, by combining the two energy level schemes and joining the

corresponding states, a correlation diagram is obtained. This diagram, therefore, represents the effect of varying the ligand field strength in a qualitative fashion.

A quantitative treatment is much more difficult, particularly for Δ values which are found in practice, i.e., the intermediate case. For the weak field case, the energy expressions for the states can be obtained by solving matrix elements of the form $\langle\langle M_L | V_{oct} | \langle M_L' \rangle\rangle$ as shown by Figgis (25). The strong field case is rather easier to handle for the octahedral case, at least. The energy separations of the strong field configurations, $t_{2g}^a e_g^b$ can be obtained from the following expression:

$$E = (-4a + 6b)\, Dq$$

which arises from the fact that the separation of the t_{2g} and e_g states is 10Dq with the t_{2g} at -4Dq, and the e_g at +6Dq.

The intermediate case is much more difficult to solve and the method of calculation will not be discussed. It can be approached from either the weak or strong field limit. Tanabe and Sugano (16) have completed such calculations, starting from the strong field limit, for all the d^n configurations. Because of the complexity of the calculations, it was necessary to assume a value for C/B. Their results are usually presented in the form of a Tanabe-Sugano diagram in which E/B is plotted versus Δ/B. In order to derive values of Δ and B from a particular spectrum, it is more accurate to use the energy matrices from which these diagrams were constructed. In some cases, however, the matrices are so large that this procedure becomes impracticable and the diagrams must be used. Thus, for an octahedral low-spin d^5 complex, which has a $^2T_{2g}$ ground state, the energy expression for this level involves a 10 x 10 matrix. Jørgensen (15) has pointed out that the results obtained

by Tanabe-Sugano can be generalised as follows: If there is only one term of a certain symmetry type, then the energy can be written in the form: $k\Delta + k_2B + k_3C$. If there are two terms of the same symmetry type, then the energy expressions involve a square root expression of Δ, B and C. For more than two terms, extremely complicated expressions are obtained.

The Tanabe-Sugano treatment does not consider the effects of spin-orbital coupling. This is quite reasonable since the theory was developed for first row transition metal complexes in which such an effect is not very important at room temperature. At low temperatures, particularly for single crystals, splitting due to spin-orbital coupling is observed. Whether or not spin-orbital splitting will be observed will depend on the relative sizes of this splitting and the ligand field splitting. A brief discussion of spin-orbital coupling is now given in which a simple classical point of view is adopted. In this sense, both the spinning of the electron and its orbital movement give rise to magnetic dipoles which can interact. In the majority of cases, the relative magnitudes of the spin-orbital coupling interaction and the term separations in the free ion are such that it can be assumed that spin-orbital coupling in one term does not influence that in a different term. In other words, spin-orbital coupling can be regarded as a small perturbation on the terms. Each of the terms is split into $(2S + 1)$ or $(2L + 1)$, whichever is the least, states. These states are designated by their J value which may take values between $(L + S)$ and $(L - S)$. The spin-orbital coupling constant λ is defined for each term of a configuration:

$$\lambda = \frac{\pm \zeta}{2S}$$

where ζ is the single-electron spin-orbital coupling constant. λ is a constant within a term and, since it depends on S, will change for terms of different spin multiplicity. The values of λ are positive for a shell which is less than half-full. Although spin-orbital coupling is often discussed with reference to the free ion terms, it can, as shown by Ballhausen (23), be applied to the ligand field states. Energy level diagrams, identical to those of Tanabe and Sugano except that the effects of this coupling on the ligand field state are included, have been published for all the d^n configurations, (see reference 26 for a list of references). However, just as the Tanabe-Sugano diagrams are limited in that only a single ratio of C/B is used, so for these diagrams assumptions regarding the values of B, ζ and C/B must be made. This obviously detracts somewhat from their usefulness and means, in fact, that separate calculations are necessary for each specific complex. Throughout the main body of this thesis, it has been found that the Tanabe-Sugano diagrams, or better, the energy matrices, for the various states are sufficient to interpret the results obtained.

With the aid of the Tanabe-Sugano diagrams, it is possible to predict the number of bands quite easily. Furthermore, by a judicious use of the selection rules discussed later, the relative intensities of the bands can be estimated. In this way, the gross features of the spectrum can be predicted.

The positions of the bands depend on the values of Δ, B and C, and it is, therefore, rather difficult to try to predict the actual band positions. The use of an average value of Δ for a particular metal, depending on its oxidation state and whether it is in the first, second or third transition series, is not of much help since

the values of B and C are more difficult to predict. It has been found that Δ and B vary for different ligands and central metal atoms in a reasonably regular order. Thus, for a particular ligand, it is found that Δ increases in the following order:

Mn(II), Ni(II), Co(II), Fe(II), Cr(III), Co(III),

Mn(IV), Mo(III), Rh(III), Re(IV), Pt(IV)

Furthermore, if a different ligand is used, the same general trend is observed although minor discrepancies do occur. For a constant metal ion, the ligands also can be arranged in order of increasing Δ value:

I^-, Br^-, F^-, H_2O, pyridine, dipy, NO_2^-, CN^-.

Once again, if the metal is changed, the same general order is observed. These two series are known as the spectrochemical series. The existence of these two spectrochemical series led Jørgensen (27) to postulate that, for any complex species, Δ can be separated into a ligand contribution and a metal contribution in the following manner:

$$\Delta = f(\text{ligands}) \cdot g(\text{central ion})$$

in which g is evaluated by choosing $f = 1$ for aquo complexes. The value of f for other ligands can then be obtained. These values of f and g can be used to predict Δ values for complexes provided that the values for the corresponding aquo ions have been obtained.

There have been many attempts to calculate 10Dq from first principles using both the crystal field and molecular orbital approaches, (see (23) for a complete discussion). On the crystal field model, the expression for 10Dq is found to be (25):

$$\Delta = 10\,Dq = \frac{5Z\,e^2\,\overline{r^4}}{3\quad a^5}$$

where: r = radius of d electrons in the central metal atom

a = metal-ligand distance

Z = charge on the ligand.

On this model, it can be seen that 10 Dq varies inversely as the fifth power of the metal-ligand distance. Such a variation can have a relatively large effect on the temperature and pressure dependance of 10 Dq. Jørgensen (27) used this relationship to explain the change in 10 Dq observed on cooling $Ni(H_2O)_6^{2+}$ by suggesting that the M - L bond length decreased. Furthermore, an increase in pressure will also decrease this bond distance and should, therefore, increase the value of Δ. Results confirming this effect have been reported by Drickamer and coworkers, e.g., for the $NiSO_4 6H_2O$ system (28). The actual values of Δ calculated by the above expression are in very poor agreement with experiment. The molecular orbital treatment has also been applied to calculations of Δ. In this case, good agreement between calculated and experimental values for $KNiF_3$ has been obtained (29).

Lee and Lever (30) have questioned Jørgensen's explanation for the temperature dependance of Δ and have suggested that it can be explained in terms of changes in the vibrational populations of the ground electronic state. On this particular model, it would appear that Δ should depend on T in an exponential fashion. This ramification of the Lee and Lever theory has not been checked experimentally. Certainly, the theory would be much more convincing if such an

experimental check was made. The explanation put forward by Jørgensen has the advantage that it can explain, in a qualitative fashion at least, both temperature and pressure variations, whereas it is difficult to understand how an increase in pressure could lead to a decrease in the population of excited vibrational states.

When the values of Δ, B and C are calculated from the spectral results using the Tanabe-Sugano matrices, it is usually found that the values of B and C are less than the corresponding free ion values. As indicated earlier, this reduction arises because of metal-ligand orbital overlap which allows the metal d electrons more space to move in and, therefore, results in a decrease in the interelectronic repulsion terms. The greater the orbital overlap, the greater the decrease in the Racah parameters and the greater the covalent character of the complex. The reduction is normally expressed in terms of the nephelauxetic parameter β defined as the ratio of B for the complex to the free ion value. In this sense, the smaller the β value, the more covalent the compound. Just as the spectrochemical series occurs for both ligands and central metal atoms, so the following nephelauxetic series are obtained (in decreasing order of β):

For the ligands:

$$F^-,\ H_2O,\ NH_3,\ Cl^-,\ CN^-,\ Br^-,\ I^-$$

For the metals:

Mn(II), Ni(II), Mo(III), Fe(III), Ir(III), Co(III), Ir(VI), Pt(VI).

An extremely detailed discussion of the nephelauxetic series has been given by Jørgensen (31).

2.2 Band Shape. The absorption spectrum which arises because of transitions between electronic levels, might at first sight, be expected to consist of very narrow lines. In practice the bands obtained in ligand field spectra have quite large widths varying from ~ 0.1 kK for the ruby lines, to ~ 3 kK in $RhCl_6^{3-}$. There are several mechanisms which can cause band broadening. Those that will be considered here are:

1. Natural line width
2. Doppler broadening
3. Collision broadening
4. Stark broadening
5. Vibrational broadening

2.2.1 Natural line width arises as a direct consequence of the Heisenberg Uncertainty Principle in that the energy levels between which a transition is taking place have a finite width ΔE. This can be written in the form:

$$\Delta E \cdot \Delta t = h/2\pi$$

where: ΔE = width of the upper energy level

Δt = lifetime in the upper energy level.

If transitions are taking place between essentially more than one energy level, then the resulting line will have some width. The calculated band widths (32) are of the order of 10^{-9} kK. An expression for the band shape can be obtained and is found to have the same general form as a Lorentzian curve, i.e.

$$I = \frac{a^2}{\frac{\delta^2}{4} + (\nu - \nu_0)^2}$$

where δ = half width, I = intensity of absorption.

Because of the wide discrepancy between the experimental and calculated band widths, it is apparent that the broadening mechanism which is operative in ligand field spectra is not the natural line width effect.

2.2.2 Doppler broadening of a spectral line occurs because the absorbing molecules are in motion and will, therefore, absorb light of slightly different frequencies. If a Maxwell-Boltzmann distribution of velocities is assumed, it can be shown (32) that the band shape will correspond to a Gaussian curve:

$$I = A\ e^{-a(\nu - \nu_0)^2}$$

Furthermore, Garbuny shows that the band width due to this effect is given by:

$$\delta = 7.17 \times 10^{-7}\ \nu_0 \left(\frac{T}{M}\right)^{1/2}$$

where: T = temperature ^{o}K

M = molecular weight

ν_0 = frequency at band maximum

Using this equation, it is found that for the band occurring at 24 kK in the spectrum of $Cr(H_2O)_6^{3+}$, the Doppler width at 300^{o} K is 2.34×10^{-5} kK. This does not agree at all well with the experimental value of ~3.7 kK indicating that Doppler broadening is not important for the systems of interest.

2.2.3 Collision broadening occurs if the rate of decay from the excited state is increased by collision with another species. In this case it is found that the absorption band will again be of the Lorentzian type. The half-widths of collision broadened bands have been estimated to be of the order of 10^{-5} kK so this effect is also negligible for ligand field spectra.

2.2.4 Stark broadening arises because of the electrostatic field associated with the surrounding ions or dipoles in the absorbing species. Once more, as Garbuny (32) indicates, this gives rise to a Lorentzian absorption band. Calculations of the half-widths are not easy to carry out for the type of species under consideration since it is very difficult to estimate the electric field strength experienced at the nucleus. This particular effect has been given an extremely thorough treatment when applied to atomic spectra but does not seem to have been investigated for ligand field spectra. In view of the complexity of the atomic spectral treatment, this is not surprising. Nevertheless, since the energy levels in transition metal complexes are given by an internal Stark effect, it would be of great value if Stark broadening effects were examined.

2.2.5 Vibrational broadening occurs in electronic transitions because each electronic level has a series of vibrational levels associated with it and the molecules will be distributed between these vibrational levels with a Maxwell-Boltzmann distribution. Excitation from these various vibrational levels to an excited electronic state will, therefore, give a band with finite width. Even if the molecules are all in the ground vibrational state, they still possess zero point vibrational energy and will give rise to a broadened band. Orgel (33) explained the band widths and their relative ordering in the spectrum of $Mn(H_2O)_6$ by means of the above vibrational argument. He explained that during a vibration the M - L distance varies and, therefore, the value of Dq varies. Now the relative band width is given by

the slope of the energy level to which the transition is taking place, as shown in the Tanabe-Sugano diagrams.

If the excited state is parallel to the ground state, the small change in Dq produced by the vibrational motion will not affect the energy of transition and, therefore, the band will be narrow. Alternatively, if the excited level has a steep slope, then small changes in Dq will correspond to rather large energy differences and a broad band will result. An examination of the Tanabe-Sugano diagrams reveals that if the excited level belongs to the same strong field configuration as the ground state, then the levels will be parallel and a transition between them will give rise to a narrow band. Considerations of this nature can be of some use in the assignment of spectral bands.

Assuming then that the main cause of the band widths is vibrational excitation, it is possible to derive an expression for the intensity distribution in an absorption band. The derivation, as reported by Sulzer and Wieland (34), is outlined below. These workers introduced the following assumptions:

(i) In the vibrational ground state of the electronic state, the molecule can be regarded as a harmonic oscillator so that the wave function will have the form $\psi = A \exp \frac{-x^2}{2a^2}$, where x = displacement, and A = amplitude of vibration.

(ii) An electronic transition between two levels takes place with unchanged nuclear displacement. Thus is the potential energy curve for the excited state has its potential energy minimum at the same displacement in all normal coordinates as the ground, the transition will take place predominantly between the ground

vibrational levels. On the other hand, if the minimum in the potential energy curve for the excited state is displaced relative to that of the ground state, then a transition from the ground vibrational level in the electronic ground state will go to an excited vibrational level of the excited state.

(iii) Since the exact form of the potential energy curve for the excited state is difficult to obtain, it was assumed that over the region directly above the ground vibrational level of the ground electronic state, the curve could be approximated by a straight line.

The mathematical treatment begins with the following equation:

$$\varepsilon(\nu) = \varepsilon_o \left[\psi_v(\nu)\right]^2$$

which states that the variation of the extinction coefficient with frequency depends on the square of the vibrational wave function. ε_o represents the absorption maximum at $0^\circ K$ when all the molecules are in the lowest vibrational state. The band shape is then given by the reflection of the squared vibrational wave function of the electronic ground state upon the potential curve of the excited state. Since the ground vibrational level is assumed to be a harmonic oscillator, then by squaring the wave function and projecting it upon a straight line, the resulting intensity profile is given by an equation of the form:

$$\varepsilon(\nu) = \varepsilon_{max} e^{\left(\frac{\nu - \nu_o}{\delta}\right)^2}$$

where: ν_o = frequency of band maximum

ε_{max} = extinction coefficient at band maximum

δ = width of band at the half-height.

It would seem, therefore, that an absorption spectrum when plotted as ε versus ν should contain bands with an approximate Gaussian shape. Experimentally, it has been found that in the spectra of regular octahedral complexes, in which the bands are well separated, then the bands do indeed possess a Gaussian shape. This has been shown in many instances; for example Jørgensen (35) reports band analysis of Cr(III), Co(III) and Ni(II) spectra. In view of the assumptions made by Sulzer and Wieland, in particular the linearity of the potential energy variation for the excited state, and also the harmonic oscillator, such an agreement is surprising. Whether or not such an agreement is fortuitous can be answered only after a completely rigorous treatment using genuine excited potential energy curves and the anharmonic oscillator model has been carried out. However, it would seem that there is some experimental and theoretical justification for assuming a Gaussion band shape. The application of wave analysis, assuming Gaussian band shapes, rests on these facts.

Sulzer and Wieland also considered the effect of temperature on the band shape. In this instance, they considered the temperature dependent extinction coefficient to be the sum of the extinction coefficients for the transitions from the populated vibrational levels weighted according to their Maxwell-Boltzmann populations, i.e.

$$\varepsilon_T = \sum_{\nu} \varepsilon_i N_i$$

The complete derivation of their final equations is not given here since it was carried out for a diatomic molecule. On the other hand, the same line of approach has been used to derive an expression for the variation of the oscillator strength as a function of temperature for an octahedral complex (36). At temperatures above $0^{\circ}K$ some

of the excited vibrational states will be occupied and because of the form of the excited vibrational wave functions, in which maxima are observed at the extremes of the vibration, it would be expected that the feet of the absorption band would be too high, suggesting that the band would approximate to a Lorentzian curve.

In this context, however, a paper by Stolarczyk (37) is of some use. By assuming a Maxwell-Boltzmann distribution in the vibrational levels, Stolarczyk considered three cases, (ν_o is the vibrational frequency of the harmonic oscillator):

(i) $kT << h\nu_o$

(ii) $kT \sim h\nu_o$

(iii) $kT >> h\nu_o$

The first case is concerned with the situation in which all the molecules are in the ground vibrational state. This will give rise, as shown by Sulzer and Wieland, (above) to a Gaussian-shaped band. The second situation arises when there is considerable population of the excited vibrational states; it is not easy to predict the general band shape but, as discussed earlier, a Lorentzian curve might be expected. When the thermal energy is much greater than $h\nu_o$, the situation can be treated in terms of a Maxwell-Boltzmann distribution, and Stolarczyk has shown that, once again, the band shape is approximately Gaussian.

2.3 Band Intensities. The bands observed in the spectra of transition metal compounds can be classified into three types according to their intensity. These are as follows:

		Oscillator Strength
Spin-forbidden,	Symmetry forbidden	10^{-7}
Spin-allowed,	Symmetry forbidden	10^{-5} - 10^{-3}
Spin-allowed,	Symmetry allowed	10^{-1}

In this classification the oscillator strength, f, rather than the molar extinction coefficient, ε, is used as a measure of intensity. The oscillator strength is preferred since it can be calculated theoretically and compared to the experimental value thereby allowing a check on the theory. Furthermore, by comparing the ε values directly, it is implicitly assumed that the bands being compared have the same half-width. The oscillator strength, on the other hand, is a measure of the area under the curve as shown by the way it is defined, namely:

$$f = 4.32 \times 10^{-9} \int_{\nu_1}^{\nu_2} \varepsilon d\nu$$

The numerical factor arises from fundamental constants which are obtained in the derivation of the formula (38).

Now in order to discuss the various band intensities and selection rules implied in the above classification, it is necessary first of all to consider the interaction of electromagnetic radiation and matter. This interaction arises because matter contains electrical charges in motion. The electric and magnetic components of the radiation induce dipole and multipole moments within matter. Of these interactions only the electric and magnetic dipole and the electric quadrupole moments are of interest for the present purpose (39). Absorption of radiation can be regarded as occurring by a coupling of the induced dipole or quadrupole and the corresponding

dipole or quadrupole component of the radiation.

2.3.1 Selection Rules. It might be thought at first that the number of bands which occurred in the spectrum would correspond to the total number of transitions between all the energy levels. Fortunately, this is not the case in as much as only transitions between certain levels are allowed. There are two steps in approaching this problem; firstly, a purely qualitative approach to determine whether the transition is allowed or forbidden, and secondly, a quantitative approach to see if the oscillator strength can be calculated theoretically. In this thesis only the qualitative results will be examined in any detail, although the quantitative aspects will be mentioned where appropriate.

The purely qualitative approach has the decided advantage that very little quantum mechanics is necessary to derive the selection rules: they can be obtained by the application of elementary group theory. The complete derivation of the expression for the intensity of absorption I_{abs} is discussed in detail in various texts e.g. Sandorfy (40). The results are as follows:

$$I_{abs} = \rho N_n B_{nm} h c \omega \Delta l \qquad 2.1$$

in which:

ρ = radiant energy per wavenumber interval

N_n = number of atoms or molecules per cm^3

B_{nm} = Einstein coefficient of absorption

Δl = thickness of the layer

ω = wavenumber of incident radiation.

The important point is that the Einstein coefficient of absorption is given by the following expression:

$$B_{nm} = \frac{8\pi^3}{3h^2c}\left[(M_x)^2_{mn} + (M_y)^2_{mn} + (M_z)^2_{mn} \right]$$

where (M_x) is the electric dipole transition moment for a transition from $n \rightarrow m$ and is given by:

$$\begin{aligned}(M_x)_{mn} &= \int \psi^*_m \sum_i e x_i \psi_n \, d\tau \\ &= e \int \psi^*_m \sum_i x_i \psi_n \, d\tau \\ &= e \, Q_{mn}\end{aligned}$$

In general, all transitions, no matter by what mechanism they occur, have a transition moment Q which can be written:

$$Q = \int \psi^*_m \, O \, \psi_n \, d\tau \qquad 2.2$$

in which O is the appropriate operator for the type of transition mechanism under consideration. The operators for the mechanisms considered here are:

For electric dipole: the radius vector $r = ix + jy + kz$

For magnetic dipole: the rotations R_x, R_y, R_z

For electric quadrupole: the components of the polarisability tensor $\alpha_{xx}, \alpha_{xy}, \alpha_{yz}, \alpha_{zz}, \alpha_{xz}, \alpha_{yy}$

On combining equations 2.1 and 2.2 it can be seen that:

$$I_{abs} \propto \left| \int \psi^*_m \, O \, \psi_n \, dz \right|^2$$

and therefore, in order for a transition to be allowed, i.e. to have finite intensity, the integral must be non-zero. An equivalent description is that the product under the integral sign must be totally symmetric for one, at least, of the components of the operator. Formulated in this fashion, the selection rule problem is amenable to treatment by the methods of group theory. For this, the symmetry types of the ground

and excited states and the transformation properties of the appropriate operator are required. The operators were written above in such a fashion that their transformation properties are easily obtained. Thus, for electric dipole transitions, the operator transforms in a manner identical to simple translation; for magnetic dipole transitions it has the same characteristics as a rotation about the x, y, or z axes, whilst for electric quadrupole transitions, it is similar to the components of the polarisability tensor, i.e. the product of two translations. Character tables for all the common molecular symmetry groups include the symmetry characteristics of the translations, rotations and the products of two translations. The procedure then is to obtain the direct product of the three representations corresponding to ψ_m^*, O and ψ_n, and see if it contains the totally symmetric representation. An easier and equivalent test is to see if the direct product of ψ_m^* and ψ_n contains the representation corresponding to O. If it does, then the transition between states n and m is allowed.

In addition to the above selection rules, there are two others of some importance, namely, the spin selection rule and the Laporte rule. The spin selection rule can be derived in the following fashion. It is assumed that the wave function of the system can be written as the product of electronic and spin wave functions:

$$\Psi = \psi_e \psi_s$$

In this case, the transition moment is given by:

$$Q = \int \Psi'^* O \Psi'' d\tau$$

$$= \int \psi_e'^* O \psi_e'' d\tau \int \psi_s' \psi_s'' d\tau$$

Now, since the spin wave functions are orthogonal, i.e. $\int \psi_s' \psi_s'' d\tau = 0$, then if the S values of the states are different, Q will be zero. This factorisation of

the total wave function into electronic (orbital) and spin parts necessarily implies that there is no spin-orbital coupling. In a sense, then, the existence of spin-forbidden bands can be regarded as an indication of the presence of spin-orbital coupling in the system and, therefore, of the breakdown of the L - S coupling scheme. Spin-orbital coupling allows states of different multiplicities to mix together, the amount of mixing being determined by the spin-orbital coupling parameter ζ and the separation between the two states.

The other selection rule which is very important for the complexes discussed later in this thesis is the Laporte rule which is a special case of the symmetry selection rule. The derivation of this rule is best seen by considering the E_g T_{2g} transition for the $Ti(H_2O)_6^{3+}$ complex (41). The intensity of this band is proportional to:

$$\int (xz)\ r\ (x^2 - y^2)\ d\,r$$

where: $r = ix + jy + kz$

On reflecting the octahedron through the centre of symmetry, its physical properties will not change, but the coordinates will change $x \rightarrow -x$, $y \rightarrow -y$, $z \rightarrow -z$. Therefore the integral undergoes the following change:

$$\int (xz)\ (ix + jy + kz)\ (x^2 - y^2)\ dr \rightarrow -\int (xz)\ (ix + jy + kz)\ (x^2 - y^2)\ d\,r$$

This change is not allowed since the integral represents a physical property of the system and, therefore, the original integral must be zero. This result can be generalized for all transitions in the Laporte rule which states "no transitions can take place between states of the same parity." In symbolic form, the rule can be written:

$$g \leftrightarrow u,\quad g \not\leftrightarrow g,\quad u \not\leftrightarrow u\ .$$

2.3.2 Intensities. The Laporte selection rule, therefore, states that for octahedral complexes, all the d - d transitions will have zero intensity. Experience shows, however, that such transitions do occur with a finite, albeit rather small, intensity. The problem of spectral intensities is, therefore, recast in the form: How do d - d transitions for octahedral complexes gain intensity? Ballhausen (41) has shown that if 'p' orbitals are mixed with the d orbitals, the bands would still have zero intensities. The answer to the dilemma lies, naturally enough, in the centre of symmetry which a perfect octahedron possesses. It is possible to remove this centre of symmetry and thus obtain intensity by distorting the complex both statically and dynamically. A static distortion, as in cis MA_4B_2 lowers the symmetry from O_h to C_{2v} and would allow some intensity. It could not explain intensities of regular O_h complexes, since it is certainly not true that all MA_6 species are distorted statically in such a way that the centre of symmetry is removed. The answer lies in the dynamic distortion, which occurs such that on the average the species still retains full octahedral symmetry. The MA_6 species, even in the ground electronic state, is vibrating. The normal modes have been worked out (42) and from these diagrams it can be seen that modes of T_{1u} and T_{2u} symmetry destroy the centre of symmetry It has, therefore, been suggested that a coupling of the electronic and vibrational (= vibronic) wave functions gives rise to the observed intensity. Such a mechanism is amenable to theoretical calculation and Ballhausen (41) gives several references which report detailed calculations of the oscillator strengths from which he concludes that the calculated and experimental values are in excellent agreement. A later review by Liehr (43) lists further references to calculations of this nature.

An important point to realise is that these calculations were carried out for electric dipole transitions which throws some doubt, therefore, on the efficacy of the magnetic dipole and electric quadrupole transitions. It is generally agreed that of the possible transition mechanisms, the electric dipole transition is by far the most important. Thus Griffith (44) gives details of the calculations of oscillator strength for the $^3T_{2g} \leftarrow {}^3A_{2g}$ transitions of $Ni(en)_3^{2+}$ assuming a magnetic dipole transition. The calculated value of 5.4×10^{-6} does not agree very well with the experimental value of 1.0×10^{-4}. The calculation for an electric quadrupole transition gives a value of 3.1×10^{-9}. These calculations show, therefore, that for the d - d bands of octahedral complexes, the main transition mechanism undoubtedly is the electric dipole coupling.

In tetrahedral complexes, pure d - d transitions are Laporte forbidden. The problem is, therefore, similar to the octahedral case and the same solution has been put forward. Calculations, however, of oscillator strengths, assuming a vibronic mechanism, give values which are too low by a factor of 10 - 100 (45). It was pointed out that p orbitals have u character so that by mixing the metal p and d orbitals together the bands will gain intensity. Actual calculations showed that this mechanism did not give rise to the experimental values. An alternative description in which the ligand field rather than a pure crystal field model was used, where the metal d orbitals overlapped with ligand orbitals, was examined. The expression for the oscillator strength derived on this model, however, contained an empirical factor which was varied so as to give good agreement with experiment. This parameter, labelled the 'covalency factor' by the authors, was regarded as a measure of the overlap. The justification for accepting this particular mechanism as the most

important one is that a separate evaluation of this 'covalency factor,' from magnetic data in fact, gave a reasonably similar value. The other selection rules, namely, the spin selection rule and the operator selection rule, can be derived in a fashion identical to that for octahedral complexes.

In the classification of bands given earlier, the most intense bands were labelled 'spin-allowed, Laporte-allowed.' This means that they were of the $g \leftrightarrow u$ variety. These bands are identified as charge-transfer or redox bands. They are envisaged as arising from the transfer of an electron from an orbital localised mainly on the metal to one localised essentially on the ligands, written as $M \rightarrow L$, or as the reverse, $L \rightarrow M$. In the spectra reported in this thesis, the positions of such bands were simply noted when they occurred in the visible or near ultra-violet regions. They do, however, play an important part in the vibronic intensity mechanism with respect to the phenomenon known as 'intensity stealing' (25). For a transition to an excited state, which becomes allowed by the vibronic mechanism, there may be a vibrational mode such that the excited term and a nearby Laporte allowed level are mixed. By this mechanism the originally forbidden transition gains more intensity than by a simple vibronic mechanism. This intensity stealing mechanism has been investigated in some detail by Englman (46, 47). This effect is inversely proportional to the energy separation between the Laporte forbidden and allowed transitions; a fact which, as Englman points out, is admirably shown in the spectra of the first transition row aquo ions as recorded by Holmes and McClure (36).

In summary, it would appear that the main ligand field bands observed in the spectra of octahedral and tetrahedral complexes are Laporte-forbidden and spin-allowed

in both cases. For octahedral complexes, the bands gain intensity by the vibronic mechanism, whilst for tetrahedral complexes metal-ligand orbital mixing is apparently the most effective mechanism.

2.3.3 Effect of Temperature on Intensity. The effect of temperature on the band intensities has been investigated by several workers. Holmes and McClure (36) considered the effect of lowering the temperature on the intensity, as given by the vibronic mechanism. It was argued that, because of the presence of a vibrational component, the oscillator strength should be strongly temperature dependant since, by lowering the temperature far enough, this vibration may be frozen out and thus the transition would become essentially Laporte-forbidden. Their treatment was as follows: It was assumed that the transition strength could be factorised into two parts – the ground state vibrations, which were temperature dependant, and the upper state vibrations, which were temperature independent. By assuming a description of the vibrational levels in terms of an equidistant spacing in both the ground state and the excited state, and that the over-all band had a Gaussian shape, they were able to derive the following expression:

$$f_T = f_o(1 + \exp - \frac{\theta}{T}) \qquad 2.3$$

in which:

f_T = oscillator strength at $T^\circ K$

f_o = oscillator strength at $O^\circ K$

θ = frequency of the intensity giving vibration in temperature units.

This equation was applied by Holmes and McClure to the data they obtained for several crystal hydrate spectra as a function of temperature. In each case, quite a

reasonable fit of the experimental results was obtained for values of θ which were acceptable for the vibrational frequency.

Essentially the same problem, i.e. the temperature dependance of vibronic transitions, has also been treated by Satten and Wong (43). This treatment contained the same assumptions, with regard to spacing of the vibrational levels and similarity in the ground and excited electronic states, as that of Holmes and McClure (36). It differed in that it was postulated that the oscillator strength is given by the sum of the oscillator strengths of the summation band f_+, corresponding to a change in vibrational quantum number $v = +1$ between the electronic states, and the difference band f_- where v changed by -1, corresponding to emission of one vibrational quantum. The expressions that were obtained are as follows:

$$f_+ = f_o \left(1 - \exp\left(-\frac{\theta}{T}\right)\right)^{-1}$$

$$f_- = f_o \left(\exp\left(\frac{\theta}{T}\right) - 1\right)^{-1}$$

which leads to:

$$f_T = f_+ + f_-$$

$$= f_o \coth\left(\theta/2T\right) \qquad 2.4$$

$$= f_o \frac{1 + \exp\left(-\theta/T\right)}{1 - \exp\left(-\theta/T\right)} \qquad 2.5$$

Equation 2.5 is similar to the Holmes and McClure expression (equation 2.3) except for the denominator term. As the temperature decreases $\exp\left(-\theta/T\right)$ becomes smaller and smaller and, therefore, the denominator in equation 2.5 approaches unity and 2.5 will, therefore, be essentially of the same form as equation 2.4 for low temperature studies. At higher temperatures, on the other hand, the two equations differ quite appreciably. If T increases, then $\exp\left(-\theta/T\right) \rightarrow 1$ and, therefore, at high

temperatures equation 2.3 tends to a limiting value of $2f_o$, whilst equation 2.5 tends to ∞. For high temperature work, the equations suggest different temperature variability of the oscillator strength. It has been suggested (49) that for high temperatures more than one vibrational level will contribute to the intensity and then equation 2.4 should be replaced by:

$$f_T = \sum_i' (f_o)_i \coth \frac{\theta_i}{2T} \qquad 2.6$$

in which the summation is carried out over the appropriate number of vibrational levels, i.e. until a reasonable fit of experimental results is obtained. Smith showed that his data for Ni(II) in $KMgCl_3$ over the range $100^oK - 800^oK$ was not reproduced by either equations 2.5 or 2.9 (nor incidentally by 2.3). Thus it may be concluded that the expressions derived by Holmes and McClure and Satten and Wong are satisfactory at low temperatures but fail to account for the experimental data at elevated temperatures. This could be due to the fact that the vibrations are more accurately represented by anharmonic motions (47) rather than harmonic ones as assumed by both the previous workers.

The effect of temperature on the intensities of tetrahedral complexes has not received much theoretical treatment. In order to explain the fact that for the spectrum of Co(II) in the LiCl - KCl eutectic an increase in temperature from 400°C to 1,000°C resulted in a decrease in the oscillator strength of the $^4T_1 \leftarrow {}^4A_2$ transition, Gruen and McBeth (5) suggested that the 'covalency factor', referred to earlier, decreased.

In this brief discussion of the ligand field spectra, it has been shown that three factors must be considered. The positions and number of bands determine the

values of Δ, B and C, and also the nephelauxetic ratio β. The shape of the bands can, with some reservations, be assumed to be Gaussian, thereby allowing wave analysis to be carried out in order to determine the positions of bands which occur close together. The intensity of the bands can be used to indicate the coordination geometry, in some cases, and, when written in a temperature dependant form, to check the acceptability of the intensity-producing mechanism.

CHAPTER III

SPECTRA OF RUTHENIUM AND OSMIUM IN FUSED CHLORIDE MEDIA

3.1 Introduction. Unlike the other elements considered in this thesis, electrode potential measurements for ruthenium and osmium have not been reported for the LiCl - KCl eutectic melt, so that prior to this spectral investigation the oxidation states of these elements in this melt were unknown. The only pertinent paper in the literature reported that a solution of $RuCl_3$ in the $KAlCl_4$ melt was deep red-brown. (50). According to Griffith (51) the most common oxidation states are Ru(III) and Os(IV) in which the complexes are almost invariably octahedral. In attempting to explain the spectra obtained in the LiCl - KCl eutectic, the results were compared with both solid and solution spectra. The spectra of Os(IV) and Ru(III) together with band assignments will now be discussed.

Ru(III). The spectral properties of simple octahedral Ru(III) complexes have not been studied in any great detail. The Tanabe-Sugano diagram (16) for this low spin d^5 configuration predicts the following ligand field transitions:

$$
\begin{aligned}
&{}^6A_{1g} \leftarrow {}^2T_{2g} \\
&{}^4T_{1g} \leftarrow \\
&{}^4T_{2g} \leftarrow \\
{}^2T_{1g},\ &{}^2A_{2g} \leftarrow \\
&{}^2E_g \leftarrow \\
&{}^2T_{2g} \leftarrow
\end{aligned}
$$

All these transitions are not necessarily observed in every spectrum. The spin-forbidden bands may lie in the near infra-red region and, since they are very weak, will only be detected if concentrated solutions are used. The spin-allowed bands, on the other hand, occur in the region where charge-transfer transitions are found for these complexes and are often obscured by them.

Jørgensen (52, 53) has obtained the spectrum of $RuCl_6^{3-}$ in hydrochloric acid and his results are shown in Table 3.1. The spectra of $Ru(H_2O)_6^{2+}$ (54) and $Ruox_3^{3-}$ (55) are also included in this Table. The spectrum quoted for the $Ru(H_2O)_6^{3+}$ case is rather misleading in that a low energy band is apparently missing. This is not strictly correct since the paper was primarily concerned with the bands at higher energy and no attempt was made to record the spectrum below 26 kK. In his first paper (52), Jørgensen suggested that the bands at 19 and 25.6 kK in the spectrum of $RuCl_6^{3-}$ were both due to spin-allowed transitions from the $^2T_{2g}$ ground state.

Table 3.1

Ligand field spectra for complexes of Ru(III)

$Ru(H_2O)_6^{3+}$		$RuCl_6^{3-}$			$Ruox_3^{3-}$	
kK	ε	kK	ε	f	kK	ε
		19	40	7×10^{-4}	15.85	11
~ 25	~ 50	25.6	600	8×10^{-3}	20.4	28
		28.7	2200	2.5×10^{-2}	26.6	350
		32.4	1700	2×10^{-2}	34.7	320
44.5	2300	43.6	16000	5.5×10^{-1}		
(54)		(52, 53)			(55)	

An examination of the spectrum in the near infra-red region, as far out as 9.1 kK in fact, revealed that no other bands were present and it was implied that the bands at 19 and 25.6 kK were due to the first two spin-allowed transitions. In the second paper, however, the band at 25.6 kK was assigned as a charge-transfer band.

The assignment proposed for the $RuOx_3^{3-}$ spectrum differs appreciably from that suggested by Jørgensen for $RuCl_6^{3-}$. Olliff and Odell (55) assign all four bands listed in Table 3.1 as ligand field transitions. Their argument is that the first two bands are quite weak, as shown by the extinction coefficient, and are due to transitions to quartet states whilst the remaining two bands are quite intense and should be assigned to spin-allowed transitions. The assignment is then as follows:

15.85	$^4T_{1g} \longleftarrow {}^2T_{2g}$
20.4	$^4T_{2g} \longleftarrow$
26.6	$^2A_{2g}, {}^2T_{1g} \longleftarrow$
34.7	^2Eg (?) $\longleftarrow$

The energy expressions for the various levels of the d^5 configuration have been quoted in a convenient form by Jørgensen (27) and are given below:

$^4T_{1g} \longleftarrow {}^2T_{2g}$	$\Delta - 5B - 4C$
$^4T_{2g} \longleftarrow$	$\Delta + 3B - 4C$
$^2A_{2g} \longleftarrow$	$\Delta - 3B - C$

The expression for the transition to the ^2Eg state was not given. Using these expressions, Olliff and Odell calculated Δ and B from the spin-forbidden bands by assuming that $C = 4B$. The difference between the two spin-forbidden bands is equal to $8B$ and therefore, $B = 570\ cm^{-1}$, which leads to $\Delta = 27.8$ kK, obtained

by taking the above-mentioned approximation. (Values of $B = 560\ cm^{-1}$ and $\Delta = 28.7$ kK quoted in the original paper are incorrect.) On substituting the correct values for Δ and B into the expression for the first spin-allowed band it is found to lie at 23.82 kK, which is not in very good agreement with the experimental value of 26.6 kK. Apart from this discrepancy, which might be ascribed to the use of spin-forbidden transitions in determining ligand field parameters, no other assignment gives any better agreement. This can be seen from the Tanabe-Sugano diagram which, in any attempt to fit the two spin-allowed bands, requires that:

$$\frac{34.7}{B} - \frac{26.6}{B} = 5\ kK$$

(This equation arises because the lines for the $^2A_{2g}$ and ^2Eg states are parallel with a separation of 5 kK.) This leads to a value of $B = 1600\ cm^{-1}$ which is almost certainly greater than the free ion value, although this latter value is not readily available.

From this discussion of the available data, sparse as it is, it would appear that an assignment such as that of Olliff and Odell is not very satisfactory. The assignment of Jørgensen, on the other hand, in which all bands, except the 19 kK band, in the spectrum of $RuCl_6^{3-}$ are due to charge-transfer transitions gains support from a comparison with charge-transfer spectra of other 4d and 5d hexahalide complexes. (For a discussic , see Chapter 9 in reference 27.) Certainly much more experimental and theoretical work is needed for simple octahedral Ru(III) complexes before a complete understanding of the spectra of such species can be achieved.

Os (IV). From the Tanabe-Sugano diagram for d^4 (16), it would be expected that the following ligand field transitions should occur:

$$^5E_g \leftarrow {}^3T_{1g}$$

$$^1T_{2g} \leftarrow$$

$$^1E_g \leftarrow$$

$$^1A_{1g} \leftarrow$$

$$^3E_{1g} \leftarrow$$

$$^3T_{1g} \leftarrow$$

$$^3T_{2g} \leftarrow$$

$$^3A_{1g} \leftarrow$$

$$^3A_{2g} \leftarrow$$

The reported band positions, and in some cases the extinction coefficients, for the spectrum of $OsCl_6^{2-}$ in both solids and solutions are listed in Table 3.2. The bands can be divided into two classes: those above and those below ~ 18 kK. Although this might not be very apparent from Table 3.2, an examination of the published spectra shows that this is true even for reflectance spectra.

TABLE 3.2

Spectra of $OsCl_6^{2-}$ in Various Environments.

K_2OsCl_6 in HNO_3	K_2OsCl_6	$OsCl_6^{2-}$ in 1NHCl ν	ε	$(Et_4N)_2OsCl_6$	$(nBu_4N)_2OsCl_6$	$OsCl_6^{2-}$ in 6NHCl ν	ε	$OsCl_6^{2-}$ in HCl ν	ε
					7.84				
					8.07				
				10.8	8.4	8.58	1.1		
	10.8	10.8		11.1	10.47	10.83	5.3		
	11.6	11.7		~11.9	10.93	11.78	4.4		
	17.12	17.09		16.98	16.99	17.24	6.7		
		17.25		17.15	17.17	17.43	3.4		
		17.42	~ 8.3	17.31	17.32	17.58	2.1		
		17.54		17.46		17.64	4.9		
23.8		17.76		~19.8		24.1(sh)	1220	24.27	1240
26.8		18.94		~23.3		27.1	8650	27.29	9810
29.3						29.4(sh)	9300	29.41	10390
30.1						30.0	9380	30.4	10810
32.9						33.1	1270		
						36.4	965		
						39.4	2330	39.53	2460
								47.8	25230
(56)	(57)	(57)		(57)	(58)	(58)		(59)	

The original expectation of a spectrum consisting of several spin-allowed bands occurring at higher energies than for weaker spin-forbidden bands has been examined with a view to band assignments for the reflectance spectrum of $Cs_2 Os F_6$ (60). By taking a value of $\Delta = 32$ kK and $B = 460\ cm^{-1}$, it was predicted (using the Tanabe-Sugano diagram) that the triplet-triplet transitions should lie between 27.5 and 31.0 kK and also that the $^5Eg \leftarrow {}^3T_{1g}$ should occur at ~ 20 kK. Bands were reported at 23.5, 30 and 33 kK in satisfactory agreement with the predictions. Although this was a reflectance study and extinction coefficients could not be obtained, the authors were aware of the high intensity of the spin-forbidden band and suggested that it gained intensity because of the relaxation of the spin selection rule by j - j coupling (see later). However, no explanation was given for the high intensities of the spin-allowed bands. If the bands listed in Table 3.2 for the chloro analogues are assigned in a similar manner, then it can be seen that extinction coefficients of ~10,000 must be assigned to two of the triplet-triplet transitions corresponding to an oscillator strength of $\sim 10^{-1}$. This does not agree very well with the expected values for octahedral complexes (see earlier P. 34). The majority of the workers in the field (57 - 59) are of the opinion that most of the bands observed above ~ 18 kK (for chloro complexes) are of the charge-transfer variety.

The bands below ~ 18 kK are very weak and are of the order of magnitude expected for spin-forbidden bands. Thus, using the first four bands observed by Johannesen and Candela (58) for the hydrochloric acid solution, for illustrative purposes, a tentative assignment would be:

$^5E_g \leftarrow {}^3T_{1g}$	8.58 kK
$^1T_{2g} \leftarrow$	10.83
$^1E_g \leftarrow$	11.78
$^1A_{1g} \leftarrow$	17.24

The structure of the band ~17 kK observed in 1NHCl by Jørgensen (57) (Table 3.2) has been ascribed to transitions to various vibrational levels of the excited electronic level. Values of the ligand field parameters were calculated using the energy expressions (27):

$^5E_g \leftarrow {}^3T_{1g}$	$\Delta - 6B - 5C$
$^1T_{2g} \leftarrow$	$6B + 2C$
$^1E_g \leftarrow$	$6B + 2C$
$^1A_{1g} \leftarrow$	$15B + 5C$

The last expression gives a value of $3B + C = 3.45$ which, in turn, does not give a very good prediction of the $^1T_{2g} \leftarrow {}^3T_{1g}$ band (6.9 versus 10.83 kK). The value of Δ found is 15.4 kK. This is rather low when compared to the values obtained for other hexahalo complexes of 5d elements: e.g. Pt(IV) 29, Ir(III) 25, Re(IV) 27.5, (27). A rough estimate of the value of Δ for $OsCl_6^{2-}$ would be ~25 kK with a value of B of ~ 360 cm^{-1} (27). This leads to a value of ~7 for Dq/B. On extending the published Tanabe-Sugano diagrams to this region (assuming that the levels are linear) the following order of transitions would be obtained:

$^1T_{2g} \leftarrow {}^3T_{1g}$	8.58 kK
$^1E_g \leftarrow$	10.83
$^1A_{1g} \leftarrow$	11.78
$^5E_g \leftarrow$	17.24

Using the expression for the $^1A_{1g} \leftarrow {}^3T_{2g}$ transition to find a value of $3B + C$, the transitions to the ^1Eg and $^1T_{2g}$ states should be degenerate and occur at 4.7 kK and the value of Δ is found to be 21.94 kK. This particular assignment obviously is not very good. There is a further argument, due to Jørgensen (57), against this assignment which is as follows: The ^5Eg state in the strong field limit arises from the $t_{2g}^3 e_g^1$ configuration so that the transition $^5Eg \leftarrow {}^3T_{1g}$ corresponds to an electron transfer from a t_{2g} to an e_g orbital. The band-widths normally found for these transitions are of the order of 2 - 3.5 kK, which is greater, by a factor or ~ 2, than found for any of the four bands discussed above. The shoulder observed at ~ 19.8 kK in the spectrum of $(Et_4N)_2 OsCl_6$ is quite broad and has been tentatively assigned to this $^5Eg \leftarrow {}^3T_{1g}$ transition (57). On the basis of the energy expressions there would appear to be four absorption bands and only three possible levels.

One possible explanation is that the complex is not perfectly octahedral. That this is not the case can be seen from the following results for $K_2 OsCl_6$. The infra-red and Raman results (61) can be interpreted using an octahedral model. A study of the chlorine quadrupole resonance spectrum (62) has shown that all the chlorine atoms are equivalent. An X-ray structure determination indicated that $K_2 OsCl_6$ was cubic with an Os - Cl distance of 2.36A (quoted in reference 51). This evidence, therefore, rules out the possiblity of a distorted octahedral symmetry.

A further possible explanation is that the levels are split by spin-orbital coupling effects. Although it is possible to discuss spin-orbital coupling in conjunction with the spectral results, historically it was first considered in an attempt to explain the magnetic results. Figgis et al. (63) pointed out that the spin-only

magnetic moment for d^4 should be 2.83 B.M., whilst the experimental value for K_2OsCl_6 was found to be 1.5 B.M. Using an L - S coupling scheme, with spin-orbital coupling as a perturbation, the coupling constant ζ was found to be 6700 cm^{-1}, which implies a larger spin-orbital coupling constant in $OsCl_6^{2-}$ than in the free ion. Estimates of the free ion value have been made by Dunn (personal communication quoted in 64) and Griffith (65) who obtained values of 4000 and 4500 cm^{-1} respectively. In view of the large ζ value, Figgis et al. (63) suggested that the L - S coupling scheme, which implies that the electrostatic repulsion terms are greater than the spin-orbital interaction parameter, is invalid and that the reverse is a closer approximation to the truth. This leads to a pure j - j coupling scheme and the value of ζ obtained for K_2OsCl_6 is 1490 cm^{-1} which is much nearer the value of ~2000 cm^{-1} expected by Figgis et al. (63). These workers also pointed out that it was unlikely that pure j - j coupling was present and that some form of intermediate coupling would be much more likely. At the same conference Griffith (65) presented the results of his calculations for such an intermediate coupling scheme which are summarised as follows: Starting from the t_{2g}^4 strong field configuration, interelectronic repulsions give rise to $^3T_1$, $^1A_1$, ^1E and $^1T_2$ terms. When the spin-orbital coupling effect is applied, the $^3T_1$ state splits into three levels specified by their values of J, namely $^3T_{10}$, $^3T_{11}$ and $^3T_{12}$ with the $^3T_{10}$ state as the ground state. The energy level diagram has been constructed by Griffith but, just as for the Tanabe-Sugano diagrams discussed in Chapter II, the analytical expressions for the energy differences are of more value from a computational point of view. These have been quoted by Johannesen and Candela (58) and are as follows:

$$^3T_{11} \longleftarrow {}^3T_{10} = W_1 = -\frac{5X}{2} + \frac{1}{2}[(5x + \zeta)^2 + 8\zeta^2]^{\frac{1}{2}}$$

$$^3T_{12} \longleftarrow {}^3T_{10} = W_2 = -\frac{3X}{2} + \frac{3\zeta}{4} + \frac{1}{2}[(5X + \zeta)^2 + 8\zeta^2]^{\frac{1}{2}} - \frac{1}{4}[(4X - \zeta)^2 + 8\zeta^2]^{\frac{1}{2}}$$

$$^1E, {}^1T_2 \longleftarrow {}^3T_{10} = W_3 = -\frac{3X}{2} + \frac{3\zeta}{4} + \frac{1}{2}[(5X + \zeta)^2 + 8\zeta^2]^{\frac{1}{2}} + \frac{1}{4}[(4X - \zeta)^2 + 8\zeta^2]^{\frac{1}{2}}$$

$$^1A_1 \longleftarrow {}^3T_{10} = W_4 = [(5X + \zeta) + 8\zeta^2]^{\frac{1}{2}}$$

where $X = 3B + C$

Johannesen and Candela used the above expressions to calculate values of $3B + C$ and ζ for $OsCl_6^{2-}$ in 6N HCl and obtained 2800 cm^{-1} and 2100 cm^{-1} respectively, with the assignment $W_4 = 17.2$ and $W_3 = 8.6$ kK. This leads to values of 3.15 and 1.52 kK for W_2 and W_1 respectively and does not give any reasonable assignment for the bands at 10.83 and 11.78 kK. Jørgensen (57) assigns the bands for $OsCl_6^{2-}$ in HCl in the following fashion:

$^1E \leftarrow {}^3T_1$	10.8 kK
$^1T_2 \leftarrow$	11.7
$^1A_1 \leftarrow$	17.24

According to this particular assignment the degenerate transition W_3 is split into its two component levels. If the baricentre of the split state is taken, then $W_3 = 11.25$ and $W_4 = 17.24$ kK. For this assignment values of 2600 and 2800 cm^{-1} are quoted for $3B + C$ and ζ respectively. Using these values in the above energy expressions the calculated band positions are as follows:

$$W_1 = 2.3,\ W_2 = 4.2,\ W_3 = 10.8,\ W_4 = 17.7 \text{ kK}$$

in which W_3 and W_4 are in reasonable agreement with the experimental values. The positions of W_2 and W_1 are very low and have not been observed although Johannesen and Candela (58) did observe some bands in the 4.5 - 5.6 kK region in the spectrum of $(nBu_4N)_2\,OsCl_6$ which they believed were due to $OsCl_6^{2-}$ and not to the $[nBu_4N]^+$ ion. No published results have been found concerning the position of W_1. The band at 8.6 kK in the spectrum of $OsCl_6^{2-}$ in HCl assigned by Johannesen and Candela to W_3 is rather suspicious. As will be discussed in Chapter IV, the absorption spectra of solutions of H_2SO_4 containing varying amounts of water have bands in the near infra-red at 6.95, 8.45 and 10.15 kK, which are due to overtones of the O - H vibrational mode. Furthermore, similar bands are obtained for aqueous systems provided that the sample and reference solutions are not absolutely identical. For example, the absorption spectrum of an aqueous solution of $(NH_4)_2\left[Fe_4(NO)_7S_3\right]H_2O$, recorded with distilled water in the reference beam, gave a very weak band at ~8.1 kK (66). It is believed that the band at 8.6 kK is, in fact, a water overtone. Some, or all, of the bands in the 7 - 8 kK region in the spectrum of $(nBu_4N)_2\,OsCl_6$ might be due to a similar overtone of the C - H vibrational mode.

The conclusion, from available date, is that the bands below ~18 kK in the spectrum of $OsCl_6^{2-}$ are due to transitions within the t_{2g}^4 configuration, which is split into several levels by spin-orbital coupling. The assignment proposed by Jørgensen is believed to be essentially correct although the mechanism by which the degeneracy of W_3 is lifted is not settled.

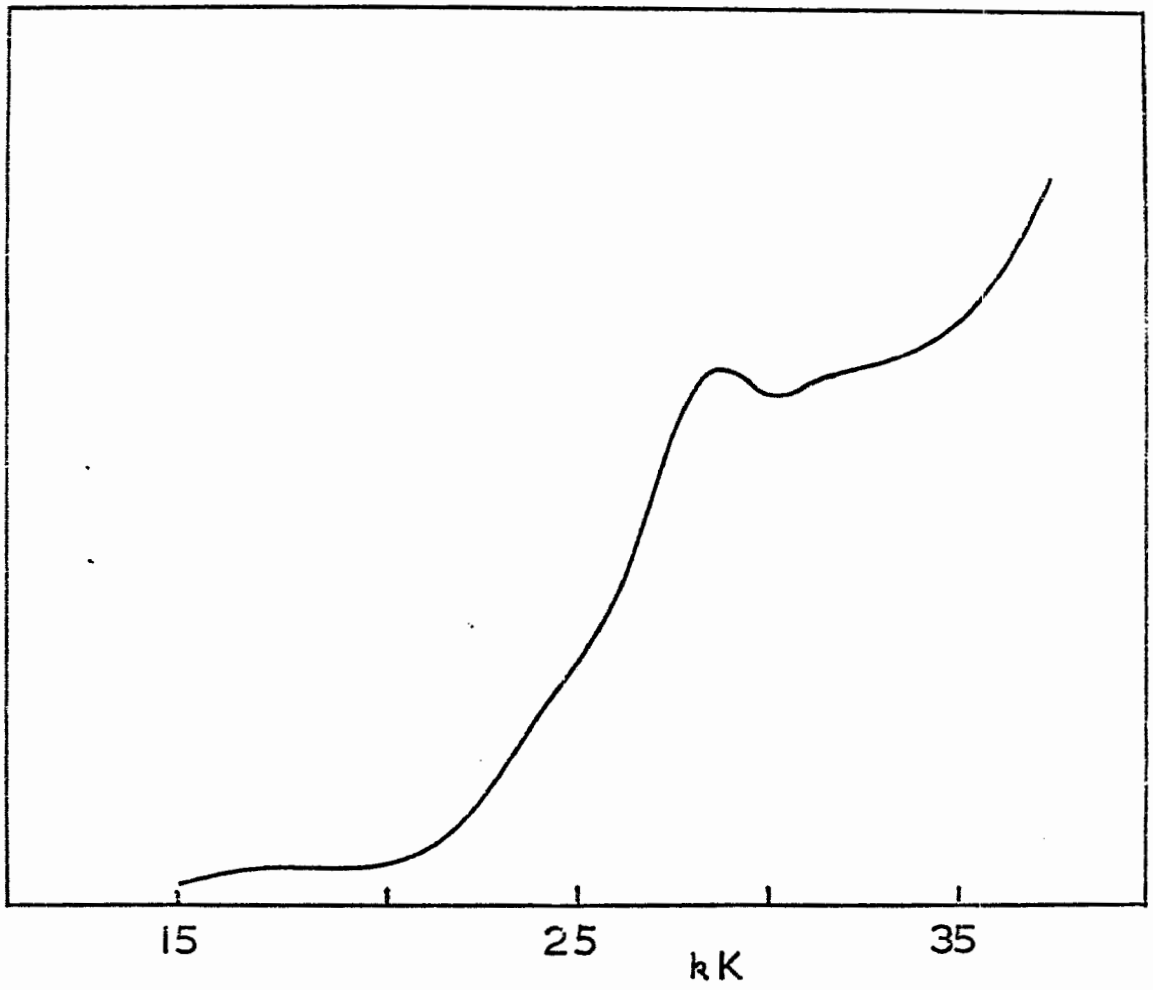

Figure 3.1

Spectrum of $RuCl_3$ in LiCl - KCl at 450°C

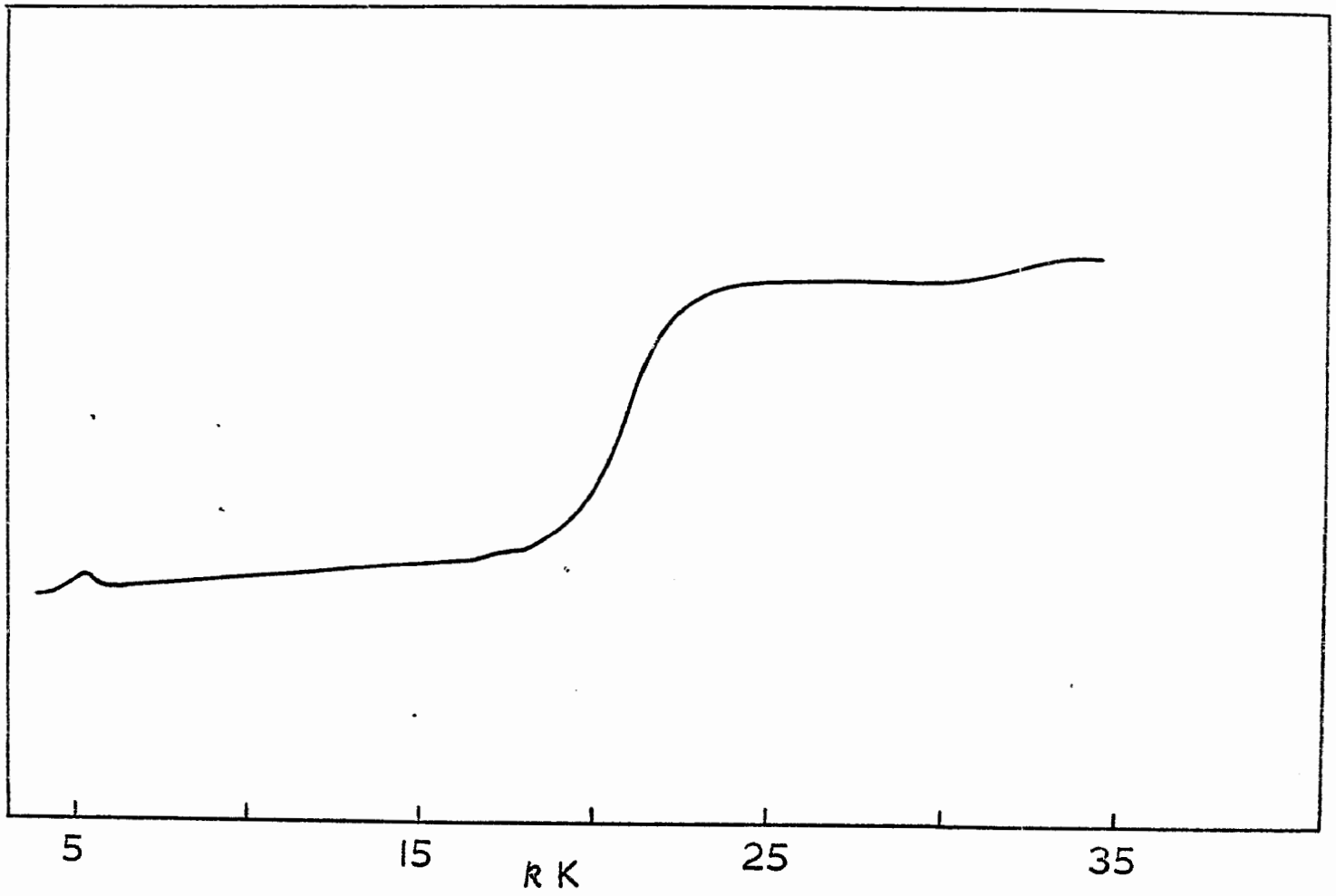

Figure 3.2

Spectrum of $OsCl_6^{2-}$ in LiCl - KCl at 450°C

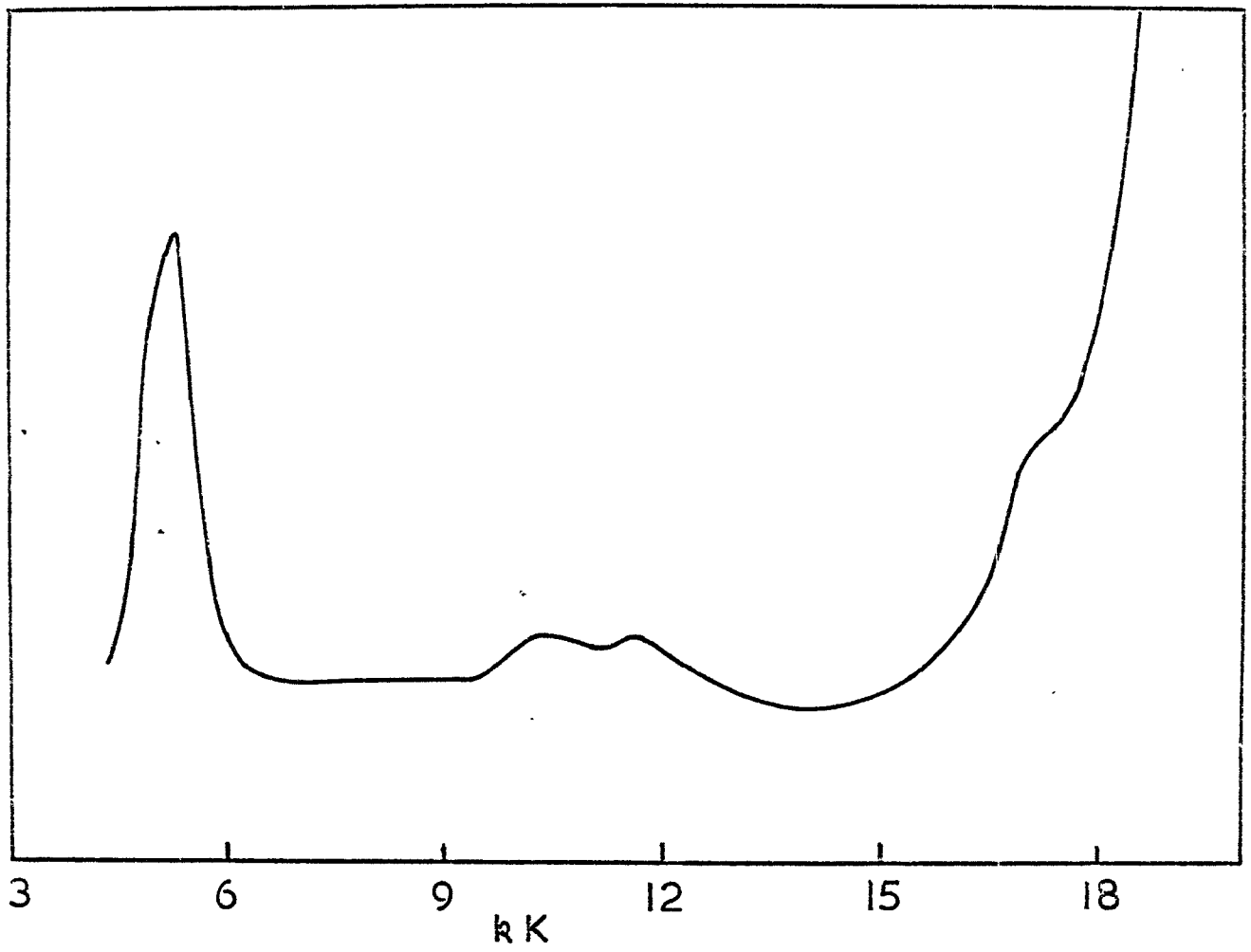

Figure 3.3

The 3 - 18 kK region of the spectrum of $OsCl_6^{2-}$ in LiCl - KCl at 450°C

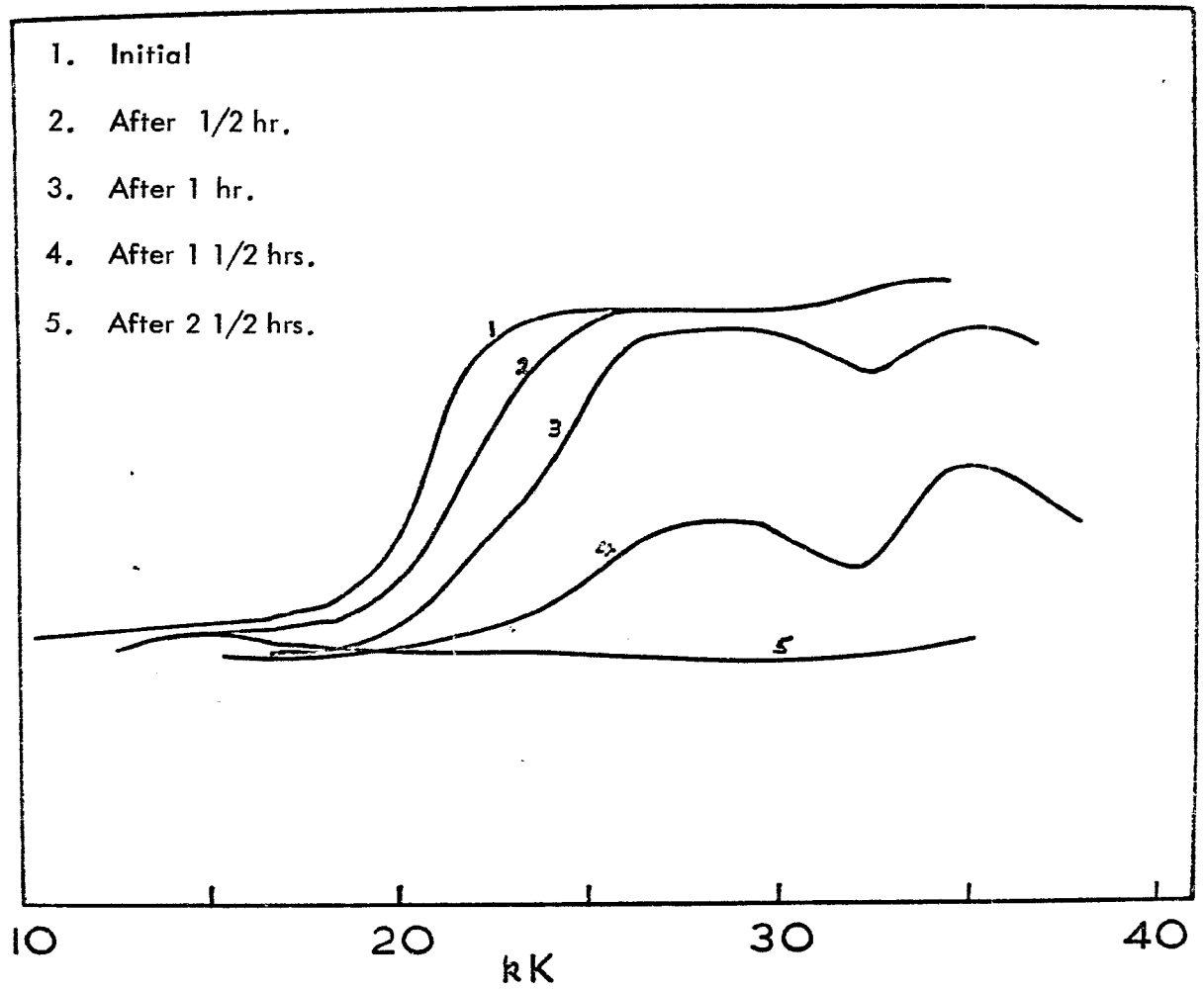

Figure 3.4

Spectrum of $OsCl_6^{2-}$ in LiCl - KCl at 450°C as a function of time

3.2 Results. The spectrum of a solution of the LiCl - KCl eutectic to which $RuCl_3$ had been added is shown in Figure 3.1 and the band maxima are listed in Table 3.3. The results for osmium are more complicated. A concentrated solution of Na_2OsCl_6 in the LiCl - KCl was prepared and had a deep red-brown colour. When a solution was prepared for spectral measurements by diluting this stock solution, the colour changed to lime green. The spectrum of this dilute solution was found to vary between samples. Furthermore, over a period of time the colour faded and an almost colourless solution was obtained. It was decided to study the spectral changes accompanying this change in colour. As a starting point the spectrum of a moderately concentrated solution, which was still red-brown in colour, was recorded at 450°C and is shown in Figure 3.2. The spectrum obtained for a more concentrated solution in the region of 3 - 18 kK is shown in Figure 3.3 and has bands at 10.4 and 11.65 kK which are not apparent in Figure 3.2. Finally, Figure 3.4 shows the spectral variations over a period of about 2 1/2 hours obtained at 450°C, with the cuvette under continuous vacuum. The band positions are reported in Tables 3.4 for the concentrated solution, and 3.5 for the time dependant spectra.

Table 3.3

Band maxima in kK for spectrum of $RuCl_3$ in LiCl - KCl at 450°C

17.5	weak
24.5 (sh)	
28.7	strong
32	strong

Table 3.4

Band maxima in 3 - 18 kK region for spectrum of Na_2OsCl_6 in LiCl - KCL at 450°C

5.3	weak
10.4	very weak
11.65	very weak
17.25 (sh)	weak

Table 3.5

Spectra of Na_2OsCl_6 in the LiCl - KCl eutectic at 450°C as a function of time

Time (hours)	Band positions (kK)				
0	5.3	17.4		24 - 30	~ 33.5
0.5		17.4		26 - 30	~ 33.5
1.0		17.1	22 sh	26 - 29	35
1.5			21 sh	28	35
2.5	15	17.2			

3.3 Discussion. Ruthenium. By comparing the band positions listed for $RuCl_6^{3-}$ in Table 3.1 to those in Table 3.3, it can be seen that the species in the LiCl - KCl eutectic melt at 450°C is the octahedral $RuCl_6^{3-}$ complex. The band at 32 kK is not as clearly resolved in the melt spectrum as it is in the HCl solution spectrum. For reasons discussed earlier the assignment of Jørgensen is preferred which, since only one band is assigned to a ligand field transition, namely $^2A_{2g} \leftarrow {}^2T_{2g}$ at 17.5 kK,

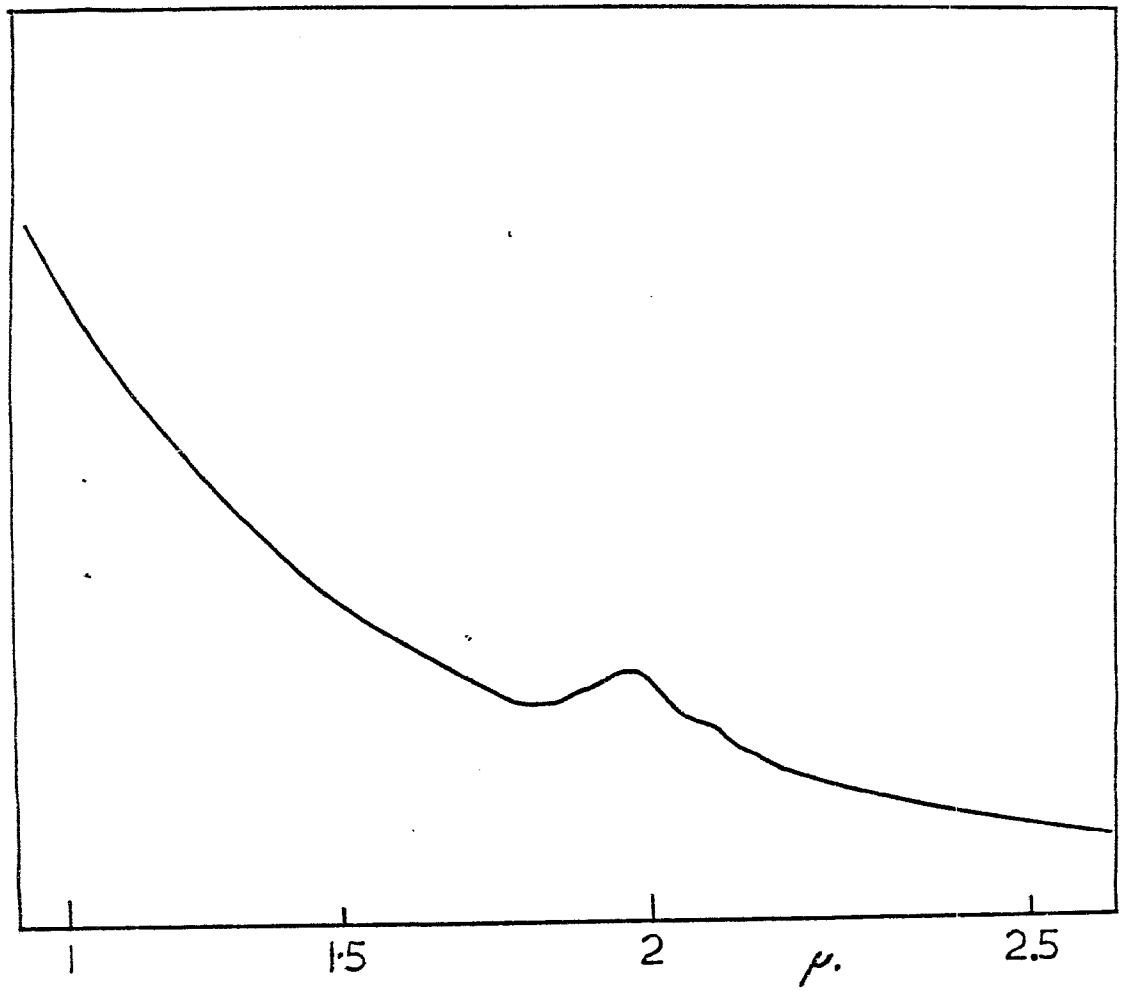

Figure 3.5
Spectrum of $OsCl_6^{2-}$ in a KBr disc

makes a calculation of Δ and B impossible. However, this band is at lower energies in the melt spectrum than in the HCl solution spectrum, which would suggest that Δ and perhaps B also are slightly lower at the higher temperature.

Osmium. The bands listed in Table 3.4, except for the one at lowest energy, are almost identical to those reported by Jørgensen for K_2OsCl_6 (Table 3.2) thereby confirming that in the LiCl - KCl eutectic octahedral $OsCl_6^{2-}$ is present. Because of this similarity it would be expected that K_2OsCl_6 should have a band at ~5 kK (W_2) and also, perhaps, another band at a lower energy (W_1). Unfortunately, K_2OsCl_6 was not available, but since the spectrum is due to the $OsCl_6^{2-}$ entity, it seemed reasonable to use Na_2OsCl_6 in its place. Accordingly, a KBr pellet containing ~ 1% w/w of Na_2OsCl_6 was prepared and the spectrum recorded over the region 7 - 2.9 kK on the Beckman DK - 2A and 1 - 4 kK on the Beckman IR8. As Figure 3.5 shows, a band was observed at 5.06 kK which can be assigned to W_2. Despite the fact that the finely ground mixture of KBr and Na_2OsCl_6 was dried by pumping at ~ 0.5 mm Hg and 140°C for 60 hours, the infra-red spectra in the 1 - 4 kK region showed bands due to water at 3.4 and 1.63 kK. Since W_1 would be expected to occur in the 2 - 3 kK region, the presence of water vibrations is rather annoying. A re-examination of the spectrum using K_2OsCl_6, which is much less hygroscopic than the corresponding sodium salt, might allow detection of W_1. The assignment for the K_2OsCl_6 spectrum is now as follows:

$$W_2 = 5.06 \text{ kK}$$

$$W_3 = 11.2$$

$$W_4 = 17.12$$

A procedure for calculating $(3B + C)$ and ζ was worked out and is described below. The expressions quoted earlier are rewritten in the following fashion.

$$W_1 = -5a + b$$

$$W_2 = -3a + b + c - d$$

$$W_3 = -3a + b + c + d$$

$$W_4 = 2b$$

where:

$$a = \frac{x}{2}$$

$$b = 1/2\left[(5x + \zeta)^2 + 8\zeta^2\right]^{1/2}$$

$$c = \frac{\sqrt{3}\,\zeta}{4}$$

$$d = 1/4\left[(4x - \zeta)^2 + 8\zeta^2\right]^{1/2}$$

$$x = 3B + C$$

In the case of interest, W_1 is not usually known and the calculation of X and ζ is more complicated than if it were. The procedure is as follows: The transition corresponding to W_4 is assigned and the value of b calculated. It can be seen from the above expressions that $W_3 - W_2 = 2d$ so that once W_3 and W_2 are assigned the value of d can be found. Using a fixed value of b and various arbitrary values of W_1, values of x and ζ were calculated and from these a range of values for d was found. Curiously enough, these values of d were rather insensitive to the values of x and ζ but were found to vary slightly with different values of b. In view of this result, the expression for W_2 can be written in the following fashion:

$$W_2 = -3a + c + \text{constant}$$

since d is a constant and b is known, b - d is a constant. Therefore:

$$\text{Constant} - W_2 = \frac{3X}{2} - \frac{3\zeta}{4}$$

The next step is to set up a table for a range of values of X and ζ from which the best values can be obtained. Thus for the spectrum of K_2OsCl_6 : b = 8.56, d = 3.07 kK, the constant term = 5.49, and W = 5.06 kK, then the above equation can be written as:

$$5.49 - 5.06 = 0.43 = \frac{3X}{2} - \frac{3\zeta}{4} \qquad 3.1$$

The values of $\frac{3X}{2}$ and $\frac{3\zeta}{4}$ for a range of X and ζ values between 2 and 5 kK are shown below:

X	2	2.5	3	3.5	4	4.5	5
$\frac{3X}{2}$	3	3.75	4.5	5.25	6	6.75	7.5
ζ	2	2.5	3	3.5	4	4.5	5
$\frac{3\zeta}{4}$	1.5	1.88	2.25	2.63	3	3.38	3.75

It can be seen that the following pairs of values of X and ζ satisfy equation 3.1:

$X = 2 \qquad \zeta = 3.5$

$X = 2.5 \qquad \zeta = 4.5$

which give a value of 0.37 for the right hand side of the equation. The next step is to consider a range of values of X between 2 and 2.5 and of ζ between 3.5 and 4.5. These are evaluated below:

X	2	2.1	2.2	2.3	2.4	2.5						
$\frac{3X}{2}$	3	3.15	3.3	3.45	3.6	3.75						
ζ	3.4	3.5	3.6	3.7	3.8	3.9	4.0	4.1	4.2	4.3	4.4	4.5
$\frac{3\zeta}{4}$	2.55	2.63	2.7	2.77	2.85	2.92	3	3.07	3.15	3.22	3.3	3.38

Once again the pairs of values which give the best fit to equation 3.1 are chosen. In this case, there are six sets of values. Each of these sets are then used to calculate the value of b and these values are as follows:

X	2	2.1	2.2	2.3	2.4	2.5
ζ	3.4	3.6	3.8	4.0	4.2	4.4
b	8.24	8.71	9.18	9.59	10.04	10.2

The experimental value of b = 8.56 kK is approached closest by the values X = 2.1 and ζ = 3.6 kK. The agreement can be further improved by repeating the whole calculation, taking values of X between 2 and 2.1 and the values of ζ between 3.4 and 3.6. The final step in the calculation is to calculate all the band positions and compare with the experimental values. Using the best values of X and ζ found above the following band positions are calculated for the K_2OsCl_6 spectrum:

$$W_1 = 3.31 \text{ kK}$$

$$W_2 = 5.27$$

$$W_3 = 10.93$$

$$W_4 = 17.12$$

The agreement between experimental and calculated values of W_2 and W_3 is seen to be satisfactory. Furthermore, W_1 is predicted to lie in the conventional infra-red region and exactly in the area where O - H stretching vibrations occur.

For the spectrum in the LiCl - KCl eutectic melt the bands are assigned as follows:

$$W_2 = 5.6 \text{ kK}$$

$$W_3 = 11.0 \text{ kK}$$

$$W_4 = 17.25 \text{ kK}$$

This leads to values of $b = 8.63$, $d = 2.25$, which gives:

$$6.38 - W_2 = \frac{3X}{2} - \frac{3\zeta}{4}$$

$$0.78 = \frac{3X}{2} - \frac{3\zeta}{4}$$

By a calculation similar to that performed earlier, the best values of X and ζ satisfying equation 3.2 are found to be:

$$X = 2 \qquad \zeta = 3$$

$$X = 2.5 \qquad \zeta = 4$$

$$X = 3 \qquad \zeta = 5$$

The expanded form of the table in the region $X = 2 - 3$ and $\zeta = 3 - 5$ leads to the sets of values:

X	2	2.1	2.2	2.3	2.4	2.5	2.6	2.7	2.8	2.9	3.0
ζ	3	3.2	3.4	3.6	3.8	4.0	4.2	4.4	4.6	4.8	5.0
b	7.76	8.18	8.62	9.11	9.55	10.0	10.43	10.91	11.34	11.8	12.25

Also shown above are the corresponding values of b from which it can be seen that the best pair of values is $X = 2.2$ kK and $\zeta = 3.4$ kK. The predicted band positions are then found to be:

$$W_1 = 3.12 \text{ kK}$$

$$W_2 = 5.11 \text{ kK}$$

$$W_3 = 10.63 \text{ kK}$$

$$W_4 = 17.24 \text{ kK}$$

The agreement between calculated and experimental values of W_2 and W_3 is quite reasonable.

The values of X and ζ in the K_2OsCl_6 and the LiCl - KCl eutectic melt spectra are, therefore, essentially identical, within the limits of the experimental error. This similarity is governed, in the main, by the difficulty in determing the position of W_4 accurately, particularly for the case of K_2OsCl_6 where the band is not as pronounced as it is in the melt spectrum. That the two sets of values are similar is not really surprising since the bands considered are all due to transitions within t_{2g}^4 and as such are not affected by the value of the ligand field splitting parameter (which is temperature dependent). One further point in favour of the assignment discussed above concerns the band intensities. These have been indicated in a qualitative fashion in Table 3.4. Griffith (65) indicates on his energy level diagram the values of j associated with each of the energy levels. The change in j value for each of the four transitions is shown in Table 3.6:

Table 3.6

Selection rules for j - j transitions within the t_{2g}^4 configuration

	$j \rightarrow j'$	Electric dipole	Magnetic dipole	Electric quadrupole
W_1	0 - 1	allowed	allowed	forbidden
W_2	0 - 2	forbidden	forbidden	allowed
W_3	0 - 2	forbidden	forbidden	allowed
W_4	0 - 0	forbidden	allowed	forbidden

Since all four transitions are within the t_{2g}^4 level, they are essentially localised on the central metal atom and can be treated in the same fashion as atomic transitions. The selection rules for transitions between states of different j values for electric

quadrupole transitions are as follows (67):

	Electric dipole	Electric quadrupole	Magnetic dipole
Δj	$0, \pm 1 (0 \nleftrightarrow 0)$	$0, \pm 1, \pm 2 (j + j' \geqslant 2)$	$0, \pm 1$

Table 3.6 also contains the result of applying these selection rules to the four transitions listed. Thus assuming a pure $j - j$ coupling scheme the order of band intensities, bearing in mind that electric dipole transitions are stronger than magnetic dipole, which in turn are stronger than electric quadrupole transitions, would be $W_4 > W_2 \sim W_3$. (W_1 is not considered since it was not observed experimentally but would appear to be the strongest of the four.) This order is not in agreement with the experimental order of $W_2 > W_4 > W_3$ (see Figure 3.3). The assumption of pure $j - j$ coupling made above in deriving the 'theoretical' order of intensities is only a first approximation, as was pointed out in the discussion of the magnetic properties of K_2OsCl_6. A closer approach to the truth is given by the intermediate coupling scheme of Griffith. Whilst in pure $j - j$ coupling there are no spin selection rules as such, since S is no longer a good quantum number, in the intermediate coupling scheme S still retains some meaning. It is probable that it is not a very good quantum number but it may have some descriptive purpose. In these circumstances W_1 and W_2 are transitions within the split levels of the $^3T_{1g}$ term and can be described as spin-allowed transitions, whilst W_3 and W_4 correspond to transitions to singlet states and are spin-forbidden. The observed order of intensities is then described in the following fashion: W_2 is the most intense band because, to a first approximation, it is a spin-allowed transition. W_4 is moderately intense because, although it is of the spin-forbidden variety, it is located close to a charge-transfer band and could possibly

gain intensity by an intensity-stealing mechanism. Finally, W_3 is weak because it is spin-forbidden and located too far away from the charge-transfer band to gain intensity.

There seems little doubt, therefore, that the species in concentrated solutions of Na_2OsCl_6 in the LiCl - KCl eutectic is the octahedral $OsCl_6^{2-}$ entity. The spectrum has not been completely interpreted, however, since the origin of the effect which splits W_3 into two bands has not been examined.

Turning now to the time dependent spectra shown in Figure 3.4, it can be seen that the initial spectrum is more or less identical to the spectrum of the concentrated solution shown in Figure 3.3. This may seem surprising when it is recalled that one solution is lime-green whilst the other is red-brown, and both apparently contain the $OsCl_6^{2-}$ entity. This type of effect has been observed before for $OsCl_6^{2-}$. Thus Jørgensen reported that whilst $OsCl_6^{2-}$ is yellow in solution, the potassium and ammonium salts are deep red, the caesium salt orange, the thallous salt olive-green, and the silver salt brown. The reflectance spectra of these salts showed that the colour effects were caused by broadening and shifting of the charge-transfer bands and were explained in terms of changes in the lattice parameters caused by the different cations (68, 69). This effect has also been observed in dilute aqueous solutions of Na_2OsCl_6 with added lithium, potassium, ammonium and barium chlorides. The qualitative results of adding an excess of the above-mentioned chlorides to a dilute solution of Na_2OsCl_6 are reported in Table 3.7.

Table 3.7

Cation effects on the colour of $OsCl_6^{2-}$ solutions

LiCl	yellow - green
KCl	red
CsCl	olive ppt formed
NH_4Cl	red
$BaCl_2$	yellow

These results can only be explained if it is assumed that in solution the added cation is having an effect on the $OsCl_6^{2-}$ entity, i.e. some form of ion pair is present in solution. The results for the LiCl - KCl eutectic melt can be explained along the same lines. In concentrated solutions the nearest cation is sodium or potassium, thereby giving a red colour. When the concentration of Na_2OsCl_6 (or Na^+) is reduced by dilution, the species in the second coordination shell is replaced by lithium, giving rise to the lime-green colour.

The identity of the species giving rise to spectra 2 and 3 in Figure 3.4 will now be examined. When a concentrated solution of Na_2OsCl_6 in the LiCl - KCl eutectic melt maintained at 450°C was subjected to a continuous vacuum over a period of ~ 12 hours, a black deposit was formed in the cooler portion of the tube. Just above the level of the melt a silvery-grey metallic film was also observed when the cell was cooled and the eutectic dissolved out. The black deposit was found to dissolve in water and gave a positive test for chloride. Furthermore, if the cell was maintained at 450°C when open to the atmosphere, chlorine gas could be detected. These results are rationalised in the following fashion. Griffith (51) reports that

$OsCl_3$ is a dark grey powder which can be formed by the thermal decomposition of $OsCl_4$ at temperatures above 350°C. The trichloride decomposes above 450°C to the metal and chlorine. The suggested mechanism is therefore:

$$Na_2OsCl_6 \longrightarrow OsCl_4 \longrightarrow OsCl_3 \longrightarrow Os + Cl_2$$

Since the LiCl - KCl melt was at 450°C, it is likely that some or all of the decomposition occurs in solution and, therefore, Os(III) might be expected to occur in the melt perhaps as the $OsCl_6^{3-}$ moiety.

Griffith (51) also reports that $OsCl_3$ is insoluble in water. However, for the rarer platinium metals both water soluble and water insoluble trichlorides are well known, e.g. $RuCl_3$, $IrCl_3$, $RhCl_3$.

The spectrum of an aqueous solution of $OsCl_6^{3-}$, produced by reduction of $OsCl_6^{2-}$ with silver powder, has been reported by Jørgensen (53). In the visible region there are bands at 17.7 and 22.4 kK and the charge-transfer bands begin at ~ 30 kK. Spectra 3 and 4 of Figure 3.4 both contain a shoulder at ~ 24 kK, together with a very small band at 17.3 kK. However, as Table 3.2 shows, the spectrum of $OsCl_6^{2-}$ also contains bands in the same region, the difference being the intensities - the band at 22.24 kK for Os(III) has $\varepsilon = 40$, whilst for Os (IV) it has $\varepsilon = 1220$. With this intensity data, plus the positions of the charge-transfer bands, spectra 3 and 4 can be shown to be due to the Os (IV) species by the following argument. Since there are relatively strong bands present at 28 and 34 kK, the Os(III) species is unlikely to be present. Furthermore, the ratio of band intensities for the bands at 24 and 28 kK is approximately 25:45 (using optical densities from spectrum 4), whilst for the reported Os(III) spectrum the ratio for the

bands at 22 and ~ 35 kK is 40:2000. It can be concluded, therefore, that spectra 1, 2, 3 and 4 are due to the octahedral $OsCl_6^{2-}$ species. The fact that spectra 1 and 4 look different is the result of two factors. Firstly, difficulties were experienced in determining the osmium concentration and even rough values of the extinction coefficients were not obtained. Because the spectra reported in Figure 3.4 were obtained for a solution from which $OsCl_3$ was being distilled off, the osmium concentration in the melt decreased in the order 1 to 5 and, therefore, the relative intensities between the different spectra are not comparable. However, the relative band intensities within one particular spectrum can be compared. Secondly, the lowered osmium concentration allows better resolution of spectral bands and explains the appearance of the shoulder at 24 kK in spectra 3 and 4.

Spectrum 5 has a pronounced peak at 15 kK and a smaller band at 17.2 kK with no detectable peaks at higher energies. The lowered osmium concentration present in this solution might result in very weak bands being missed. Certainly, the solution appeared virtually colourless. The species producing this spectrum cannot, with the data at present available, be identified. It is interesting to note that Griffith (51) refers to work published in 1863 where it is suggested that a violet-blue solution of $OsCl_6^{4-}$ may be obtained by the reduction of $OsCl_6^{3-}$. The spectrum of this Os (II) solution has not been reported in the literature but, by virtue of its colour, would be expected to have absorption bands in the red region of the spectrum. Positive identification of the species giving rise to spectrum 5 must await further study. In order to study it in any detail, a better preparative procedure must be found. It is very important that concentrated solutions be used in such a study. Such solutions

could probably be obtained by electrochemical reduction.

3.4 Experimental. The preparation of the LiCl - KCl eutectic melt is reported in Appendix C together with the details of recording spectra at elevated temperatures. The salt Na_2OsCl_6 was obtained from Johnson, Matthey and was used without further purification although it was dried at 120°C for two days before addition to the melt.

The ruthenium trichloride obtained from Johnson, Matthey was the hydrated form and on drying at 120°C gave a black solid. Addition of this solid to the LiCl - KCl eutectic melt resulted in chlorine evolution. Griffith (51) reports that commercial hydrated $RuCl_3$ often contains Ru (IV) species, in which case the chlorine evolution observed can be rationalised:

$$2Ru^{4+} + 2Cl^- \longrightarrow 2Ru^{3+} + Cl_2$$

A sample of anhydrous $RuCl_3$ obtained from Alfa Inorganics was, therefore, used to prepare the solutions for spectral work.

CHAPTER IV

SPECTRA OF Co(II) IN AQUEOUS AND FUSED SULPHATE MEDIA

4.1 Introduction. Investigations of the stereochemistry of Co(II) compounds have shown that in a large number of cases the metal atom is surrounded by either four ligands arranged tetrahedrally or six arranged octahedrally. The tetrahedral complexes are usually blue, whilst the octahedral ones are pink. The criterion of colour, however, cannot be used to determine stereochemistry since quite a few exceptions to the above general statement are known, e.g. Co SiO_4 is blue and octahedral and Co dipivaloylmethanide is pink and tetrahedral (70). Whilst tetrahedral and octahedral ligand arrangements are the most common, by a suitable choice of ligand other symmetries and coordination numbers are possible. This may be illustrated by the examples shown in Table 4.1.

Table 4.1

Some Coordination Geometries for Co(II) Complexes

Compound	Coordination Number	Stereochemistry	Reference
Co phthalocyanine	4	Square planar	71
Co(trenMe)X	5	Trigonal bipyramid	72
$Co(NO)(S_2CNMe_2)_2$	5	Square pyramid	73

(trenMe = tris (2 dimethylaminoethyl) amine)

A recent review of the stereochemistry of Co(II) compounds has been published by Carlin (70).

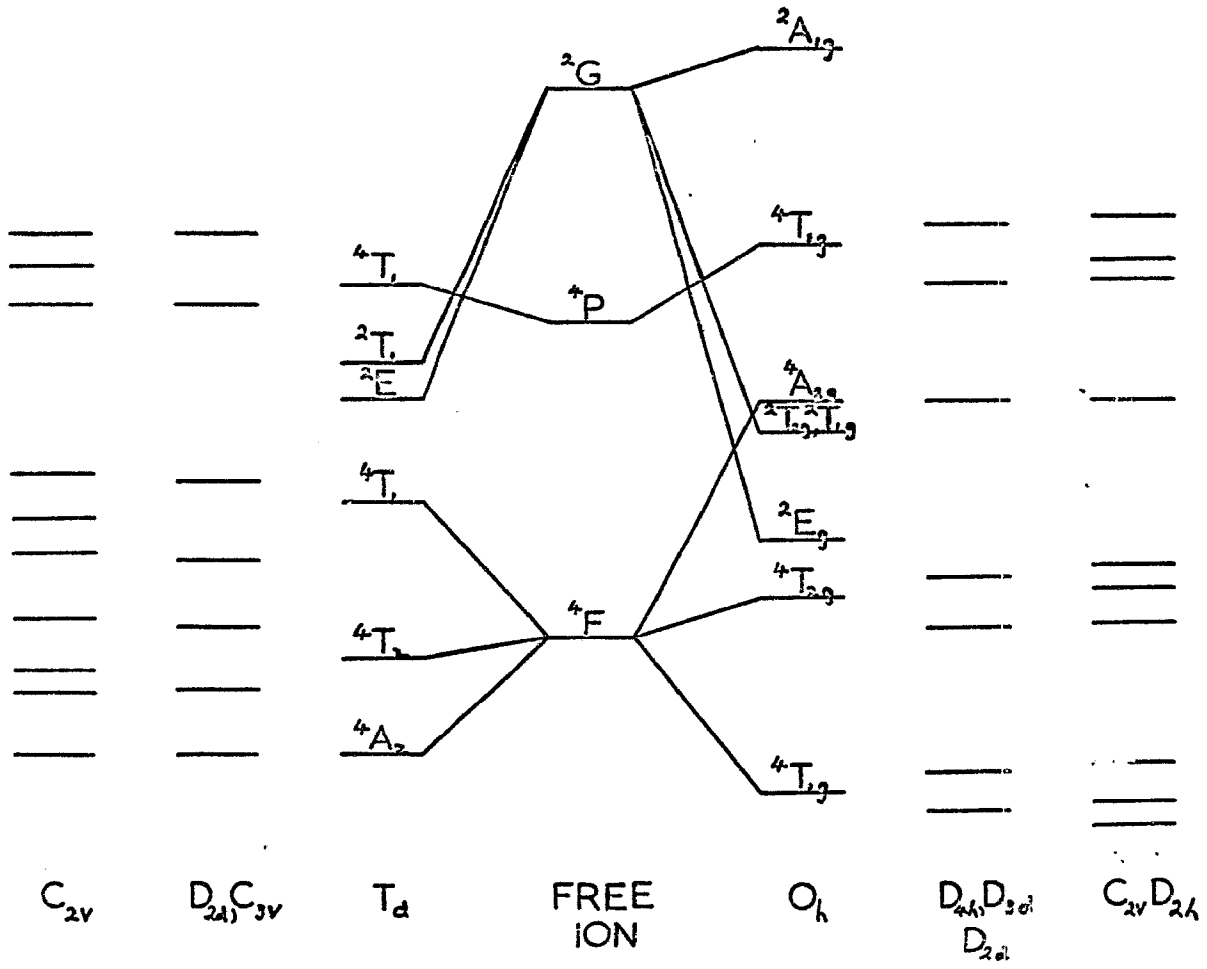

Figure 4.1

Energy level diagrams for cubic and distorted cubic Co(II) compounds

4.2 Spectral Assignments. The Co(II) ion has a d^7 electron configuration which, on applying the Russell-Saunders coupling scheme, gives rise to the following terms in order of increasing energy: ^4F, ^4P, ^2G, ^2P, ^2H, ^2D, ^2F. The ^4P state lies approximately 15 kK above the ^4F ground state in the free ion. When the Co(II) ion is incorporated into a complex, all these states, with the exception of the P states in cubic symmetry, are split. The symmetry of the ligand field determines the size of the splitting, the number of levels, and also the relative ordering of these levels. For the tetrahedral (T_d) and octahedral (O_h) cases, the splitting is as shown in Figure 4.1. Although low-spin octahedral complexes of Co(II), which have a ^2E_g ground state are known, these are not considered here since the complexes of interest have relatively small ligand field splittings and are, therefore, of the high-spin variety.

The spectral assignments for tetrahedral and octahedral complexes will now be considered in some detail. Following this, a discussion of the effects of lower symmetry ligand fields on the octahedral and tetrahedral levels is presented.

4.2.1 Tetrahedral Symmetry. Using Figure 4.1, it would be predicted that the spectrum of tetrahedral Co(II) complexes should contain three relatively strong bands corresponding to transitions from the quartet ground state to the three excited quartet states. Such a spectrum has, in fact, been observed. The three bands are normally found in the 3 - 5 kK, 6 - 8 kK, and 12 - 17 kK regions of the spectrum (74). There are two reasons why the position of the first band has not always been reported in the literature (74, 75). Firstly, the band is located on the edge of, or actually within, the conventional infra-red. Secondly, although the band is due to a spin-allowed transition, it is electric-dipole-forbidden and thus appears in the spectrum as a weak band.

It has been observed that the bands in the spectrum are not single bands but consist of several components. These components may be explained in terms of either low symmetry ligand fields splitting the various levels, or of spin-orbital coupling, or a combination of the two. Ferguson (76), in a detailed study of the spectrum of Cs_2ZnCl_4 doped with cobalt, concluded that the principal effect causing the width and structure of the band in the near infra-red was, in fact, due to low symmetry fields. Although the assumption of tetrahedral symmetry was satisfactory in explaining the overall position of the band, it could not account for the fine details which were observed on cooling the crystal, even with the inclusion of spin-orbital coupling effects.

Ferguson's conclusions were confirmed by Pappalardo et al. (77) who showed that the experimental band width was always greater than the band width calculated assuming spin-orbital coupling. Indeed, Lever and Nelson (78) explained the large band width and three components of the near infra-red band in the spectra of pseudo-tetrahedral $Co(amine)_2X_2$ complexes as arising principally from the low (C_{2v}) symmetry rather than from spin-orbital coupling effects.

With regard to the band in the visible region, a further complication arises in that there is a doublet level very close to the ^4P level and these two levels may intermix. This would result in the transition from the ground state to this particular doublet level gaining intensity. The highest energy component of the visible band is normally attributed to this transition.

Expressions for the energies of the quartet-quartet transitions have been derived by Cotton et al. (75) from the energy matrices obtained by Tanabe and Sugano (16). These are as follows:

$$
\begin{aligned}
{}^4T_2(F) &\longleftarrow {}^4A_2(F) && \Delta && \nu_1 \\
{}^4T_1(F) &\longleftarrow {}^4A_2(F) && 1.5\,\Delta + 7.5B - Q, && \nu_2 \qquad 4.1 \\
{}^4T_1(P) &\longleftarrow {}^4A_2(F) && 1.5\,\Delta + 7.5B + Q, && \nu_3
\end{aligned}
$$

Where $Q = 1/2(225B^2 - 18B\Delta + \Delta^2)^{1/2}$

Thus if the bands in the near infra-red and visible regions are obtained, values of Δ and B may be calculated.

To summarize, it can be said that the absorption spectra of tetrahedral Co(II) complexes consist of three band systems which are split due to symmetry distortions and spin-orbital coupling effects in the two lowest energy bands. The highest energy band shows splitting due to these effects and also due to intermixing with a nearby doublet state.

4.2.2 Octahedral Symmetry. As in the tetrahedral case, three relatively strong bands in the absorption spectra of octahedral Co(II) complexes, corresponding to the quartet-quartet transitions, would be expected. In actual practice only two separate band systems are found, the first in the 6 - 8 kK, and the second in the 18 - 20 kK regions. The second band system contains at least two relatively strong bands together with some weaker components. It is this band system which has been the subject of much discussion with regard to assignment. The most obvious assignment is that quoted by Figgis (25) and Phillips and Williams (79), who assign the two strong components to the transitions:

$$
\begin{aligned}
{}^4A_{2g}(F) &\longleftarrow {}^4T_{1g}(F) \\
{}^4T_{1g}(P) &\longleftarrow {}^4T_{1g}(F)
\end{aligned}
$$

This assignment has been questioned since for the aqueous Co(II) system, for example, the first transition would be more intense than the second. However, since the

$^4A_{2g}(F) \leftarrow {}^4T_{1g}(F)$ transition corresponds to a two electron transition, it should have a lower intensity than the one electron transition $^4T_{1g}(P) \leftarrow {}^4T_{1g}(F)$. Indeed, Koide (80) has reported a semi-empirical calculation of the intensity of this two electron transition and obtained a value of the oscillator strength of 4.8×10^{-6}. This is the order of magnitude which spin-forbidden transitions are expected to have and it would, therefore, give rise to a weak band in the spectrum. Such a band is often observed at the low energy foot of the 18 - 20 kK band system and it is now generally agreed that this band is due to the $^4A_{2g}(F) \leftarrow {}^4T_{1g}(F)$ transition. Lever and Ogden (81), however, have questioned the automatic assignment of a weak band at the foot of the visible band to this transition and they have shown, by considering the energy expressions for the various transitions, (see later), that the ratio of ν_1/ν_2 should lie between 2.1 and 2.2 for all reasonable values of Δ and B. (ν_1 is the frequency corresponding to the $^4T_{2g}(F) \leftarrow {}^4T_{1g}(F)$ transition, and ν_2 corresponds to the $^4A_{2g}(F) \leftarrow {}^4T_{1g}(F)$ transition.) These authors state that ν_2 should not be greater than $2.2\,\nu_1$ but that due to the limitations of the theory it may be slightly less than $2\,\nu_1$. Thus, by using the result of Koide's calculation and the criterion of Lever and Ogden, the assignment of the $^4A_{2g}(F) \leftarrow {}^4T_{1g}(F)$ transition is fairly satisfactory.

Alternative assignments must now be considered in order to explain the two strong components of the visible band. Whilst one of the components must be due to the $^4T_{1g}(P) \leftarrow {}^4T_{1g}(F)$ transition, there have been several suggestions put forward to explain the presence of a second component. Among those which have been considered are the following:

(i) Presence of vibrational structure.

(ii) Spin-orbital coupling.

(iii) Presence of a spin-forbidden band.

(iv) Distortion from octahedral symmetry.

(i) Vibrational Structure Although the transitions under consideration are between electronic levels, excitation of vibrational modes also takes place and, in fact, accounts for the band widths of the electronic transitions. Vibrational structure is rarely resolved at room temperature but is sometimes observed in crystal spectra recorded at low temperatures. It normally occurs as a fine structure on the spectral bands and it is highly unlikely that the two bands in question are due to this effect.

(ii) Spin-Orbital Coupling This effect has been considered in some detail by both Koide (80) and Pappalardo et al. (77). They have shown that the magnitude of the spin-orbital splitting should be of the order of 0.6 kK. Since the observed splitting is of the order of 1.8 - 2.0 kK, it would appear that spin-orbital coupling is not the principal effect.

(iii) Spin-Forbidden Transitions It has been suggested by several workers that the high energy shoulder is due to a transition to a doublet state. As in the tetrahedral case, this spin-forbidden transition gains intensity by mixing with the $^4T_{1g}(P) \longleftarrow {}^4T_{1g}(F)$ transition. The situation is rather confused since the various authors do not assign the transition to the same doublet state. Thus, Low (82) assigned the high energy component which occurred at 20.5 kK in the spectrum of Co(II) in MgO to the transition $^2T_{1g}(P) \longleftarrow {}^4T_{1g}(F)$, whilst Hatfield et al. (83)

assigned the same component in the $Co(H_2O)_6^{2+}$ spectrum to transitions to the $^2T_{2g}$ and the $^2T_{1g}$ states, which may have the same energy, arising from the ^2G free ion state.

(iv) Symmetry Lowering The effect of lowering the symmetry from octahedral does not explain the presence of the two components. This is shown by the fact that the crystal spectrum of $Co(ClO_4)_2 \cdot 6H_2O$ is identical to that of Co(II) in aqueous solution (84), whilst West (85) has shown that in this particular crystal the Co is surrounded by a regular octahedral arrangement of water molecules. Furthermore, Low (82) has shown by ESR measurements that the CoO_6 system in MgO is accurately cubic, whilst the visible band still contains two strong components.

In summary then, it can be said that the first strong band in the near infra-red arises from the $^4T_{2g}(F) \longleftarrow {}^4T_{1g}(F)$ transition. The weak band at the low energy foot of the main visible band is, always remembering the Lever and Ogden criterion, due to the $^4A_{2g}(F) \longleftarrow {}^4T_{1g}(F)$ transition. The strongest component of this main band is assigned to the $^4T_{1g}(P) \longleftarrow {}^4T_{1g}(F)$ transition. Whilst the assignment of the high energy shoulder is still ambiguous, a spin-forbidden transition is probably the most favoured explanation.

Papparlardo et al. (77) have tabulated the expressions for the energies of the quartet-quartet transitions derived in the same manner as for the tetrahedral case. These are as follows:

4.2

$^4T_{2g}(F) \longleftarrow {}^4T_{1g}(F)$	$1/2(\Delta - 15B + Q)$,	ν_1
$^4A_{2g}(F) \longleftarrow {}^4T_{1g}(F)$	$1/2(3\Delta - 15B + Q)$,	ν_2
$^4T_{1g}(P) \longleftarrow {}^4T_{1g}(F)$	Q,	ν_3

Where $Q = (225B^2 + 18B\Delta + \Delta^2)^{1/2}$

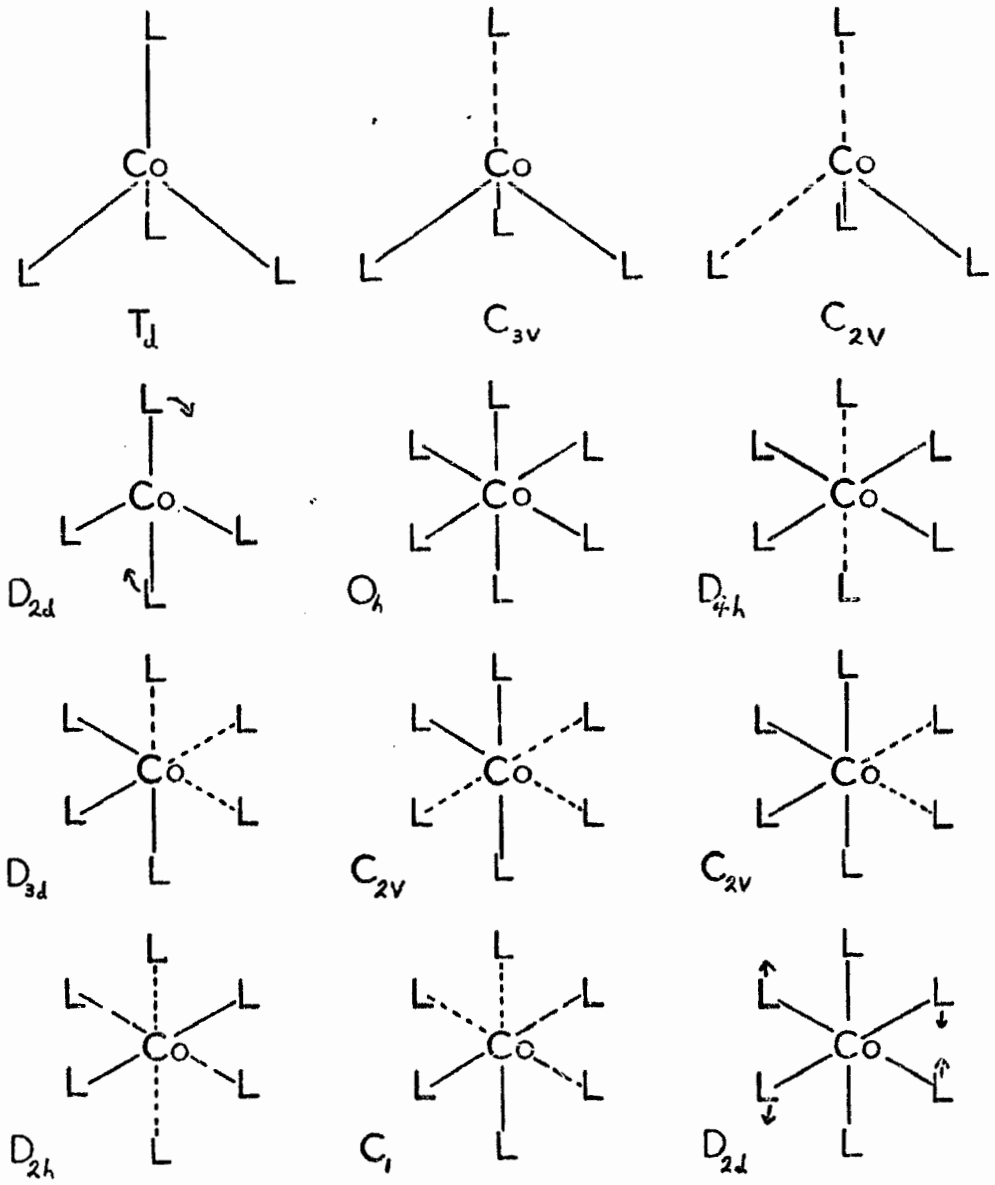

Figure 4.2

Some distortions for cubic Co(II) compounds

4.2.3 Distortions From Cubic Symmetry Even in the case where all the ligands are identical, the complex need not remain regularly octahedral or tetrahedral. The reasons for this are not well understood. Certainly in the crystals, whether single crystals of a cobalt complex or a host crystal doped with cobalt, the cobalt species may be forced to adopt a lower symmetry than cubic. In solutions, however, the factors are much less clearly understood although in molten salts, viewed on the quasi-crystalline model, it may be that the actual structure of the melt itself causes the distortions.

In this section then, various distortions and their effects on the parent energy levels will be considered. It would obviously be futile to attempt to discuss all possible distortions from both octahedral and tetrahedral parent symmetries, and so the choice has been restricted to those distortions which may be useful in explaining the experimental results.

Tetrahedral Parent Symmetry. The most feasible distortions from tetrahedral symmetry are shown in Figure 4.2. Although these distortions have all been obtained by essentially stretching bonds, other distortions may be possible. The effects of these distortions on the tetrahedral energy levels are shown in Figure 4.1. Note that the direction of the splitting need not be the same as shown here. It is not possible to specify unequivocally the direction of the splitting from simple symmetry principles. Only the effects on the quartet levels have been considered since these would be the most easily observed.

Octahedral Parent Symmetry. The symmetry species obtained from the octahedron by bond stretching, except for the case of D_{2d} which involved twisting as well, are shown in Figure 4.2. Figure 4.1 contains the effects of such distortions on the octahedral energy levels.

For both the tetrahedral and octahedral cases, the splittings of the parent energy states were obtained from the correlation tables of Wilson, Decius and Cross (20).

4.3 Previous Work. The spectrum of cobalt sulphate dissolved in a Li_2SO_4 - Na_2SO_4 - K_2SO_4 eutectic melt and recorded at 550° C has been reported by Johnson and Piper (87). The spectrum, which consisted of a single band system centred at ~17 kK, was interpreted in favour of a distorted tetrahedral arrangement of ligands about the Co(II) by virtue of the band shape and intensity. The interpretation has been criticised by Gruen (6) principally on the grounds that the extinction coefficient was too low for tetrahedral Co(II). It was decided that a detailed re-investigation of the spectrum of Co(II) in the Li_2SO_4 - Na_2SO_4 - K_2SO_4 eutectic melt was necessary, and in particular, a more careful look at the near infra-red region where bands for both octahedral and tetrahedral Co(II) complexes are expected.

A classic approach to the interpretation of melt spectra was adopted in which the melt spectrum was compared with appropriate solution spectra, and also with spectra of crystalline sulphato-complexes of Co(II) of known structure where possible. A search of the literature revealed that Arris and Duffy (88) had reported the spectrum of Co(II) dissolved in concentrated sulphuric acid and recorded at room temperature. On comparing this spectrum with the aqueous spectrum of Co(II) they found that the position, shape and intensity of the absorption bands were very similar. In view of the fact that the spectra of Co(II) salts dissolved in aqueous solution were independent of the salt used (84), over a cobalt concentration of 10^{-3} - 1M, it was suggested that the spectra were due to the presence of a common Co(II) species. This was shown to be the $Co(H_2O)_6^{2+}$ complex by comparison with the spectrum of

$Co(ClO_4)_2 \cdot 6H_2O$ as discussed earlier. Arris and Duffy, therefore, concluded that the Co(II) species in concentrated sulphuric acid was octahedral but they were unable to specify the nature of the ligands. During the course of the present investigation, Duffy et al. (89) reported further work designed to determine the nature of this species. This work involved the use of both hydrogen sulphate and sulphate melts and will be discussed in detail at a later stage.

In the preliminary experimental work it was observed that on heating a solution of Co(II) in concentrated sulphuric acid a definite change in colour from lilac, at room temperature, to blue, at 200°C, was observed. In the light of work reported by Scaife and Wood (90), for a Co(II) system, where they observed a similar change in colour and were able to correlate it with an octahedral-tetrahedral equilibrium, it was decided to investigate the spectra of the sulphuric acid solution as a function of temperature. In this context, Swift and Connick (91) reported that at 94.5°C the spectrum of aqueous solutions containing Co(II) was due to a mixture of octahedral $Co(H_2O)_6^{2+}$ and tetrahedral $Co(H_2O)_4^{2+}$. Since it was felt that the experimental method for determining the presence of $Co(H_2O)_4^{2+}$, which consisted of subtracting the room temperature spectrum from the spectrum at 94.5°C, completely neglected the effect of temperature on intensity, an experimental investigation of this effect was included.

The aqueous and sulphuric acid results are considered first since more is known about the solution spectra and also the results for the sulphuric acid are required as a basis for examining the sulphate melt spectrum.

TABLE 4.2

Band positions and extinction coefficients for the spectra of Co(II) in aqueous sulphuric acid solutions.

Solution	ν_1(kK)	ε_1	ν_2	ε_2	ν_3	ε_3	ν_4	ε_4	ν_5	ε_5
Water (1)	8.0	1.52	16.36	0.34	19.11	3.84	20.96	3.02	23.58	0.39
Water (2)	-	-	15.79	0.39	19.23	3.74	20.98	2.92	23.58	0.50
25% H_2SO_4	7.9	1.62	16.04	0.33	19.00	3.73	20.85	3.18	23.68	0.45
50% H_2SO_4	7.6	1.76	15.10	0.34	18.97	5.73	21.08	3.56	24.17	0.44
75% H_2SO_4 (1)	6.8	3.64	12.69	0.64	18.37	8.28	20.51	3.71	23.33	0.39
75% H_2SO_4 (2)	6.8	3.16	13.25	0.47	18.28	8.68	20.41	3.62	23.51	0.47
98% H_2SO_4	6.8	1.3	12.54	0.52	17.84	8.22	19.55	4.57	25.85	0.87

TABLE 4.3

Oscillator strengths for the spectra of Co(II) in acqueous sulphuric acid solutions.

Solution	f_1	f_2	f_3	f_4	f_5
Water (1)	0.92×10^{-5}	7.85×10^{-6}	3.7×10^{-5}	3.76×10^{-5}	6.1×10^{-6}
Water (2)	-	8.56	3.56	3.74	13.5
25% H_2SO_4	1.91	6.10	3.57	4.28	11.9
50% H_2SO_4	2.24	6.10	6.22	4.27	5.53
75% H_2SO_4 (1)	2.65	9.57	9.10	4.18	7.75
75% H_2SO_4 (2)	1.83	7.28	9.75	4.19	10.50
98% H_2SO_4	1.17	8.92	8.80	6.60	-

TABLE 4.4

Ligand field parameters for the spectra of Co(II) in aqueous sulphuric acid solutions.

Solution	Δ(kK)	B(cm^{-1})	β	Pred. position of ν_1(kK)
Water (1)	8.73	836	0.86	7.63
Water (2)	8.43	856	0.88	7.36
25% H_2SO_4	8.56	839	0.865	7.48
50% H_2SO_4	8.08	866	0.89	7.02
75% H_2SO_4 (1)	6.81	896	0.925	5.87
75% H_2SO_4 (2)	7.11	874	0.90	6.14
98% H_2SO_4	6.75	866	0.89	5.80

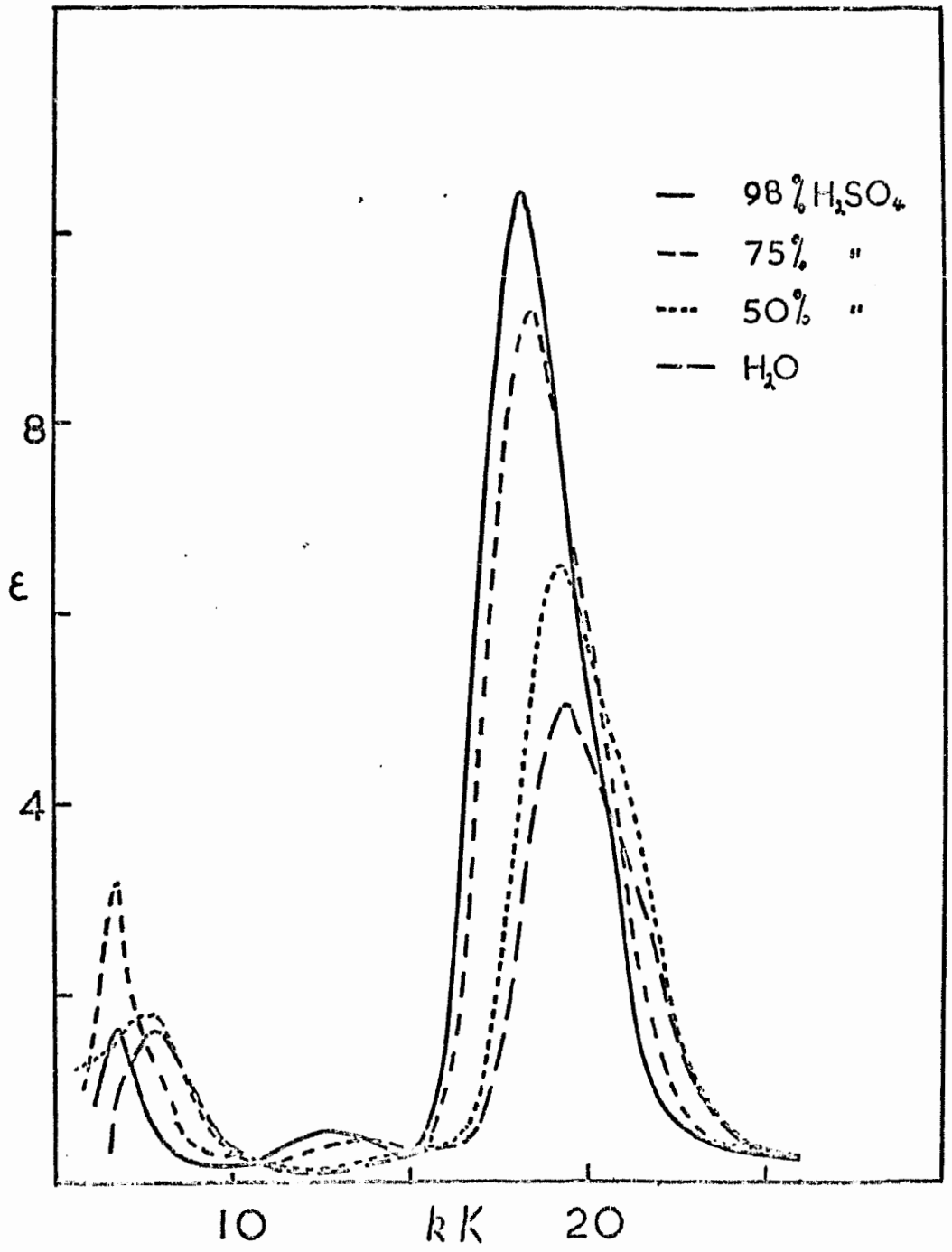

Figure 4.3

Spectra of Co(II) in aqueous and sulphuric acid solutions

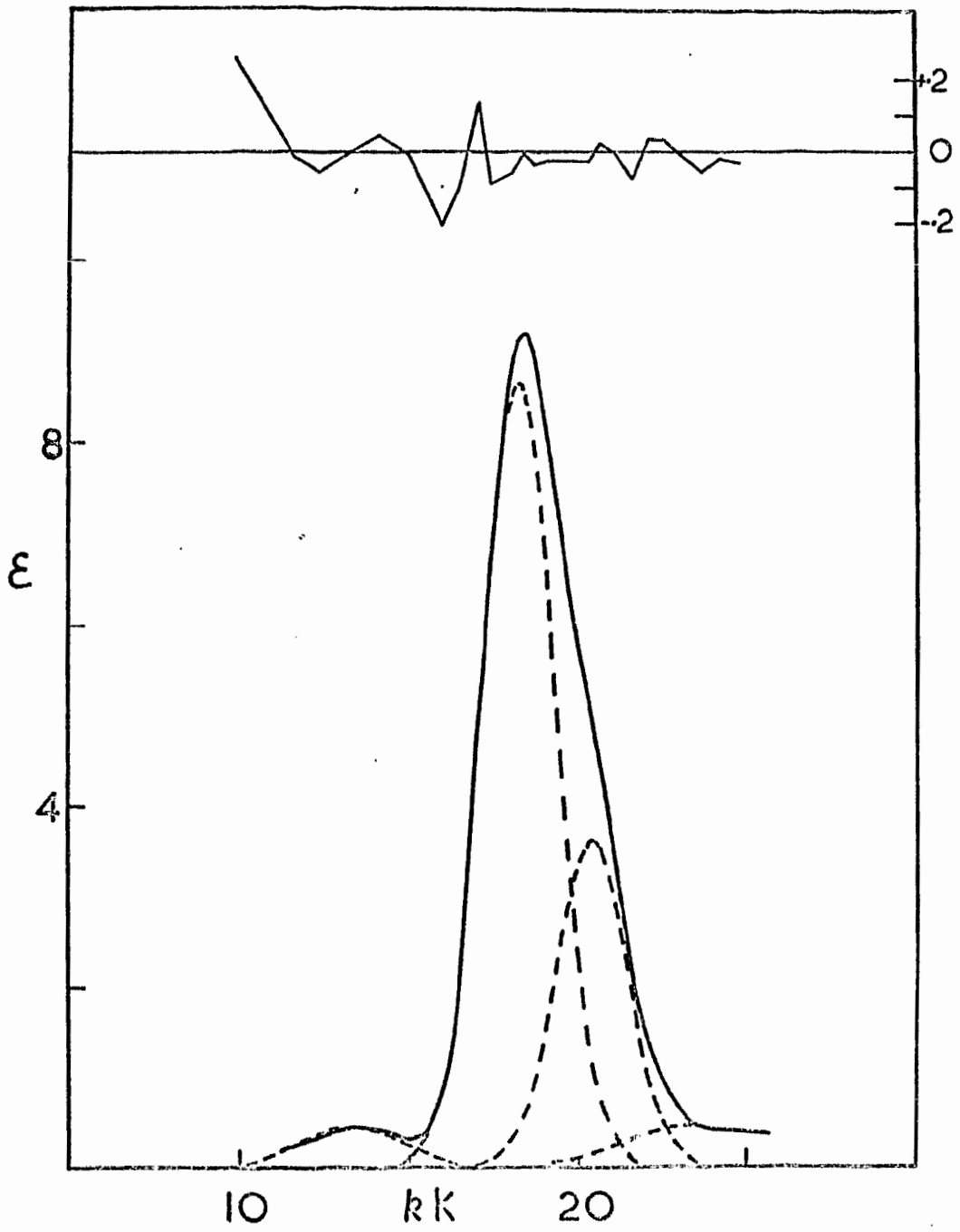

Figure 4.4

Gaussian analysed spectrum of Co(II) in 75% H_2SO_4 solution

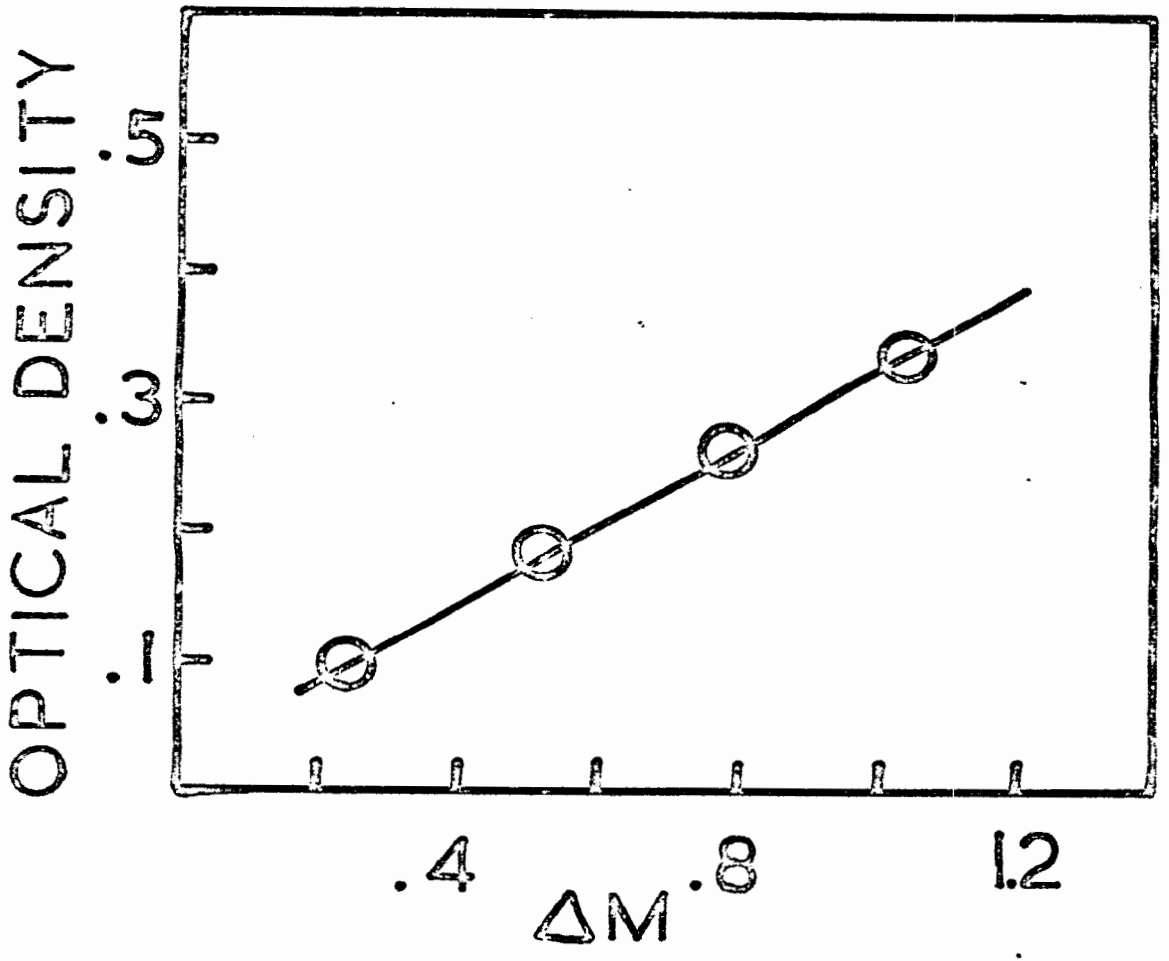

Figure 4.5

Graph of optical density as a function of water-content for a 75% H_2SO_4 solution measured at 1435 mμ. (Δ M is the difference in sulphate molarity between reference and sample solutions.)

4.4 Present Work.

4.4.1 Co(II) In Aqueous And Sulphuric Acid Solutions The spectra of Co(II) in aqueous solution and in solutions of 50%, 75% and 98% sulphuric acid are shown in Figure 4.3. Each spectrum was analysed into Gaussian components using a computer programme which was based on the procedure of Chatt et al. (92). (See Appendix A for details.) An example of such an analysis is shown in Figure 4.4 for the spectrum in 75% H_2SO_4 solution. The figure includes the residual, which is the difference between the experimental curve and the sum of the Gaussian components. The full results of the Gaussian analyses are collected in Tables 4.2 and 4.3 where the maxima, extinction coefficients and oscillator strengths are given. The assignments chosen are in line with the previous discussion. The bands represented by ν_4 and ν_5 are believed to be due to spin-forbidden transitions, the ν_4 being more intense because of 'intensity stealing' from ν_3. Using these assignments, values of Δ, the ligand field splitting parameter, B, the Racah parameter, and β, the ratio of the value of B in the complex to that in the free ion, were calculated and are presented in Table 4.4. Δ and B were found using the expressions for ν_2 and ν_3, (equation 4.2), and then the position of ν_1 was calculated. This particular procedure was chosen because the position of ν_1 was not very easy to determine from the spectra, particularly when the solution had a high sulphuric acid concentration. The reason for this is that in the region of the spectrum where ν_1 occurs, 6 - 8 kK, overtones of the O - H stretching vibration occur. This does not cause much difficulty when the water concentration is very high since the difference between the reference and the sample solutions is not very large. At lower water concentrations, however, these effects

become much more noticeable and, despite the fact that care was taken to ensure that the water content in both reference and sample solutions was identical, overtone bands were obtained. These bands were found to occur at 10.15, 8.45 and 6.97 kK. In order to confirm that these bands were, in fact, due to water, the behaviour of the band at 6.97 kK was investigated as a function of water concentration. The reference solution used was 75% sulphuric acid, and the sample solution was the same solution with varying amounts of water added. Figure 4.5 shows a plot of optical density versus the difference in acid molarity between the reference and sample solutions. The straight line relationship confirms that the band was due to the presence of water.

It has been shown earlier, (p. 84), that the spectrum of Co(II) in aqueous solutions is due to the octahedral $Co(H_2O)_6^{2+}$ ion. It is evident from Figure 4.3 that as the solution changes from water to 98% sulphuric acid, the species retains basically the same symmetry. There is an increase in intensity and a bathochromic shift of the bands but these are almost certainly due to a change in the coordinating species from H_2O to HSO_4^- or H_2SO_4. Since the band positions depend on Δ and B, this shift indicates that these are decreasing also. In point of fact, as Table 4.4 shows, B does not change appreciably but the main effect is incorporated in changes in Δ.

The effect of temperature on the spectrum of Co(II) in aqueous solution is shown in Figure 4.6. The variation in the oscillator strength is shown in Table 4.5 and depicted in Figure 4.7.

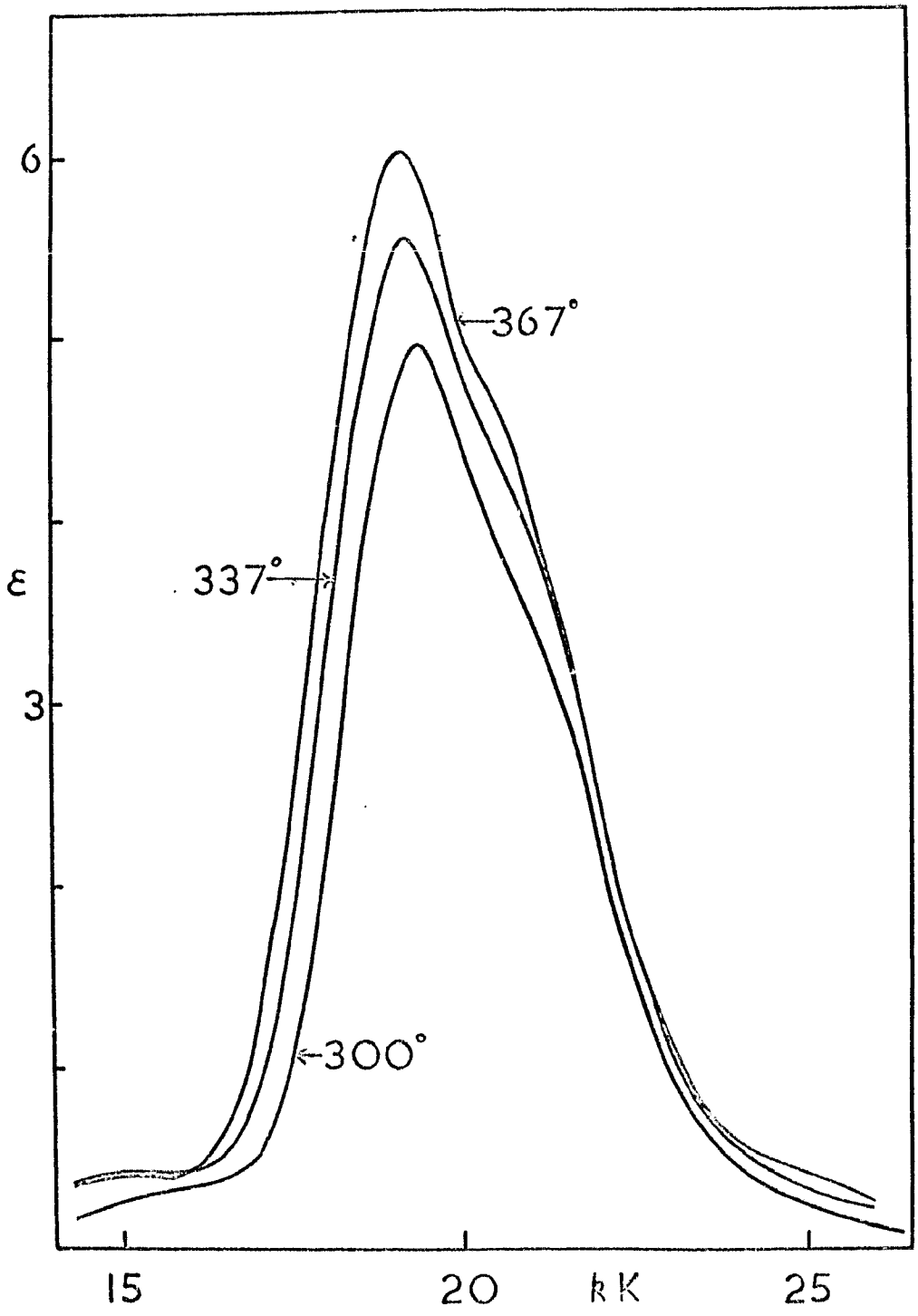

Figure 4.6

Spectra of Co(II) in aqueous solution as a function of temperature

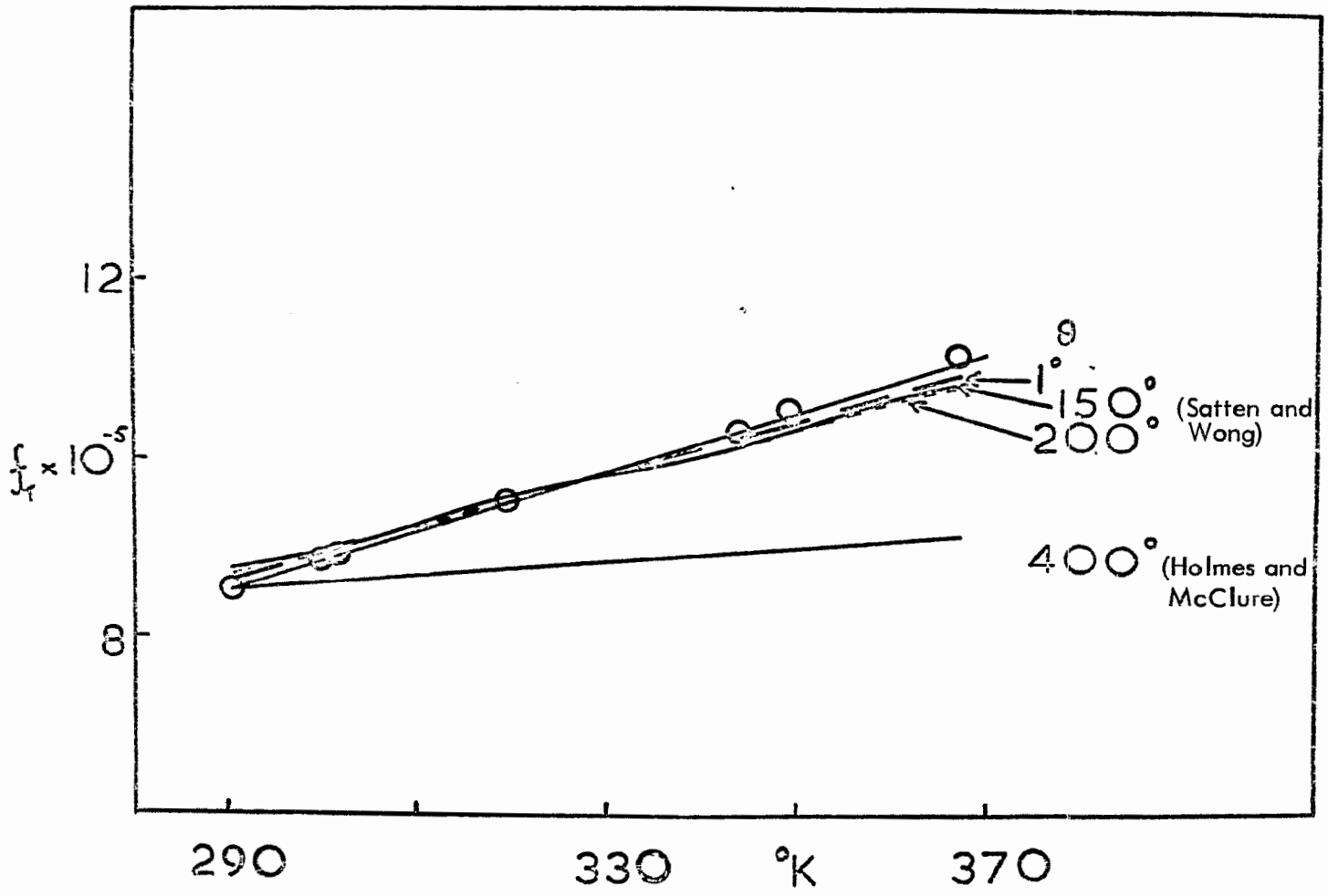

Figure 4.7

Temperature dependence of the oscillator strength for Co(II) in aqueous solutions

Table 4.5

Temperature dependence of the oscillator strength for Co(II) in H_2O

Temperature °K	$f_T \times 10^5$
290	8.55
290.4	8.62
290.5	8.64
300	8.87
302	8.90
304	8.99
319	9.54
320	9.38
337	9.95
344	10.32
349	10.57
367	11.17

From Figure 4.6 it seems apparent that the Co species in aqueous solution, which has been shown to be $Co(H_2O)_6^{2+}$ (p. 84) at room temperature, retains the same shape as the temperature increases, i.e. the spectral differences can be explained in terms of the effect of temperature on the oscillator strength. Certainly, if the results of Scaife and Wood (90) in which they studied a temperature dependent equilibrium between $[CoCl_2 \cdot 4MeOH]$ and $[CoCl_3 \cdot MeOH]^-$, can be regarded as a norm for this type of behaviour, then the aqueous spectra cannot be

explained on this basis. The reason for this is that these authors reported spectra in which the intensity of the visible band due to the octahedral species decreased and a new band at lower energy rapidly gained intensity as the temperature was raised. No such effects are obtained for the aqueous system.

An attempt to fit the experimental results to the various models used for the temperature dependence of intensities, as discussed in Chapter II, was made. Both the formula of Holmes and McClure (36),

$$f_T = f_o(1 + e^{-\Theta}/T) \qquad 2.3$$

and that of Satten and Wong (49),

$$f_T = f_o \coth(\Theta/2T) \qquad 2.4$$

were applied.

In using the Holmes and McClure equation the results were fitted at the lowest experimental temperature for a series of values of Θ. The best fit was obtained for $\Theta = 400^{\circ}K$ and is shown in Figure 4.7. The Satten and Wong expression was fitted over the entire range of temperatures for which measurements were made, again using a series of values of Θ. For this expression it was found that the fit was not very dependent on the actual value of Θ. This is illustrated in Figure 4.7 where the Satten and Wong expressions for values of Θ of 1°, 150°, and $200^{\circ}K$ are shown. From Figure 4.7 it can be seen that the Holmes and McClure expression does not reproduce the experimental results at all. Whilst the Satten and Wong expression gives reasonable agreement, it is rather disturbing that the value of Θ is so ill-defined. Now Holmes and McClure (36) reported that the results they obtained for the temperature dependence of the intensity of the crystal spectrum of $CoSO_4 \cdot 7H_2O$ over the

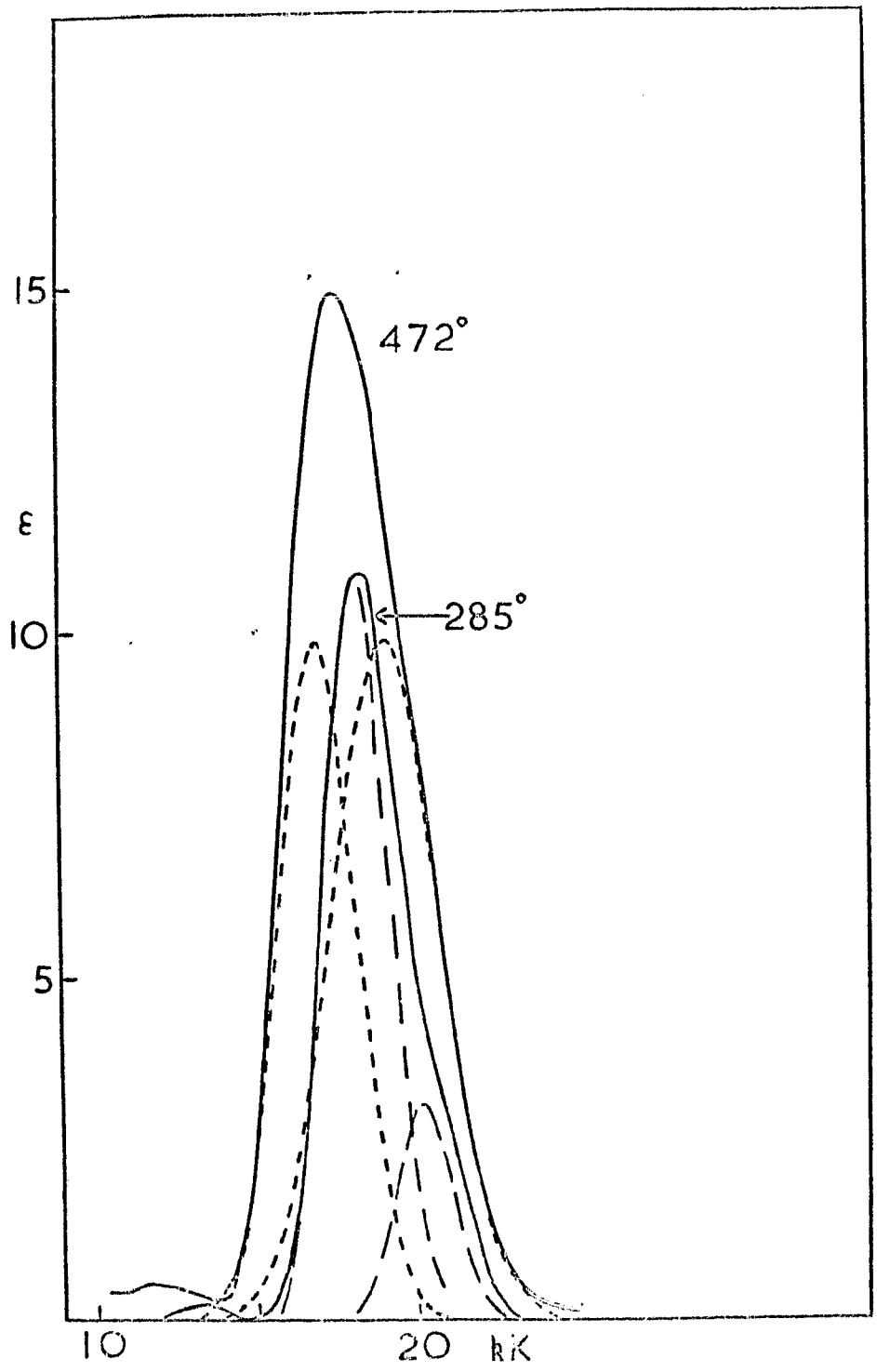

Figure 4.8

Resolved spectra of Co(II) in 98% H_2SO_4 at 285° C and 472° K

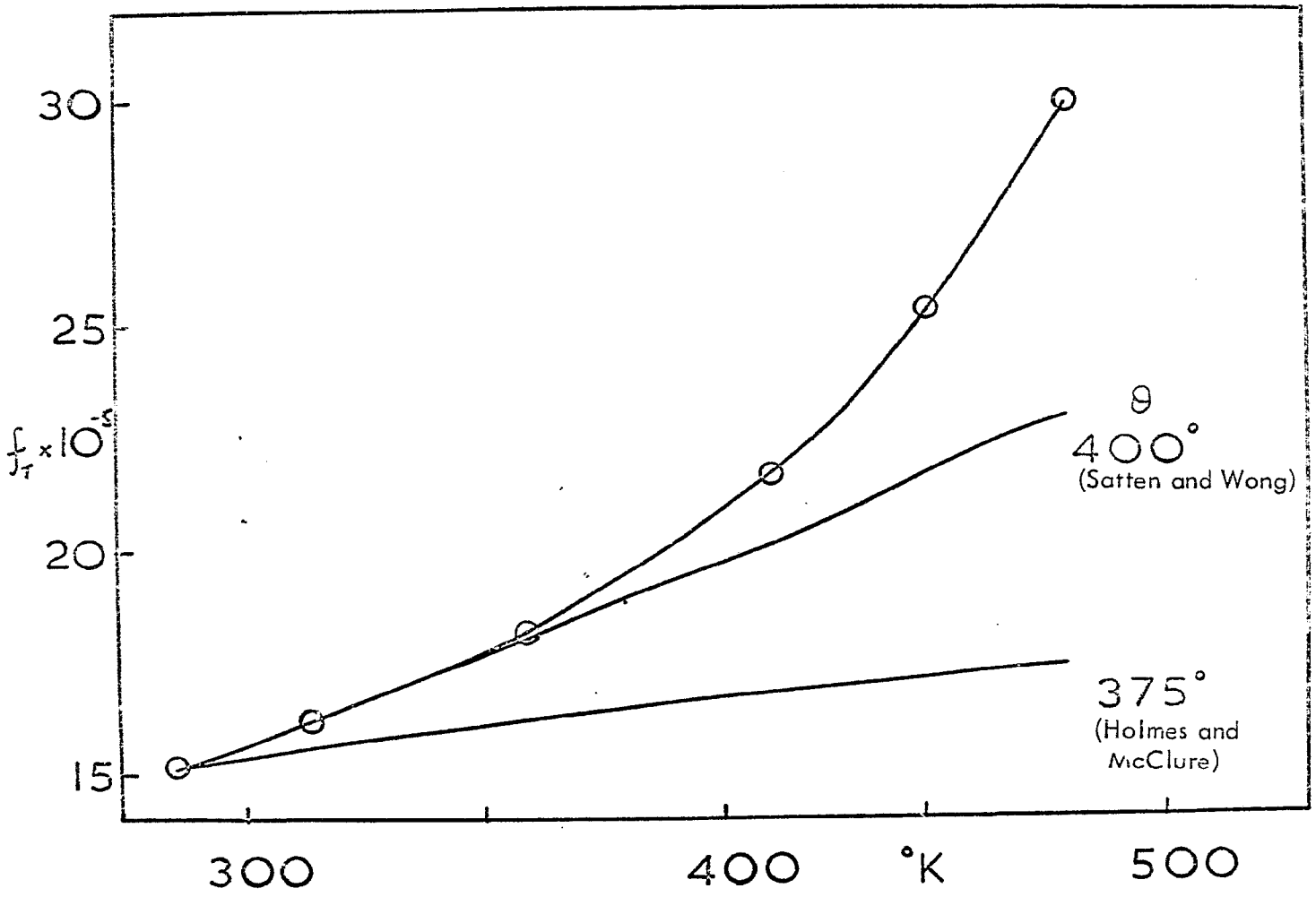

Figure 4.9

Temperature dependence of the oscillator strength for Co(II) in 98% H_2SO_4

temperature range 95° - 298° K were reproduced by equation 2.3 with a θ value of 250° K. The crystal spectrum of $CoSO_4 \cdot 7H_2O$ at 298°K suggests that the $Co(H_2O)_6^{2+}$ species is present in the crystal and it is, therefore, extremely puzzling why one equation should fit the crystal data and the other the aqueous spectra. Certainly, since the aqueous spectra fit the Satten and Wong relationship, which was derived assuming an octahedral species, the octahedral-tetrahedral transformation $Co(H_2O)_6^{2+} \rightleftharpoons Co(H_2O)_4^{2+}$ suggested by Swift and Connick is no longer feasible. As well as this spectral evidence against the presence of $Co(H_2O)_4^{2+}$ in aqueous solution, Chmelnick and Fiat (93) have shown that the interpretation of the NMR data of Swift and Connick on H_2O^{17} exchange in aqueous Co(II) solutions, (which first led to the suggestion of a $Co(H_2O)_4^{2+}$ species), was, in fact, incorrect. Chmelnick and Fiat state that they "wish to emphasise that no positive NMR evidence has been found hitherto, or now, in favour of this interpretation," (i.e. the presence of $Co(H_2O)_4^{2+}$ in aqueous solution).

The spectra, resolved into Gaussian components, at 285°K and 472°K for Co(II) in 98% sulphuric acid solution are shown in Figure 4.8. The band positions and oscillator strengths for all the temperatures at which spectra were recorded are reported in Table 4.6. Included in this table are the values of Δ and B, which were obtained by assuming an octahedral coordination and using the same assignment as was employed previously. It has been established earlier that the spectrum of Co(II) in 98% sulphuric acid at room temperature is consistent with an octahedral species. However, as the resolved components in Figure 4.8 show, for the spectrum at 472°K, a change has taken place. Moreover, the results in Table 4.6 show that the greatest

TABLE 4.6

Temperature dependance of the spectral parameters for Co(II) in H_2SO_4

Temperature °K	ν(kK)	$f_T \times 10^5$	Δ(kK)	B(cm^{-1})
285	13.15	0.198	7.06	871
	18.19	12.03		
	20.20	3.08		
313	12.79	0.336	6.87	872
	18.06	12.20		
	20.10	3.94		
359	12.54	0.573	6.74	870
	17.93	13.60		
	20.16	4.57		
410	12.19	0.816	6.55	869
	17.75	15.30		
	20.06	6.32		
442	11.80	0.79	6.35	872
	17.63	18.40		
	20.19	6.86		
472	11.69	0.75	6.29	831
	16.99	12.50		
	19.09	17.40		

change occurs in the 442° - 472° K region. This is shown by the sudden increase in the intensity of the high energy component of the main band and also, curiously enough, in a sudden change in B. In point of fact, there is a reversal in the position of the most intense component. At room temperature the high energy component is believed to be due to a spin-forbidden transition. At 472° K it is suggested that the Co(II) species is no longer octahedral but has suffered some degree of distortion. Since in pure octahedral symmetry the main component of the visible band corresponds to the $^4T_{1g}(P) \leftarrow {}^4T_{1g}(F)$ transition, a distortion would remove the degeneracy of the T states and split them into two or three components. Only two bands were observed on Gaussian analysis and it is, therefore, suggested that the $^4T_1(P)$ state has been split so as to produce both a $^4A_2$ and a ^4E component. Such a splitting would be caused, as shown in Figure 4.1, by lowering the symmetry from O_h to D_{4h}, D_{3d} or D_{2d}. The data available do not allow a distinction to be made between these possibilities. If the suggestion that the spectrum at 472° K is due to a distorted octahedral complex is accepted, then the pseudo-octahedral ligand field parameters may be evaluated by taking the arithmetic centre of the split band as the energy corresponding to the $^4T_{1g}(P) \leftarrow {}^4T_{1g}(F)$ transition. In this case, the values of Δ and B were found to be 6.29 KK and 993 cm^{-1} respectively. The value of Δ has remained unchanged but the value of B has increased such that it is now greater than the free ion value of 970 cm^{-1}. This discrepancy would seem to be due to the nature of the approximation used in the calculation and emphasises the fact that comparisons of this nature should only be made between systems that have been treated in exactly the same way.

The variation of the oscillator strength with temperature for the 98% sulphuric acid was treated in the same fashion as the results for the aqueous system. Figure 4.9 shows that neither the expression of Holmes and McClure nor that of Satten and Wong describe the results at all well, although the latter expression gives a reasonable fit over the temperature range 285° - 390°K with a Θ value of 400°K. Above ~390°K the band would appear to be too intense on the basis of the octahedral model of Satten and Wong. This could be explained in terms of a distortion destroying the centre of symmetry and thereby removing, in part at least, the Laporte-forbidden nature of the transition. As Figure 4.2 shows, both the D_{3d} and the D_{2d} models would achieve this result. However, this argument is not strong enough to rule out models, e.g. D_{4h} , with any degree of certainty.

Thus, both the oscillator strength variation and the ligand field splitting parameter Δ can be interpreted in favour of a distorted octahedral species being present in 98% sulphuric acid at 472°K. In an attempt to obtain more information concerning this distortion, it was decided to carry out magnetic susceptibility measurements over the temperature range 313° - 465°K. This investigation was performed using the NMR method of Evans (94), (see Appendix B for details). The experimental results are reported in Table 4.7 and a plot of $1/\chi_A'$ versus T is shown in Figure 4.10. χ_A' is the atomic magnetic susceptibility corrected for the diamagnetism of sulphuric acid, which was taken to be -39.8×10^{-6} cgs units for 98% H_2SO_4 extrapolated from the data of Cini and Pernicone (95), and the diamagnetism of the Co(II) ion which was taken to be -12×10^{-6} cgs units from the compilation of Figgis and Lewis (96).

As Figure 4.10 shows, $1/\chi_A'$ varies linearly with temperature within the

TABLE 4.7

Temperature dependence of the magnetic moment for Co(II) in 98% H_2SO_4.

Temperature (°K) ±1°	Shift (Hz) ±1 Hz	$1/\chi_A^1 \times 10^3$	μ_{eff} B.M.
311	40.7	.936±0.026	5.16±0.07
313	41.1	.927 .025	5.20 .07
334	37.9	1.005 .025	5.16 .08
359	35.1	1.088 .027	5.14 .07
375	31.6	1.205 .038	4.99 .07
383	32.0	1.189 .038	5.08 .08
396	30.8	1.237 .040	5.06 .09
410	29.6	1.287 .044	5.05 .09
413	29.0	1.314 .046	5.02 .09
419	28.0	1.360 .049	4.97 .09
426	27.2	1.401 .051	4.93 .09
441	26.5	1.438 .055	4.96 .10
457	24.9	1.531 .062	4.89 .11
465	24.8	1.537 .062	4.92 .11

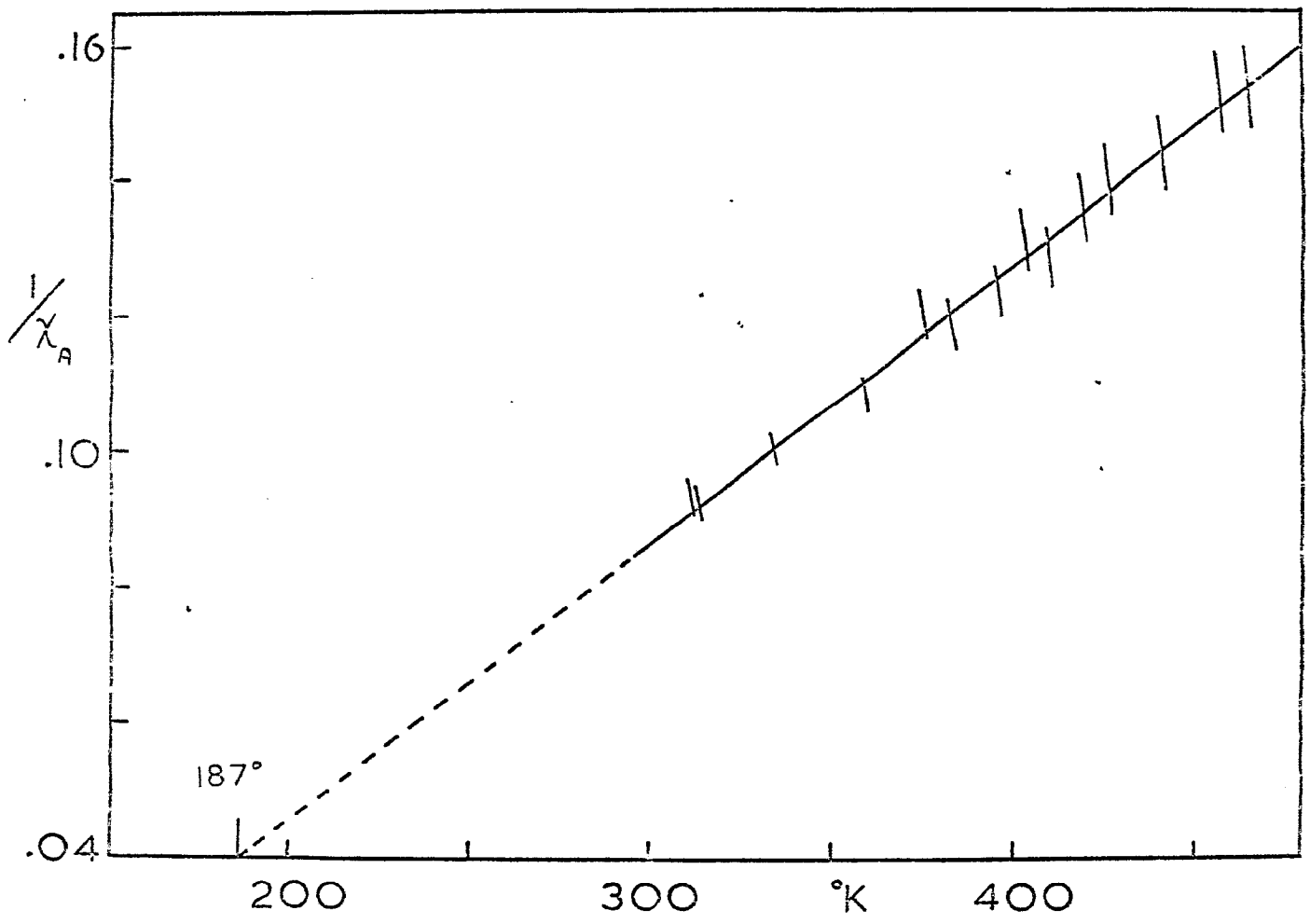

Figure 4.10

Graph of reciprocal susceptibility as a function of temperature for Co(II) in 98% H_2SO_4

errors of the experiment. This means, therefore, that the Curie-Weiss law is obeyed for this system. The average value of the magnetic moment over the temperature range 311° to 465 °K is 5.03 $\pm$ 0.09 Bohr magnetons. This value is in substantial agreement with a value of 5.02 Bohr magnetons reported for Co(II) in H_2SO_4 solutions measured by a semi-differential Gouy method (97). Furthermore, the value of the magnetic moment is within the range of values for typical octahedral Co(II) complexes (96). However, as can be seen from Figure 4.10, the error increases as the temperature is raised. This arises principally because the percentage error in the shift increases by about 1%. It would certainly seem necessary to use a more precise method to measure the magnetic susceptibilities at the highest temperatures. From this work then, no evidence has been obtained to confirm the existence of a distortion.

4.4.2 Co(II) in the Li_2SO_4 - Na_2SO_4 - K_2SO_4 Eutectic Melt. The spectrum of anhydrous cobalt sulphate dissolved in the Li_2SO_4 - Na_2SO_4 - K_2SO_4 eutectic melt and recorded at 550°C is shown in Figure 4.11. It can be seen that the spectrum consists of two band systems, the lower energy one being located in the near infra-red, and the higher energy and more intense one in the visible region of the spectrum. The band positions, extinction coefficients and oscillator strengths of the components of the bands, as obtained by Gaussian analysis (see Appendix A for details) are presented in Table 4.8 together with the results of Johnson and Piper (87). Since these latter authors reported the positions and extinction coefficients of the maxima and the shoulders, Figure 4.11 must be used to compare the results. With regard to position, the results are in good agreement.

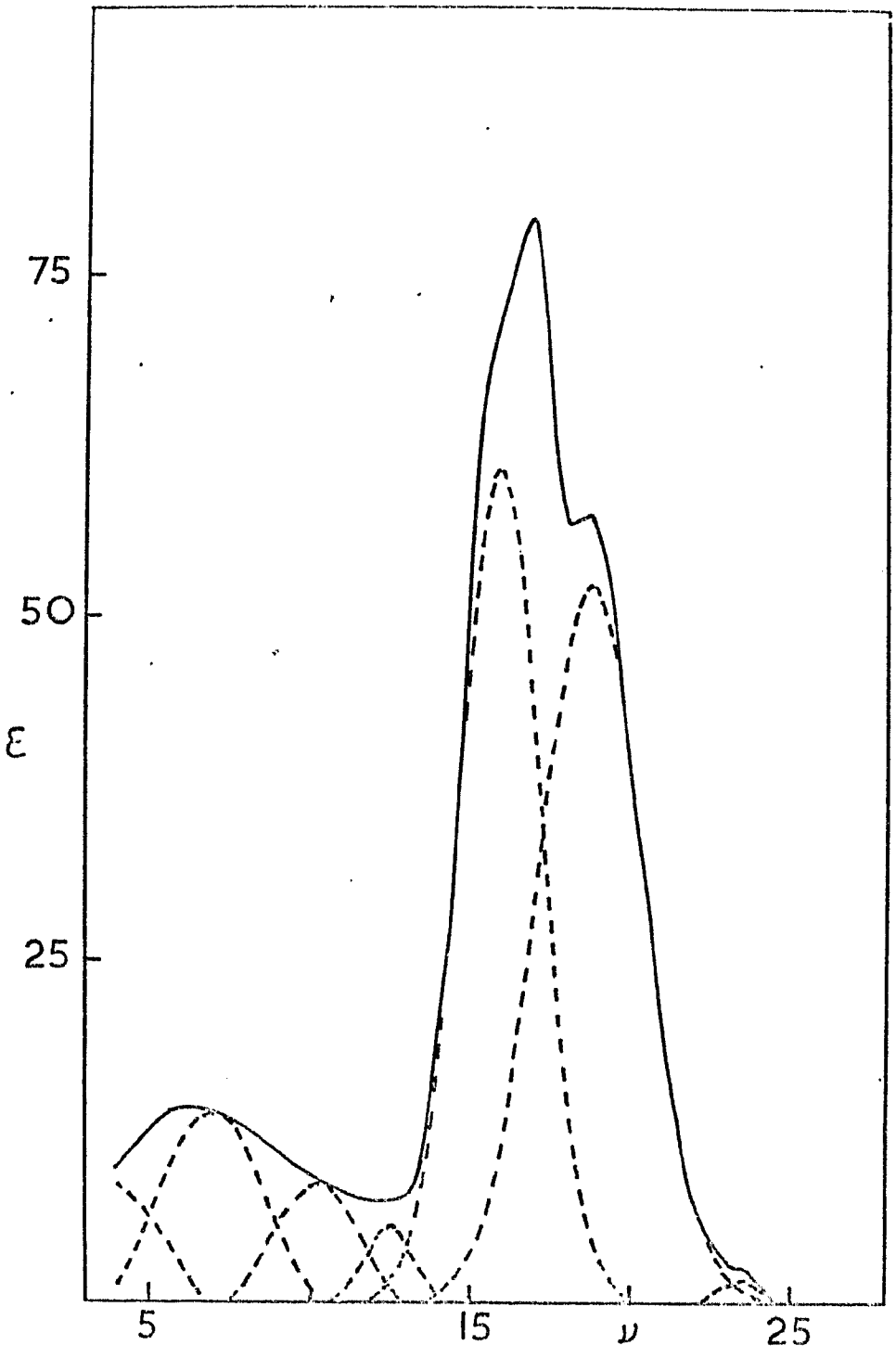

Figure 4.11

Spectrum of Co(II) in Li_2SO_4 - Na_2SO_4 - K_2SO_4 at 550°C

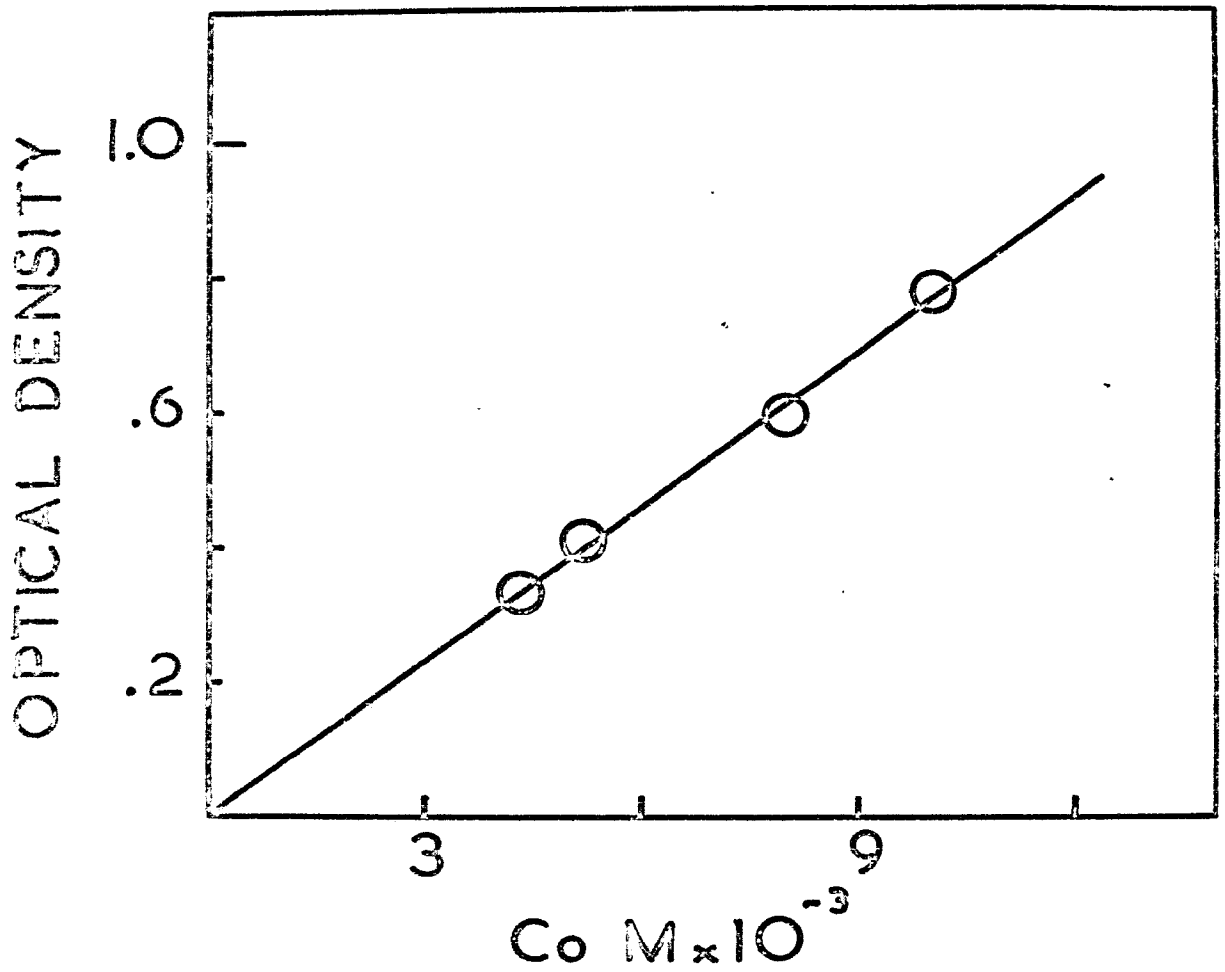

Figure 4.12

Beer's law plot for Co(II) in Li_2SO_4 - Na_2SO_4 - K_2SO_4 at 550°C

In Figure 4.12 a plot of optical density, measured at 17.0 kK, which corresponds to the highest over-all absorbance, as a function of cobalt concentration, is presented. The slope of this line, which proves that Beer's law is obeyed for this system, gives a value for the extinction coefficient of 76, which is somewhat lower than that reported by Johnson and Piper, (see Table 4.8). The main difference, however, is the characterisation of the band system in the near infra-red. In comparison with the visible band system it is relatively weak, which perhaps explains why it was not resolved previously.

Table 4.8

Spectrum of Co(II) in Li_2SO_4 - Na_2SO_4 - K_2SO_4 at 550°C

ν(kK)	ε	f x 10^4	ν (87)	ε
7.0	14.0	2.35		
10.24	8.75	1.29		
12.50	5.5	0.43		
16.0	61.0	8.35	16.1	
18.82	52.5	9.26	17.1	93.5
23.50	1.75	0.096	19.0	83.0

These results will now be discussed in terms of the three properties which characterise absorption bands: namely shape, position and intensity.

A. Shape. In the absence of large distortions, the shape of the bands can be a useful guide to the symmetry of the species. The usual procedure is to compare the band shape with that due to a species with known symmetry. Johnson and Piper (87) noted that the shape of the visible band for the cobalt species in the sulphate

eutectic melt closely resembled that due to a distorted tetrahedral species reported by Gruen (6). This latter author reported the spectral changes which took place as LiCl - KCl eutectic was added to a solution of anhydrous cobalt nitrate dissolved in the $LiNO_3$ - KNO_3 eutectic. The spectral changes were interpreted as being due to a change from an octahedral nitrato-complex, which was postulated to be $Co(NO_3)_4^{2-}$, to tetrahedral $CoCl_4^{2-}$. That the spectrum in solutions containing large proportions of LiCl - KCL was, in fact, due to tetrahedral $CoCl_4^{2-}$, was shown by comparison with the spectrum of Co(II) substituted in a Cs_2ZnCl_4 crystal. Certainly, as far as shape is concerned, spectrum E of Figure 5.5 in reference (6) is virtually identical to the sulphate melt spectrum. Furthermore, this spectrum lies towards the 'tetrahedral end' of the octahedral-tetrahedral change. The comparison is weakened somewhat in that the environment about the Co(II) ion is being changed from six oxygens to four chlorides so that in the intermediate region there is considerable doubt as to the nature of the species present. The fact that there are different types of ligands present further complicates the problem since these will also affect the band shape due to their differing ligand field strengths.

A similar study, also by Gruen et al. (98) is perhaps more applicable, since in this case the effect of added $ZnCl_2$ on the spectrum of Co(II) in an $AlCl_3$ melt was reported where, of course, the ligating atom remained the same. Again the spectral changes were interpreted in terms of an octahedral-tetrahedral change, the species becoming tetrahedral as the amount of $ZnCl_2$ was increased. The spectrum of melts containing up to 39.9 mole % $ZnCl_2$ are very similar in shape to the sulphate melt spectrum, whilst at 54.3 mole % $ZnCl_2$ the spectrum is similar to a

tetrahedral spectrum obtained for Co(II) in CsCl. Thus, once again the shape of the sulphate melt spectrum occurs close to a tetrahedral spectrum.

Turning to aqueous systems, there is a strong resemblance between the visible band of $Co(OH)_2$ dissolved in NaOH (99), and the sulphate melt spectrum. It was suggested that the cobalt species in the sodium hydroxide solutions was $Co(OH)_4^{2-}$ although some $[Co(OH)_3H_2O]^-$ may have been present. Certainly there was no resemblance between this particular spectrum and that reported for $Ba_2[Co(OH)_6]$ (83), see Table 4.9.

Table 4.9

Band positions, in kK, of T_d and O_h Hydroxo-complexes of Co(II)

$Co(OH)_4^{2-}$	7.3		14.6 - 14.8		
$Co(OH)_6^{4-}$	8.2	11.7	15.0	19.2	21.2

A discrepancy arises, however, when the spectrum of Co(II) in a pure $AlCl_3$ melt at 227°C and 6 atmospheres pressure is considered (100), since the visible band in this spectrum has the same general shape as the sulphate melt spectrum. However, Gruen has interpreted this spectrum in favour of an octahedral Co(II) species which he suggests may be $Co(Al_2Cl_7)_2$. The interpretation was based on the similarity between the $AlCl_3$ melt spectrum and the spectrum of $CsCdCl_3$ doped with Co(II) where only a single band at ~ 17 kK was found. Whilst this spectrum has not been published in the literautre (101), Gruen does state (5) that it is reminiscent of the spectrum of Co(II) in aqueous solution. If this is, in fact, the case, then there should be some similarity between the $AlCl_3$ melt spectrum and the aqueous spectrum. Such a comparison is not very encouraging. In a $CsCdCl_3$ crystal, Siegel (102) has

shown that there are two types of $CdCl_6^{4-}$ octahedra. The first type, constituting one-third of the total, consist of regular octahedra, each chlorine being shared with another octahedron, whilst the second type involve octahedra sharing a face with another type II species, the remaining three chlorine atoms being shared with type I octahedra. These type II octahedra are "appreciably distorted". Thus, if the Co(II) ion substitutes in the type II Cd sites, the spectrum will be due to a $CoCl_6^{4-}$ octahedron having a D_{3d} distortion.

In a later paper (103) Gruen states that "the similarity of the spectrum to those of $CoCl_2$ and $Co(AlCl_4)_2$ leaves little doubt that Co(II) is octahedrally coordinated (in $AlCl_3$)". However, the spectrum of $CoCl_2$ as reported by Ferguson et al. (104) does not contain the low energy 'anomalous shoulder', nor is the higher energy, partially resolved, band as intense as in the $AlCl_3$ or the sulphate melt. The spectrum of $CoCl_2$ represents an almost perfect octahedral type spectrum by comparison with the spectrum of $Co(H_2O)_6^{2+}$. The structure of $Co(AlCl_4)_2$, as reported by Ibers (105), shows that each Co(II) ion is surrounded by four $AlCl_4^-$ groups, two of which act as bidentate and two as unidentate ligands, the resulting symmetry being of the C_{2v} type. The spectrum of $Co(AlCl_4)_2$ was reported by Gruen for a polycrystalline sample but, presumably because of the sample state, it was not at all well resolved. The main band in the visible has an unusual bell shape with a partly resolved high energy band.* On the basis of these criticisms, it

* The low energy shoulder has been described as 'anomalous' since it has been shown by Gaussian analysis that for the sulphate melt spectrum it does not correspond to another absorption band, but arises because of extensive band overlapping. However, it is useful when comparing spectra.

would appear that the assumption of octahedral symmetry for the species in $AlCl_3$ is not completely justified.

The spectrum of a calcium fluoride crystal doped with Co(II) has been reported by Stahl-Breda and Low (106). By assuming that the Co(II) substituted for the Ca(II) ions, it was suggested that the Co ion was surrounded by eight fluorides. The shape of the visible band in the spectrum bears a marked resemblance to that of the sulphate melt spectrum. However, the existence of a cubic CoF_8 species in this crystal has not been generally accepted. Nevertheless, the fact that both the CaF_2 and the sulphate melt spectra have similar shapes is unexpected. It may be that the Co(II) does not occupy a regular Ca(II) site but instead the fluoride lattice distorts so as to produce a tetrahedral arrangement of fluorides in the first coordination shell. That this mechanism is possible is shown by the Pauling radii of 0.99 Å and 0.72 Å for the Ca(II) and Co(II) ions respectively. Furthermore, the value of the ligand field splitting parameter, 3.40 kK, is very reasonable for a tetrahedral complex but too low by a factor of 2 for Co(II) with eight-fold coordination.

In the light of these comparisons it would seem reasonable to conclude that the shape of the visible band system for the cobalt species in the sulphate eutectic melt is compatible with a tetrahedral or distorted tetrahedral species, although a distorted octahedral species is not completely ruled out.

B. Position. It has been pointed out earlier that the main band in the visible region is found in the 18 - 20 kK and 12 - 17 kK regions for octahedral and tetrahedral Co(II) complexes respectively. The position depends, of course, on the ligand field strength of the particular ligand and it may also be influenced by the

temperature. The temperature effect is related to the ligand field strength in the following way. The expression for Δ contains a term in r^{-n}, where r is the metal-ligand distance. As the temperature increases, the vibrational amplitude of the M - L stretching vibrations also increase, leading, in turn, to an increase in the average distance r. Since r increases, Δ must then decrease and the bands will move to lower energy.

Thus, as far as position is concerned, the cobalt species in the sulphate melt may be either octahedral or tetrahedral. However, more information can be obtained by examining this criterion in a critical fashion, namely by the evaluation of the ligand field parameters Δ and B. The assignments of the bands to both the octahedral and tetrahedral cases, (including distortions), will now be considered.

(i) Octahedral Case. In the light of the discussions earlier, the following assignment seems most reasonable:

$$^4T_{2g}(F) \leftarrow {}^4T_{1g}(F) \qquad 7.0\ \text{kK.},\quad \nu_1$$
$$^4A_{2g}(F) \leftarrow {}^4T_{1g}(F) \qquad 12.5\ \text{kK.},\quad \nu_2$$
$$^4T_{1g}(P) \leftarrow {}^4T_{1g}(F) \qquad 16.0\ \text{kK.},\quad \nu_3$$

By applying the Lever and Ogden criterion it is found that $\nu_2/\nu_1 = 1.78$ which is slightly below that predicted. Using the energy expressions for the octahedral case, equations 4.2, the following values of the ligand field parameters are obtained, $\Delta = 6.65$ kK and $B = 730\ cm^{-1}$. These values were obtained by using the expressions for ν_2 and ν_3. They can, therefore, be used to predict the value of ν_1, which was found to lie at 5.85 kK. By comparison with the values obtained for the sulphuric acid media, (Table 4.4), it can be seen that the value of Δ is

quite reasonable but the value of B is considerably lower and corresponds to a β value of 0.75. This lower value of β would mean that the complex in the sulphate melt has a greater degree of covalency than the species in sulphuric acid. On this assignment the band at 18.82 kK would presumably be assigned to a quartet-doublet transition as discussed earlier. This is extremely unlikely since, as Table 4.8 shows, this particular band has a larger oscillator strength than the quartet-quartet transition at 16.0 kK. Furthermore, the band at 10.24 kK, which is quite a strong band, would have to be assigned to the spin-forbidden transition $^2E_g(G) \leftarrow {}^4T_{1g}(F)$. However, since the oscillator strength of this band is too large, by a factor of ~ 100, the intensity would have to be explained in terms of 'intensity stealing' from the nearby spin-allowed band but, because this is 3.24 kK to lower energy, it is unlikely that this mechanism is operative. When all these factors are considered, it can be seen that this particular assignment is not very satisfactory.

It is possible to consider the spectrum as due to a distorted octahedral species. In this case, the two pairs of bands at 7.0 and 10.24 kK, and at 16.0 and 18.82 kK, arise because the parent octahedral states $^4T_{2g}(F)$, and $^4T_{1g}(P)$ respectively are split. Various types of distortions have already been considered (see Figure 4.2). It seems reasonable to discard those distortions which split each of the parent octahedral T states into three components in favour of those producing only two components since, in fact, only two bands were found. From Figure 4.1, therefore, it would seen that the complex must be either of the D_{3d} or D_{4h} symmetry species.

As stated earlier (p. 86), since the direction of the splitting cannot be predicted from symmetry principles, it is not possible to determine the baricentre of

the split state. As an approximation, the arithmetic centre of the split bands was used to calculate the pseudo-octahedral parameters. Taking the centres to be 8.62 and 17.4 kK, the values of Δ and B were found to be 9.65 kK and 655 cm^{-1} respectively. The position of ν_2 is then predicted to lie at 18.3 kK. Now the weak band at 12.5 kK may, in fact, be ν_2, in which case the assignment is unsatisfactory. Alternatively, a small absorption band may be present but be completely hidden by the two large bands. If this is the case, then the band at 12.5 kK may be assigned to the $^2E_g(G) \leftarrow {}^4T_{1g}(F)$ transition. In theory, an E_g state should split on lowering the symmetry from O_h to D_{4h} but remain unsplit if the symmetry is lowered to D_{3d}. Despite the fact that only one band is observed, it seems unreasonable to use this criterion to distinguish between these possibilities on the grounds that the band is such a weak one. Moreover, the over-all assignment is not very satisfactory if the values of the ligand field parameters are examined. However, because of the approximation of taking an arithmetic centre instead of a baricentre, it is only justifiable to compare the values of Δ and B for the sulphate melt with values derived in a similar manner for other distorted octahedral Co(II) compounds. To make the comparison valid, distorted sulphato-complexes of Co(II) would seem the most reasonable choice.

The only compounds readily available were anhydrous cobalt sulphate and cobalt sulphate monohydrate. Although these are blue and lilac respectively, both are distorted octahedra. Whilst only the anhydrous compound is of interest, the monohydrate was also examined since it appeared that Johnson and Piper (87) reported the spectrum of the monohydrate as being due to the anhydrous compound.

The reflectance spectra of anhydrous cobalt sulphate and the monohydrate are

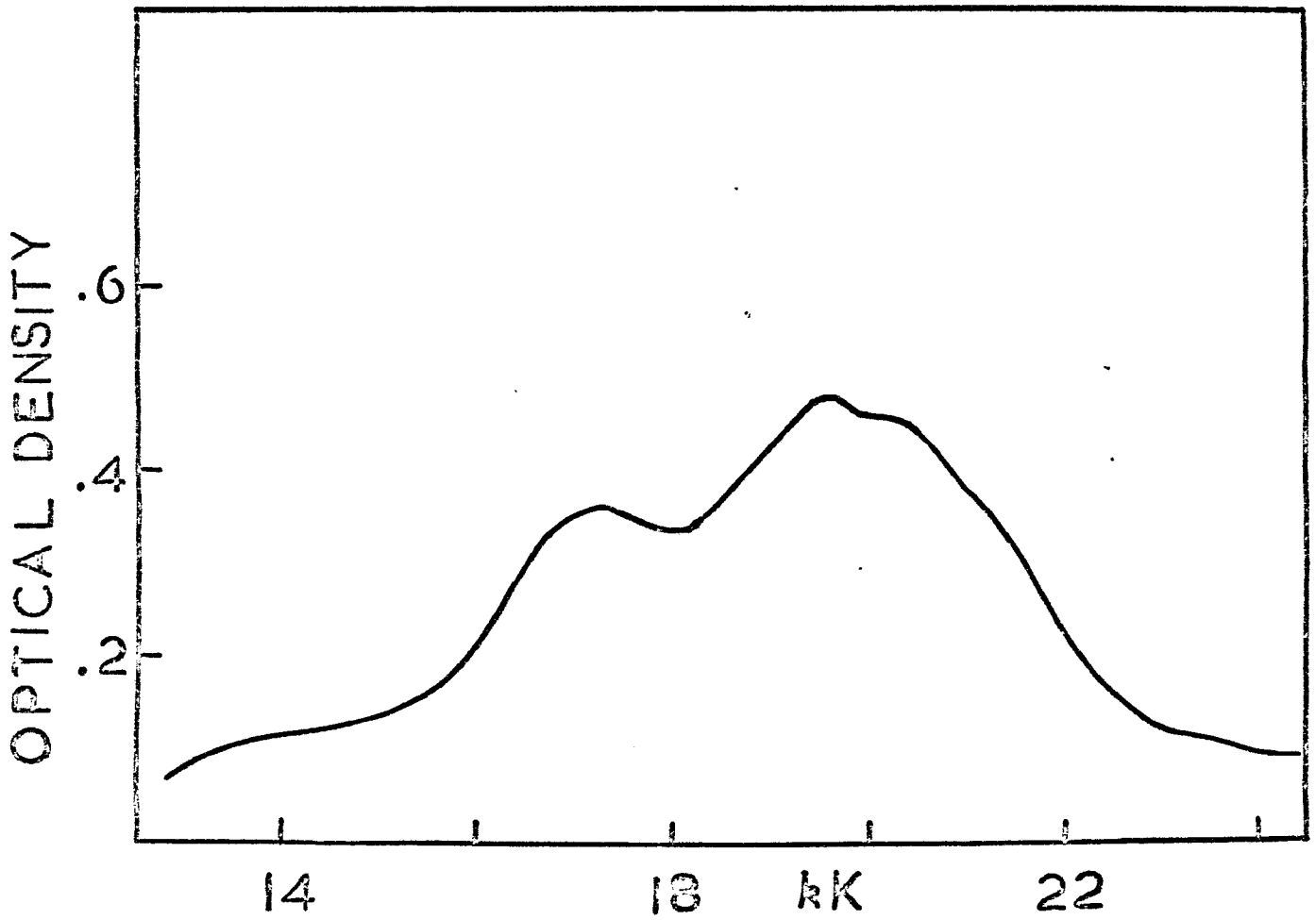

Figure 4.13

Reflectance spectrum of anhydrous $CoSO_4$

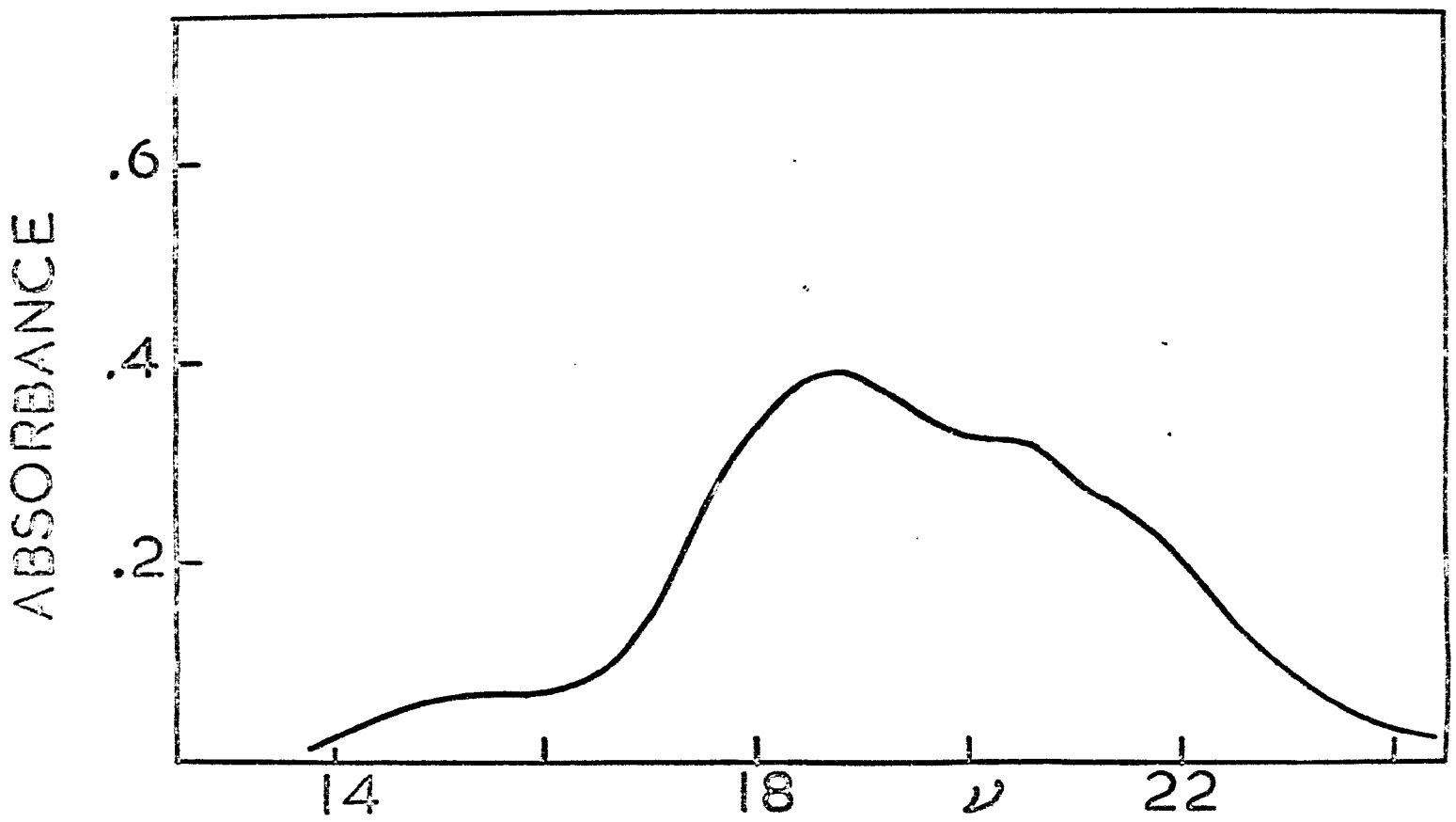

Figure 4.14

Reflectance spectrum of $CoSO_4 \cdot 1\,H_2O$

shown in Figures 4.13 and 4.14 respectively. The band positions and suggested assignments in octahedral symmetry are shown in Table 4.10.

Table 4.10

Reflectance spectra of $CoSO_4$ and $CoSO_4 \cdot 1H_2O$

Assignment in O_h Symmetry	$CoSO_4 \cdot 1H_2O$	$CoSO_4$
$^4A_{2g}(F) \leftarrow {}^4T_{1g}(F)$	15.3	13.8
$^4T_{1g}(P) \leftarrow {}^4T_{1g}(F)$	18.7, 20.3	17.2, 19.6, 20.2
Doublet Level $\leftarrow {}^4T_{1g}(F)$	21.5	21.5

The crystal structure of $CoSO_4 \cdot 1H_2O$ has been reported by Goring-Bayat and Bassi (107). The Co(II) ion is surrounded by four sulphate groups, in a plane with Co - O distances of 2.00 and 2.01 Å, and two water molecules, one above and the other below the plane, the Co - OH_2 distances being 2.16 Å. The structure may, therefore, be described as a tetragonally distorted octahedron with the molecule belonging to the D_{4h} symmetry group. From Figure 4.1, the spectrum in the visible region may be predicted to have the following characteristics.

a. A relatively weak band corresponding to the $^4A_{2g}(F) \leftarrow {}^4T_{1g}(F)$ two electron-transition in octahedral symmetry.

b. A strong band at higher energy which is split into two components.

c. Higher energy shoulders which may be due to spin-forbidden transitions.

The experimental results are in good agreement with these predictions. By taking the arithmetic centre of the split band, the ligand field parameters listed in

Table 4.11 were obtained, i.e. the assignment used was:

$$^4A_{2g}(F) \longleftarrow {}^4T_{1g}(F) \qquad 15.3 \text{ kK}$$

$$^4T_{1g}(P) \longleftarrow {}^4T_{1g}(F) \qquad 19.6 \text{ kK}$$

Table 4.11

Ligand field parameters for $CoSO_4$ and $CoSO_4 \cdot 1H_2O$

	ΔkK	B cm^{-1}	β
$CoSO_4 \cdot 1H_2O$	7.93	916	0.945
$CoSO_4$	7.56	940	0.97

For the case of anhydrous cobalt sulphate, the crystal structure has been reported by Dunitz and Pauling (108). In this structure each cobalt ion is surrounded by six sulphate groups arranged with three different Co - O distances, namely 2.00, 2.10, and 2.29 Å. It is not clear from this paper how the different Co - O bonds are orientated with respect to each other. There are two regular arrangements which are feasible. Firstly, the pairs of identical Co - O distances may be cis to one another, leading to a structure which belongs to the C_1 symmetry group, (see Figure 4.2). Secondly, the pairs of distances may be trans to one another, in which case the species belongs to the D_{2h} symmetry group, (see Figure 4.2). The effects of descending to these symmetries are included in Figure 4.1 where it can be seen that each of these symmetries should give rise to three components of the $^4T_{1g}(P)$ level of the octahedral parent symmetry.

The values of the ligand field parameters shown in Table 4.11 were obtained using the following assignments:

$$^4A_{2g}(F) \leftarrow {}^4T_{1g}(F) \qquad 13.8\ kK$$

$$^4T_{1g}(P) \leftarrow {}^4T_{1g}(F) \qquad 19.0\ kK$$

Again, the approximation of an arithmetic centre instead of a baricentre was used.

A rough check of the validity of these assignments for the reflectance spectra can be made if the Rule of Average Environment (25) is invoked. This states that, for a complex with a mixed set of ligands, the value of Δ will be a weighted average of the Δ values of the individual ligands. This can be used to calculate Δ for $CoSO_4 \cdot 1H_2O$ as follows. The value of Δ for $Co(H_2O)_6^{2+}$ was found to be 8.58 kK (Table 4.4) and from Table 4.11, Δ for $Co(SO_4)_6$ is 7.56. Thus the value for $[Co(SO_4)_4(H_2O)_2]$ is:

$$(4/6 \times 7.56) + (2/6 \times 8.58) = 7.90\ kK.$$

This is in excellent agreement with the experimental value of 7.93 kK.

It is now possible to compare the values of Δ and B obtained from the sulphate melt spectrum, assuming a distorted octahedral species, with those for anhydrous cobalt sulphate. It can be seen that Δ is substantially higher for the sulphate melt, whilst B is very much smaller. Thus for a change in temperature of $\sim 500^\circ C$, Δ increases if, as a first approximation, the difference in symmetry between D_{2h} and D_{3d} or D_{4h} is neglected. Now Johnson and Piper (87) found that for the Ni(II) species in the $Li_2SO_4 - Na_2SO_4 - K_2SO_4$ eutectic melt, Δ decreased as the temperature was raised from $550^\circ C$ to $700^\circ C$. This is reasonable as it would be expected that the Ni - O bond distances would increase as the temperature was raised, (see earlier discussion). For the same reason it would be expected that for Co(II) Δ should decrease as the temperature rose. Also the low

B value, corresponding to a relatively large covalency effect, is also unexpected if the average M - L distance increases with temperature.

In summary, it can be said that on assuming a distorted, possibly D_{3d} or D_{4h}, octahedral species, an unconvincing result is obtained.

(ii) Tetrahedral Case. In the earlier discussion of the assignment of the spectra of tetrahedral Co(II) species, it was pointed out that, although only two bands were expected in the near infra-red and visible regions of the spectrum, the spectra invariably contain complex bands in these regions. Furthermore, evidence was cited which showed that the complex bands were best explained as arising from distortions from a pure tetrahedral species. On this basis then, the following assignments were made, again taking the arithmetic centre rather than the baricentre:

$$^4T_1(F) \longleftarrow {}^4A_2(F) \qquad 8.62 \text{ kK}$$

$$^4T_1(P) \longleftarrow {}^4A_2(F) \qquad 17.41 \text{ kK}$$

Following this, the band at 12.5kK was assigned to a spin-forbidden transition; since it was now in tetrahedral symmetry, the oscillator strength for such a band could be of this order of magnitude. The ligand field parameters were then calculated using the expressions quoted earlier, (equations 4.1). These values are listed togehter with the values for other tetrahedral Co(II) complexes in Table 4.12. It can be seen that while the value of Δ is a little higher for the sulphate melt species, the value of B is quite reasonable. On this assignment, the band at 23.5 kK may be identified as a spin-forbidden transition. In other tetrahedral Co(II) complexes, e.g. $CoCl_4^{2-}$, it occurs much closer to the spin-allowed transition and, presumably by an 'intensity stealing' mechanism, is found as a much more intense component. In the present

TABLE 4.12

Ligand field parameters for various T_d Co(II) complexes.

	$Co(N_3)_4^{2-}$	$Co(NCO)_4^{2-}$	$Co(NCS)_4^{2-}$	$Co(OH)_4^{2-}$	$CoCl_4^{2-}$	Co in ZnO	Co in CdS	Co in SO_4 Melt
ν_2 kK	6.75	7.15	7.78	7.3	5.22-9.7	6.75	5.50	8.62
f_2	1.49×10^{-3}	1.37×10^{-3}	3.44×10^{-3}	5.81×10^{-4}	0.721×10^{-3}	-	1.2×10^{-3}	2.35×10^{-4}
ν_3 kK	14.9	16.1	16.25	16.6	14.6-14.8	15.5	13.95	17.41
f_3	8.58×10^{-3}	6.70×10^{-3}	1.46×10^{-2}	2.98×10^{-3}	5.09×10^{-3}	-	8×10^{-3}	1.77×10^{-3}
Δ kK	3.92	4.15	4.55	4.23	2.99-3.28	3.9	3.16	5.10
B cm^{-1}	658	720	691	747	690-730	700	664	714
β	0.68	0.745	0.715	0.770	0.72-0.75	0.72	0.68	0.735
Reference	(75)	(75)	(75)	(99)	(99)	(77)	(109)	

case, however, it is ~ 4.7 kK above the nearest strong component compared to ~ 1 kK in the case of $CoCl_4^{2-}$. This distance is apparently too large for any degree of 'intensity stealing' to take place.

On the basis of band position, it has been shown that the sulphate melt spectrum gives a better fit for a distorted tetrahedral than for a distorted octahedral species and since the bands were split into two components, as Figure 4.11 shows, this is compatible with a C_{3v} or D_{2d} species.

C. Intensity. It has often been stated that the band intensities of tetrahedral complexes are higher, by a factor of about 100, than those of octahedral complexes (25). This is often the case, e.g. the absorption band ~ 15 kK in the spectrum of $CoCl_4^{2-}$ has $\varepsilon = 520$, whilst for $Co(H_2O)_6^{2+}$ the band at 19.1 kK has $\varepsilon = 3.84$. This does not mean, however, that band intensities can be indiscriminately used as a criterion for characterising coordination geometries. Consider, for example, the various nitrato-complexes of Co(II) listed in Table 4.13.

Table 4.13

Spectra of some Co(II) nitrato complexes

	Symmetry	Maxima in visible (kK)	ε	Reference
$[NMe_4]_2Co(NO_3)_4$	T_d	18.7	120	110
$NO[Co(NO_3)_3]$	O_h	20.83 19.23	35 44	111
$Co(NO_3)_2$ in $LiNO_3$ - KNO_3 at 160°C	O_h	18	90	6

That the first two species are, in fact, tetrahedral and octahedral respectively was supported by other evidence. It can be seen that for the first two species, which were at room temperature, the extinction coefficient of the tetrahedral species is greater by a factor of ~ 3 than for the octahedral species, and that as the temperature is raised to include the last case, the factor decreases to about 1.3. However, emphasis should not be placed on these examples since the comparison embodies the same fault as that used by Gruen (6) in his criticism of Johnson and Piper 's interpretation (87) - namely that the extinction coefficient is a true measure of the intensity. This is not strictly correct. The true intensity is measured by the oscillator strength, which involves the extinction coefficient and also the band width. The values of the total oscillator strengths of the two band systems for the Co(II) species in the sulphate melt are included in Table 4.12, where it can be seen that the oscillator strengths for this species are in line with the other tetrahedral species.

Again, as in the discussion of band shape, the spectrum of Co(II) in the $AlCl_3$ melt appears anomalous. The oscillator strengths for a wide range of chloride melts have been measured by Øye and Gruen (103), including the $AlCl_3$ system, and are shown in Table 4.14. The first point to be noted is that over the range of symmetries suggested by these authors, the oscillator strength does not change by more than a factor of ~ 5. This is in contrast to aqueous and solid systems where the oscillator strengths for octahedral complexes are found to be 10^{-5} to 10^{-4} (Table 4.4) and for tetrahedral complexes ~ 10^{-3} (Table 4.12), a factor of 10 to 100.

The increase in intensity for melt systems has been examined by Gruen and McBeth for the V(II) system in the LiCl - KCl eutectic at 400°C (112). The

TABLE 4.14

Oscillator strengths for Co(II) in various chloride melts (103).

Melt	Temperature °C	Band Positions in kK (ε max)			$fx10^3$
Tetrahedral and Distorted Tetrahedral Species.					
$C_5H_5N.Cl$	150	14.3 (630)	14.9 (570)	15.9 (360)	5.42
$KCl-AlCl_3$ (50.3% KCl)	300	14.4 (406)	15.1 (395)	16.3 (250)	4.48
CsCl	800	14.2 (292)	14.8 (298)	16.4 (176)	3.82
KCl	800	14.2 (249)	14.8 (245)	16.4 (152)	3.35
NaCl	820	14.2 (223)	15.0 (223)	16.5 (140)	3.25
LiCl	800	14.3 (173)	15.1 (179)	16.7 (117)	2.89
$CdCl_2$	650	14.2 (173)	15.0 (176)	16.6 (121)	2.83
$MgCl_2$	800	14.4 (154)	15.1 (156)	16.8 (101)	2.54
$PbCl_2$	600	14.0	14.8	16.3	
Octahedral Species.					
$AlCl_3$	227	~14.8	15.7 (76)	~16.7	0.97
$GaCl_3$	150	~14.8	15.8 (58)	~16.7	0.78
$KCl-AlCl_3$ (35.5% KCl)	300	~14.6	15.8 (73)	~16.7	1.05
Strongly Distorted Octahedral Species.					
$HgCl_2$	350	13.6 (228)	15.4 (197)	16.8 (188)	3.8
$KCl-AlCl_3$ (49.9% KCl)	300	13.6 (218)	15.6 (145)	17.0 (137)	3.0

values of the oscillator strengths for the VCl_6^{4-} species in aqueous solution and in the LiCl - KCl eutectic were found to be ~ 0.3 x 10^{-4} and 4.3 x 10^{-4} respectively, an increase by a factor of ~ 10 for a 400° temperature rise. The Holmes and McClure equation for intensity as a function of temperature (equation 2.3) was shown to predict an increase in the oscillator strength of 10 - 30% for this temperature rise. An alternative mechanism, involving distortion of the complex such that the centre of symmetry was destroyed, thereby lifing the Laporte selection rule, was suggested. The effectiveness of a mechanism of this sort has not been examined on a quantitative basis. Such studies would be extremely useful.

Gruen has argued that, since the oscillator strength for the tetrahedral species cannot be described completely by a vibronic mechanism, the covalency mechanism of Ballhausen and Liehr (45) must be invoked to describe the large values. Such a mechanism suggests that the intensity would increase with increasing covalency of the Co - Cl bond. Thus, if the cations present can reduce the covalency of the Co - Cl bond, there should be a decrease in intensity. As Table 4.14 shows, for the alkali halide melts the intensity decreases in the order Cs - Li. On this argument the stronger the polarising power of the cation, the lower the intensity. Thus, in an $AlCl_3$ melt, where the ligating species is a covalent entity, (whether it is $AlCl_4^-$ or $Al_2Cl_7^-$ is unimportant), the covalency of the Co - Cl bond would be even lower than in the alkali halide melts. As Table 4.14 shows, such a decrease is, in fact, observed; thus a fair case can be made, on intensity grounds, for a tetrahedral or distorted tetrahedral species. Similar arguments could be put forward for the other covalent melts.

However, the whole problem is complicated even further by the oscillator strength of $\sim 1.5 \times 10^{-3}$ found for the spectrum of Co(II) in the $LiNO_3$ - KNO_3 eutectic at 160°C by Gruen (6) where, by comparison with the Co(II) aqueous system, the Co(II) species is almost certainly octahedral.

To return to the original problem concerning the species in the Li_2SO_4 - Na_2SO_4 - K_2SO_4 eutectic melt, it is felt that because of the doubt associated with the octahedral interpretation of the $AlCl_3$ melt spectrum, comparison with better understood systems is to be preferred. There are thus two points of reference: the aqueous spectra as an octahedral example on the one hand, and on the other, the KCl melt spectrum at 800°C as a typical tetrahedral example. The following conclusions are arrived at:

(i) The species is not perfectly octahedral but it may be a distorted octahedron.

(ii) The species is not tetrahedral, or more exactly, it does not have the same symmetry as the species in the KCl melt which itself may be distorted.

(iii) Since reasonable ligand field parameters are obtained for both a distorted tetrahedral and a distorted octahedral species, and in view of the above conclusions, it would seem likely that the species could be described in either fashion.

In view of these conclusions, and bearing in mind that a detailed treatment of the $AlCl_3$ system, which involves a close examination of the complete spectrum in terms of a critical discussion of the ligand field parameters, could reverse the emphasis

towards the octahedral side, it would appear reasonable to discuss the results of Duffy et al. (89), already referred to, from a distorted tetrahedral point of view.

However, a further possibility remains: namely, that the spectrum in the Li_2SO_4 - Na_2SO_4 - K_2SO_4 melt was due to a mixture of octahedral and tetrahedral Co(II) species. Various combinations of band assignments for the octahedral and tetrahedral cases were investigated. In no case were reasonable values of the ligand field parameters for both symmetries obtained. Furthermore, since an octahedral-tetrahedral equilibrium would be temperature dependent, a change in temperature should result in a spectrum of a different shape. As the results for the Na_2SO_4 - K_2SO_4 - $ZnSO_4$ melt, (to be discussed later), show, no such effect was observed.

On the basis of simple crystal field theory, it has been shown that Δ for a tetrahedral species should be approximately 4/9 that of the octahedral complex with the same ligands (25). Thus for the case of sulphato-complexes of Co(II) it is found, using the Δ value for anhydrous cobalt sulphate, that, for a tetrahedral species, the value of Δ should be 3.38 kK. This is substantially smaller than the experimental value of 5.1 kK. This may be due, in part, to the inherent assumption in the derivation of the 4/9 factor that the M - L distances must remain the same in the octahedral and tetrahedral species. Furthermore, if the ligand changes from unidentate to bidentate then this too would invalidate this type of calculation.

Whilst the calculations listed above have consistently been carried out using the arithmetic centres of the split bands, McClure (113) in his study of the $[Co(NH_3)_n X_{6-n}]^{(3-n)-}$ systems used the fact that the T state was split into

two components of unequal intensity, to determine the baricentre. It was implied that a transition to an E state would be more intense than a transition to an A state. If this procedure is applied to the Li_2SO_4 - Na_2SO_4 - K_2SO_4 melt spectrum, then the assignment is as shown in Figure 4.15 for the octahedral case. A similar result is obtained for the tetrahedral case except that the levels $^4A_2(F)$ and $^4T_1(F)$ are reversed.

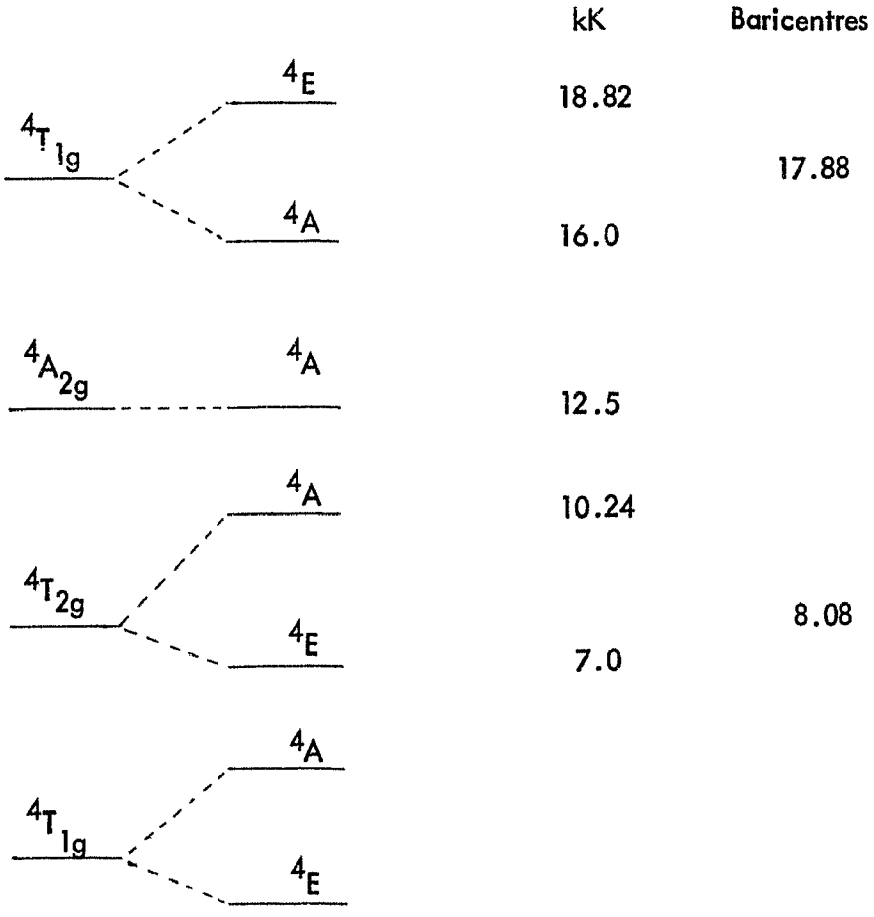

Figure 4.15

Energy level diagram for a distorted octahedral Co(II) complex

Then by using the appropriate energy expressions, equations 4.1 and 4.2, the values of Δ and B listed in Table 4.15 are obtained.

Table 4.15

Ligand field parameters for Co(II) in Li_2SO_4 - Na_2SO_4 - K_2SO_4 at 550°C

	Δ kK	B cm^{-1}
O_h	6.73	869
T_d	4.68	795

Similar energy level diagrams can be obtained for the other Co(II) species considered earlier and the ligand field parameters evaluated. However, for purposes of comparison it is perfectly possible to retain the concept of an arithmetic mean provided that this same procedure is applied to all the systems within the group being compared. Both the sets of parameters in Table 4.15 are quite reasonable for their respective symmetries and it might be argued that the octahedral values are an embarrassment in view of the previous arguments in favour of a tetrahedral or distorted tetrahedral species. However, it must be emphasised once again that all the factors defining a spectrum should be taken into account and, on this basis, a distorted tetrahedral model gives the best fit for all the spectral features.

4.4.3 Co(II) In Other Sulphate Containing Media. As was mentioned earlier, during the course of the investigations reported in this thesis, Duffy et al. (89) reported their results on Ni(II) and Co(II) in sulphate containing media. Only the Co(II) results will be discussed here. (The results for the Ni(II) system will be considered in Chapter VI.) The primary purpose of their work was an attempt to further characterise the cobalt species in concentrated sulphuric acid which they had

previously studied (88).

The approach they chose was to investigate the spectra of Co(II) in the following media:

a. K_2SO_4 - $ZnSO_4$ glass at 25°C.

b. $NaHSO_4$ - $KHSO_4$ glass and melt over the temperature range 25° - 230°C.

c. 98% H_2SO_4 at 25° and 190°C.

The results obtained were compared with the spectrum of Co(II) in the Li_2SO_4 - Na_2SO_4 - K_2SO_4 eutectic melt as reported by Johnson and Piper (87).

Table 4.16 contains the results as quoted by Duffy et al. The effect of temperature on the spectrum in $NaHSO_4$ - $KHSO_4$ is reproduced in Figure 4.16, (by kind permission of the author).

TABLE 4.16

Spectral results for Co(II) in sulphate media reported by Duffy (24).

Li_2SO_4-Na_2SO_4-K_2SO_4 550°C		K_2SO_4-$ZnSO_4$ Glass, 25°C		H_2SO_4 25°C		H_2SO_4 190°C		$NaHSO_4$-$KHSO_4$ 25°C		$NaHSO_4$-$KHSO_4$ 190°C	
ν	ε	ν	ε	ν	ε	ν	ε	ν	ε	ν	ε
		13.6	0.9	13.0	0.5			13.1	0.4		
17.1	94	17.5	30	18.4	11.0	17.4	21	18.4	13.0	17.3	31
19.0	83	18.6sh		20.5sh		20.5sh		20.5sh		18.6sh	

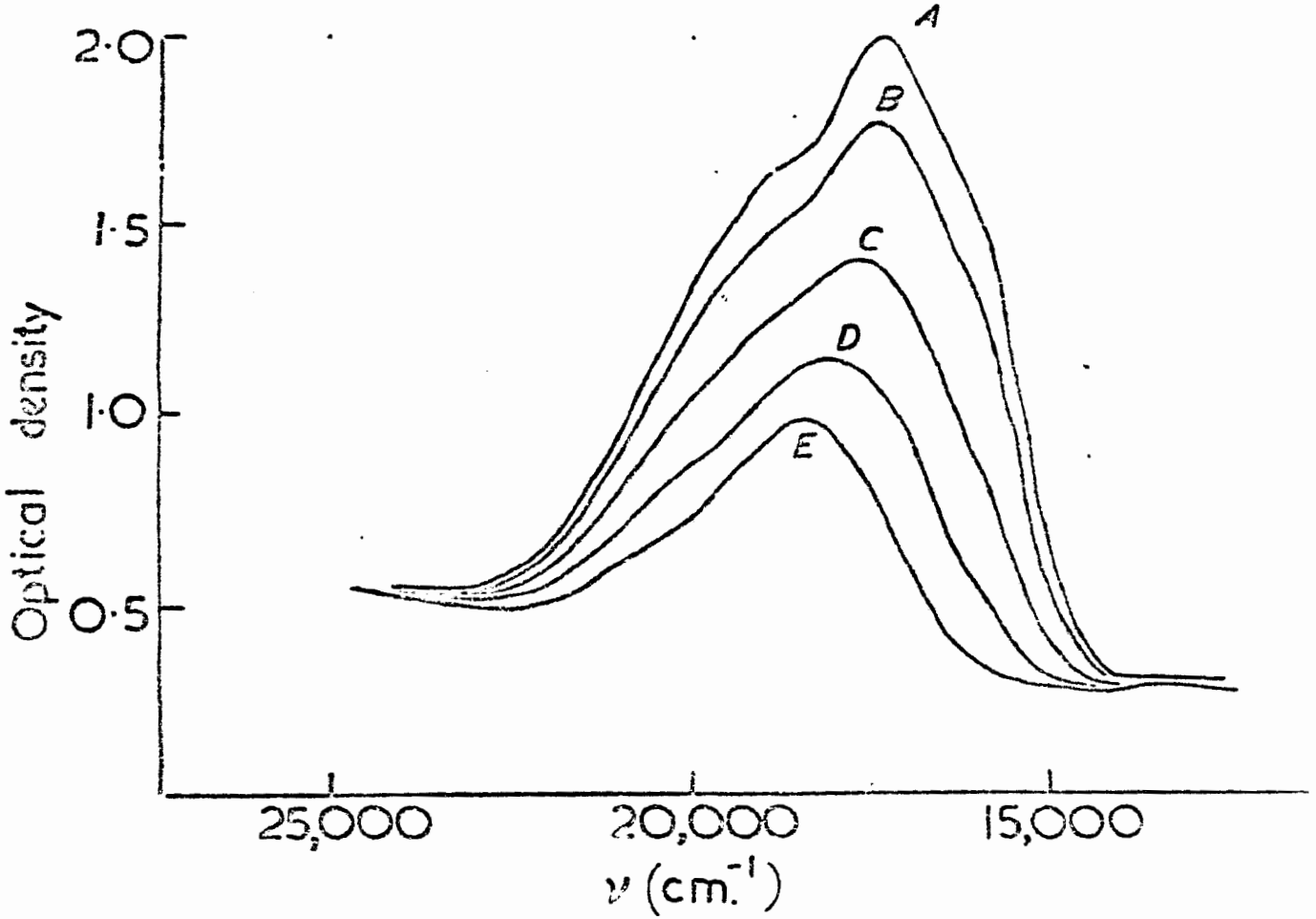

Figure 4.16

Spectra of Co(II) in $NaHSO_4$ - $KHSO_4$ as a function of temperature (reproduced from reference 89 with permission)

The results for the sulphuric acid spectra can be compared with those found in the present investigation. These band positions and extinction maxima may be obtained from Figure 4.8, and are found to be as follows (Table 4.17).

Table 4.17

Spectra of Co(II) in 98% H_2SO_4 at 12° and 199°C

12°C		199°C	
ν	ε	ν	ε
13.4	0.25	12.0	0.5
18.35	10.9	17.6	14.9
20.5 sh		20.3 sh	

It can be seen that the two sets of results are in substantial agreement except that there is a difference in extinction coefficient at 199°C.

There is a discrepancy between the results for the hydrogen sulphate melt at 230°C, reported in Table 4.16, and the spectrum as reproduced in Figure 4.16. The spectrum clearly shows the presence of an 'anomalous' shoulder located at ~ 15.8 kK. Furthermore, the results of Johnson and Piper (87) were quoted with the 'anomalous' shoulder, which occurred at 16.1 kK in this case, being omitted.

By comparing the spectrum of Co(II) in the K_2SO_4 - $ZnSO_4$ glass with that for the 98% H_2SO_4, Duffy concluded that the cobalt species present in the glass was octahedral but since the absoprtion maximum was at 17.5 kK, with $\varepsilon = 30$ for the sulphate glass, compared to 18.4 kK, with $\varepsilon = 11$, for the sulphuric acid, both at 25°C, it was suggested that Co(II) could form two distinct octahedral complexes with sulphate as the ligand. Apparently in sulphuric acid the behaviour of sulphate as a ligand had been modified, presumably by protonation.

The suggestion was made that the spectrum in K_2SO_4 - $ZnSO_4$ glass was similar to that obtained in the hydrogen sulphate melt at 230°C. Furthermore, the hydrogen sulphate glass spectrum at 25°C was the same as that for the sulphuric acid solution at 25°C and also the spectrum in the sulphuric acid, over the temperature range 25° - 190°, underwent a similar shift to that observed for the hydrogen sulphate system over the same temperature range.

The authors offered two explanations to account for these results. Firstly, protonation of the sulphate ligands was possible at either of two different oxygen sites: the donor oxygen atom or the outer oxygen atom. Protonation of the donor oxygen would be expected to affect the crystal field experienced by the Co(II) to a greater extent than protonation of the outer oxygens. Then, on this basis, the hydrogen sulphate melt at 230°C contained an octahedral complex with outer oxygen protonation and was similar to the complex in the K_2SO_4 - $ZnSO_4$ glass. Protons were then assumed to migrate to the inner oxygens as the temperature dropped and thus the band positions moved to higher energy. Duffy et al. rejected this explanation on the grounds that it should be very sensitive towards the acidity of the solvent, which they had not found to be the case, in as much as the temperature effect was very similar for both the sulphuric acid and the hydrogen sulphate media.

The preferred second explanation utilised the ability of sulphate to act either as a bidentate or a monodentate ligand. The suggestion was that at high temperatures the sulphate acted as a bidentate group but as the temperature was lowered it changed from bidentate to monodentate, with the increased charge being counteracted by protonation. The conversion in the K_2SO_4 - $ZnSO_4$ glass apparently did not

occur, due either to the absence of protons or the rigidity of the medium preventing the attainment of equilibrium. This conclusion of Duffy et el., namely that the species in the K_2SO_4 - $ZnSO_4$ glass at 25°C represented the bidentate, 'high temperature' form, as found in the other media, is important when compared with work reported later (p. 141).

There are two points concerning these results and their interpretation:

(i) The hydrogen sulphate melt spectrum at 230°C bears a marked resemblance to the spectrum in the Li_2SO_4 - Na_2SO_4 - K_2SO_4 eutectic melt at 550°C, cf:

	kK		
$NaHSO_4$ - $KHSO_4$	15.8	17.3 (31)	18.6 (sh)
Li_2SO_4 - Na_2SO_4 - K_2SO_4	16.1	17.1 (93.5)	19.0 (83)

(ii) The spectrum in the K_2SO_4 - $ZnSO_4$ glass at 25°C is similar to the hydrogen sulphate spectrum at 180°C (Spectrum C in Figure 4.16) rather than the spectrum at 230°C (Spectrum A in Figure 4.16). Figure 4.17, which contains the spectrum of Co(II) in the K_2SO_4 - $ZnSO_4$ glass at 14°C, allows this comparison to be made.)

As a result of this report by Duffy et al., further work on the Co(II) system was undertaken. This consisted of the following experiments:

(a.) An investigation of the Co(II) spectrum in K_2SO_4 - $ZnSO_4$ over the range 25°C to 600°C.

(b.) An investigation of the Co(II) spectrum in the Na_2SO_4 - K_2SO_4 - $ZnSO_4$ eutectic over the temperature range 420° - 620°C. This particular eutectic was chosen because it was found that the lowest temperature at which a spectrum could

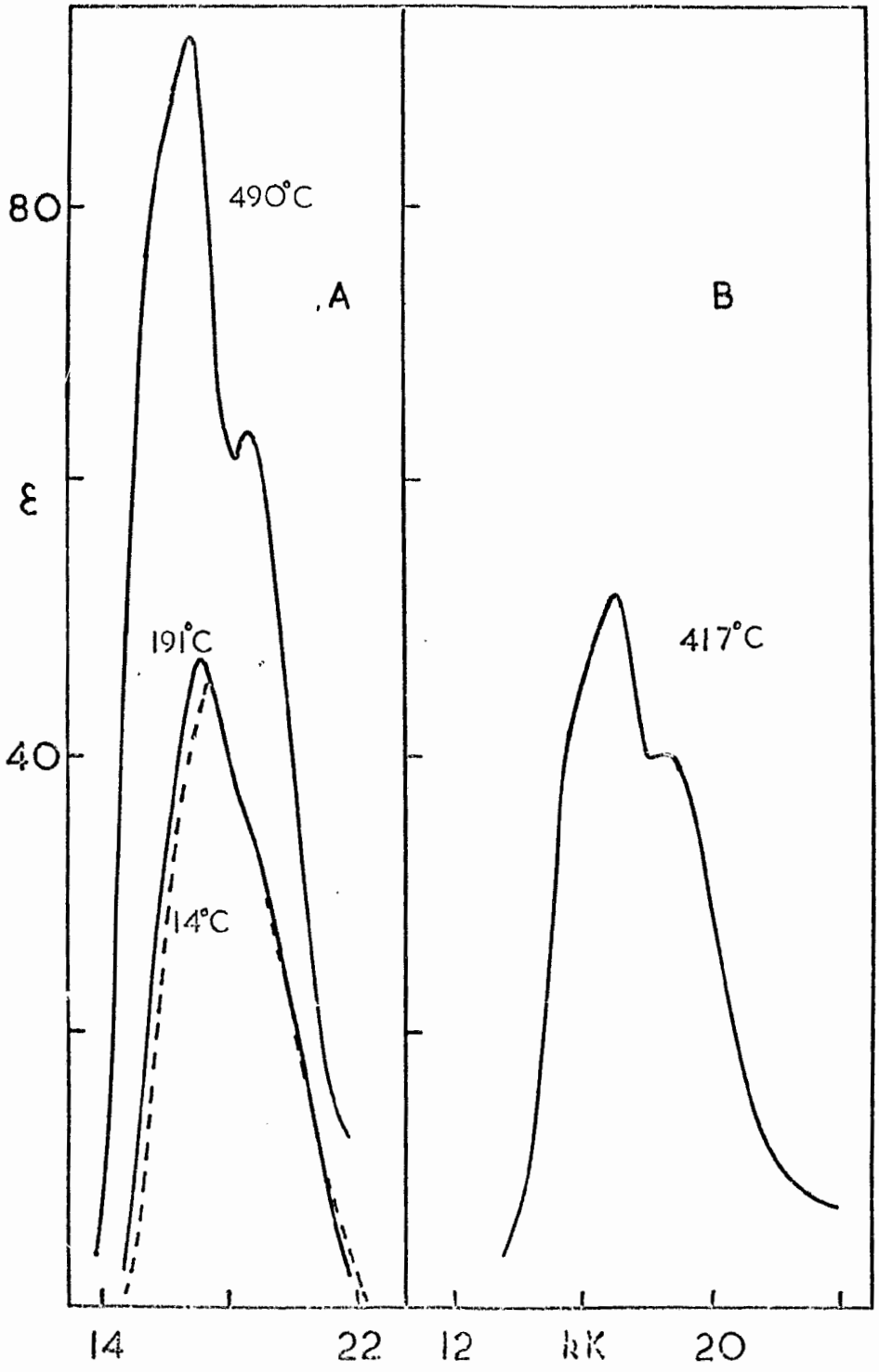

Figure 4.17

A. Spectrum of Co(II) in K_2SO_4 - $ZnSO_4$ at 14°, 191°, and 490° C

B. Spectrum of Co(II) in Na_2SO_4 -K_2SO_4 - $ZnSO_4$ at 417° C

be recorded for the K_2SO_4 - $ZnSO_4$ melt was approximately 500°C. Furthermore, despite the fact that this latter melt could be quenched to form a glass, the spectrum could not be obtained in the temperature range 200° - 500°C since the glass began to nucleate above 200°C. The Na_2SO_4 - K_2SO_4 - $ZnSO_4$ eutectic was chosen because its lower melting point of 382°C (114) allowed spectral measurements to be made at slightly lower temperatures.

(c.) It was decided to investigate the NMR spectrum of Co(II) dissolved in 98% H_2SO_4 at low temperatures in an attempt to rule out the first explanation offered by Duffy et al.

The spectrum of Co(II) in K_2SO_4 - $ZnSO_4$ at 14°, 191° and 490°C is shown in Figure 4.17A. The band positions, band maxima and oscillator strengths are listed in Table 4.18 for the resolved bands.

Table 4.18

Temperature dependence of the spectrum of Co(II) in a K_2SO_4 - $ZnSO_4$ melt

Temperature °C	ν(kK)	(ε)	ν (kK)	(ε)	f
14	17.42	(45.2)	18.9 (sh)	(33)	8.1×10^{-4}
191	17.21	(46.8)	18.7 (sh)	(34)	8.7×10^{-4}
580	16.81	(92.4)	18.66	(63.6)	1.97×10^{-3}

The oscillator strengths, f, in the table refer to the total intensity of the visible band. Although spectra were recorded at temperatures between 14° and 191°, they are not reported, since only a very gradual change took place over this temperature range.

The results for the Na_2SO_4 - K_2SO_4 - $ZnSO_4$ eutectic melt over the temperature range 417° - 620°C were very similar, the only difference being that the band maxima moved to slightly lower energy as the temperature was raised. The actual movement over the temperature range in question was approximately 0.3 kK. The spectrum at 417°C is shown in Figure 4.17B.

The spectrum in the K_2SO_4 - $ZnSO_4$ at 14°C bears a marked resemblance to that obtained by Duffy et al. (Table 4.16), the only real difference being the value of the extinction coefficient.

By comparing the melt spectra in Figures 4.17A and 4.17B, it can be concluded that the cobalt species is the same in both melts. Furthermore, these two spectra are very similar to the spectra in the hydrogen sulphate melt at 230°C (Figure 4.16), and the Li_2SO_4 - Na_2SO_4 - K_2SO_4 eutectic melt at 550°C (Figure 4.11). The total oscillator strength of the visible band for the four melts is shown in Table 4.19.

Table 4.19

Oscillator strengths for the spectra of Co(II) in various sulphate containing melts

Melt	T °C	f
Li_2SO_4 - Na_2SO_4 - K_2SO_4	550	1.76×10^{-3}
Na_2SO_4 - K_2SO_4 - $ZnSO_4$	417	1.25×10^{-3}
K_2SO_4 - $ZnSO_4$	580	1.97×10^{-3}
$NaHSO_4$ - $KHSO_4$	230	0.9×10^{-3}

The result for the hydrogen sulphate melt was estimated from Figure 4.16. By virtue of the arguments put forward in the discussion of the Li_2SO_4 - Na_2SO_4 - K_2SO_4 results, it is suggested that the cobalt species in these melts has a distorted

tetrahedral shape.

Since the spectrum of Co(II) in the K_2SO_4 - $ZnSO_4$ melt is very similar to that of the $NaHSO_4$ - $KHSO_4$ melt at 230°C, it is obvious that the Co(II) species in the K_2SO_4 - $ZnSO_4$ glass at 25°C cannot be the 'high temperature' form as postulated by Duffy et al. These workers were apparently misled on this point by the very large value of the oscillator strength for the visible band in the glass spectrum. Certainly a value of ~ 8×10^{-4} is rather large for an octahedral complex, but as discussed earlier, the whole problem of intensities in melts, (a glass can be regarded as a supercooled melt), is not at all well understood.

The results for the $NaHSO_4$ - $KHSO_4$ system can then be interpreted as a change from octahedral at low temperature, (Curve E of Figure 4.16 is identical to the spectrum of Co(II) in 98% sulphuric acid shown in Figure 4.8), to a species which may be described as distorted tetrahedral at high temperatures. The species in the hydrogen sulphate melt at 180°C (Spectrum C in Figure 4.16) is very similar to the spectrum in 98% H_2SO_4 at 194°C (Figure 4.8) and would presumably have the same type of distortion. The change from octahedral to tetrahedral can be described in several ways of which the following is an example:

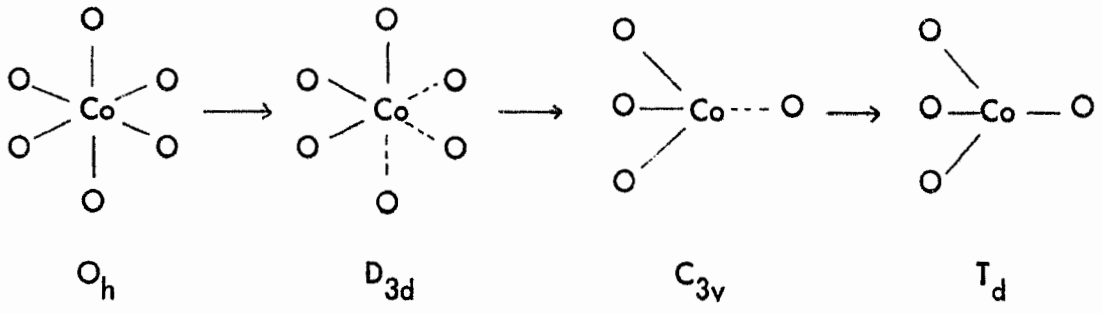

This distortion mechanism is compatible with the previous discussion. Thus it was shown earlier that the species in 98% sulphuric acid at 472°K could be described as D_{4h}, D_{3d}, or D_{2d} and also that the species in the Li_2SO_4 - Na_2SO_4 - K_2SO_4 eutectic melt at 550°C could be described as C_{3v} or D_{2d} on the tetrahedral model.

According to the first explanation of Duffy et al. the low temperature form of the cobalt complex in 98% H_2SO_4 must contain the hydrogen bonded to the inner oxygen atom. Now Robinson and Stokes (115) have summarised the experimental results of studies on the H_2SO_4 - H_2O system which showed that at 98% H_2SO_4 the solution is approximately 9M in HSO_4^-, $H_3SO_4^+$ and H_2SO_4, the first two species arising from the autoprotolysis reaction:

$$2H_2SO_4 \rightleftharpoons H_3SO_4^+ + HSO_4^-$$

Taking this solvent reaction into account, it can be seen that there are five different proton environments present, which, in theory at least, should give rise to five different resonance frequencies. These environments are as follows:

(a) Undissociated H_2SO_4

(b) Free $H_3SO_4^+$

(c) Free HSO_4^-

(d) Complexed HSO_4^-, inner oxygen protonation

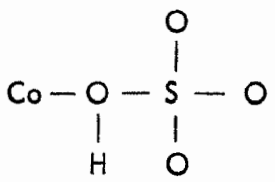

(e) Complexed HSO_4^-, outer oxygen protonation

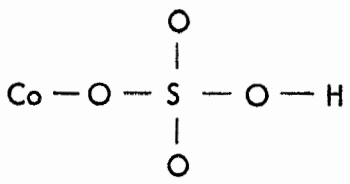

On consideration, it would be expected that the species (a), (b), (c) and (e) would give rise to lines at similar frequencies, whereas species (d) would be quite different.

It was found earlier (p.106), in the magnetic susceptibility measurements, that only one resonance line for the paramagnetic solution was obtained at room temperature. This is almost certainly due to the fact that at this temperature rapid proton exchange between the various species is taking place, thereby giving only one line. In cases of this sort, the usual procedure is to cool the sample down thereby slowing the rate of exchange and allowing separation of the different resonant frequencies. Accordingly, a 0.02M Co(II) solution in 98% H_2SO_4, to which some $(Me_4N)HSO_4$ was added, was placed in an NMR sample tube. The NMR spectrum was recorded at a series of temperatures between $+40^\circ C$ and $-30^\circ C$. As the temperature decreased the peak due to the solvent became broader and broader, but it was not possible to resolve it. Furthermore, only one peak was observed, although the full range of the instrument was scanned. This result would apparently rule out the existence of the protonated inner oxygen type complex, thereby disproving the first hypothesis put forward by Duffy et al.

With the data at present available it is not possible to determine whether the sulphate groups are acting as uni- or bidentate ligands. An integral part of this problem lies in assigning relative positions, within the spectrochemical series, to

these essentially different sulphate ligands. Certainly, complexes which have been shown, usually by IR study of the sulphate vibrations, to contain sulphate acting as a uni- or bidentate or as a bridging ligand are well known (116, 117). However, these complexes have invariably had other ligand groups, usually NH_3, present at the same time,which thereby renders the relative values of Δ meaningless for the present purpose. In the only well-characterised compound of Co(II) containing only sulphate ligands, namely anhydrous cobalt sulphate, the sulphate acts as a bridging ligand. In the sulphate melt systems it seems unlikely that the sulphate groups would act in this fashion.

The solution to the problem would appear to lie in the entropy term involved in the chelate effect. A possible appraoch to this problem would be to use the electrode potential measurements of Johnson and Laitinen (118) to obtain a Δ G value for the reaction:

$$Co \longrightarrow Co(II) \text{ complexed}$$

in the Li_2SO_4 - Na_2SO_4 - K_2SO_4 eutectic melt. This would then have to be compared with values calculated for the hypothetical reactions:

Co	$\longrightarrow$	$Co(SO_4)_6^{10-}$	O_h	Unidentate
Co	$\longrightarrow$	$Co(SO_4)_3^{4-}$	O_h	Bidentate
Co	$\longrightarrow$	$Co(SO_4)_4^{6-}$	T_h	Unidentate
Co	$\longrightarrow$	$Co(SO_4)_2^{2-}$	T_d	Bidentate

The final conclusion concerning the Co(II) species in sulphate media is as follows: In concentrated sulphuric acid at temperatures up to ~ 160°C and in the hydrogen sulphate melt up to ~ 150°C, the species is almost certainly octahedral.

As the temperature is increased, the species distorts until, at 230°C, it is the same as in the sulphate melts. The identity of this latter species has not been confirmed absolutely, but it would seem to be so severly distorted that it can be described on either a tetrahedral or an octahedral basis.

4.5 Experimental. The solutions for the aqueous and sulphuric acid spectra were prepared from a stock solution of $CoSO_4 \cdot 7H_2O$ (Baker Analysed Reagent) in water. In the case of the 75% and 98% sulphuric acid solutions, it was found that precipitation occurred very easily. It order to obtain solutions containing sufficient cobalt it was necessary to add the required amount of a saturated aqueous $CoSO_4 \cdot 7H_2O$ solution to the sulphuric acid solution cooled in an ice bath. In this way solutions that were stable for a few hours were obtained. The spectra were recorded using a Beckmann DK2A instrument. Aliquots for analytical purposes were obtained at the same time. Cobalt analyses were performed by the EDTA titration method (119) using murexide as an indicator. Sulphate was determined gravimetrically as barium sulphate.

Cobalt sulphate monohydrate was prepared by heating the seven hydrate in air at 120°C overnight. In order to prepare the anhydrous cobalt sulphate, it was found necessary to heat the seven hydrate at 150°C and $\sim 10^{-2}$ mm. of Hg overnight. Analyses for sulphate in both cases confirmed the products. The reflectance spectra of these compounds were obtained using a Beckmann DU spectrometer fitted with a standard reflectance assembly and using magnesium carbonate as a standard.

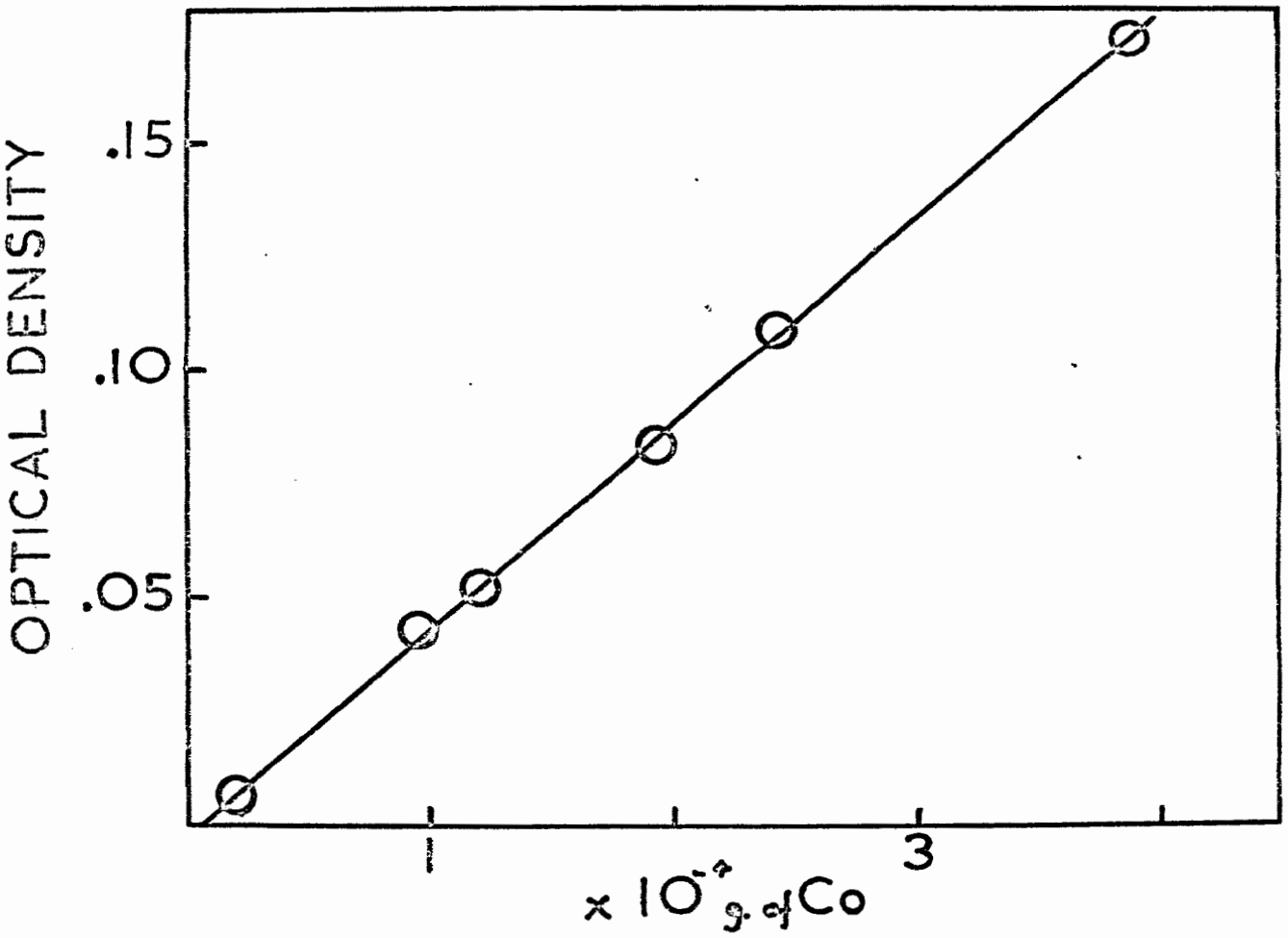

Figure 4.18

Plot of optical density versus cobalt molarity for the Co/SCN^- analytical method

For the eutectic melt solution, the total amount of cobalt present was rather small. Johnson and Piper (87) used the EDTA titration method to determine cobalt, but had some difficulties observing the end point. It was decided, therefore, to use another method and that finally chosen was a colourimetric determination using thiocyanate (120). The colour was developed by adding chlorostannous acid, followed by acetone and then KSCN, and was measured at 625m μ using the Beckmann DU spectrometer. Standard solutions containing $CoSO_4 \cdot 7H_2O$ were prepared and a plot of optical density versus cobalt molarity was obtained. The resulting graph, Figure 4.18, shows that over the concentration range studied, Beer's Law was obeyed. This graph was then used to determine the amount of cobalt present in the known weight of the frozen eutectic. The density of the eutectic melt was taken to be 2.13 g/ml and it was assumed that this was the same for the Co solution as for the pure melt. Molar extinction coefficients were then calculated.

For the case of the Li_2SO_4 - Na_2SO_4 - K_2SO_4 and the Na_2SO_4 - K_2SO_4 - $ZnSO_4$ melts, the spectra were recorded with solvent in the reference beam of the Beckmann DK2A spectrophotometer. Due to the difficulty in obtaining an isotropic glass for the K_2SO_4 - $ZnSO_4$ system, the reference was an empty silica cell. However, the spectrum of the solvent was obtained over the temperature range 14° - $580^\circ C$, and was subtracted from the spectra obtained with the solution containing Co(II). The densities of the glasses and melts containing $ZnSO_4$ were measured (see Appendix C for details) and the values listed in Table 1 in Appendix C were used to calculate the molar extinction coefficients.

CHAPTER 5

SPECTRA OF Rh AND Ir IN FUSED CHLORIDE AND SULPHATE MEDIA

5.1 Introduction. The most common oxidation state for rhodium is Rh(III) which occurs in a wide range of octahedral complexes. In the case of iridium, whilst an oxidation state of four is quite important, Ir(III) complexes are still common and, for reasons stated later, only this latter oxidation state will be considered in the following discussion. Both these ions have a d^6 configuration and for the ligands of interest, viz. Cl^- and SO_4^{2-}, give rise to low spin complexes. The Tanabe-Sugano diagram (16) for d^6 predicts the following transitions:

$$^3T_{1g} \leftarrow {}^1A_{1g} \qquad \Delta - 3C \quad (+50B^2/\Delta)$$

$$^3T_{2g} \leftarrow \qquad \Delta + 8B - 3C \quad (+14B^2/\Delta)$$

$$^1T_{1g} \leftarrow \qquad \Delta - C \quad (+86B^2/\Delta)$$

$$^1T_{2g} \leftarrow \qquad \Delta + 16B - C \quad (+2B^2/\Delta)$$

$$^5T_{2g} \leftarrow \qquad 2\Delta - 5B - 8C \quad (+120B^2/\Delta)$$

The energy expressions quoted for each transition were obtained from the compilation of Jørgensen (27). The expressions in brackets arise because there are several states which have the same symmetry classification present and these interact and modify the energies. The bracketed terms were taken from a review article by Jørgensen (15). The procedure used to calculate values of Δ and B deserves description. B is calculated by letting the energy difference between the two spin-allowed bands be 16B. Each of the band energies is then divided by B to give a series of E/B

values which are then fitted to the Tanabe-Sugano diagram from which a value for Dq/B can be found. A corrected B value can be obtained using the value of 10 Dq (=Δ) found above in the complete expression for the energy difference between the spin-allowed bands, which is:

$$16B - \frac{84B^2}{\Delta}$$

With this corrected B value the previous steps are repeated so as to yield a corrected value of Δ . This new value of Δ is then used to find a second corrected value of B and the entire procedure repeated until B and Δ no longer change. The final corrected values of B and Δ are checked for consistency by calculating the energy difference between the two spin-allowed bands. The last step in the calculation is to predict the positions of the two spin-forbidden bands. As with the majority of ligand field calculations, at least one assumption has been made in order to obtain the correction terms listed above. In this case it was assumed that C = 4B, an approximation often made and which is based essentially upon experience.

As with a large number of the 4d and 5d hexahalo complexes, the first spectral investigation reported has been that of Jørgensen (53, 121).

The results for $RhCl_6^{3-}$ are listed in Table 5.1 together with the results obtained by other workers.

Table 5.1

Spectra of $RhCl_6^{3-}$ in aqueous HCl solutions

ν(kK)	ε	ν (kK)	ε	ν(kK)	ε
14.7	3				
19.3	102	19.3	111.5	19.3	109
24.3	82	24.0	93.8	24.4	98
39.2	30,000				
	(53, 121)		(122)		(3)

Substantial agreement is observed for the visible bands at least, both for position and intensity. The first weak band, however, is not always observed. In his first paper (121) Jørgensen discusses the assignment of the first three bands and suggests that this should be as follows:

$^3T_{1g} \longleftarrow {}^1A_{1g}$	14.7 kK
$^1T_{1g} \longleftarrow$	19.3
$^1T_{1g} \longleftarrow$	24.3

On considering the transitions predicted from the Tanabe-Sugano diagrams, two points emerge. Firstly, the second spin-forbidden transition is not observed and, secondly, the singlet-quintet transition is also missing. Both of these missing bands are almost certainly hidden by the more intense spin-allowed bands. Using Jørgensen's assignment, the values of Δ and B may be calculated by the procedure outlined above and are found to be 20.3 kK and 340 cm^{-1} respectively. The check on the consistency of these values, given by evaluating $16B - 84B^2/\Delta$, gives a value of 5 kK which is identical to the experimental value for the energy difference between the spin-allowed bands. The spin-forbidden bands are predicted, using the above values of Δ and B, to lie at 15.5 and 18.1 kK. The agreement between the calculated and experimental band position for the first spin-forbidden band is not perfect. The discrepancy almost certainly arises because of the assumption that $C = 4B$ mentioned earlier, since, as the energy expressions quoted show, the spin-forbidden transitions contain a term 3C whilst the spin-allowed transitions contain C only. Thus, if the value of C is too low, i.e. C should be greater than 4B, then the spin-forbidden bands will be predicted to lie at energies higher than experimentally

found. The discrepancy will not be as large for the spin-allowed bands. The predicted position of the second spin-forbidden band is quite close to the spin-allowed band at 19.3 kK and confirms the explanation offered above for the absence of this band from the observed spectrum. It seems, therefore, that, within the limitations imposed by the calculations, the assignment suggested by Jørgensen is almost certainly correct. That the species giving rise to the spectra reported in Table 5.1 is, in fact, $RhCl_6^{3-}$ has been confirmed by Wolsey et al. (122) using an ion-exchange technique to determine equilibrium constants in the Rh(III) - Cl^- - H_2O system.

The spectrum of $IrCl_6^{3-}$ has not received a great deal of attention. Some of the results available for spectra recorded in aqueous media are listed in Table 5.2.

Table 5.2

Spectra of $IrCl_6^{3-}$ in aqueous HCl solutions

ν	ε	ν	ε
16.3	7		
17.9	10	17.4	9.8
24.1	76	24.1	88
28.1	84	28.2	69
48.5	28,000		
	(121)		(123)

Once again, the results are in substantial agreement, although it must be pointed out that the band positions and extinction coefficients obtained from reference (123) were estimated from the published spectrum. An assignment of the bands listed in Table 5.2 has been put forward by Jørgensen (121) along the same lines as for

$RhCl_6^{3-}$, except that two spin-forbidden bands are now observed. The complete assignment is therefore:

$^3T_{1g}$	$\leftarrow$ $^1A_{1g}$	16.3 kK
$^3T_{2g}$	$\leftarrow$	17.9
$^1T_{1g}$	$\leftarrow$	24.1
$^1T_{2g}$	$\leftarrow$	28.1

If the procedure outlined above is carried out using this assignment, then the values of Δ and B are found to be 24.9 kK and 265 cm^{-1} respectively. The calculated separation of the two spin-allowed bands is found to be 0.08 kK larger than the experimental value using the above values of Δ and B. The two spin-forbidden transitions are predicted to lie at 21.5 and 24.04 kK. The agreement is much worse than for the $RhCl_6^{3-}$ case and the same explanation may be put forward. However, an alternative and probably more correct description of the spectrum of $IrCl_6^{3-}$ has been put forward by Schroeder (124). Using the fact that, on going from 3d through 4d to 5d, the electronic coupling departs from the L - S variety and approaches a j - j type, Schroeder calculated the energy levels appropriate to Ir(III) in the intermediate coupling scheme. The results that were obtained show that in intermediate coupling the singlet terms remain unchanged, whilst the triplet terms are split into four levels. The spin-forbidden bands, therefore, should show considerable fine structure, a result which is not obtained for the spectra in aqueous solution listed in Table 5.2, although Schroeder does assign the two weak bands observed by Jørgensen to transitions to the components of $^3T_{1g}$. It is almost certain that this particular scheme would be essential to interpret low temperature single crystal spectra

of Ir(III) compounds, in which there is a likelihood of obtaining better band resolution. However, Schroeder's calculations give no better agreement with experiment, for the spin-allowed bands, than the assignment and calculation of Jørgensen. It is interesting to compare the ligand field parameters obtained by Jørgensen and by Schroeder, since Schroeder used the band positions found by Jørgensen, so that the two different calculations had a common starting point. The results are as follows:

	Δ kK	B cm^{-1}	C cm^{-1}	ζ cm^{-1}
Jørgensen	24.9	265	(1060)	-
Schroeder	22.75	338	1520	2820

The value of C quoted in Jørgensen's results was obtained from the assumption C = 4B. The difference between the two approaches involves, in the main, the values of B and C. It would seem, therefore, that the gross features of the spectrum of $IrCl_6^{3-}$ can be described within the L - S coupling scheme, although finer details of the spin-forbidden bands must be described by an intermediate type of coupling scheme. The results reported later for the melt spectra will be discussed using the assignment suggested by Jørgensen.

It has been implied in the previous discussion that the species which are to be discussed in conjunction with the spectral results are complexed forms of Rh(III) and Ir(III). That this is, in fact, true was known before the spectral investigations were initiated, as a result of electrochemical studies. These studies showed that in the chloride eutectic the stable species were Rh(III) and Ir(III) and for the ternary sulphate melt Rh(III) was stable in solution (see reference 125 for original papers.) An attempt to anodise Ir in the sulphate melt and thus obtain the redox potential and the oxidation state was unsuccessful (126).

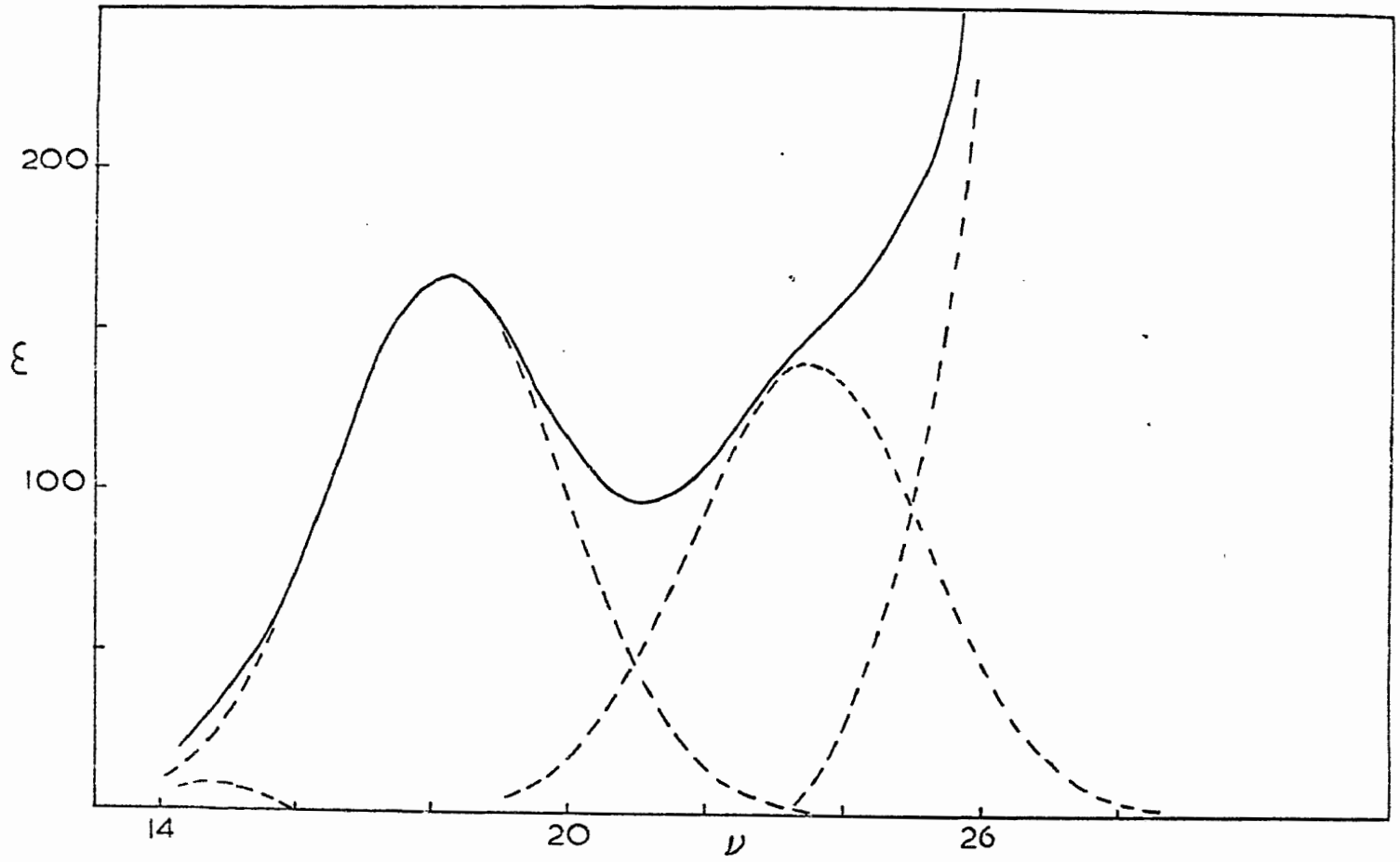

Figure 5.1

Spectrum of Rh(III) in LiCl - KCl at 450° C

5.2 Results. The spectrum of Rh(III) in the LiCl - KCl eutectic recorded at 450°C is shown in Figure 5.1 together with the Gaussian components obtained as described in Appendix A. The band positions and extinction coefficients are listed in Table 5.3.

Table 5.3

Band positions for Rh(III) in the LiCl - KCl melt at 450°C

ν	ε
14.8	8
18.2	167
23.5	140

The values of Δ, B and the predicted positions of the spin-forbidden bands, obtained by the method outlined earlier, are listed in Table 5.4.

Table 5.4

Ligand field parameters for $RhCl_6^{3-}$

	LiCl - KCl	Aqueous HCl
Δ (kK)	19.3	20.3
B (cm^{-1})	370	340
$^3T_{1g} \longleftarrow {}^1A_{1g}$	14.5	15.5
$^3T_{2g} \longleftarrow {}^1A_{1g}$	17.4	18.1

The results for the aqueous HCl spectrum discussed earlier are also included in Table 5.3 to facilitate comparison.

Tables 5.5 and 5.6 contain the corresponding results for Ir(III), whilst the spectrum is shown in Figure 5.2.

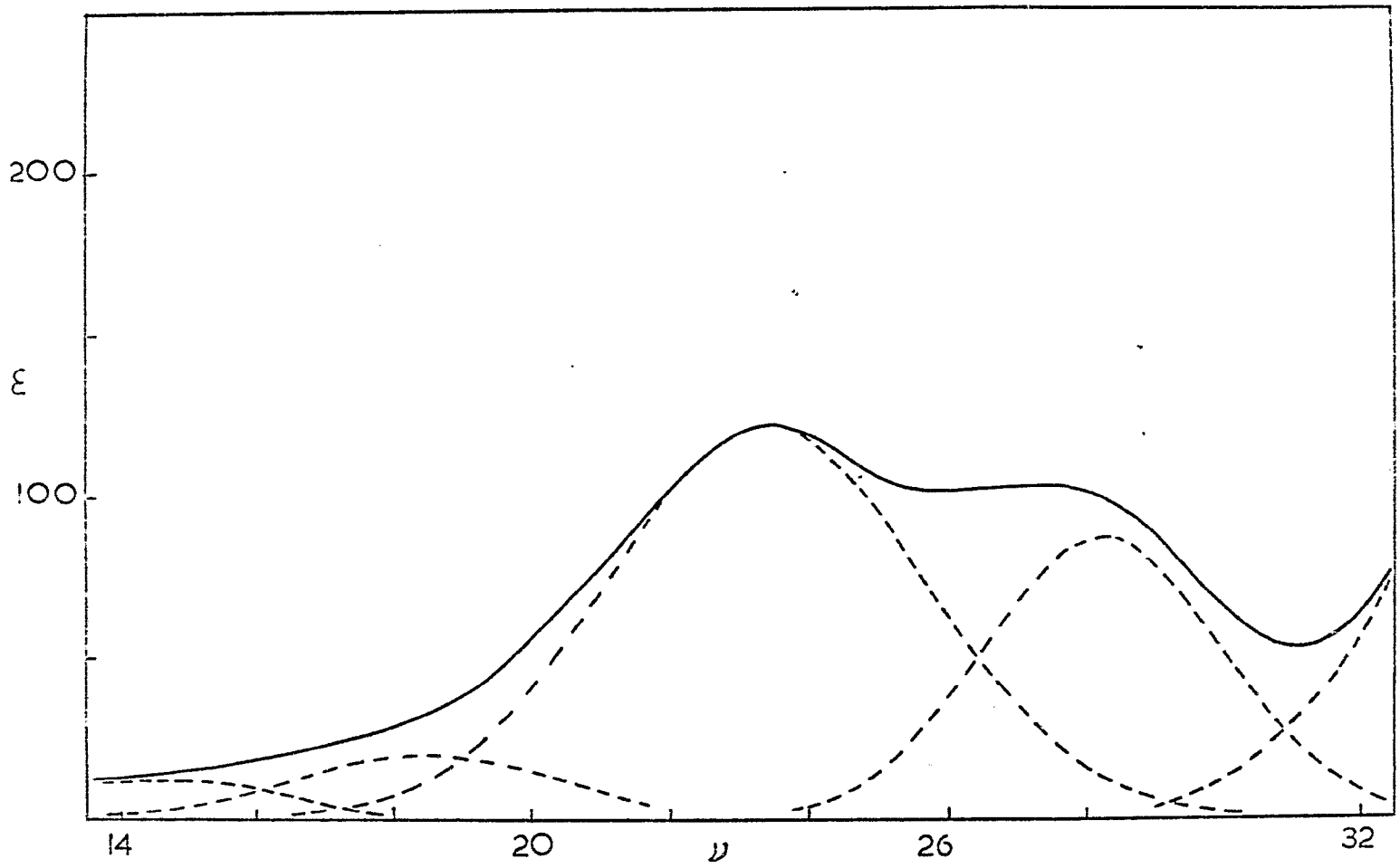

Figure 5.2

Spectrum of Ir(III) in LiCl - KCl at 450° C

Table 5.5

Band positions for Ir(III) in the LiCl - KCl eutectic at 450°C

ν (kK)	ε
15.0	12
18.5	20
23.4	121
28.1	86.5

Table 5.6

Ligand field parameters for $IrCl_6^{3-}$

	LiCl - KCl	Aqueous HCl
Δ (kK)	24.7	25.0
B (cm^{-1})	300	270
$^3T_{1g} \leftarrow {}^1A_{1g}$	20.5	21.5
$^3T_{2g} \leftarrow {}^1A_{1g}$	23.4	24.0

The spectrum of Rh(III) in the Li_2SO_4 - Na_2SO_4 - K_2SO_4 eutectic at 550°C is shown in Figure 5.3. Unlike the chloride melt, no indication of the second spin-allowed band is discernible even after a Gaussian analysis. The band positions and extinction coefficients are listed in Table 5.7.

Table 5.7

Band positions for Rh(III) in Li_2SO_4 - Na_2SO_4 - K_2SO_4 at 550°C

ν	ε
12.4	3
18.5	12
21	150

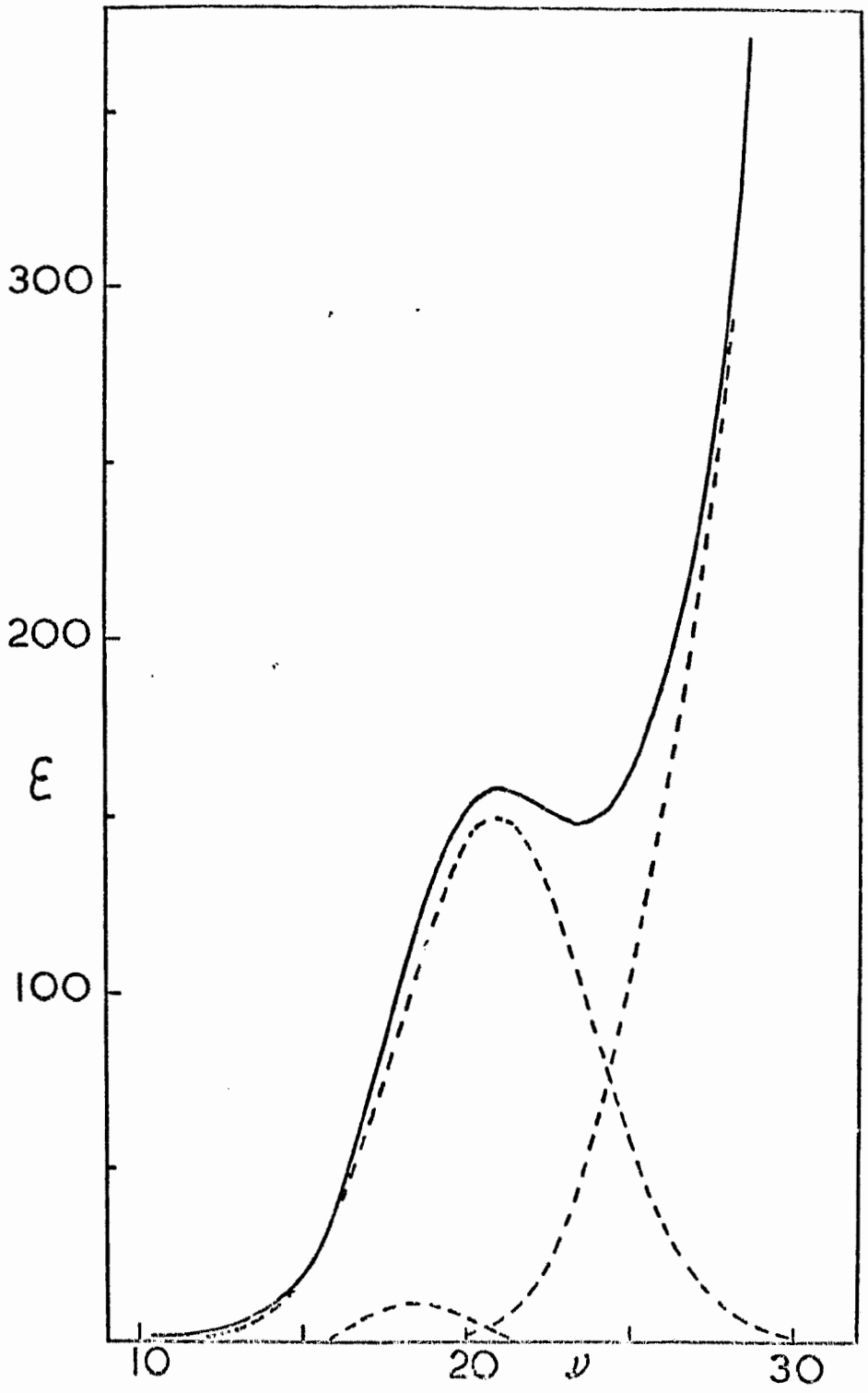

Figure 5.3

Spectrum of Rh (III) in Li_2SO_4 - Na_2SO_4 - K_2SO_4 at 550° C

5.3 Discussion.

5.3.1 LiCl - KCl Spectra. Immediately prior to the commencement of this portion of the work, Ogilvie and Holmes (3) had reported the spectrum of Rh(III) in the LiCl - KCl. Their spectrum was very similar to that shown in Figure 5.1, except that the inflection point at ~ 24 kK was not apparent. The position of the first maximum at 18.2 kK, with $\varepsilon = 160$, agrees very well indeed with the results in Table 5.3. They attempted to explain their spectrum as being due to octahedral $RhCl_6^{3-}$, but, because the second spin-allowed band was not detected, felt obliged to consider other species — in particular, dimeric or polymeric chloro-bridged complexes. The conclusion finally reached was that it was unlikely that the species in the chloride melt was $RhCl_6^{3-}$.

A comparison of the results for the chloride melt and aqueous HCl solutions, Tables 5.1, 5.3, and 5.4, leaves little doubt that in the LiCl - KCl eutectic the rhodium species is the octahedral $RhCl_6^{3-}$ complex. This particular example shows the usefulness of wave analysis, without which the position and intensity of the second spin-allowed band could not have been determined with much accuracy.

Ir(III) in the LiCl - KCl eutectic melt, which has not been previously reported, is, as a comparison between Tables 5.2, 5.5 and 5.6 confirms, present as the octahedral $IrCl_6^{3-}$ species.

Tables 5.4 and 5.6 show that the value of Δ decreases when the solvent is changed from aqueous HCl to the chloride melt. This is consistent with an increase in the metal-ligand distance as the temperature increases, due probably to a greater vibrational amplitude at the higher temperatures. If the M - L distance is, in fact,

increased, then the extent of orbital overlaps between the metal and the ligand should also be decreased. A measure of this overlap is afforded by the nephelauxetic ratio β (which has been discussed in Chapter 2). For Rh(III) and Ir(III) the values of β for the melt and aqueous spectra are then shown in Table 5.8.

Table 5.8

β values for $RhCl_6^{3-}$ and $IrCl_6^{3-}$

	Aqueous	Melt
Rh(III)	0.47	0.51
Ir(III)	0.41	0.48

The increased values in the melt confirm, therefore, that the species is becoming more ionic in character, i.e. the orbital overlap is decreased.

5.3.2 Li_2SO_4 - Na_2SO_4 - K_2SO_4. As Figure 5.3 shows, three ligand field bands are discernible in the spectrum of Rh(III) in this melt after Gaussian analysis has been carried out. The two weak bands are assigned to the spin-forbidden transitions whilst the strong band is due to the first spin-allowed band. The spectrum in the sulphate melt is, therefore, rather different from the chloride melt in that a spin-allowed band is lost. Nevertheless, because of the general similarily between these spectra, it is believed that in the sulphate melt the Rh(III) is present as an octahedral complex. That the second spin-allowed band is not found, even by Gaussian analysis, is unfortunate in that a calculation of Δ and B, by the method outlined for $RhCl_6^{3-}$, is not possible. However, an estimate of Δ , B and C can be obtained if the bracketed terms in the energy expressions are neglected. On this basis, Δ , B and C are found to be 25.3 kK, 490 cm^{-1}, 4.3 kK respectively. The value of the ligand

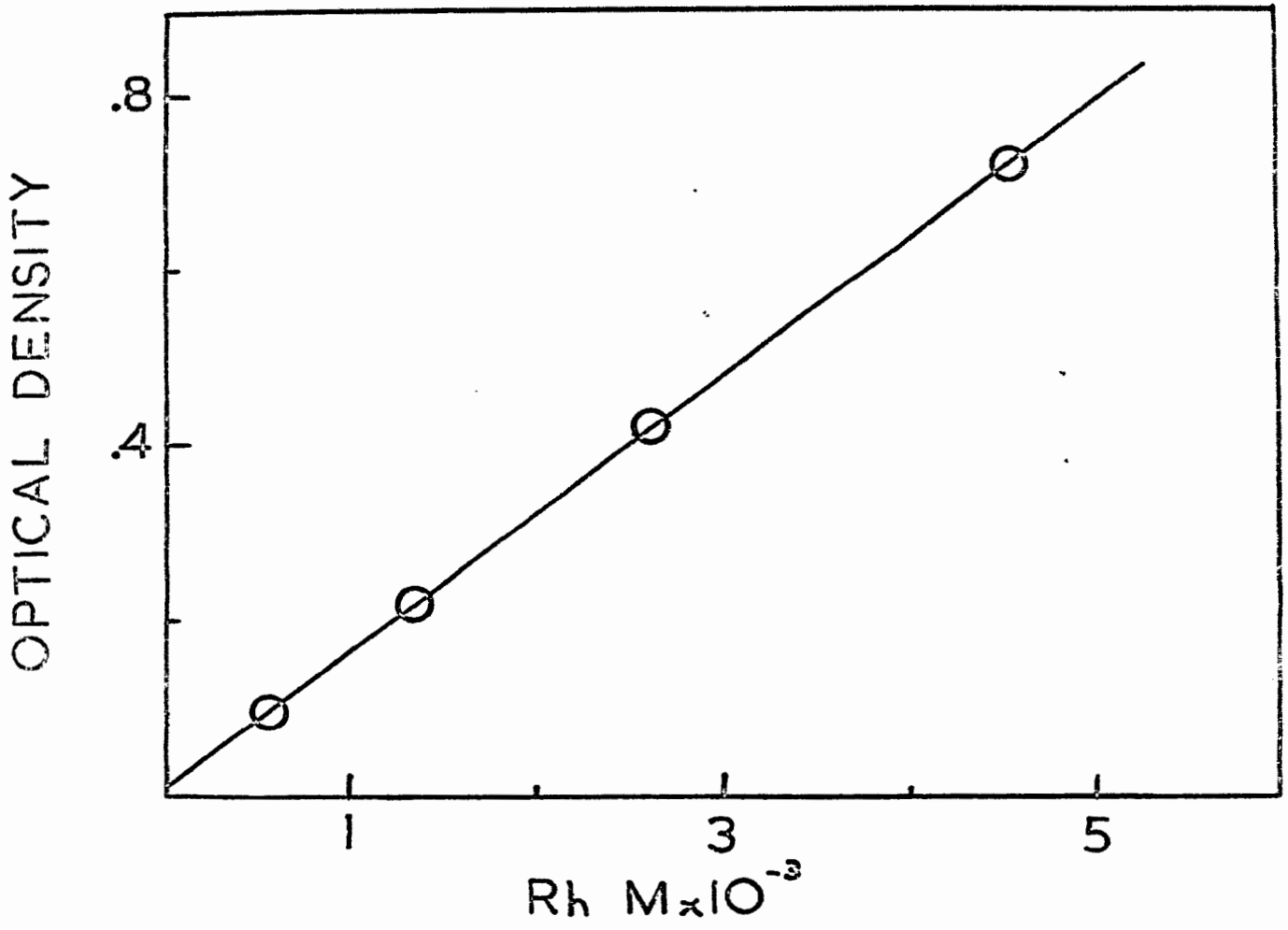

Figure 5.4

Beer's law plot for Rh(III) in Li_2SO_4 - Na_2SO_4 - K_2SO_4 at 550°C

field splitting is probably on the low side when the extent of the shift of the peak maxima on changing from the chloride to the sulphate melt is considered (cf 18.2 versus 21 kK). It is this shift which is undoubtedly the reason why the second spin-allowed band is not observed. It would, therefore, be expected that SO_4^{2-} should lie above Cl^- in the spectrochemical series and this has been confirmed for other systems (127). Just as with the case of Co(II), it is impossible to specify whether the sulphate groups attached to the rhodium are acting as unidentate, bidentate or even tridentate ligands.

The value of the extinction coefficient at the highest point of the band due to the spin-allowed transition, i.e. the point on the spectrum and not on the Gaussian component, was determined with solutions of varying rhodium concentrations in an attempt to determine the accuracy of such measurements and to see if Beer's law was obeyed. The average value of the extinction coefficient was found to be 160 ± 3 from four measurements. As Figure 5.4 shows, Beer's law is obeyed for Rh(III) in the sulphate melt. That the straight line does not go exactly through the origin is almost certainly due to experimental errors.

An attempt was made to obtain a solution of iridium in the sulphate melt by anodisation after oxide had been removed from the melt by pyrosulphate treatment (Appendix C): this was not successful and, therefore, a spectrum could not be obtained. The addition of an anhydrous iridium sulphate complex, e.g. $K_3[Ir(SO_4)_3]$ might be more fruitful but was not attempted in the present work.

5.4 Experimental. The melts were obtained by the methods outlined in Appendix C, as were the concentrated solid solutions used to obtain appropriate

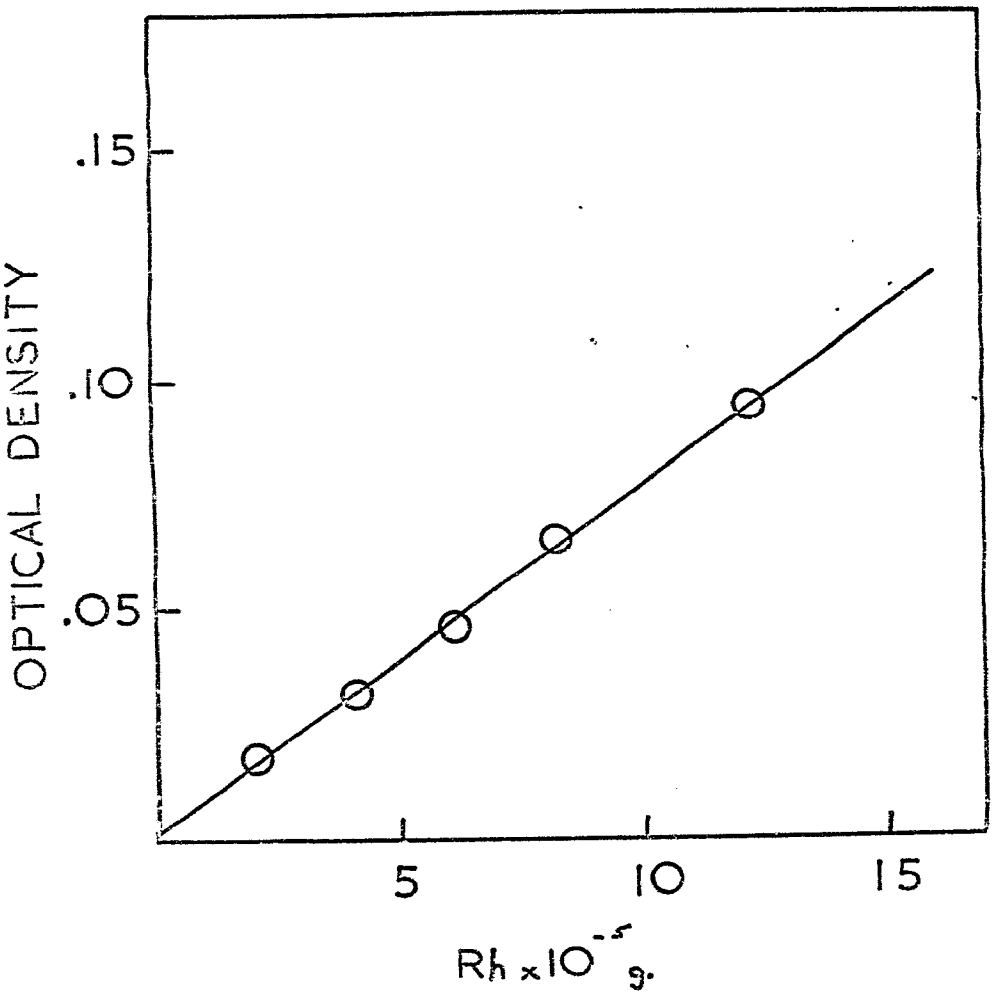

Figure 5.5

Calibration curve for Rh(III) analysis using $SnCl_2$

solutions for spectral investigation. For the chloride melts, the salts used were K_3RhCl_6 and K_3IrCl_6 (both supplied by Johnson Matthey) which were dried at 120°C prior to addition to the melt. In the sulphate melt, on the other hand, the rhodium solution was obtained by anodisation in a sintered frit of a rod of rhodium metal (Johnson Matthey) using a platinum cathode.

The analysis for rhodium was carried out using the stannous chloride method of Ayres et al. (128). This involves boiling an aliquot containing rhodium with concentrated HCl and stannous chloride for ten minutes, diluting to the appropriate volume and measuring the absorbance at 475mμ. The calibration curve, which was obtained using the starting material K_3RhCl_6 as a standard, is shown in Figure 5.5.

The analysis for iridium presented some problems in that two of the recommended methods did not give good results with the standard solution. These were the colourimetric methods of MacNevin and Kriege (129), using an Ir(IV) EDTA complex, and of Maynes and McBryde, using ceric sulphate (130). Much more consistent results were obtained with the mixed acid method of Ayres and Quick (131). This involved developing a purple colour by heating the iridium solution together with the mixed acid (10 : 10 : 1 of 72% $HClO_4$: 85% H_3PO_4 : conc. HNO_3). The optical density was then measured at 564 mμ. The calibration curve, using K_3IrCl_6 as a standard, for this method is shown in Figure 5.6.

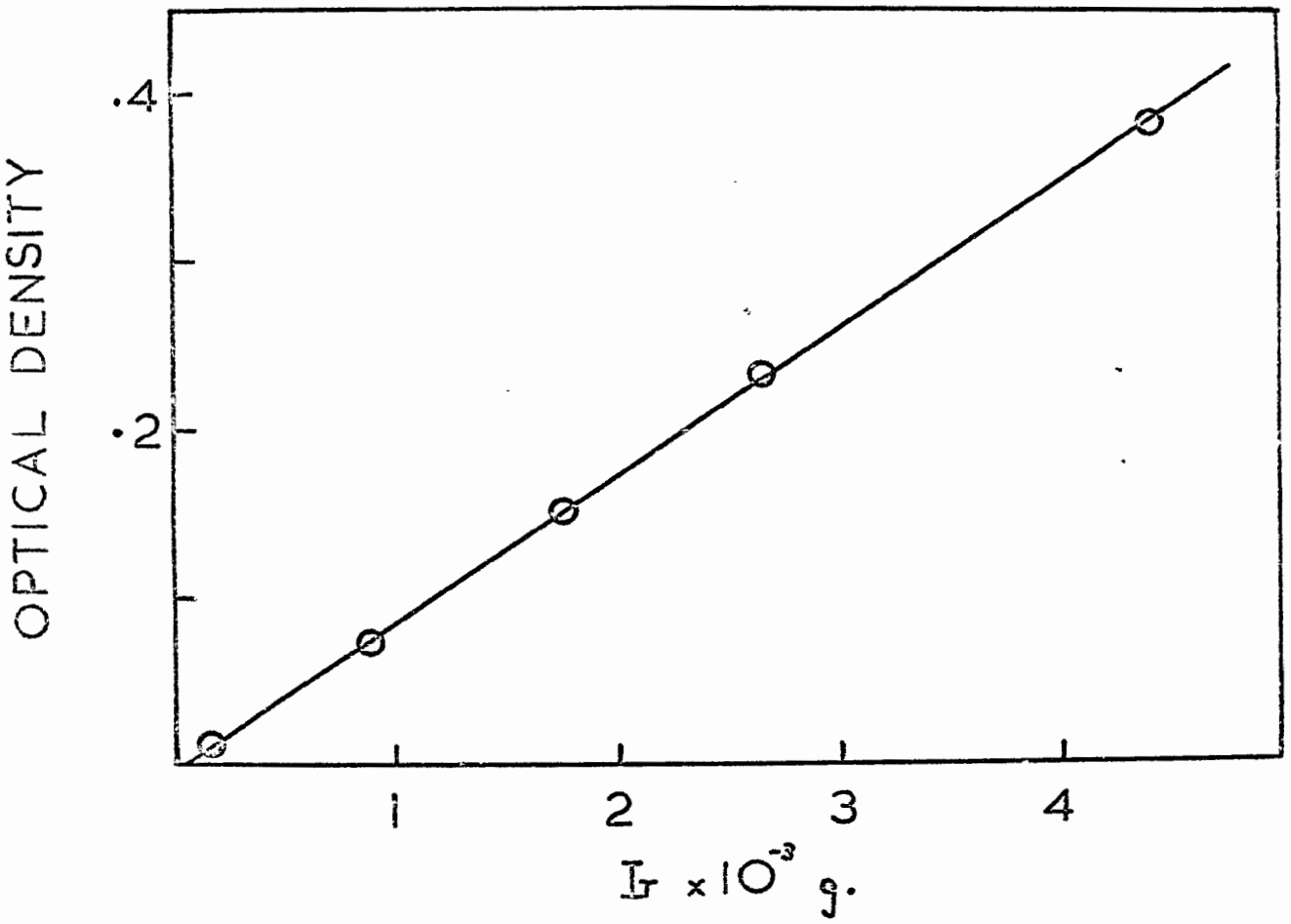

Figure 5.6

Calibration curve for Ir(III) analysis using the mixed acid method

CHAPTER 6

SPECTRUM OF Ni(II) IN FUSED Li_2SO_4 - Na_2SO_4 - K_2SO_4 EUTECTIC

6.1 Introduction. The spectrum of a solution of anhydrous nickel sulphate in the sulphate melt has been reported previously and interpreted in favour of a distorted octahedral species (87). This interpretation was questioned (7) on the grounds that the highest energy peak contained more than one band, whilst the corresponding peak in the spectrum of octahedral $Ni(H_2O)_6^{2+}$ in aqueous solution is almost perfectly Gaussian shaped. On the basis of an octahedral model for the nickel species in the sulphate melt, it was predicted that a third band, occurring at ~ 6 kK, should also be present in the spectrum. The published spectrum showed no clearly discernible band at this energy.

Spectral measurements for this system were repeated so that some of the above points could be investigated. Emphasis was placed on the following details:

(i) The value of the extinction coefficient of the main band.

(ii) The position of the low energy 'third' band.

(iii) The shape of the main band.

6.2 Results. The spectrum of nickel sulphate in the sulphate eutectic melt at 550°C is shown in Figure 6.1, which also includes a Gaussian analysis of the spectrum. The band positions and extinction coefficients of the unresolved spectrum are shown in Table 6.1 together with the values at 550°C and 700°C obtained by Johnson and Piper (87).

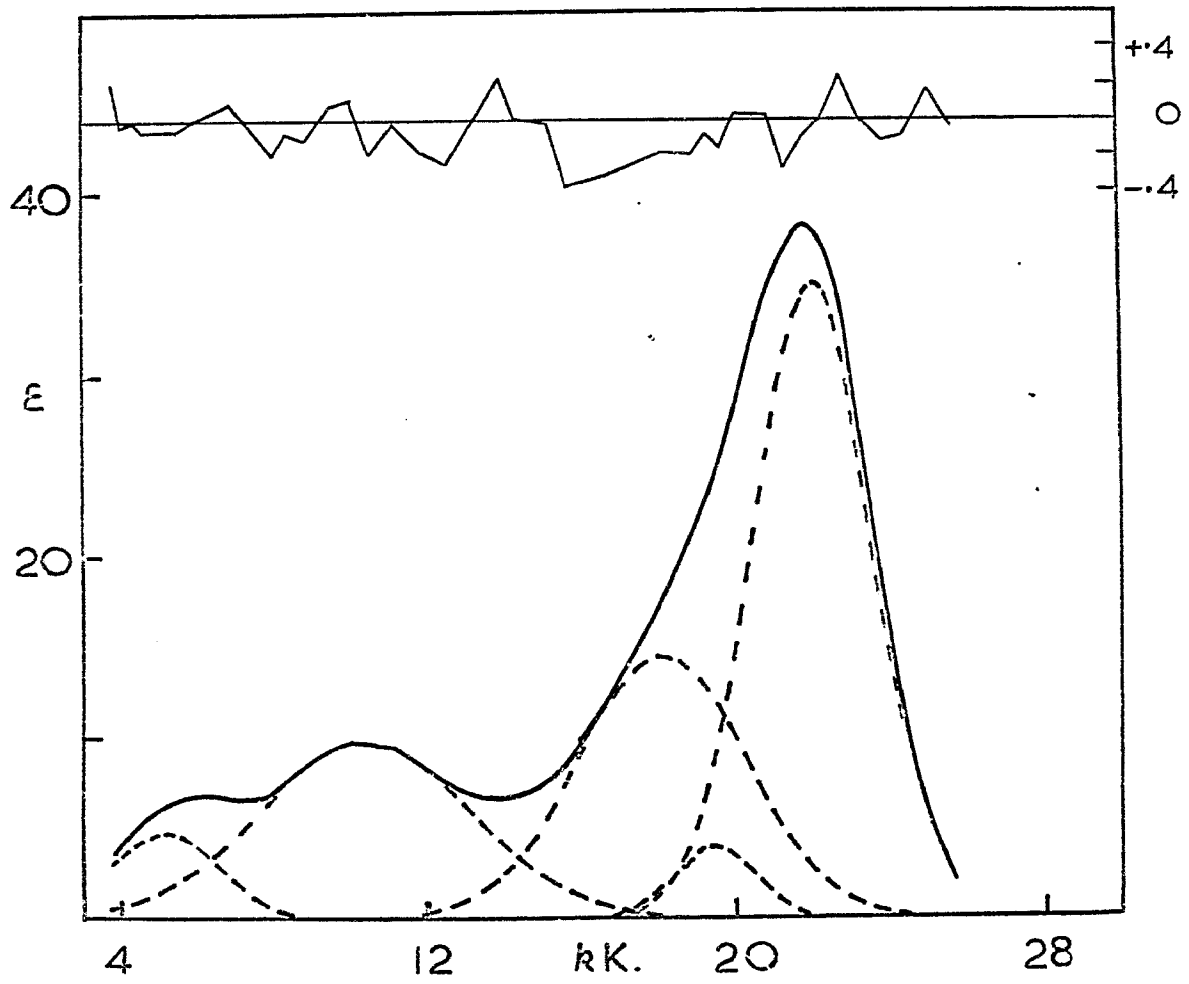

Figure 6.1

Spectrum of Ni(II) in the Li_2SO_4 - Na_2SO_4 - K_2SO_4 melt at 550°C

Table 6.1

Spectrum of Ni(II) in Li_2SO_4 - Na_2SO_4 - K_2SO_4

ν(kK)	ε	ν(kK)	ε	ν(kK)	ε
5.8	6.8				
10.0	9.8	10.4	11.6	9.9	11.3
10.9 (sh)	9.4				
21.9	38.4	22.0	44.6	21.6	42
550°C		550°C		700°C	
		(87)		(87)	

The results in Table 6.1 for the spectrum at 550°C show substantial agreement with those reported earlier. A Beer's law plot for the main peak, over the concentration range $5 - 25 \times 10^{-3}$M, gave a straight line which on extrapolation passed very close to the origin. The results are shown in Figure 6.2 and confirm that Beer's law is obeyed for this system.

The initial Gaussian analysis was carried out assuming that only four bands were present but gave such a large residual that it was clear that at least one further band was present. By estimating the peak positions, heights and half-widths for five bands, the analysis shown in Figure 6.1 was obtained. However, because of the difficulty of estimating the peak parameters for the fifth band, i.e. the one whose presence is not clearly indicated in the spectrum, a second Gaussian analysis, starting from slightly different parameters, gave the result shown in Figure 6.3. The band positions and extinction coefficients for both the Gaussian analyses are shown in Table 6.2.

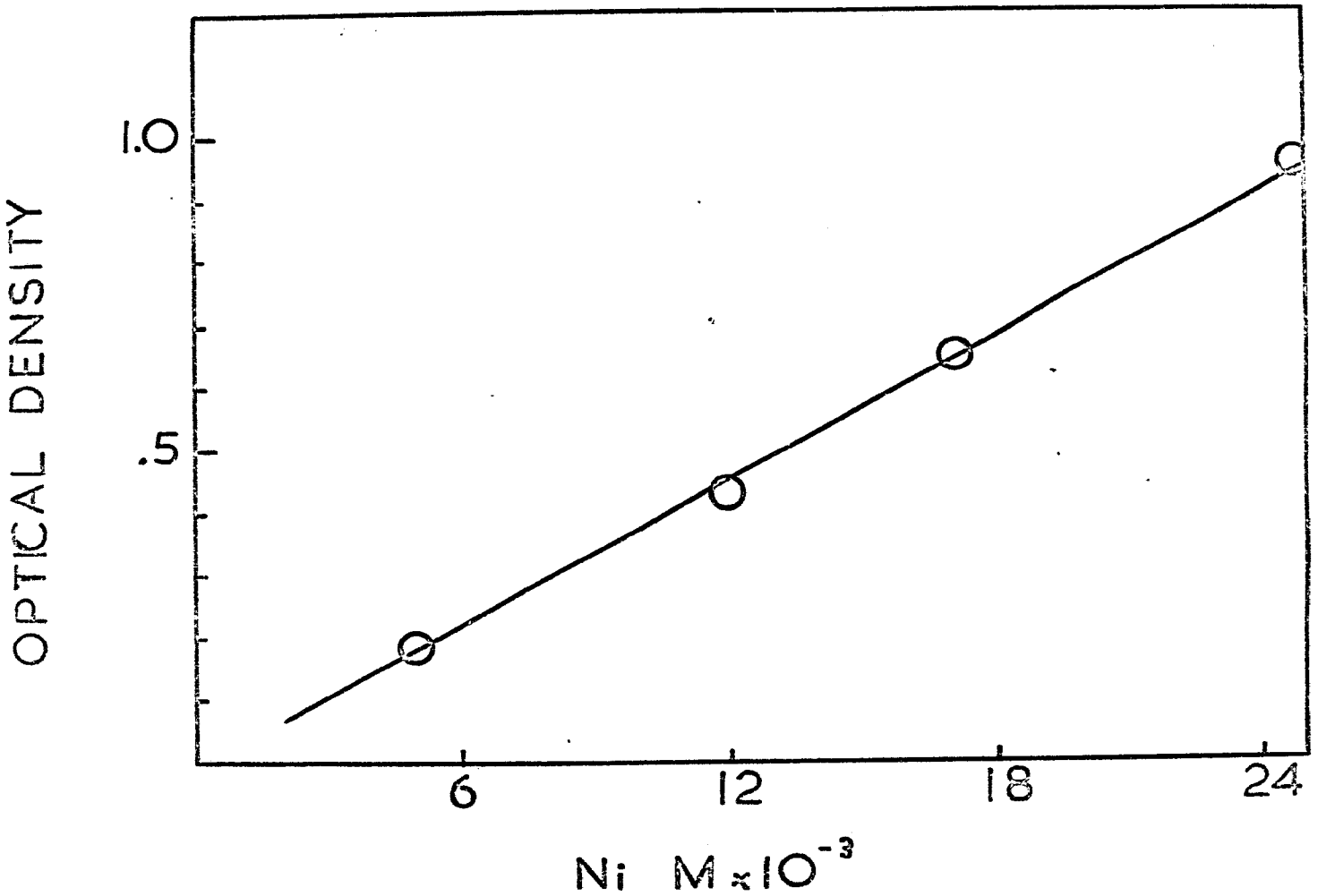

Figure 6.2

Beer's law plot for Ni(II) in Li_2SO_4 - Na_2SO_4 - K_2SO_4 at 550° C

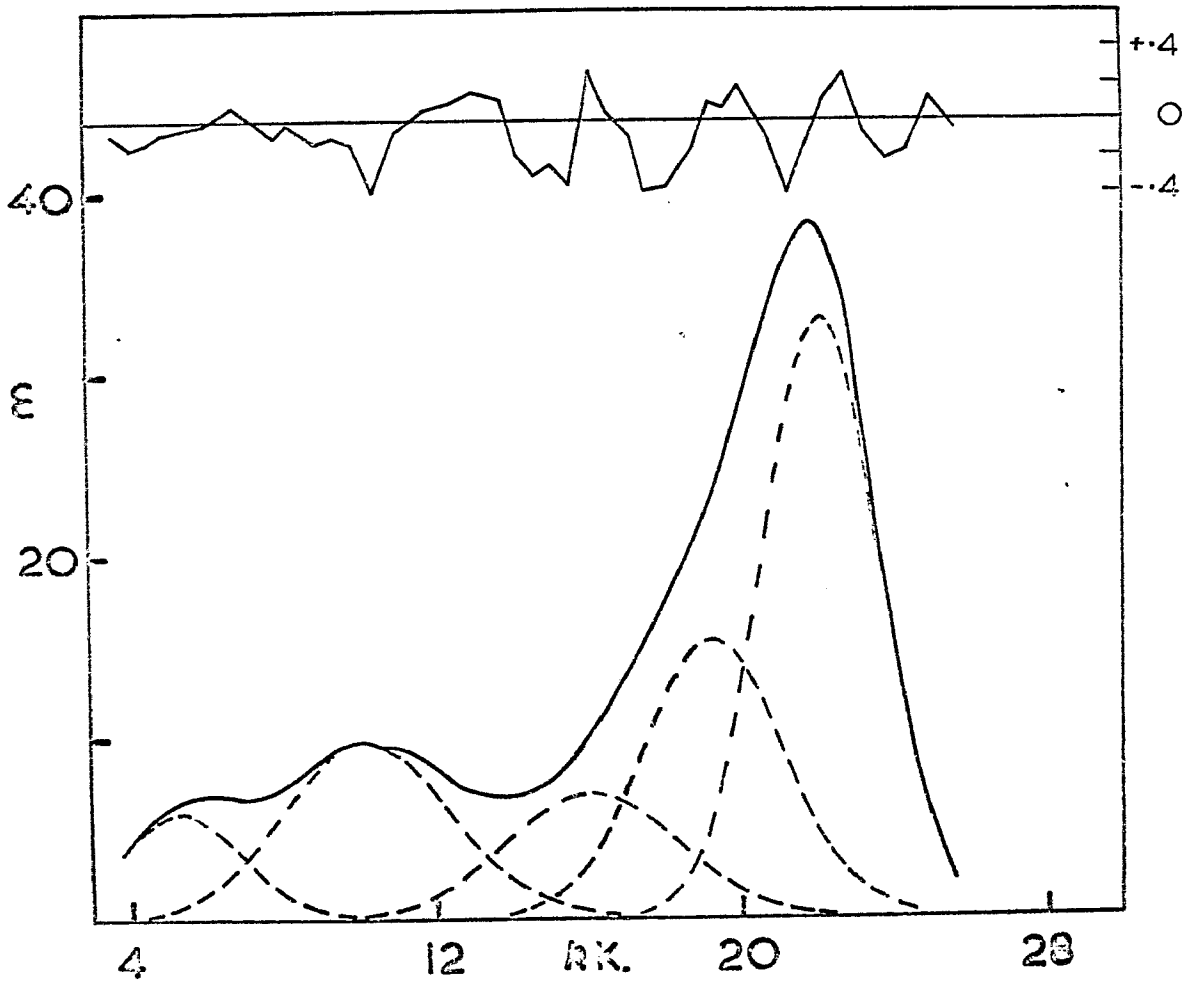

Figure 6.3

Second Gaussian analysis for the Ni(II) spectrum in the sulphate melt

Table 6.2

Gaussian components for the spectrum of Ni(II) in the sulphate melt

Figure 6.1		Figure 6.3	
ν (kK)	ε	ν (kK)	ε
5.18	4.8	5.4	5.9
10.4	9.7	10.2	9.8
18.1	14.5	16.1	6.8
19.5	3.98	19.3	15.3
22.0	35.0	22.1	33.1

Both Figures 6.1 and 6.3 also contain the residual obtained by subtracting the sum of the Gaussian components from the recorded spectrum. One point to be noted is that, for clarity, the residual has been plotted on an expanded scale compared to the spectrum. As both the diagrams and the table show, the Gaussian analyses are reasonably similar to one another. The two lowest energy bands and the highest energy one are relatively invariant; it is the two bands which produce the skewed shape of the main visible band that are varying. In view of this discrepancy, which incidentally shows the limitations of Gaussian analysis and proves, quite conclusively, that such an analysis is never mathematically unique (see Appendix A), a classical approach to the interpretation of the melt spectrum was adopted. This involved a comparison of the melt spectrum with the crystal spectrum of a compound of known structure.

6.3 Discussion. The crystal spectrum of $NiSO_4 \cdot 7H_2O$, which contains regularly octahedral $Ni(H_2O)_6^{2+}$ entities (132), has been shown to be essentially

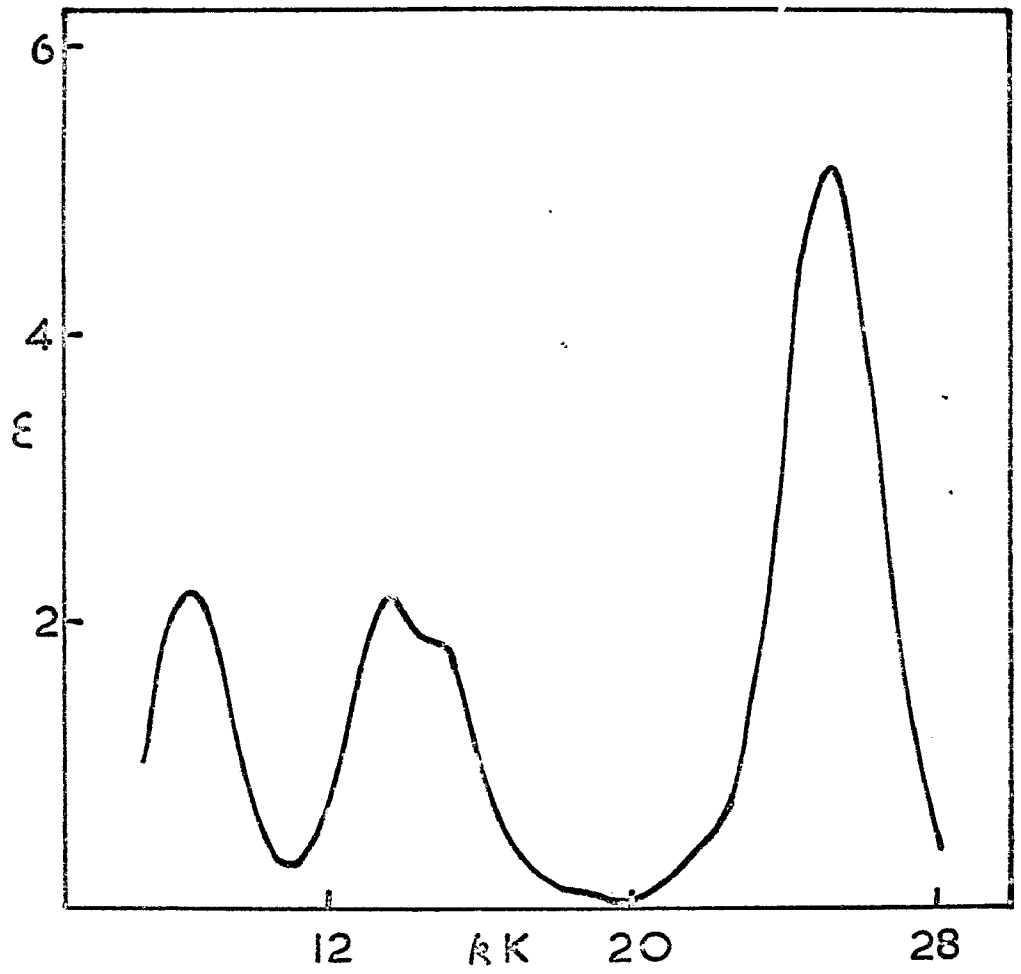

Figure 6.4

Spectrum of Ni(II) in aqueous solution

identical to the aqueous solution spectrum (36). Both spectra consist of three relatively strong bands, which are assigned to the three triplet-triplet transitions that are possible for an octahedral d^8 complex. Close examination of the spectrum indicates that the highest energy band contains a small distortion on the lower energy foot. This same distortion has also been observed in the spectrum of $KNiF_3$ (29) at 300°K, except that in this case the small band is rather better resolved. In both cases, the main band, which has been assigned to the $^3T_{1g}(P) \leftarrow {}^3A_{2g}$ transition, is quite symmetrical except for the distortion arising from overlap with the small band. The above two spectra can be regarded as being typical of Ni(II) in octahedral ligand fields. It must be borne in mind that as the ligand is changed the relative positions of all the bands in the spectrum may also change. The result is that, although the band corresponding to a certain transition may be well defined in one spectrum, it may change to such an extent that it is no longer readily discernible.

A comparison of the spectrum shown in Figure 6.1 with the two spectra mentioned above indicated that the principal difference arises because of the unsymmetrical nature of the highest energy band. The two lowest energy bands bear a marked resemblance to the corresponding bands in the typical octahedral spectra with the exception that in the sulphate melt the two bands are not as well separated. For reference purposes the spectrum of an aqueous solution of $NiSO_4$ is shown in Figure 6.4. The highest energy peak certainly contains bands which are not apparent in the aqueous spectrum. It would seem, therefore, that identification of the species in the sulphate melt in terms of an octahedral entity is not really justified unless some explanation of the band structure is put forward. The problem is compounded somewhat

in that other melt spectra of Ni(II) which also contain this asymmetric band have also been interpreted on the octahedral model (100).

An important factor that has not been considered so far is the effect of temperature on the spectrum. It could be argued that a detailed comparison of spectra recorded at widely differing temperatures may not be valid. This particular problem has been treated in some detail by Smith et al. who studied the crystal spectrum of $KMgCl_3$ doped with Ni(II) over the range 80 - 763°K (49). The spectrum at 298°K showed that the main visible band was fairly symmetrical, whereas at elevated temperatures this band developed a distortion in the low energy tail. The reason for this can be seen if the results at 80°, 298°, and 763°K are compared. At 80°K the main band, corresponding to the $^3T_{1g}(P) \leftarrow {}^3A_{2g}$ transition, occurs at 20.3 kK with the spin-forbidden $^1T_{2g} \leftarrow {}^3A_{2g}$ transition at 18.05 kK. Because the main band is quite narrow, (the half-width is only ~ 1.3 kK) the spin-forbidden band is quite clearly resolved. The spectrum at 293°K shows the main band at 20.13 kK having a half-width of ~ 2 kK with the spin-forbidden band, which is less well resolved than at 80°K, occurring at 17.7 kK. At 763°K, the half-width of the main band has increased to ~ 3 kK and it occurs at 19.76 kK whilst the spin-forbidden is not resolved at all. This last spectrum bears a marked resemblance to the sulphate melt spectrum. As a consequence of the increasing band width of the main band as the temperature is increased, the low energy foot overlaps the small spin-forbidden band and results in the unsymmetrical shape.

The spectrum in the sulphate melt (Figure 6.1) might then be interpreted in the same fashion, in which case the band assignments are shown in Table 6.3.

Table 6.3

Band assignments for Ni(II) in the sulphate melt

	ν (kK)	ε
$^3T_{2g}(F) \longleftarrow {}^3A_{2g}$	5.18	5.8
$^3T_{1g} \longleftarrow$	10.4	9.7
$^1T_{2g} \longleftarrow$	18.1	14.5
	19.5	3.98
$^3T_{1g}(P) \longleftarrow$	22.0	35

The assignment of the band at 18.1 kK to a spin-forbidden transition requires some comment. An examination of the values of the extinction coefficients reported by Smith et al. (49), as shown below, indicates that, as the spin-allowed band approaches the forbidden band, the extinction coefficient increases such that at 763° K it has approximately the same intensity as the first spin-allowed band.

	$^1T_{2g}$	^1E_g	$^3T_{1g}(F)$	$^3T_{2g}$
80° K	1.6	0.5	3.1	2.3
293°	~2	0.5	5.4	2.7
763°	~3	<1	8.6	3.1

The increase in intensity of the $^1T_{2g} \longleftarrow {}^3A_{2g}$ transition may be rationalised as a combination of the increase in temperature (compare the increases in the other bands) together with some 'intensity stealing' from the overlapping $^3T_{1g}(P) \longleftarrow {}^3A_{2g}$ transition.

The assignment of the band at 10.4 kK to the transition to the $^3T_{1g}$ state is confirmed if Figures 6.1 and 6.3 are compared. In both cases the second band

has a shoulder occurring very close to the maximum. The presence of this shoulder has been satisfactorily explained in terms of spin-orbital coupling by Ballhausen (23). Since the bands were very close together, no attempt was made to separate them by Gaussian analysis. As the results in Table 6.2 show, this approximation did not cause a significant difference in the position of the Gaussian component for the two analyses that were carried out.

Energy expressions for the transitions listed in Table 6.3 were obtained from the matrices quoted by McClure (133) and are as follows (only the triplet terms are considered):

$$^3T_{2g} \longleftarrow {}^3A_{2g} \qquad \Delta$$

$$^3T_{1g}(F) \longleftarrow \qquad 1.5\,\Delta + 7.5\,B - Q$$

$$^3T_{1g}(P) \longleftarrow \qquad 1.5\,\Delta + 7.5\,B + Q$$

$$Q = 1/2\,[225B^2 - 18\,B\,\Delta + \Delta^2]^{1/2}$$

The values of Δ and B were then found to be 5.2 kK and 1120 cm^{-1} respectively. The corresponding values obtained by the same type of calculation for the $KMgCl_3/Ni$ spectrum at 763 °K are 5.8 kK and 840 cm^{-1}. These values compare quite well with the values reported by Smith et al. of 5.0 and 850 cm^{-1} which were obtained using a treatment involving spin-orbital coupling (23). The value of B for the sulphate melt is, unfortunately, larger than the free ion value of 1,042 cm^{-1} quoted by Liehr (26). Such a high value for B undoubtedly arises because the third band is at too high an energy. This is seen to be the case if an alternative assignment of the band at 18.1 kK to the $^3T_{1g}(P) \longleftarrow {}^3A_{2g}$ transition is considered. In this case, Δ is once again 5.2 kK whilst B is now 860 cm^{-1}. This assignment,

however, does not take into account the highest energy component occurring at 22 kK. Suggestions as to the origin of this band can be made, e.g. it could be due to the presence of a small amount of a tetrahedral or even a square planar Ni(II) species. However, in view of the lack of definite evidence in favour of either of these possibilities they will not be pursued further.

In spite of the ligand field calculation reported above, the very close similarity between the melt spectrum and the $KMgCl_3$/Ni spectrum still suggests that the same type of species is present in both environments. The contention that the nickel species in $KMgCl_3$ is octahedral is supported by the crystal structure determination of $KMgCl_3$ at 298°, 383° and 448° K which showed that over this temperature range the $MgCl_6^{4-}$ remained octahedral. Of course, the assumption was made that substitution of Ni(II) for Mg(II) did not cause any distortion of the octahedral site. It is not very easy to determine whether a small distortion of the octahedron has occurred or not, but if it is assumed that by replacing a host cation with a cation of much the same size, then because Mg^{2+} is very similar to Ni^{2+} (Pauling radii of 0.65 and 0.69Å respectively), the distortion will be quite small. It would appear, therefore, that the nickel species in the sulphate melt has some similarity with an octahedral model but no satisfactory explanation has been put forward for the observed band structure of the main band.

This same problem has been encountered by Smith et al. (134, 135) in their studies of the effects of solvent composition and temperature on the spectrum of Ni(II) in the LiCl - KCl melt. They showed that at 526° C the spectra obtained by varying the KCl concentration could be described in terms of an equilibrium

mixture of two types of 'nickel centres'. A 'nickel centre' was defined as 'a nickel ion together with whatever surrounding ions play a substantial role in the light absorbing process with no implication concerning the degree of geometrical order'. The first type of centre, which became predominant as the KCl concentration increased, was labelled a T centre and was shown, by comparison with the spectrum of a $CsCl - NiCl_2$ melt, to be essentially tetrahedral. The second type, labelled an O centre, was similar in many respects, but certainly not identical to, the Ni(II) species in the $KMgCl_3$ spectrum. The spectrum of the O centres, moreover, is similar to the sulphate melt spectrum reported earlier. It was suggested that there was a distribution of geometries clustered about an average which is not very different from octahedral. In order to account for the high extinction coefficients for the LiCl - KCl spectrum, it was postulated that some of these O centres were of such a geometry that they lacked a centre of symmetry and should, therefore, give rise to more intense absorption bands.

The sulphate melt spectrum might also be interpreted in a similar fashion although, because of the suggested wide range of geometries constituting an O centre and their lack of definition, a detailed interpretation of the spectrum is not feasible. Such a range of geometries might perhaps explain why the resolution of the spectrum into Gaussian components is not unique. Although an explanation along these lines might be satisfactory when the molecular motion in the fused solvent is taken into account, it is still somewhat surprising that the principal effects are observed on one band alone and that the other two are relatively unperturbed.

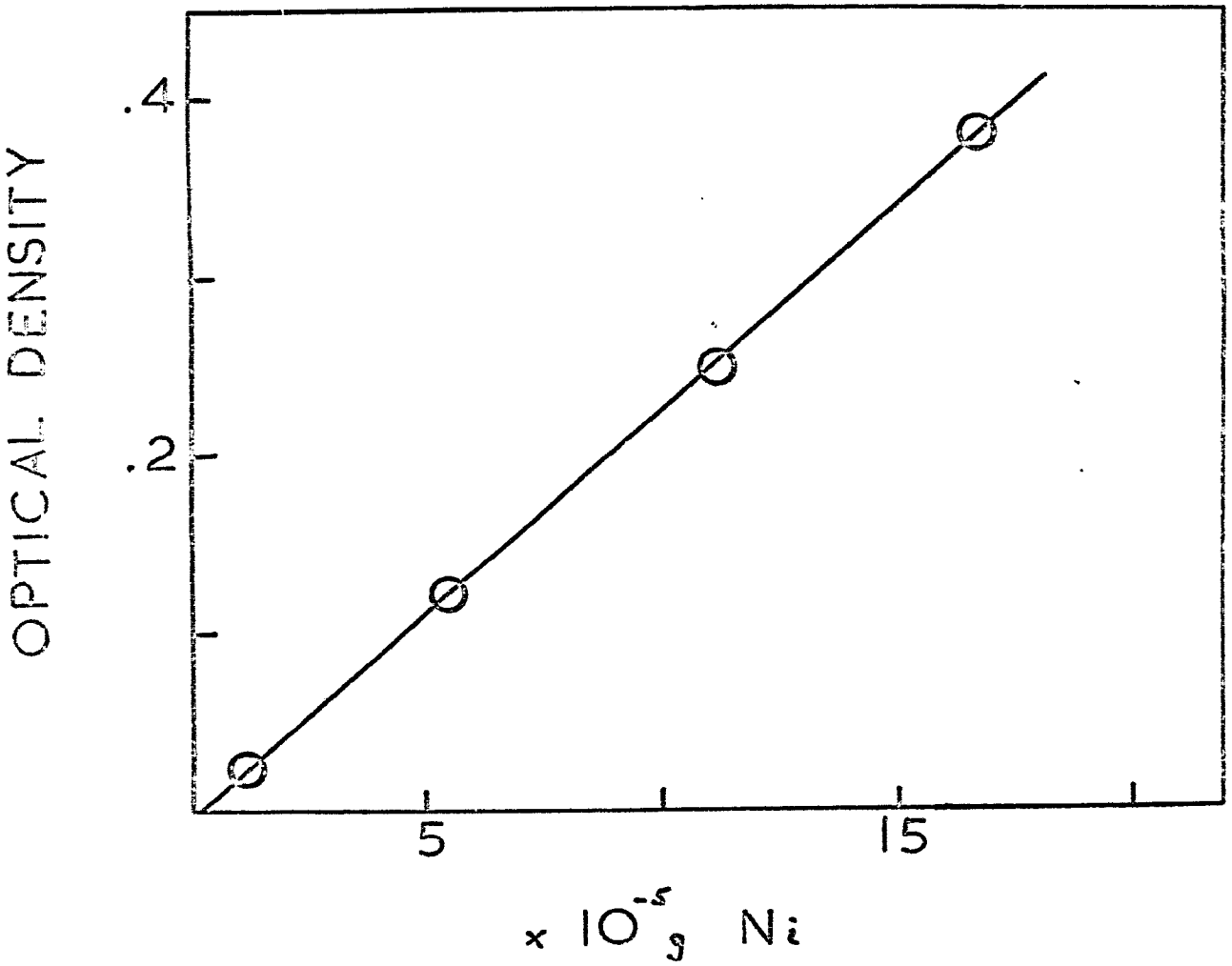

Figure 6.5

Calibration curve for Ni(II) analysis

To summarise the discussion, it is believed that in the sulphate melt the nickel species are not perfectly octahedral but may be described, with some reservations, in terms of the O centre concept.

6.4 Experimental. The preparation of the melt and the solutions for spectral work are described in Appendix C. Anhydrous nickel sulphate was prepared by heating $NiSO_4 \cdot 6H_2O$ (Baker Analysed Reagent) at 120 °C overnight. Nickel analyses were carried out using the colourimetric method reported by Charlot and Bezier (136). This involved oxidation of Ni(II) to Ni(IV) followed by the formation of the soluble Ni(IV) dimethylglyoxime complex. The optical density of the final solution was measured at 465 mμ. Figure 6.5 shows the calibration curve which was used for the analysis.

The Gaussian components shown in Figures 6.1 and 6.3 were obtained by the method outlined in Appendix A.

CHAPTER 7

SPECTRA OF Pd(II) AND Pt(II) IN FUSED CHLORIDE AND SULPHATE MEDIA

7.1 Introduction. By far the most important oxidation states for palladium and platinum are the 2+ and 4+ states. The majority of M(II) compounds are found to be square planar, whilst for the M(IV) complexes the stereochemistry is centred around the octahedron.

The orange solution obtained by anodisation of platinum in the LiCl - KCl melt has been known almost since the first days of electrochemical studies in this melt. This is because the Pt(II)/Pt electrode is perhaps the most commonly used reference electrode for this melt. The stable oxidation state was, therefore, known to be Pt(II) well before the melt spectra were investigated. Pd(II) had also been identified in the melt from potential measurements. In the Li_2SO_4 - Na_2SO_4 - K_2SO_4 melt, the situation is similar to that of rhodium and iridium in that the 4d element can be obtained in solution by anodisation whilst the 5d element is not oxidised by this method. In this sulphate melt containing palladium, electrochemical studies have shown that a Pd(II) species is present (125), although the nature and degree of solvation of the species cannot be ascertained by studies of this nature. In the melts considered later, the metals when present are in the divalent state and it might be tempting to suggest that the species are, therefore, square planar.

Before the spectra in the melts are considered, however, a review of the spectra of MCl_4^{2-} complexes in crystals and in solutions is necessary. The subject

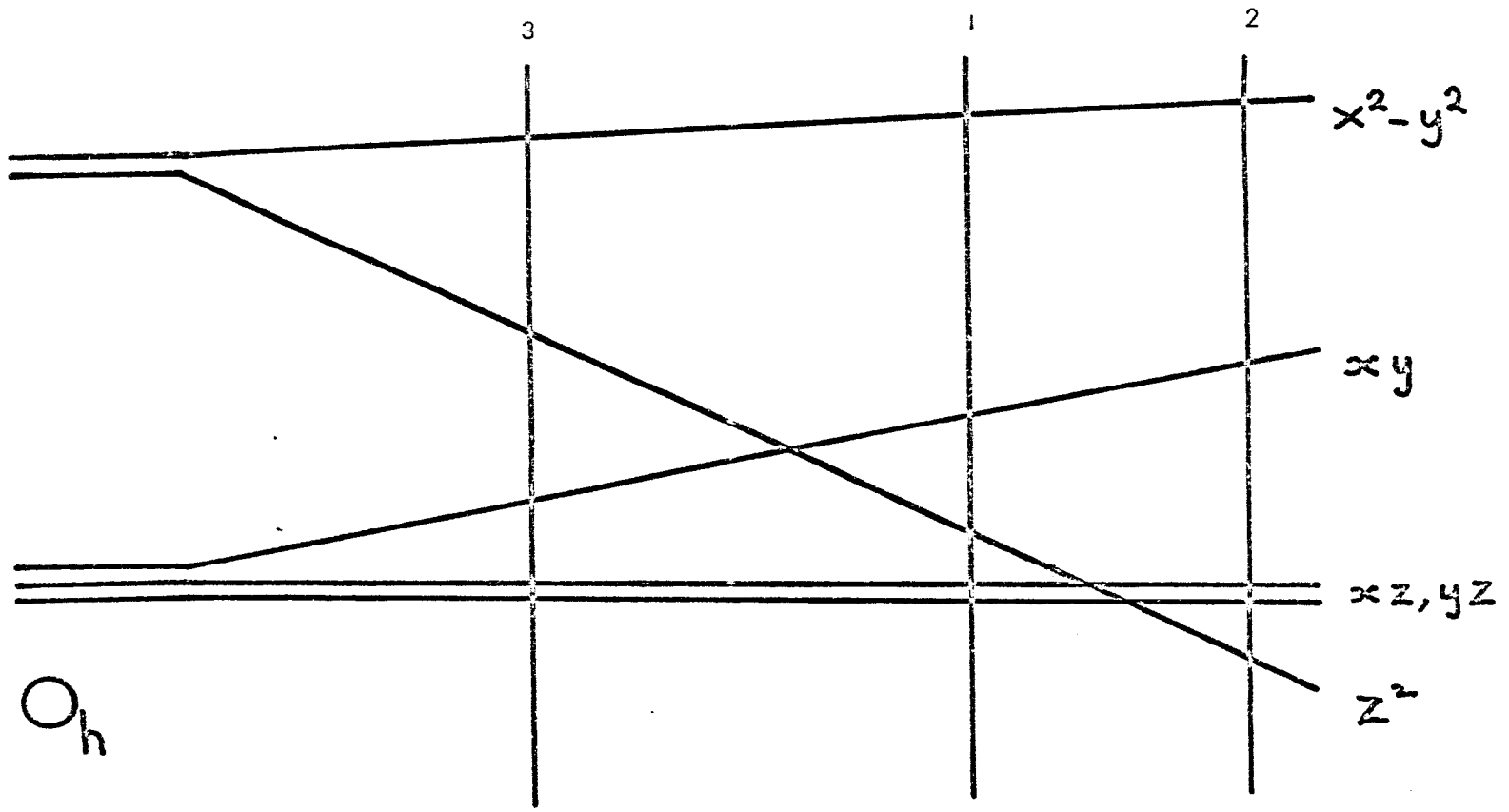

Figure 7.1

d^8 energy level diagram for D_{4h} symmetry

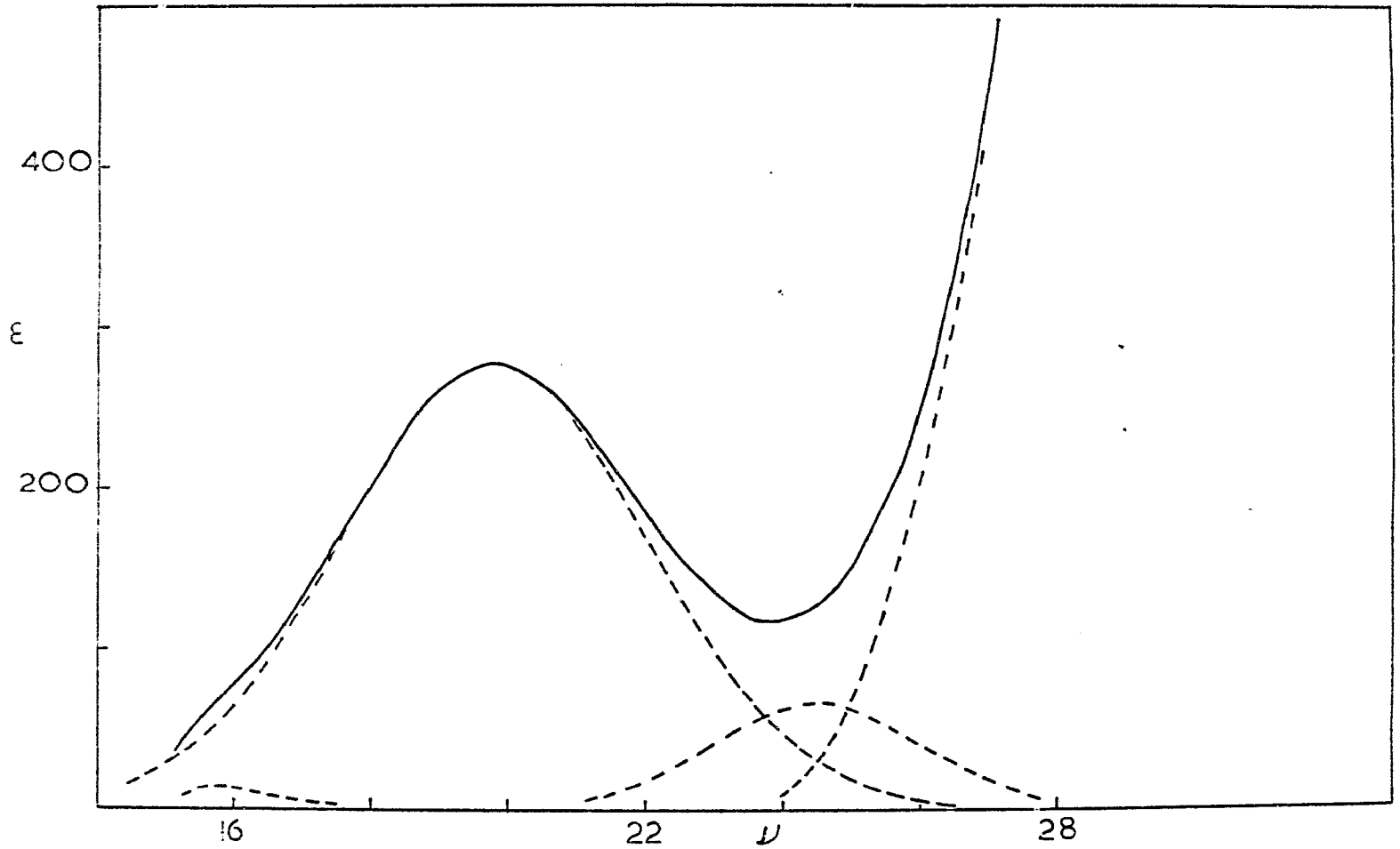

Figure 7.2

Spectrum of Pd(II) in the LiCl - KCl melt at 450°C

has been partly reviewed by Gray (137) but complete agreement has still not been reached in spite of the very large volume of work reported on the subject. Some of the published spectra, both in solids and in solution, are shown in Tables 7.1 for $PdCl_4^{2-}$ and 7.2 for $PtCl_4^{2-}$.

Table 7.1

Spectra of $PdCl_4^{2-}$ in solids and solution

ν (kK)	ε	ν (kK)	ε	ν (kK)	ε	ν (kK)	ν (kK)
				16.6	7.9	16.7	17.5
21.3	180	21.2	170	21.1	157	21.5	20.0
						23.3	22.8
30.3	500	30.3	650				29.5
35.7	10,000	35.97	12,000				
1M HCl (138)		10M HCl (139)		2M HCl (140)		Reflectance (139)	Crystal (141)

Table 7.2

Spectra of $PtCl_4^{2-}$ in solids and solution

ν (kK)	ε	ν (kK)	ε	ν (kK)	ε	ν (kK)	ν (kK)	ν (kK)
17.7	2.6			17.2	(2)			17.3
21	15	21	17	21	15	20	20.3	20.3
25.5	59	25.5	59	25.4	57	26.7	25.7	26.0
30.2	64	30.2	64	30.3	62	29.4	29	28.9
37.9	250							
46	9,580							
H_2O (92)		H_2O (142)		.3M HCl (143)		Crystal (142)	Crystal (143)	Crystal (141)

Both these tables show that, as far as the experimental results are concerned, there is substantial agreement between the different investigators. For $PdCl_4^{2-}$ there are three relatively weak bands in the visible region and two intense charge-transfer bands in the near uv. An extra weak band is observed in the spectra of $PtCl_4^{2-}$ in addition to the other three weak ones and the two intense ones. The weak bands are usually assigned to ligand field transitions, whilst the strong ones are normally associated with charge-transfer transitions between the ligand and the central metal atom.

Although the spectra both in solution and in the solid state are quite well characterised, there has been, and still is, a great deal of controversy concerning the band assignments. The majority of both the theoretical and experimental work has been concerned with Pt(II) and will be discussed in some detail, after which the Pd(II) case will be considered. Both ions in the chlorocomplexes, e.g. K_2PtCl_4, have the d^8 configuration and have been found to be diamagnetic, suggesting therefore, that the ground state is $^1A_{1g}$. Under the influence of L - S coupling, the d^8 configuration gives rise to the following terms: ^3F, ^1D, ^3P, ^1G, ^1S. The square-planar configuration, having D_{4h} symmetry, can conveniently be regarded as an octahedron to which an infinite trans distortion has been applied. The effects of both an octahedral ligand field and this infinite trans distortion on the free ion terms have been investigated by means of group theory and are quoted by Cotton (24). The result is that in D_{4h} symmetry the free ion terms are split into 5, 4, 3, 7 and 1 components respectively for the order of free ion terms listed above. This particular ordering of the free ion terms is the one experimentally

found for the case of Ni(II) (144). The $^1A_{1g}$ ground state in D_{4h} symmetry could possible arise from any one of the free ion singlet states although the ^1S lies at such high energy in the free ion as to be the least likely centre of origin. According to the energy level diagram reported by Fenske et al. (142), the order of free ion terms in Pt(II) is the same as in Ni(II) and the $^1A_{1g}$ ground state arises from the ^1D free ion state. The ligand field bands are described in the literature either in the usual fashion, i.e. as transitions from the $^1A_{1g}$ ground state to excited states described by their symmetry type, or as transitions from one d orbital to another. This latter scheme arises in the following fashion. In the free ion the five d orbitals are degenerate but when it is incorporated into an octahedral complex these orbitals split into two levels. When the ligands on the z axis are removed, corresponding to a D_{4h} distortion, the two sets of orbitals are further split. This splitting is shown schematically in Figure 7.1 where it can be seen that the order of levels is dependent on the extent of the splitting. In order for the complexes to be diamagnetic, the separation between the $d_{x^2-y^2}$ and the d_{z^2} orbitals (which will be written $x^2 - y^2$ and z^2 in the following discussion with the three other d orbitals xy, xz, and yz) must be greater than the energy required for spin-pairing. Irrespective of the ordering of the levels, with the exception that the $x^2 - y^2$ is always at highest energies, the electron configuration for $PtCl_4^{2-}$ can be written:

$$(z^2)^2 \quad (xz, yz)^4 \quad (xy)^2$$

Transitions are possible from each of these three levels to the empty $x^2 - y^2$ orbital. The transitions with their corresponding symmetry classifications are listed in Table 7.3 (143).

Table 7.3

Symmetry classification of d - d transitions in d^8 square-planar compounds

$x^2 - y^2$	$\longleftarrow$ xy	$^1A_{2g}$	$\longleftarrow$ $^1A_{1g}$
	$\longleftarrow$ xz, yz	^1E_g	$\longleftarrow$
	$\longleftarrow$ z^2	$^1B_{1g}$	$\longleftarrow$

The above correspondence between orbitally labelled and symmetry labelled transitions remains the same irrespective of the ordering of the d orbitals in the complex. As Table 7.3 implies, the excited state for the first transition (to the $^1A_{2g}$ state) can be written as $(z^2)^2$ $(xz, yz)^4$ $(xy)^1$ $(x^2 - y^2)^1$ and, as the singlet label specifies, the two unpaired electrons must have anti-parallel spins. The alternative possibility, that the spins are parallel, gives rise to a triplet state $^3A_{2g}$. Three singlet-triplet transitions corresponding to the three singlet-singlet transitions would be expected. It is very rarely that all three spin-forbidden bands, together with the three spin-allowed bands, are resolved in Pt(II) or Pd(II) complexes.

The assignments which have been postulated in the literature for the spectrum of $PtCl_4^{2-}$ are listed in Table 7.4. The experimental band positions of Martin et al. (143) have also been included in this table in order to label the transitions. Since all the transitions are considered to arise from the $^1A_{1g}$ ground state, only the excited state is listed. Also included in the table are the different orders of the d levels as shown in Figure 7.1.

Table 7.4

Band assignments for the $PtCl_4^{2-}$ spectrum

ν (kK)	ε						
17.2	(2)	$^3A_{2g}$			$^3A_{2g}$	^3E_g	$^3A_{2g}$
21	15	^3E_g	$^3A_{2g}$, ^3E_g	$^1B_{1g}$	$^1A_{2g}$	$^3A_{2g}$	^3E_g
25.4	57	$^1A_{2g}$	$^1A_{2g}$	$^1A_{2g}$	$^1B_{1g}$	$^1A_{2g}$	$^1A_{2g}$
30.3	62	^1E_g	$^1B_{1g}$	^1E_g	^1E_g	^1E_g	^1E_g
energy level scheme		2	1	3	1	2	2
		(92, 148)	(142)	(143)	(145)	(18, 146)	(147)

Arguments, pro and con, for each of the above assignments are given in the appropriate paper and will not be considered in detail. Although the assignments do vary considerably, it seems generally agreed that the band at 25.4 kK is due to the $^1A_{2g} \leftarrow {}^1A_{1g}$ transition. Gray and Ballhausen (145) had originally assigned this band to a transition to the $^1B_{1g}$ state but, in later papers (18, 146), Gray and co-workers changed their assignment to agree with the majority of other workers. That this band is due to the $^1A_{2g} \leftarrow {}^1A_{1g}$ transition is shown conclusively in the crystal spectra work of Martin et al. (143). These workers investigated the crystal spectrum of K_2PtCl_4 with light polarised parallel (z) and perpendicular (x, y) to the tetragonal symmetry axis of the crystal. They showed that on a vibronic mechanism, the $^1A_{2g} \leftarrow {}^1A_{1g}$ transition should occur in x - y polarisation only, which describes exactly the behaviour of the band at ~ 25 kK. The assignment was further confirmed by a magnetic circular dichroism measurement reported by McCaffery et al. (149). Furthermore, these MCD results are in agreement with the assignment of the band at 30.3 kK

to the $^1E_g \leftarrow {}^1A_{1g}$ transition, although the possibility of this band also containing the $^1B_{1g} \leftarrow {}^1A_{1g}$ transition is not completely ruled out.

As far as the band at 21 kK is concerned, the majority of workers are of the opinion that this is due to a spin-forbidden transition. Martin and Lenhardt (143) originally assigned this band as the $^1B_{1g} \leftarrow {}^1A_{1g}$ transition, but Martin et al. (148) changed the assignment as a result of energy level calculations carried out later. The final order of the triplet levels has not been settled. The two latest papers, both appearing within months of one another, give different assignments (146, 147).

A considerable amount of doubt still surrounds the $^1B_{1g} \leftarrow {}^1A_{1g}$ transition. As noted earlier, this may be contained in the band at 30.3 kK. On the other hand, Gray et al. (146) have assigned a band occurring at 37.03 in the spectrum of $PtCl_4^{2-}$ in MeCN to this transition. In an earlier work (145) it was suggested that the corresponding band at 37.09 kK in aqueous solution might possibly be a "spin-forbidden" charge-transfer transition.

It seems clear that the assignment of the $PtCl_4^{2-}$ spectrum is not yet settled. For a discussion of the melt spectrum of $PtCl_4^{2-}$ only the two spin-allowed bands will be considered and the latest assignment of Day et al. (147) will be used. The energy expressions for these transitions have been evaluated (145) but, because the assignment is somewhat different from that given in this paper, the repulsion terms have to be interchanged. The corrected expressions, which were used in reference 146, are as follows:

$$^1A_{2g} \leftarrow {}^1A_{1g} \qquad \Delta_1 - 35F_4$$
$$^1E_g \leftarrow \qquad \Delta_1 + \Delta_2 - 3F_2 - 20F_4$$
$$^1B_{1g} \leftarrow \qquad \Delta_1 + \Delta_2 + \Delta_3 - 4F_2 - 15F_4$$

F_2 and F_4 are the Slater-Condon repulsion terms and values for these are usually assumed so that Δ_1, Δ_2 and perhaps Δ_3 (which are defined below) can be obtained. The same values of F_2 and F_4 as chosen by Gray (146), i.e. $F_2 = 10F_4 = 1$ kK, were used for the melt spectra.

The assignment of the spectrum of $PdCl_4^{2-}$ follows that of its platinum analogue with the possible complication that fewer bands are resolved. As Table 7.2 indicated, the spectrum of a crystal of K_2PdCl_4 differs somewhat from the corresponding solution spectrum in that a second component of the main band in the visible region is observed. This component, which occurs at 20 kK (141), is at a lower energy than the main component at 22.8 kK (141); furthermore, this low energy shoulder occurs in x - y and z polarisations. In analogy to the Pt(II) case, this shoulder can be assigned to the $^1A_{2g} \leftarrow {}^1A_{1g}$ transition and the main component to the $^1E_g \leftarrow {}^1A_{1g}$. As mentioned earlier, these two components are not resolved for the aqueous solution spectrum and the MCD results (149) have been interpreted in favour of the band at 21 kK being due to the $^1E_g \leftarrow {}^1A_{1g}$ transition. In favourable cases, however, the components of the main visible band can be resolved and this has been found to be the case for $Pd_2Cl_6^{2-}$ in MeCN (146). In this case, as shown by both Gray et al. (146) and Day et al. (147), the dimer behaves as if it were a single $PdCl_4^{2-}$ unit. The two bands found at 22.2 and 24.94 kK were assigned to the transitions to $^1A_{2g}$ and ^1E_g states respectively, which is identical to the assignment for the

crystal spectrum of K_2PdCl_4.

Again, as for Pt(II), there is some doubt concerning the identity of the small spin-forbidden band occurring at ~17 kK. Day and co-workers (141) argue that, because it is present in both x - y and z polarisations, it must be due to a transition to the ^3E_g, as seen from the results listed in Table 7.5.

Table 7.5

Polarisations for the bands in square-planar d^8 systems

$^{1,3}A_{2g}$	xy
$^{1,3}B_{1g}$	xy, z
$^{1,3}E_g$	xy, z

These results have been confirmed by Martin et al. (148).

It would seem, therefore, that the best assignments for both $PdCl_4^{2-}$ and $PtCl_4^{2-}$ are as shown in Table 7.6.

Table 7.6

Assignments for $PdCl_4^{2-}$ and $PtCl_4^{2-}$

$PdCl_4^{2-}$		$PtCl_4^{2-}$
	$^3A_{2g} \longleftarrow {}^1A_{1g}$	17.2
16.7	$^3E_g \longleftarrow$	21
21.5	$^1A_{2g} \longleftarrow$	25.4
23.3	$^1E_g \longleftarrow$	30.3
(139)		(143)

These assignments, together with the energy expressions of Gray quoted earlier, will be used to discuss the spectra obtained in the chloride and the sulphate melts.

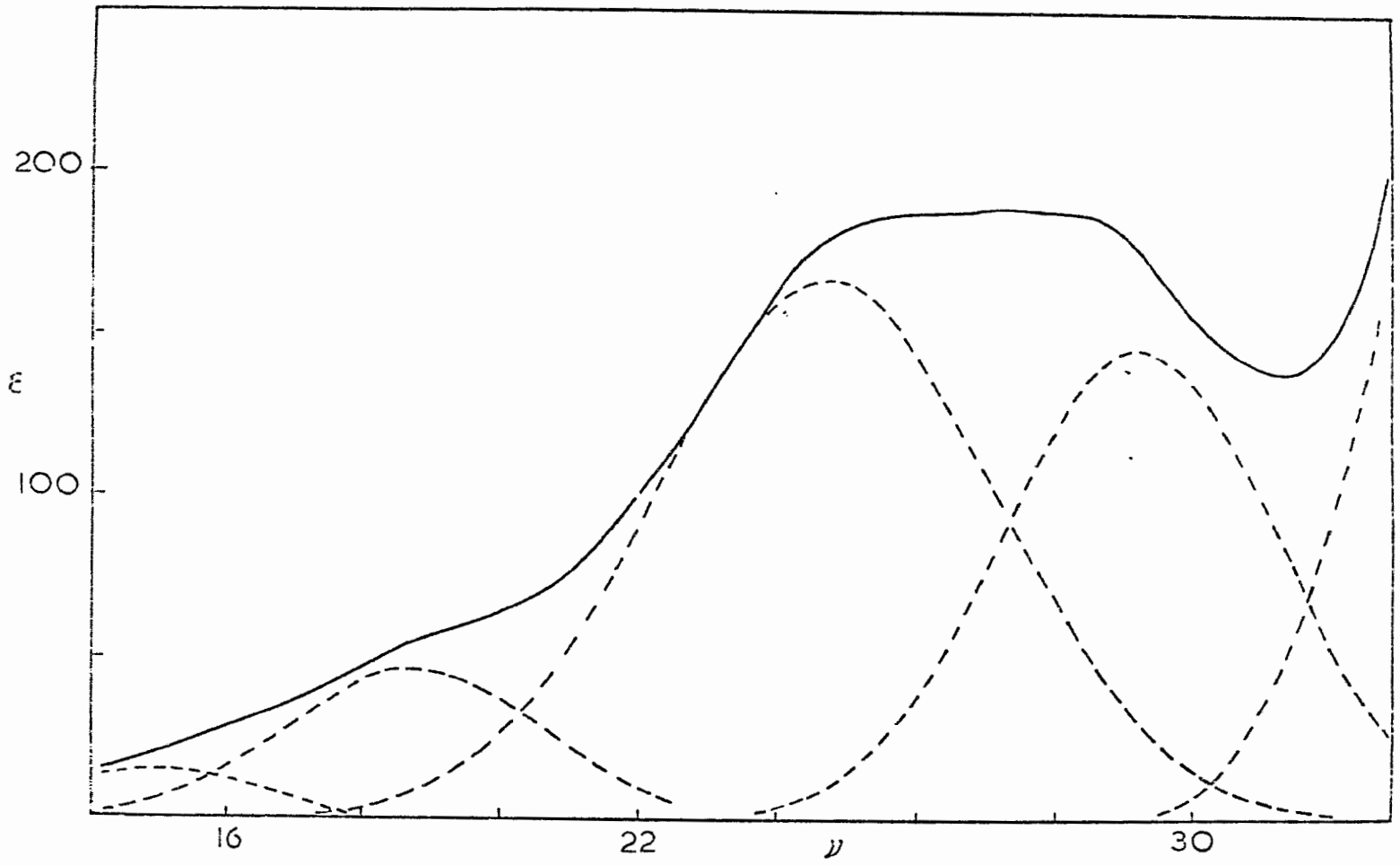

Figure 7.3

Spectrum of Pt(II) in the LiCl - KCl melt at 450° C

7.2 Results. The spectrum of Pd(II) in the LiCl - KCl eutectic at 450°C is shown in Figure 7.2. Also shown in this diagram are the Gaussian components obtained by the method outlined in Appendix A. Figure 7.3 shows the corresponding spectrum for Pt(II). The band positions and extinction coefficients for both Pd(II) and Pt(II) are listed in Table 7.7.

Table 7.7

Spectra of Pd(II) and Pt(II) in the LiCl - KCl melt at 450°C

Pd(II)		Pt(II)	
ν (kK)	ε	ν(kK)	ε
15.8	14	15	15
19.8	278	18.8	47
24.5	65	24.7	167
		29.2	146

The results for Pd(II) in the Li_2SO_4 - Na_2SO_4 - K_2SO_4 melt at 550°C are shown in Figure 7.4, with the band positions listed in Table 7.8.

Table 7.8

Spectrum of Pd(II) in the Li_2SO_4 - Na_2SO_4 - K_2SO_4 melt at 550°C

ν(kK)	ε
17.8	33
21.75	368

Figure 7.5 shows the spectra of Pd(II) in aqueous solutions of sulphuric acid: spectrum A in 1.2 M, B in 7.4 M and C in 17.4 M. The complete results for the aqueous sulphuric acid spectra are shown in Table 7.9.

Table 7.9

Spectra of Pd(II) in aqueous sulphuric acid solutions

H_2SO_4 molarity	ν(kK)	ε	ν(kK)	ε	ν(kK)	ε
1.2	18.7	8	25.9	135	--	--
2.45	18.0	6	25.4	128	30	17
6.23	17	25	25	174	29.7	32.5
7.44	17.4	24	25.3	185	31.6	44
14.03	17.5	14	23.5	153	--	--
17.36	16	8	22.65	156	--	--

An attempt was made to obtain a solution of Pt(II) in the sulphate melt by anodisation. No dissolution was observed even with the lowest current-density ~ 0.05 mA/cm^2 available. Although there are references in the literature to sulphato-complexes of Pt(II) (150) and to solutions of 'platinum sulphate' (151), well characterised complexes of Pt(II) containing only sulphate as a ligand are unknown. The preparation of $PtSO_4$ and a sulphato-complex of platinum was attempted, starting from $PtCl_2$ and K_2PtCl_4, using the Me_2SO_4 method of Lautie (152). In both cases, a dark brown or black solid was obtained which had no infra-red bands attributable to S - O stretches. On refluxing K_2PtCl_4 with concentrated sulphuric acid, a similar dark solid was obtained. Another method that was tried was to add K_2PtCl_4 to the sulphate melt. This resulted in decomposition of the K_2PtCl_4 and the production of bright silvery globules, presumably of platinum metal. No spectra are reported, therefore, for Pt(II) in sulphate media.

7.3 Discussion.

7.3.1 LiCl - KCl melt. A comparison of the results in Tables 7.1, 7.2 and 7.5 indicates quite clearly that the species present in the melt are very similar to those present in both aqueous solutions and crystals. This would tend to suggest that in the chloride melt both platinum and palladium are square planar. This will be examined in some detail later.

During the course of the work reported in this chapter, Bailey and McIntrye (4) published their results on the spectra of Pd(II) and Pt(II) in the LiCl - KCl eutectic. The results obtained at 400°C are shown in Table 7.10.

Table 7.10

Spectra of Pd(II) and Pt(II) in LiCl - KCl

(Bailey and McIntyre)

Pd(II)		Pt(II)	
ν(kK)	ε	ν(kK)	ε
20.3	240	19.5	8
		25.6	15
		28.8	15

The result for palladium, bearing in mind that Bailey and McIntyre did not carry out a Gaussian analysis and thus did not obtain the bands at 15.8 and 24.5 kK, is very similar to that obtained in this work. The band positions for platinum are also in reasonable agreement and would be even better after Gaussian analysis since, as Figure 7.3 shows, the maxima of the Gaussian components do not occur in the same position as the spectral maxima. The extinction coefficients, however, differ

almost exactly by a factor of 10. The calculations performed in order to obtain the values of the extinction coefficients listed in Table 7.7 were checked, but no such discrepancy could be detected. In the paper (4) no details of the analytical method were given, neither were they reported in the thesis of McIntyre (153), so that no check is available on their values. The fact that the values in Table 7.7 are greater than for the aqueous spectrum is a point in their favour, since, if the symmetry does not change, a decrease in extinction coefficient on raising the temperature is not to be expected. The answer to the problem lies in a Beer's law study of the type reported for Rh(III) in the sulphate melt in Chapter 5. This was not carried out because at the time of the study the cells being used were prepared from square cross-section quartz tubing as described in Appendix C. It would be unfair to argue that the discrepancy arises because these cells were not uniform since the results for Pd(II) in the chloride melt, where agreement was achieved, were obtained using the same type of spectral cell.

Turning now to the question of assignments for the melt spectra, the platinum (II) case will be considered first. Because of the very great similarity between the aqueous, crystal and melt spectra, it seems appropriate to use the square-planar assignments discussed earlier. Accordingly, the band assignments are shown in Table 7.11, together with representative crystal and aqueous spectra which will be used in the subsequent discussion.

Table 7.11

Band assignment for the spectrum of Pt(II) in LiCl - KCl

	Melt	Aqueous (92)	Crystal (141)
$^3A_{2g} \longleftarrow {}^1A_{1g}$	15.0	17.7	17.3
$^3E_g \longleftarrow$	18.8	21.0	20.3
$^1A_{2g} \longleftarrow$	24.7	25.5	26.0
$^1E_g \longleftarrow$	29.2	30.2	28.9

Using the values for the spin-allowed bands only, together with the energy expressions quoted earlier, assuming $F_2 = 10F_4 = 1$ kK, the values of Δ_1 and Δ_2 for the melt, aqueous and crystal spectra shown in Table 7.12 were obtained.

Table 7.12

Ligand field parameters for Pt(II)

	Melt	Aqueous	Crystal
Δ_1 (kK)	28.2	29	29.5
Δ_2 (kK)	6.0	6.2	4.4
$\Delta_1 + \Delta_2$ (kK)	34.2	35.2	33.9

The assignment listed in Table 7.11 corresponds to the order of d orbitals labelled 2 in Figure 7.1. The energies Δ_1 and Δ_2, therefore, represent the splitting between the $x^2 - y^2$ and the xy and (xz, yz) orbitals respectively. If the effect of decreasing the tetragonal distortion, i.e. moving the ligands on the z axis closer to the xy plane which, in turn, corresponds to a movement towards the left in Figure 7.1, is considered, then the following results should be obtained:

(i) Δ_2 should decrease

(ii) $\Delta_1 + \Delta_2$ should decrease.

The effect on Δ_1 is rather difficult to predict with any certainty because the relative slopes of the $x^2 - y^2$ and the xy orbitals are difficult to estimate. From Table 7.12 it can be seen that Δ_2 decreases in the order aqueous, melt, crystal with the same order for the decrease in $\Delta_1 + \Delta_2$. It would, therefore, appear that in the crystal the effect of the ligands on the z axis is greater than in the melt which, in turn, is greater than in the aqueous solution. Now the crystal structure of K_2PtCl_4 has been shown to consist of a columnar arrangement of $PtCl_4^{2-}$ units (154) with a Pt - Pt distance of 4.13 Å. It is not strictly correct to compare directly the aqueous, melt and crystal spectral parameters because of the difference in ligands situated on the z axis. Thus, in the crystal there are two $PtCl_4^{2-}$ units on the z axis; in aqueous solution they are liable to be water molecules, although if a large excess of Cl^- is available there will be competition between H_2O and Cl^-, whilst in the melt they could be Cl^- ions or even cations.

An equivalent argument was put forward by Bailey and McIntyre (4) who concluded that the ligands on the z axis were having more effect in the melt than in aqueous solution. These authors did not, however, consider the crystal spectra. On the other hand, the difference between Cl^- and $PtCl_4^{2-}$ as a ligand might be such that a direct comparison is misleading.

One difference between the melt and aqueous spectra that has not been discussed so far is that of temperature. The effect of temperature on the Pt(II) spectrum in the chloride melt was investigated by Bailey and McIntrye (4) at 400°

and 450°C. They observed that the first spin-allowed band did not move, i.e. Δ_1 remained constant, whilst the second spin-allowed and the second spin-forbidden bands moved to lower energies, i.e. Δ_1 and $\Delta_1 + \Delta_2$ decreased. This was interpreted in terms of a cation-anion association in the melt.

The conclusion to be drawn, therefore, is that in the chloride melt Pt(II) exists essentially as the $PtCl_4^{2-}$ species which has some species, whether anionic or cationic is uncertain, although cationic would appear to be indicated from the temperature studies of Bailey and McIntyre, above and below the plane of the complex. Further work, including studies at various temperatures in different alkali metal halide solvents, is necessary before a complete description of the species present in this melt is possible.

The band positions and assignments for the Pd(II) spectrum in the chloride melt are shown in Table 7.13, together with representative solution and crystal spectra for comparison purposes.

Table 7.13

Band assignments for Pd(II) in the LiCl - KCl melt

	Melt	Aqueous (140)	Crystal (139)
$^3A_{2g} \leftarrow {}^1A_{1g}$	15.8	16.6	17.5
$^3E_g \leftarrow$			20.0
$^1A_{2g} \leftarrow$			
$^1E_g \leftarrow$	19.8	21.1	22.8
	24.5	25.3	

The aqueous spectrum reported by Miller (140), did not contain the band at 25.3 kK. This band was obtained as a result of Gaussian analysis,although Day et al. (147) quote results of Harris and co-workers (139) in which bands at 22.1 and 25.0 kK with extinction coefficients of 200 and 250 respectively are listed. The original paper (139), however, contains no such spectrum. The band at 21.1 kK in the aqueous spectrum has been assigned to the $^1E_g \longleftarrow {}^1A_{1g}$ transition on the basis of the MCD results of McCaffery et al. (149). The similarity between the aqueous and melt spectra leads to an identical assignment for the melt. The much weaker spin-forbidden band occurring at 15.8 kK in the melt is assigned as the $^3E_g \longleftarrow {}^3A_{2g}$ transition, in accordance with the aqueous and the crystal spectra. Assignment of the band at 25.3 kK in the aqueous and 24.5 kK in the melt spectra presents a few problems. The possibilities are as follows:

(a) $^3B_{1g} \longleftarrow {}^1A_{1g}$ transition. However, it has an extinction coefficient ~ 4.5 times greater than for the lower energy spin-forbidden band as shown in Table 7.7.

(b) $^1B_{1g} \longleftarrow {}^1A_{1g}$. In the crystal and the aqueous spectra this transition has been assigned to the band occurring at 29.5 and 30.3 kK respectively.

(c) $^1A_{2g} \longleftarrow {}^1A_{1g}$. This would lead to the ordering of d orbitals designated 3 in Figure 7.1. If this suggestion is correct, then on going from the crystal to solutions there is quite a drastic change in the ordering of the d levels (scheme 2 to scheme 3 in Figure 7.1).

In view of the lack of sufficient data to distinguish between these three possible assignments, the remaining discussion will centre on the main spin-allowed band which has been assigned to the $^1E_g \longleftarrow {}^1A_{1g}$ transition. Assuming that this is the second spin-allowed band, i.e. energy scheme 2 (Figure 7.1), then as the tetragonal distortion decreases (a movement to the left in Figure 7.1), $\Delta_1 + \Delta_2$ should decrease and the band should move to lower energy. As shown in Table 7.13, this is exactly what happens on going from crystal to aqueous to melt. If the same decrease in tetragonal distortion is considered for scheme 3 (Figure 7.1) in which this band is now the first spin-allowed band, the same result would be obtained, i.e. the band should move to lower energies. The effect of increasing the temperature, as Bailey and McIntyre (21) showed, was to move the main visible band 0.4 kK to lower energies for a temperature change of 200° between 400° and 600° C.

For both Pt(II) and Pd(II) it has been shown that the spectral changes which occur on going from the aqueous to the melt system may be correlated with a decrease in the tetragonal distortion of the parent octahedron. In other words, the ligands on the z axis are exerting more effect in the melt than in aqueous solution. This result led to an attempt to fit the results using an octahedral model. As mentioned earlier, the principal coordination number for Pd(II) and Pt(II) is four, however, coordination numbers greater than four are reasonably well established. Thus, Griffith et al. (155) reported a series of nitric oxide complexes of Pd(II) and Pt(II) which, they argued, were octahedral. The UV-visible spectra of these compounds were not investigated. Several authors have suggested that in aqueous solution molecules of solvent are bonded above and below the plane (139, 143, 156).

The Tanabe-Sugano diagram (16) for an octahedral d^8 complex shows that for reasonable values of Δ and B ($\sim$25 kK and 500 cm^{-1} respectively) two spin-forbidden and two spin-allowed bands should occur in the spectrum. A further spin-allowed band at much higher energies will almost certainly be hidden by charge-transfer transitions. As Table 7.7 shows, such a spectrum does occur for Pt(II) whilst for Pd(II) one of the weaker bands is apparently missing. The octahedral assignment is then as shown in Table 7.14 which also includes the energy expressions for the transitions as quoted in Jørgensen (27).

Table 7.14

Octahedral assignment for Pd(II) and Pt(II) in the LiCl - KCl melt

	Pd(II)	Pt(II)	
$^1E_g \leftarrow {}^3A_{2g}$		15	8B + 2C
$^1A_{1g} \leftarrow$	15.8	18.8	16B + 4C
$^3T_{2g} \leftarrow$	19.8	24.7	Δ
$^3T_{1g} \leftarrow$	24.5	29.2	Δ + 12B

The values of the ligand field parameters Δ and B evaluated for both the melt and aqueous spectra are shown in Table 7.15.

Table 7.15

Ligand field parameters for Pd(II) and Pt(II) in octahedral symmetry

	Pd(II)		Pt(II)	
	Aqueous	Melt	Aqueous	Melt
Δ	21.1	19.8	25.5	24.7
B	350	392	392	375

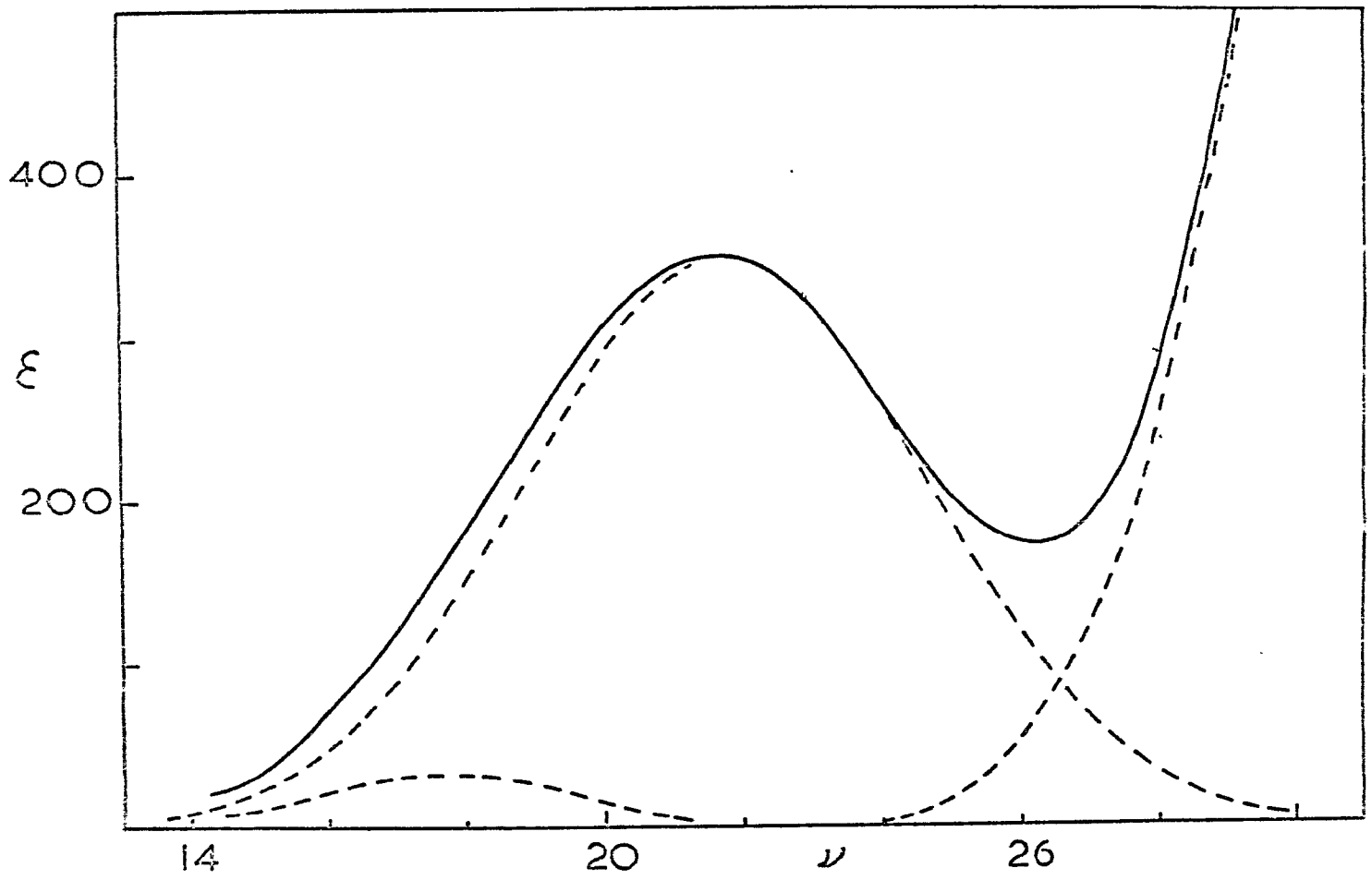

Figure 7.4

Spectrum of Pd(II) in the Li_2SO_4 - Na_2SO_4 - K_2SO_4 melt at 550° C

The values of Δ are very reasonable for second and third row elements and, furthermore, for both palladium and platinum they show a decrease as the temperature is raised to 450°C.

This comparison between the melt and aqueous spectra is invalid, however, because as discussed earlier, the MCD results confirm that the ground state in aqueous solutions is a singlet whilst for an octahedral entity it must, as indicated in Table 7.14, be a triplet. The nature of the ground state in the melt must be determined before the species present in the melt can be further characterised. This could be done either by MCD measurements or a direct magnetic susceptibility measurement.

The conclusion that can be drawn from the above discussion is that in the chloride melt Pd(II) and Pt(II) are present as tetragonally distorted octahedral species with the degree of distortion undetermined.

7.3.2 Pd(II) in sulphate media. The spectrum of Pd(II) in the sulphate melt is very similar to the chloride melt spectrum and there seems little doubt that the type of species present in both melts are also very similar. The main difference between Figures 7.2 and 7.4 is that the smaller band, occurring at slightly higher energies than the main visible band, is missing in the sulphate spectrum. The fact that both the bands in the sulphate melt spectrum have moved by 2 kK to higher energies compared to the chloride melt suggests that both bands are transitions to the same type of excited states which are, as discussed earlier, believed to be the ^3E_g and ^1E_g states. Furthermore, the movement to higher energies suggests that the SO_4^{2-} ligand lies above Cl^- in the spectro-chemical series.

The results for the aqueous sulphuric acid solutions containing Pd(II) show

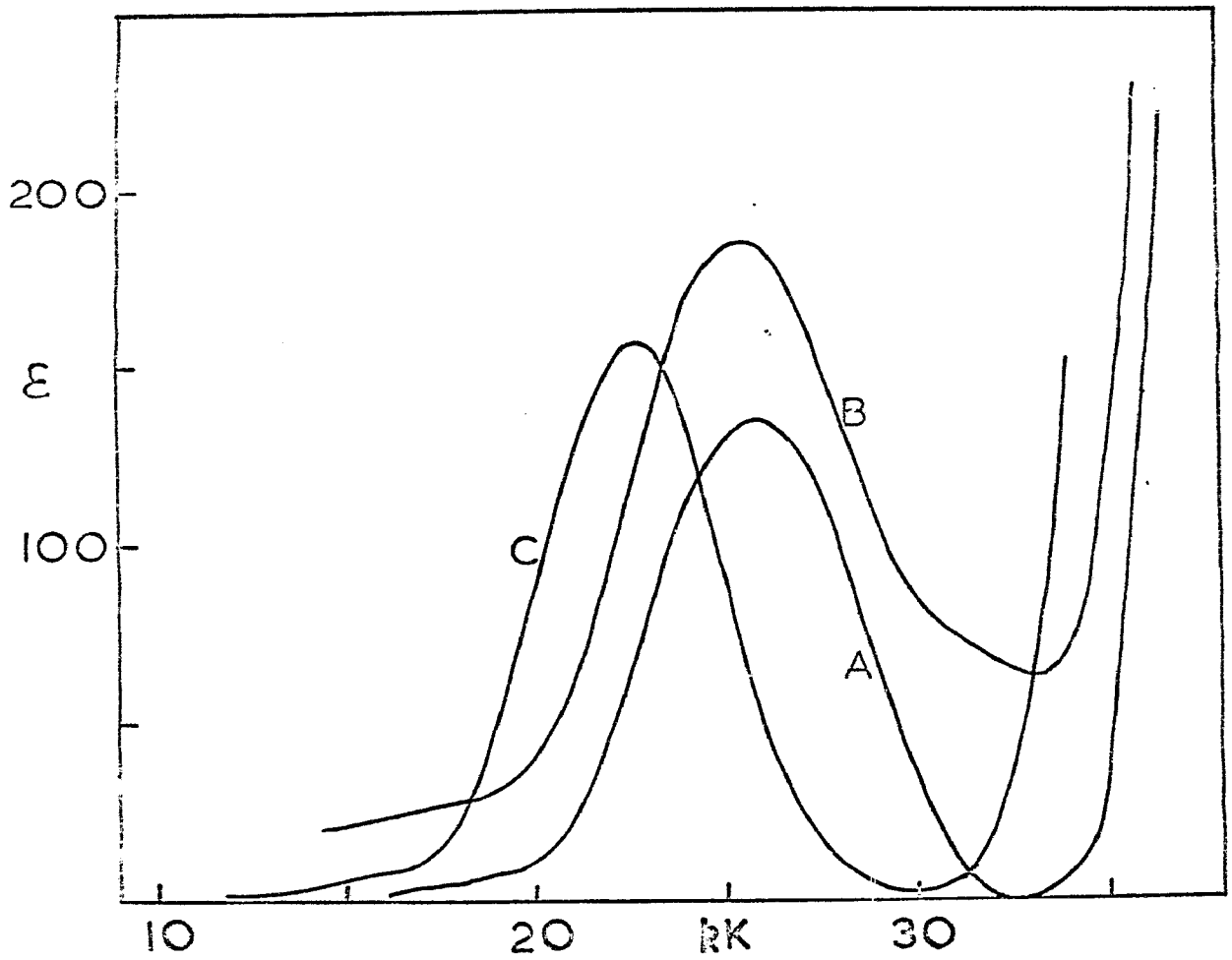

Figure 7.5

Spectrum of Pd (il) in 1.2 M(A), 7.4 M(B), and 17.4 M(C) sulphuric acid

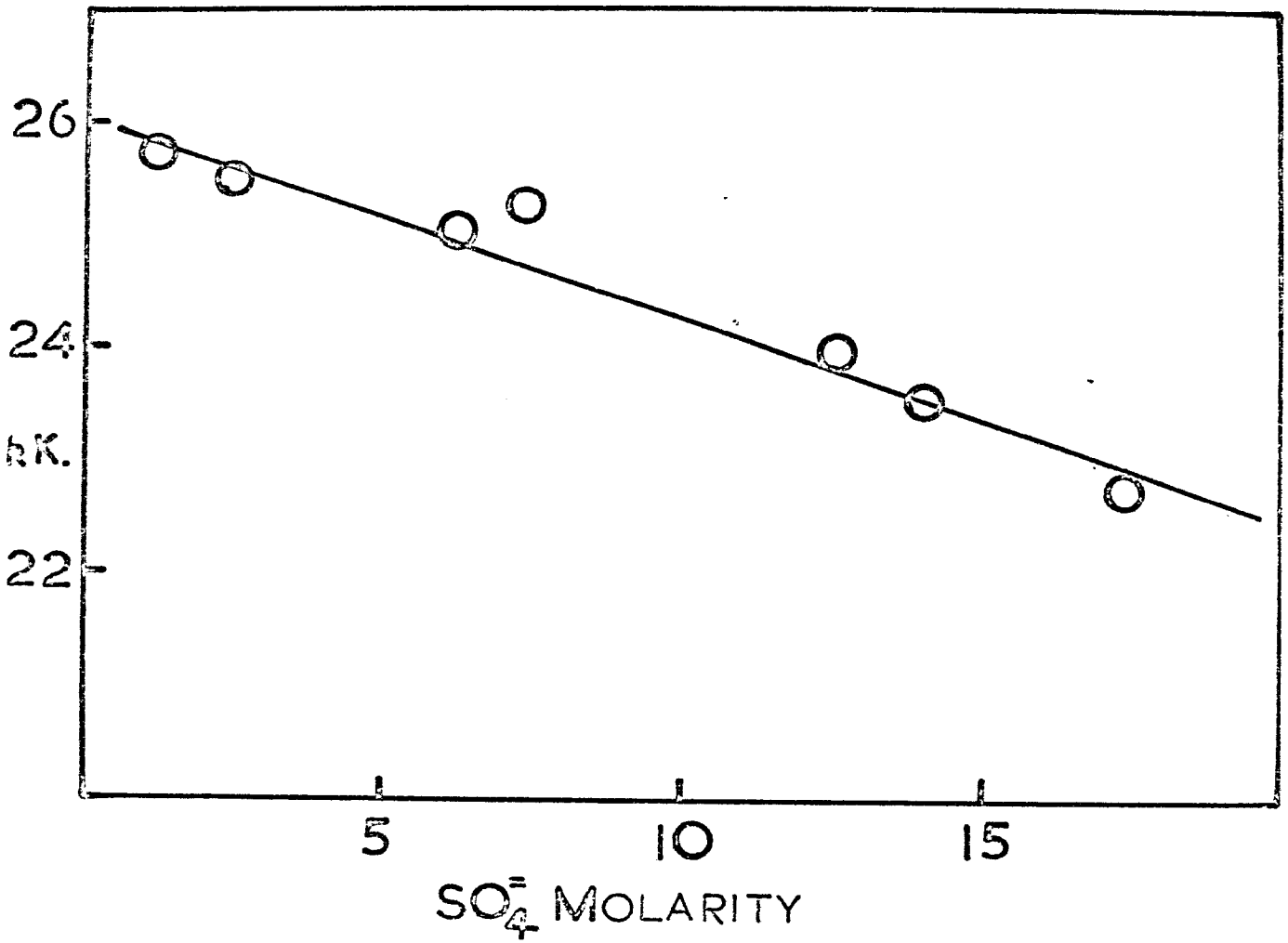

Figure 7.6

Band position of Pd(II) spectra in sulphuric acid as a function of sulphate molarity

considerable similarity to the Pd(II) spectra discussed previously. As Table 7.9 shows, there are two rather curious effects at intermediate acid strengths. Firstly, the third band appears and then, as the acid strength increases further, disappears again. Secondly, the extinction coefficient of the main band, on the whole, is larger than for both dilute and concentrated acid solutions. Too much emphasis cannot be placed on the extinction coefficients because insufficient data were obtained to allow an error to be determined for each of the quoted values. The position of the main visible band is dependent on the acid molarity as shown by Figure 7.6. Whether any significance can be attached to the more or less straight line is a moot point. Two things are certain, however. Firstly, the coordinating atom throughout the range of solutions is oxygen, so that large spectral changes are not expected. Secondly, it is extremely unlikely that the only change between very dilute solutions, which almost certainly contain $Pd(H_2O)_4^{2+}$, and the very concentrated ones is solely a matter of protonation; in other words, a change of ligand is indicated. Furthermore, because the bands are moving to lower energies, this ligand lies below water in the spectrochemical series. Any attempt to characterise the ligand further, i.e. to distinguish between SO_4^{2-}, HSO_4^- or H_2SO_4 is not easy to carry out.

The identification of the spectrum in dilute acid solutions as being due to the $Pd(H_2O)_4^{2+}$ species is based on the published spectrum of this compound. This has been reported by both Jørgensen (27) and Livingstone (157) who obtained a band at 26.4 ($\varepsilon = 86$) and 26.2 kK ($\varepsilon = 200$) respectively. In sulphuric acid the band is found at 25.9 kK with $\varepsilon = 135$ whilst in dilute perchloric acid it was found at 26 kK with $\varepsilon = 86$, in reasonable agreement with Jørgensen's results.

A detailed explanation of the appearance and disappearance of the third band is not easy to formulate. Certainly, within this acid concentration replacement of H_2O by the incoming ligands must be taking place, but whether this is the sole effect occurring is impossible to say.

In view of the previous discussion concerning solvation of square-planar entities in solution, an NMR low temperature study of Pd(II) in concentrated H_4SO_4 was carried out. The results, however, were all negative: even at $-25^{\circ}C$ only a single solvent line was observed. Although at the lowest temperatures it had broadened considerably, it showed no tendency to split into different components.

The work reported in this chapter has shown that in aqueous solution, sulphuric acid solutions and both the sulphate and chloride melt, the M(II) species are very similar to one another. By comparison with the crystal spectra, it is evident that they may be described, to a first approximation at least, as square-planar. No direct evidence concerning the nature and importance of the ligands on the z axis was obtained.

7.4 Experimental. Both the melts and the concentrated solid solutions used in preparing the solutions for spectral work were made as outlined in Appendix C. The metals used to prepare the solutions by anodisation (Pd in the sulphate melt and sulphuric acid, and Pt in the chloride melt) were obtained from Johnson Matthey, who also supplied the K_2PdCl_4 and $PtCl_2$. K_2PtCl_4, used in the attempt to prepare solutions of sulphato-complexes, was obtained from Alfa Inorganics.

Analysis for palladium was carried out using dithizone (158) for the chloride melt and α-furildioxime for the sulphate-containing solutions (159). The calibration

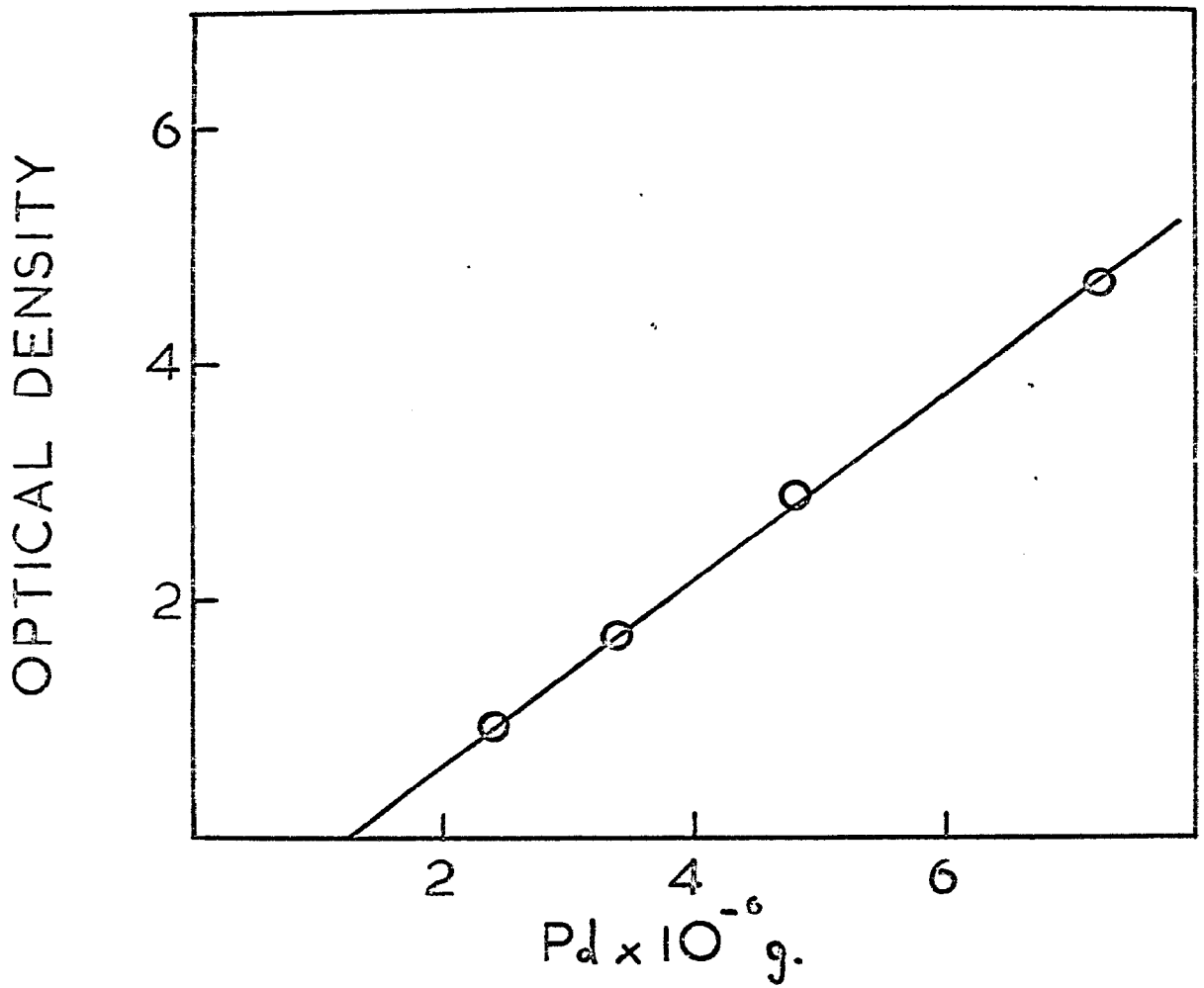

Figure 7.7

Beer's law plot for Pd analysis using dithizone

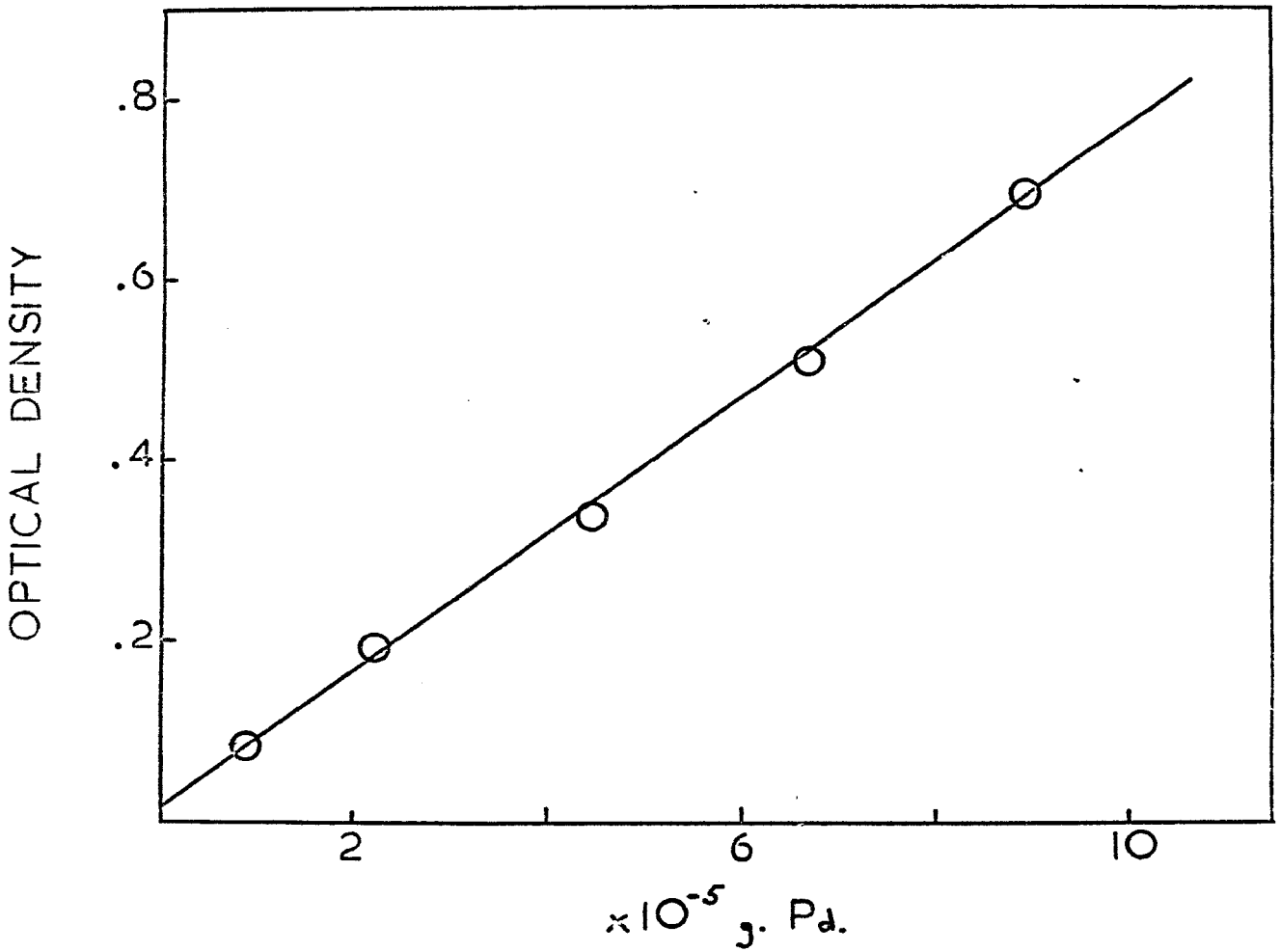

Figure 7.8

Beer's law plot for Pd analysis using α-furildioxime

curves are shown in Figures 7.7 and 7.8 respectively. The optical density was measured at 450 mμ using dithizone and 380 mμ using α-furildioxime. Whilst the dithizone reaction gave a calibration curve which could be used with the chloride media, it was not at all satisfactory when large quantities of sulphate were present. As Figure 7.7 shows, the calibration curve is a straight line but it does not pass through the origin, thereby indicating that Beer's law is not obeyed for low palladium concentrations using this analytical method. The deviation is the result of a combination of factors, of which experimental error and dissociation of the palladium-dithizone complex are probably the largest. The α-furildioxime method approaches closer to ideal Beer's law behaviour, although here, once again, the line does not pass through the origin, a fact which is almost certainly due to experimental error.

The platinum analyses were carried out using the standard stannous chloride method (160) in which the optical density is measured at 403 mμ after the colour had been developed by boiling the aliquot with $SnCl_2$ and HCl. The standard curve is shown in Figure 7.9.

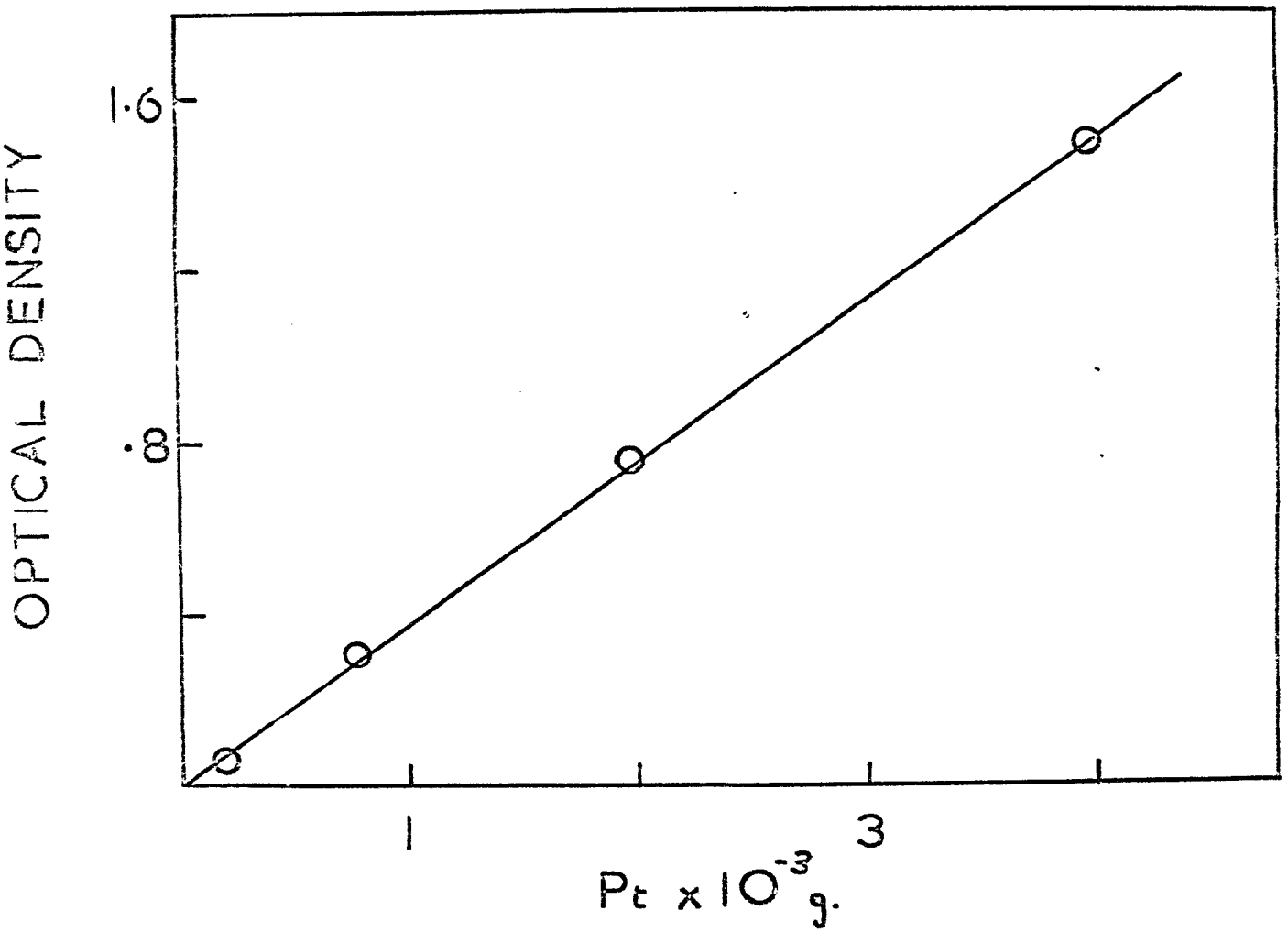

Figure 7.9

Beer's law plot for Pt analysis using $SnCl_2$

CHAPTER 8

GENERAL DISCUSSION OF RESULTS

The diverse nature of the results reported in Chapters 3 - 7 precludes any comprehensive general discussion. That this is the case can be seen from the fact that in the chloride melt the stable oxidation states are four for osmium, three for rhodium and iridium, and two for palladium and platinum. Nevertheless, a few generalisations can be made.

The second and third row elements exist in both the chloride and sulphate eutectic melts in oxidation states and coordination geometries which are directly comparable with the aqueous system. In most cases the stable species has a high degree of symmetry, e.g. octahedral for Os(IV), Ir(III). Palladium and platinum, however, approximate to square-planar but do not appear to be completely identical, in as much as the solvating species, situated above and below the plane of the molecule, are likely to be different from those in aqueous solution. On the other hand, the first row elements are not the same as the stable aqueous species. For cobalt it is not easy to decide whether Co(II) or Co(III) is the more common oxidation state as far as complex formation is concerned. However, as will be mentioned later, it is complex formation by the solvent species, which may be regarded as a special case of solvation, which is under discussion. In this case, the most common oxidation state is probably Co(II), with the majority of complexes being octahedral or slightly distorted. Tetrahedral cobalt complexes in solution

are known, e.g. $CoCl_4^{2-}$, but solvated species are very rare. (The tetrahedral $Co(H_2O)_4^{2+}$ species postulated by Swift and Connick (91), which unfortunately has found its way into the textbooks (161), has, as the result of further experimental work, since been discarded (see Chapter 4)). In the sulphate eutectic melt, the cobalt (II) species can be described as distorted tetrahedral. For Ni(II) also, the sulphate melt species is distorted. In this case, though, the distortion, which is not well defined, proceeds from an octahedral species, which is also the most common geometry for aqueous solutions. With the information at present available, it can be concluded that the first row elements do not give regular solvated species. The second row elements, on the other hand, produce fairly symmetrical species in the melt. Whether this situation would remain the same after an intensive investigation, entailing variations of both temperature and melt composition, remains to be seen. Such an investigation involving Pd(II) or Pt(II) in the LiCl - KCl system might produce sufficient information to allow the species present in the eutectic melt to be defined more precisely.

The irregular nature of the first row elements has been explained, particularly for Co(II) in chloride melts, in terms of the cobalt species reflecting the structure of the melt. A comparison with the aqueous system, where Li^+ promotes a greater degree of structure of the iceberg type than do the higher elements in the same group, is not very satisfactory. Thus for the nickel sub-group, in the melt, where the charges remain the same although the basic stereochemistry changes, the lighter member should promote a greater degree of uniform structure in the melt. The results, on the other hand, indicate that the nickel species is distorted whereas the palladium and

platinum entities are more nearly regular. The situation in the melt could be such that, whereas nickel, rather than actually promoting structure within the melt, reflects the actual structure present, for palladium and platinum the ion itself distorts the melt structure so as to adopt a structure which is amenable to the metal ion. A similar analysis for the cobalt sub-group and for Ru(III) and Os(IV) is not quite as simple because of the different ionic charges which these species have in the melt.

If the spectra of Rh(III) (Figure 5.1) and Pd(II) (Figure 7.2) in the chloride melt are compared, it can be seen that there is a great deal of similarity between them. Such an effect has been pointed out before for the aqueous spectra (27) where it was shown that the ratio of the first spin-allowed bands for the corresponding Pd(II) and Rh(III) complexes are very nearly constant in the range 1.02 to 1.10. The values for the chloride and sulphate melts are 1.09 and 1.03 respectively. The result for the chloride melt compares rather well with the value of 1.09 quoted for the chloro-complexes in aqueous solution. The agreement between the aqueous and melt values can be regarded as confirming the assignments suggested earlier. More correctly the melt spectral assignments have been brought into line with those for the aqueous spectrum which themselves are reasonably well accepted. An exactly similar situation is found for Pt(II) and Ir(III). In this case, the ratio of the first spin-allowed bands is 1.06 for both the aqueous hydrochloric acid and the chloride melt spectra.

It has been mentioned earlier that the species present in the melt should be regarded as a special class of solvated species. However, it has been assumed, and

indeed shown, that these species are quite well defined. Thus the $RhCl_6^{3-}$ species present in the melt is virtually identical with that present in concentrated hydrochloric acid solutions. In this respect then, the melt species could also be described as a complex in much the same way as the $Co(H_2O)_6^{2+}$ entity in aqueous solutions can be regarded as both a complex and a solvated species. In both cases no attempt is made to define the stability although it is certainly not suggested that $IrCl_6^{3-}$ for example, in the chloride melt, exists in a definite unchanged situation in which no chloride exchange is occurring. The present study, however, has shown that the relaxation time of the complexes is less than the characteristic relaxation time of UV-visible spectroscopy ($\sim 10^{-11} - 10^{-12}$ sec). The controversy surrounding the existence of complex ions or ion pairs in solution (162, 163) is not meaningful for the results reported here. However, if the existence of covalent character in the bond between the metal ion and the solvent, as indicated by the reduction of the Racah parameter B from the free ion value, is regarded as a suitable definition of a complex, then the species should be regarded as complexes.

In Chapter 2 it was suggested that Δ is inversely proportional to the n^{th} power of the metal-ligand distance. On raising the temperature, the M - L distance would be expected to increase, thereby causing Δ to decrease and the absorption bands to move towards the red. Such an effect is indeed observed, e.g. for Rh(III) (Chapter 5) and Pd(II) (Chapter 7). Furthermore, if the M - L distance increases then the degree of covalency, as measured by B, should also decrease. In other words, the value of B should be closer to the free ion value in the melt than for the corresponding aqueous spectrum. Once again, this prediction is borne out by the

results reported earlier. In both cases, therefore, the ligand field description of complex formation is satisfactory in explaining the results obtained.

It might be concluded that on the whole, the second and third row elements are too regular to warrant much experimental work. Such a naive assumption is unjustified since the present investigation was designed primarily to determine new fields of interest. That this was successful, to some extent at least, has been shown in the suggestions already made concerning future work. For example, a more detailed study of the Os(IV) chloride melt spectra, especially on a kinetic basis, is required; the Pd(II) and Pt(II) systems mentioned earlier also look promising. Taken in perspective it is likely that a detailed study of the spectra of second and third row elements is capable of producing a multitude of experimental results which may have some bearing on the structure and composition of molten salts.

APPENDIX A

Method of Gaussian Wave Analysis

It has been assumed throughout this thesis that the ligand field bands which occur in the absorption spectra of transition metal species can be represented by Gaussian error curves provided the spectra are plotted on an energy scale. The correctness of such an assumption has been examined in Chapter II. In many instances it has been found that a particular absorption band appears to consist of two overlapping bands. These may consist of two relatively strong bands, e.g. Co(II) in 75% sulphuric acid solution (Figure 4.4), or of a strong band with a much smaller band distorting the foot, e.g. Pd(II) in the Li_2SO_4 - Na_2SO_4 - K_2SO_4 melt at 550° C (Figure 7.4). In either case, it is difficult to determine the maxima of the component bands from the shoulders or points of inflection in the spectra. Moreover, in some cases, the presence of small bands is not at all apparent.

By assuming that the bands are represented by Gaussian error functions, it is possible to determine band positions and intensities a little more precisely. The simplest method of resolution is to assume that one side of the band is perfectly Gaussian and then just reflect through the band axis. An alternative and potentially more accurate method has been described in some detail by Chatt et al. (92). In this method the strongest peaks are fitted to the expression:

$$\varepsilon = \varepsilon_{max} e^{-x^2/2}$$

in which ε_{max} is an estimated value of the extinction coefficient at the peak

maximum and x is the value on the abscissa measured from the estimated peak maximum. Values of $e^{-x^2/2}$ were obtained from mathematical tables and then the scale of x was adjusted so as to fit the band. By varying the value of ε_{max} and the peak position, which need not necessarily coincide with the spectral maximum, it is possible to obtain a reasonable fit to the experimental curve provided that the spectral band contains only one component. If more than one band is present, then the fit will not be very good. In this case, the procedure is to choose one set of parameters for the most intense band, or if the components have approximately the same intensity, for the band which is more apparent, and subtract this band from the spectrum. The difference curve is then treated in exactly the same way and the procedure continued until no more bands are apparent. In this way the total number of component bands in the spectrum can be obtained fairly easily. The next step is to vary the peak positions, maxima and band widths of each of the component bands until the difference curve is as small as possible. Although such a procedure would appear to be extremely tedious, in practice fairly good estimates of the peak positions and maxima can be obtained by visual examination of the spectrum. In point of fact, it is the refining of the parameters which constitutes the time consuming part of the curve analysis. It was decided, therefore, to use computer techniques for this refining process.

Although several investigators have reported the use of computer programmes for resolving spectra, (164), it was felt that a relatively simple programme would suffice for the present work. Accordingly, a programme based essentially on the method of Chatt et al. was compiled by Mr. L. G. Boxall. The procedure was as follows: The number of peaks present in the spectrum was determined by inspection

and rough estimates of the peak maxima, height and half-width were made. The difference between the sum of the component Gaussian curves and the experimental curve was calculated. The peak positions, heights and half-widths of all the constituent bands were then varied so as to give the smallest difference curve. The values of the peak positions, heights and half-widths which gave this best fit were recorded. If parameters for n peaks were supplied in the data feed-in and there were, in fact, less than n peaks, say (n - m), then the computer programme was designed such that these m extraneous peaks were eliminated, i.e. they had a final value of zero for their peak heights and half-widths.

It must be borne in mind that no resolution is mathematically unique and, therefore, more than one fit of the experimental curve is possible. Furthermore, if two Gaussian curves with the same half-width are superimposed then the resultant curve is very nearly Gaussian. It is also possible for two bands to overlap to such an extent that the resultant curve becomes almost Gaussian and resolution then becomes difficult, if not impossible. Whilst both of these drawbacks are liable to occur in the systems studied here, it would appear that overlapped, as against superimposed bands, would be the most likely, particularly in the area of regular complexes which have been slightly distorted. Where the complexes are severly distorted it is possible that the levels arising from two different states will be superimposed, in which case, however, splittings of other levels would give an indication of such a distortion.

In spite of these drawbacks, which are relatively minor compared to the initial assumption of Gaussian band shape, it is felt that wave analysis is of some

use in interpreting spectra.

The complete programme listing, including the sub-routines, for Gaussian wave analysis is given below.

```
C..... Gaussian numerical analysis
      Dimension DMS(15, 15)
      Dimension G(3,5,50),R(50), ST(3,5),EX(50),WX(50),DM(15,15),RS(15)
      Dimension WR(3)
      Dimension KPT(5)
      Common DM,G,R,ST,EX,WX,RS,KPT
      Equivalence (G(1,1,1),DMS(1,1))
101   Format (3E11.4,A1)
100   Format (I1,I2,I3)
C..... Read in data subroutine
20    Call G402R(NN,NC,N,K,IND)
C..... Calculate peak variations with each variable G matrix
41    Call G402W(N,K)
C..... Calculate remainder terms
      Do 77 I3=1,K
      R(I3) = EX(I3)
      Do 7 I2=1,N
7     R(I3)=R(I3) - ST(1,I2,)* G(1,I2,I3)
      If (EX(I3) - R(I3)) 32,32,77
32    R(I3)=0.
77    R(I3)= - R(I3)
      L=3*N
      N=L
C..... Calculate normal DETERMINANT
      IE=0
      IF=1
      Do 17 IA=1,L
      IE=IE+1
      If (IE-4) 16,13,13
13    IE=1
      IF=IF+1
16    IC=0
      ID=1
      Do 8 IB=1,L
      IC=IC+1
      If (IC-4) 12,9,9
9     IC=1
      ID=ID+1
```

```
12      DM(IA, IB)=0.
        Do 8 I3=1,K
8       DM(IA,IB)=DM(IA,IB)+G(IC,ID,I3)*G(IE,IF,I3)
        RS(IA)=0.
        Do 17 I3=1,K
17      RS(IA)=RS(IA)-R(I3)*G(IE,IF,I3)
C.....  Solve by Crammers Rule
        Do 500 KJL=1,N
        Do 500 KJK=1,N
500     DMS(KJO,KJK)=DM(KJO,KJK)
        Call G402D(N,D)
        IF(D)18,19,18
19      Write (5,104)
104     Format ('ODET.=0')
C.....  Remove lowest peak to eliminate zero det.
        N=N/3
        IF(N-1)39,39,46
46      X=99999.0
        Do 42 I2=1,N
        IF(ST(1,I2)-X)43,42,42
43      X=ST(1,I2)
        I3=I2
42      Continue
        ST(1,I3)=ST(1,N)
        ST(2,I3)=ST(2,N)
        ST(3,I3)=ST(3,N)
        KPT(I3)=KPT(N)
        N=N-1
        Go to 41
18      DS=D*2.0
C.....  Solve for each variables' correction
        Do 21 I2=1,N
        Do 502  KJL=1,N
        Do 502  KJK=1,N
502     DM(KJL,KJK)=DMS(KJL,KJK)
        Do 22 I3=1,N
22      DM(I3,I2)=RS(I3)
        Call G402D(N,D)
        D=D/DS
        KJK=I2-(I2/3)*3
        KJL=I2/3+1
        IF(KJK)23,23,24
23      KJK=3
        KJL=KJL-1
```

```
      WR(KJK)=D+ST(KJK,KJL)
      Write (5,105)WR(1),WR(2),WR(3), KPT(KJL)
105   Format('OE=',E11.4,' W=',E11.4,' F=',E11.4,' PT.=',A1)
      Write (2,107)WR(1),WR(2),WR(3),KPT(KJL)
      IF(NC-1)33,33,34
C.....Adjust results to repeat calculations
34    IF(WR(1))35,36,36
35    WR(1)=ST(1,KJL)/2.0
36    ST(1,KJL)=WR(1)
      X=(ST(2,KJL)-WR(2))
      Y=X*X
      IF(Y-1.0)51,51,50
50    IF(X)52,51,53
52    WR(2)=ST(2,KJL)-1.0
      Go to 51
53    WR(2)=ST(2,KJL)+1.0
51    ST(2,KJL)=WR(2)
      IF(WR(3)-0.3)37,37,38
37    WR(3)=0.3
38    ST(3,KJL)=WR(3)
      Go to 21
33    Write (2,107)WR(1),WR(2),WR(3),KPT(KJL)
107   Format (3E11.4,A1)
      Go to 21
24    WR(KJK)=D+ST(KJK,KJL)
21    Continue
      NC=NC-1
      IF(NC)39,39,40
40    N=N/3
      Go to 41
39    IF(NN)25,25,26
25    IF(IND-1)20,20,4
C.....Load repeat peak cards
26    Read (2,100)NN,NC,N
      IF(N)26,26,27
27    Do 28 L=1,N
28    Read (2,101)ST(1,L),ST(2,L),ST(3,L),KPT(L)
      K=K+1
      Read (2,106)KJK
106   Format (A1)
      Go to 41
4     Call exit
      End
```

```
Core requirements for
 Common 3470  Variables 46  Program 1070
C..... Read in data for Gaussian analysis
       Subroutine G402R(NN,NC,N,K,IND)
       Common DM(15,15),G(3,5,50),R(50),ST(3,5),EX(50),WX(50),RS(15),KPT(15)
101    Format (3E11.4,A1)
100    Format (I1,I2,I3)
103    Format (I1,4X,F5.0,F5.0)
C..... Load peak cards
20     Read (2,100)NN,NC,N
       IF(N)20,20,503
503    Do 1 L=1,N
1      Read (2,101)ST(1,L),ST(2,L),ST(3,L),KPT(L)
C..... Load data cards
       Read (2,109)(EX(K),K=1,10)
109    Format (5X,10A6)
       Write (5,110)(EX(K),K=1,10)
110    Format ('1',10A6)
       Read (2,102)C
102    Format (4X,E11.4)
       K=1
5      Read (2,103)IND,EX(K),WX(K)
       IF(IND-1)2,3,3
2      EX(K)=EX(K)/C
       K=K+1
       IF(K-51)5,5,54
54     Write (5,111)WX(50)
111    Format ('OEXCESS Data Last W=',E11.4)
55     Read (2,103)IND
       IF(IND-1)55,3,3
3      K=K-1
       Read (2,106)KJK
106    Format (A1)
       Return
       End
Core requirements for G402R
 Common 3470  Variables 10  Program 264
C..... Calculate wave functions
       Subroutine G402W(N,K)
       Common DM(15,15),G(3,5,50),R(50),ST(3,5),EX(50),WX(50)
       YY=0.0
       Do 44 I2=1,N
       IF(ST(1,I2)-YY)44,44,45
```

```
45      YY=ST(1,12)
44      Continue
        YY=YY*0.01
        Do 6 12=1,N
        Do 6 13=1,K
C..... Gaussian wave analysis
        X= ((ST(2,12)-WX(13))*ST(3,12))
        X=X*X/2.0
        G( 1,12,13)=2.71828**(-X)
        X=G(1,12,13)*ST(1,12)-YY
        IF(X)30,30,31
30      G(1,12,13)=0.
31      X=G(1,12,13)
        G( 2,12,13)= - ST(1,12)*ST(3,12)*ST(3,12)*(ST(2,12)-WX(13))*X
        X=G(2,12,13)
6       G(3,12,13)=X*(ST(2,12)-WX(13))/ST(3,12)
        Return
        End
Core requirements for G402W
 Common 3420   Variables  24   Program 282
C..... Pivitol method to solve determinant
        Subroutine G402D(N,D)
        Common A(15,15)
        D=1
        NN=N-1
        Do 10 K=1,NN
        IF(A(K,K))3,2,3
2       Do 5 L=K,N
        IF(A(L,K))6,5,6
5       Continue
        D=0
        Go to 11
6       Do 7 J=K,N
        X=A(L,J)
        A(L,J)=A(K,J)
7       A(K,J)= -X
3       D=D*A(K,K)
        X=A(K,K)
        Do 9 L=K,N
9       A(K,L)=A(K,L)/X
        KK=K+1
        Do 10  L=KK,N
        X=A(L,K)
```

```
      Do 10  J=K,N
10    A(L,J)=A(L,J-X*A)K,J)
      D=D*A(N,N)
11    Return
      End
```

Core requirements for G402D
Common 676 Variables 10 Program 262

APPENDIX B

Measurement of Paramagnetic Susceptibilities by the NMR Method

The magnetic field experienced, and, therefore, the frequency at which resonance occurs for a proton in solution depends on the bulk susceptibility of the solution. If this susceptibility is changed by the addition of a paramagnetic species, then there is a change in the resonance frequency.

Evans (94) has reported a method for measuring the paramagnetic susceptibility of the solute which depends on the above change. In essence this consists of measuring the resonance frequency of a reference compound in both the pure solvent and the solution containing the paramagnetic species of interest. Since it was required to measure the paramagnetic susceptibility in sulphuric acid solutions at temperatures up to 200°C, it was felt that an alternative reference compound to TMS, which boils at 24°C, was required. Furthermore, the compound chosen had to be soluble in sulphuric acid to the extent of ~3% so that signals of reasonable intensity were obtained. The compound chosen was a salt of the tetramethylammonium cation. In order to avoid the presence of chloride ions in the test solution, the sulphate or hydrogen sulphate were deemed most suitable, since in that way no foreign anions would be introduced into the system. Accordingly, a solution of 20 g of $(Me_4N)Cl$ (Matheson, Coleman and Bell Company) in water, to which excess sulphuric acid was added, was evaporated to near dryness several times using a water bath and a vacuum line. This was repeated until no more HCl was detected in the traps. The mixture was then dissolved in ethanol to which a small amount of water had been

added and the solution filtered hot. The product was separated by precipitation with acetone, recrystallised and finally dried at 120 °C. Analysis for sulphate showed that the product was, in fact, $(Me_4N)HSO_4$ rather than the sulphate.

A solution of cobalt sulphate in 98% H_2SO_4 which contained 3% w/v $(Me_4N)HSO_4$ was placed in an NMR tube. A sealed capillary tube containing exactly the same solution, with the exception of the Co(II), was then placed inside the NMR tube which was then degassed and sealed. The NMR spectrum was recorded, using a Varian A-60A spectrometer fitted with a variable temperature probe, over the range 40° - 200 °C. The spectrum obtained is shown schematically in Figure 1.

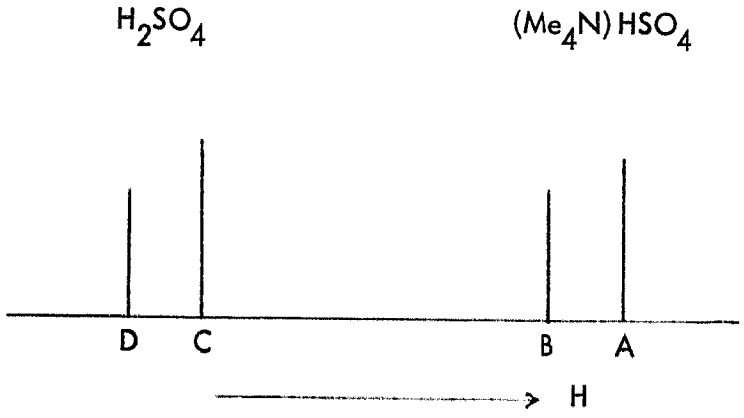

Figure 1

NMR spectrum of Co(II) in 98% H_2SO_4 with $(Me_4N)HSO_4$ as an external reference (schematic)

B - A = true susceptibility shift

D - C = solvent susceptibility shift togehter with Co(II) - solvent interaction effects.

In the temperature range 40° - $200^{\circ}C$ the rate of proton exchange between bulk and coordinated solvent, assuming that some of the ligating species, at least, are HSO_4^-, is sufficiently rapid that only one line was obtained for the cobalt solution.

Evans has shown that the mass susceptibility of the paramagnetic solution is given by:

$$\chi = \frac{3\Delta f}{2\pi fm} + \chi_o + \frac{\chi_o(d_o - d_s)}{m}$$

where:

Δf = frequency shift of the reference signal between the diamagnetic and paramagnetic solutions.

f = frequency at which the resonance is being studied.

m = concentration of paramagnetic species in g/ml.

χ_o = mass susceptibility of solvent.

d_o = density of solvent.

d_s = density of solution.

The third term in this equation is usually ignored since it gives rise to only a very small correction. It has been assumed above that the distance B - A is a true susceptibility shift. LaMar (165), however, has shown that ion pair formation between the $(C_6H_5)_3PCoI_3^-$ complex and the $(Bu_4N)^+$ cation can occur. This ion pair effect can be detected quite readily by changing the concentration of the reference compound. For the case under consideration no change in the shift, at constant temperature, was observed for a solution containing 6% w/v $(Me_4N)HSO_4$

The calculation of χ for the paramegnetic entity is relatively simple, once B - A is identified as the true susceptibility shift. For the instrument which was used in these studies the frequency term f is 60 MHz.

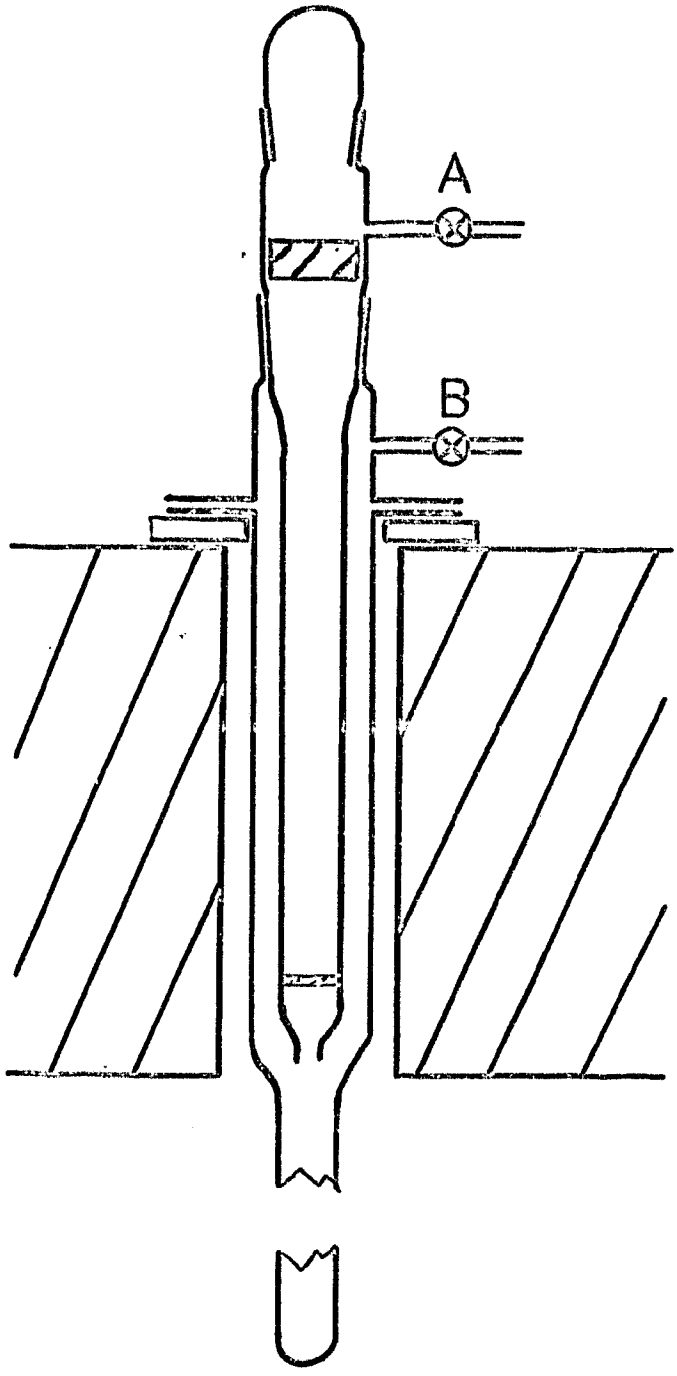

Figure C 1

Melt preparation apparatus

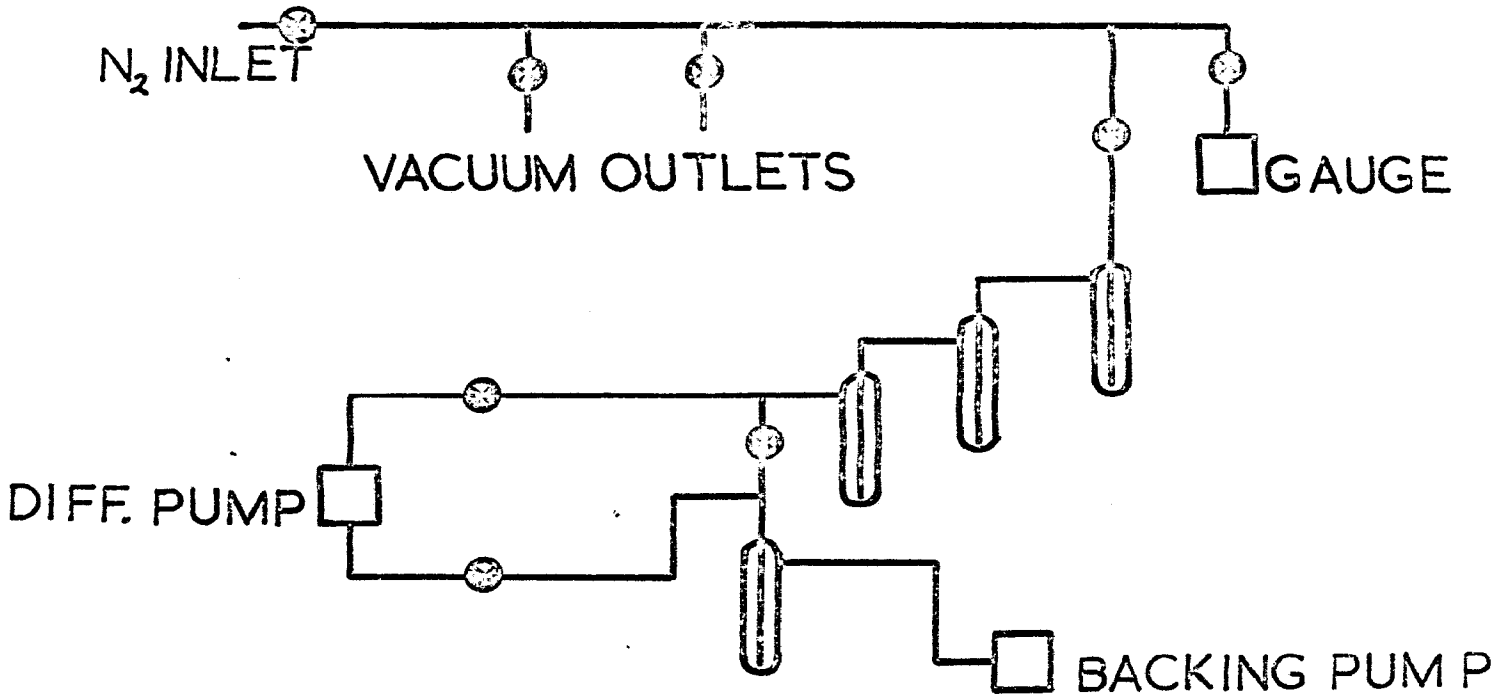

Figure C 2

Vacuum line assembly

APPENDIX C

1. Melt Preparation.

1.1 LiCl - KCl. Although lithium chloride can be obtained commercially with a purity of 99.8% (Baker Analysed Reagent), it is extremely hygroscopic. On fusion, if there is any water present, hydrolysis occurs producing the oxide or hydroxide, which attacks both glass and silica containers. As far as spectral measurements in the LiCl - KCl eutectic melt are concerned, this hydrolysis constitutes the main problem. A critical evaluation of the methods which have been employed in the preparation of the chloride eutectic has been presented by Mackenzie and Johnson (166). The purification procedure that was employed in the present work was the method of Maricle and Hume (167). The eutectic mixture, containing 59 mole % LiCl and 41 mole % KCl, which melts at 352 °C, was placed in the innermost tube above the sintered glass frit (Figure 1). The complete assemply was then placed in a tube furnace and connected to the vacuum line assembly shown schematically in Figure 2. The apparatus was evacuated and left pumping overnight with the tube furnace at ~ 100°C. No attempt was made to control the temperature beyond the use of Variac powerstats. The temperature in the furnace was measured with a chromel-alumel thermocouple and a Cropico P3 potentiometer. The following morning the temperature was gradually increased to 300°C whilst maintaining the vacuum. After several hours at 300°C the vacuum was released and chlorine, which had been scrubbed by concentrated sulphuric acid and passed through a molecular sieve column, was passed up through the bottom of the frit and

through the powdered sample. The eutectic mixture was then melted by raising the temperature to ~360°C whilst chlorine was passing through the system and the chlorine treatment was continued for two hours. After this period of time, the chlorine flow was stopped, stopcock A (Figure 1) was closed and the assembly connected to the vacuum line through stopcock B. In this way a slight negative pressure was applied to the outermost tube, sufficient to slowly filter the melt through the frit and into the storage tube projecting out of the bottom of the furnace. When all the melt had been filtered into this tube, it was sealed under a slight vacuum and stored in a dry box until required. The frozen melt still contained excess chlorine, as shown by its pale yellow colour, which had to be pumped off prior to use as a spectral solvent.

1.2 Li_2SO_4 - Na_2SO_4 - K_2SO_4. The salts, which were all Baker Analysed Reagent grade, were anhydrous except for the lithium one which was supplied as the monohydrate. They were dried in an oven at 120°C to constant weight (which removed the water from the lithium salt as shown by a weight loss experiment) and then a eutectic mixture consisting of 78 mole % Li_2SO_4, 8.5 mole % Na_2SO_4 and 13.5 mole % K_2SO_4 was prepared. This mixture, which has a melting point of 512°C (169), was melted in a pyrex tube inserted in a tube furnace and maintained at 550°C, to ensure uniform mixing. In some cases, the melt was not perfectly clear but on addition of a very small amount of potassium pyrosulfate it soon cleared due, presumably, to the conversion of oxide to sulfate:

$$S_2O_7^{2-} + O^{2-} \longrightarrow 2SO_4^{2-}$$

The frozen melt was stored in sealed bottles until required.

1.3 K_2SO_4 - $ZnSO_4$ and Na_2SO_4 - K_2SO_4 - $ZnSO_4$. In both these mixtures the sodium and potassium salts were the same as in C1.2. The zinc sulphate, on the other hand, was Fisher Reagent grade and required purification. It was recrystallised three times from an ethanol-water mixture and finally dried in an oven, at 120°C, overnight. The anhydrous zinc sulphate was obtained by heating the hydrate at 350°C and 0.015 mm of Hg for 24 hours.

For the K_2SO_4 - $ZnSO_4$ melt the same mixture as used by Duffy et al. (89) was prepared. This consisted of 40 mole % K_2SO_4 and 60 mole % $ZnSO_4$ and had a melting point of ~ 480°C. The mixture was melted and filtered prior to addition to the silica cells.

The Na_2SO_4 - K_2SO_4 - $ZnSO_4$ mixture, in the proportion 25.8, 19.0 and 55.2 mole % respectively, corresponds to a eutectic having a melting point of 385°C (114). Homogeneous mixing of the constituents was obtained by melting and filtering the eutectic prior to use.

2. Determination of Melt Density.

In order to calculate molar extinction coefficients, the density of the melt is required. For the LiCl - KCl eutectic, the density at 450°C is 1.648 g/ml (169), whilst that for the K_2SO_4 - $ZnSO_4$ melt is 2.64 g/ml at 550°C (169). Values for the remaining sulphate melts have not been reported in the literature. The densities of the three sulphate melts were measured using an extremely simple experimental set-up. This consisted of a piece of pyrex tubing, sealed at one end, on which two marks about 5 cms apart had been scratched. The volume of the tube up to each of the scratch marks in turn was determined by adding a known volume of

water. The tube was then dried and weighed, and a weighed quantity of the frozen melt was added. The weight of melt taken was such that the level, when molten, was between the two marks. The tube was then placed inside another tube which contained molten LiCl - KCl eutectic together with a thermocouple. This salt bath was maintained at the desired temperature by having the lower end located in an RF furnace. When the sulphate mixture was molten the inner tube was slowly evacuated to remove any air bubbles. High vacuum on melts containing $ZnSO_4$ was avoided since it appeared that this compound dissociated and the melt went cloudy, probably due to formation of ZnO.

When the system was stable, the temperature along the length of the vertical sample tube was measured with the thermocouple. This was found to be fairly constant, varying by about 3°. The temperatures at which the densities were obtained are thus accurate to about ± 2 C. The height of the lower mark, the meniscus and the upper mark were then found using a cathetometer. By assuming that the pyrex tube was uniform between the two marks, the total volume of the melt was obtained. From the known weights of solid added, the densities could then be calculated.

In order to check the accuracy of the method, the density of a $NaNO_3$ melt which, as a function of temperature over the range 127° - 427°C, has been reported in the literature (168), was measured. The density of this melt was determined at 467°C, which is just outside the range of the reported measurements but close enough to assume that the same expression still holds.

The results obtained are shown in Table 1.

Table 1

Density measurements of the sulphate melt

	Temp °C	Density g/ml
Li_2SO_4 - Na_2SO_4 - K_2SO_4	575	2.2
K_2SO_4 - $ZnSO_4$	590	2.6
Na_2SO_4 - K_2SO_4 - $ZnSO_4$	436	2.7
Na_2SO_4 - K_2SO_4 - $ZnSO_4$	572	2.6
$NaNO_3$	467	1.8(2)
$NaNO_3$ (calc)	467	1.79

The density of the K_2SO_4 - $ZnSO_4$ glass, at 24°C, was also measured using the liquid-displacement method and was found to be 2.9 g/ml. The value found for the K_2SO_4 - $ZnSO_4$ melt at 590°C is in very good agreement with the reported literature value of 2.64 g/ml (169). The usefulness of the method is shown by the very good agreement between the experimental and calculated values for the $NaNO_3$ melt.

3. Melt Spectra.

Instrumentation for fused salt spectrophotometry has progressed far since Gruen first reported his work on molten nitrates using a Beckmann DU spectrometer (170). For obvious reasons recording instruments were soon modified for this work until at the present there is a spectrometer specifically designed for high temperature work of this nature. Reviews of fused salt spectrophotometry and, in particular, instrumentation have been published and the criteria evaluated (171). The modification of the Beckmann DK2 was described by Sandoe and Johnson (172) and will not be

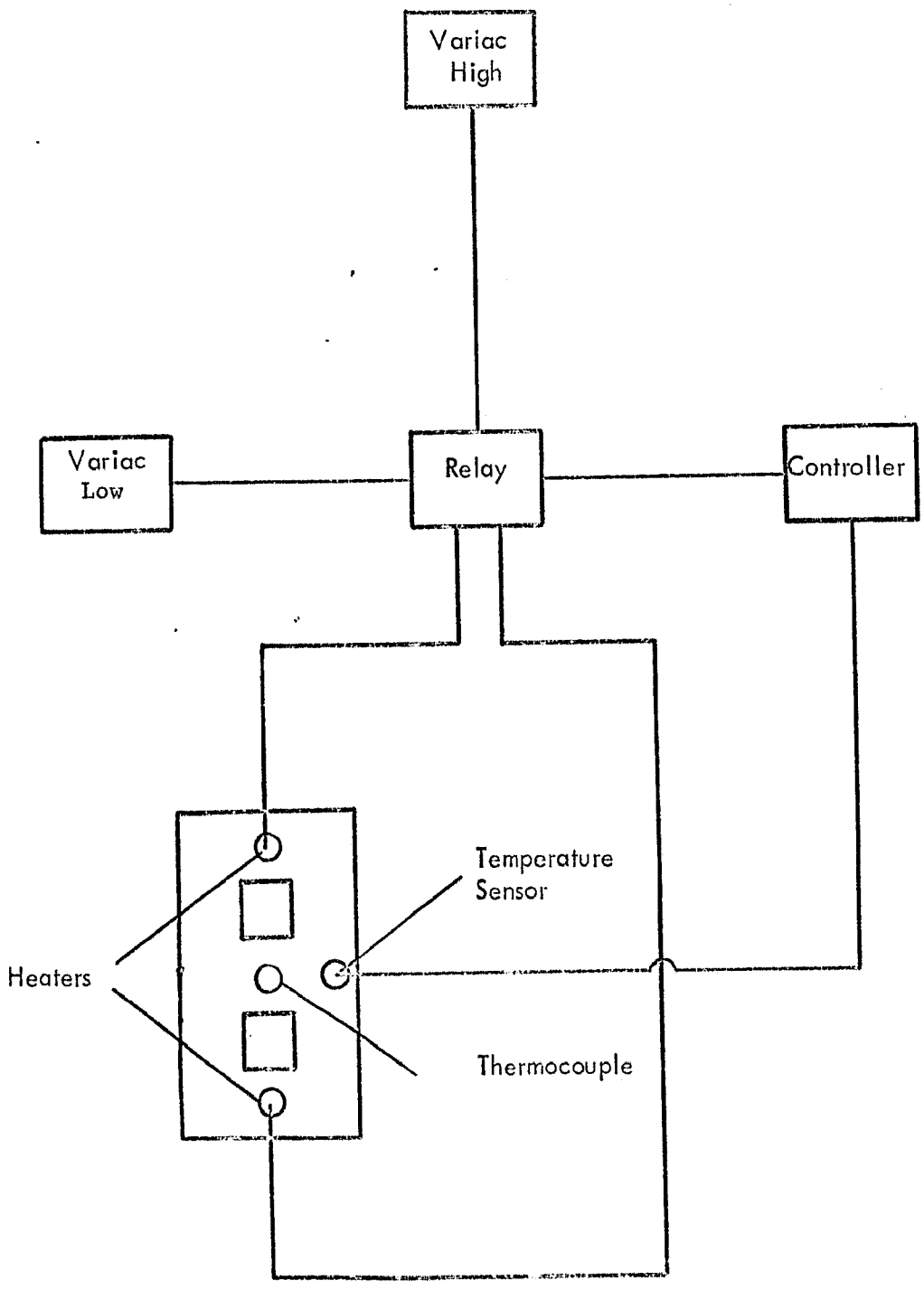

Figure C 3

Block diagram for the spectrophotometer furnace arrangement

discussed in this thesis except for some details which differ slightly. In the present case, the steel furnace block was heated by two nichrome wound resistors connected in series, with a total resistance of 5 ohms. A block diagram of the circuit, which involved a Cole-Palmer Proportio-Null temperature controller, is shown in Figure 3. The relay, which was activated by the controller, switched between a high and low voltage set on two separate Variacs. The temperature stability measured by connecting a chart recorder across the heating element was $\pm 0.5^{\circ}C$. The cells used in the latter part of the work reported here, namely Ru and Os in the chloride melt, Co, Rh and Pd in the sulphate melt, were 1 cm^2 fused silica cells (supplied by Pyrocell) to which silica B14 ground joints were sealed, thereby allowing the cells to be sealed by means of stopcocks. For the earlier work, i.e. Rh, Ir, Pd and Pt in the chloride melt, the cells were constructed from 1 x 1 cm square silica tubing (supplied by Karel Hackel).

On scanning through the visible and near ultra-violet regions, with pure solvent in both beams, it was found that the base-line was not coincident with the zero line over the entire region. For this reason, the base-line was always recorded immediately preceding the recording of any particular spectrum. The procedure which was used is as follows: Two cells, each containing pure solvent, and a third cell, containing the solution of the transition metal compound, were prepared. Both solvent cells were placed in the spectrophotometer furnace and allowed to equilibriate. The third cell was placed in a small tube furnace whose temperature was maintained as close as possible to that of the block furnace. After the base-line had been recorded, the cell in the sample beam was replaced by the third cell and the

spectrum recorded after allowing this sample to attain the equilibrium temperature of the block. The time-lag between placing the sample in the spectrophotometer furnace and recording the spectrum depended on the temperature difference between the two furnaces but was usually between 10 and 20 minutes. By subtracting the base-line from the recorded spectrum, the true spectrum was obtained and replotted on a wave number scale, as against the wavelength scale on which it was recorded.

After the spectrum had been recorded, the sample cell was removed from the furnace and inclined at such an angle that the melt ran down the side of the connecting tube and solidified well away from the cell faces, thereby lowering the risk of cracking the cell. The weight of the sample was found by weighing the cell before and after the contents had been dissolved out. The sample solution was made up to volume and analysed quantitatively for the metal by the methods indicated in the appropriate chapters.

Addition of the pure transition metal salt to the eutectic is not a very good method of obtaining solutions of known concentrations for two reasons:

(i) All of the solid may not reach the melt and on subsequent cooling, dissolving and analysing, the transition metal concentration will be too high.

(ii) It is difficult to obtain a series of solutions of increasing concentration such that the optical density is less than 2 (the maximum using the Beckmann DK2A) at the highest peak maximum.

For these reasons, the following procedure was used in preparing all the melt solutions used. For the chloride melt and the sulphate ones containing zinc, all

operations were carried out in a dry box. Portions of the chloride eutectic contained in a central tube above a frit were melted and subjected to a vacuum, about 10^{-3} mm Hg, for several hours to remove excess chlorine. To this solution a large excess of the transition metal chloride, which had previously been dried, was added. This concentrated solution was then filtered, the filtrate allowed to cool and stored in sample bottles until required. Samll lumps of the solid filtrate were added to the spectrophotometer cell containing pure, degassed solvent. For the Pt(II) case, however, the concentrated solid solution was, in fact, a reference cell donated by Dr. J. R. Mackenzie, which had been prepared by anodisation. An exactly analogous procedure was used in preparing the sulphate solutions containing Rh(III) and Pd(II), using pure metal rods obtained from Johnson Matthey, with a Pt cathode, the two electrodes being contained in separate, fritted compartments.

REFERENCES

1. Boston, C. R., and G. P. Smith, J. Phys. Chem, 62, 409 (1958).
2. Bailey, R. A., and J. A. McIntyre, Inorg. Chem., 5, 1940 (1966).
3. Ogilvie, F. B., and O. G. Holmes, Can. J. Chem., 44, 447 (1966).
4. Bailey, R. A., and J. A. McIntyre, Inorg. Chem., 5, 1824 (1966).
5. Gruen, D. M., and R. L. McBeth, Pure and Appl. Chem., 6, 23 (1963).
6. Gruen, D. M., in Fused Salts ed. B. R. Sundheim, McGraw-Hill (1964).
7. Smith, G. P., in Molten Salt Chemistry ed. M. Blander, Interscience (1964).
8. Katzin, L. I., J. Chem. Phys., 35, 467 (1961).
9. Blomgren, G. E., and E. R. Van Artsdalen, Annual Reviews, Inc. 11, 273 (1960).
10. Bloom, H., and J. O'M. Bockris, in Fused Salts, ed. B.R. Sundheim, McGraw-Hill (1964).
11. Stillinger, F. H. Jr., in Molten Salt Chemistry, ed. M. Blander, Interscience (1964).
12. Sundheim, B. R., and M. Kukk, Disc. Fara. Soc. No. 32, 49 (1961)
13. Øye, H.A. and D.M. Gruen, in Selected Topics in High-Temperature Chemistry ed. by T. Førland, Universitetsforlaget (1966).
14. Juza, R., H. Seidel and J. Tiedemann, Angew. Chem. (Int. ed.) 5, 85 (1966)
15. Jørgensen, C. K., Adv. Chem. Physics, 5, 33 (1963)

16. Tanabe, Y., and S. Sugano, J. Phys. Soc. Japan, 9, 753, 766 (1954).

17. Gray, H. B., J. Chem. Educ., 41, 2 (1964).

18. Basch, H., and H. B. Gray, Inorg. Chem., 6, 365 (1967).

19. Cotton, F. A.,and C. B. Harris, Inorg. Chem., 6, 369 (1967).

20. Cotton, F. A., and C. B. Harris, Inorg. Chem., 6, 376 (1967).

21. Fenske, R. F., and D. D. Radtke, Inorg. Chem., 7, 479 (1968).

22. Condon, E. U., and G. H. Shortley, Theory of Atomic Spectra, Cambridge University Press, 2nd. Edition (1963).

23. Ballhausen, C. J., Introduction to Ligand Field Theory, McGraw-Hill, (1962).

24. Cotton, F. A., Chemical Applications of Group Theory, Interscience (1963).

25. Figgis, B. N., Introduction to Ligand Fields, Interscience (1966)

26. Liehr, A. D., J. Phys. Chem., 67, 1314 (1963).

27. Jørgensen, C. K., Absorption Spectra and Chemical Bonding inComplexes, Addison-Wesley (1962).

28. Parsons, R. W., and H. G. Drickamer, J. Chem Phys. 29, 930 (1958)

29. Shulman, R. G., and S. Sugano, Phys. Rev. 130, 517 (1963).

30. Lee, J., and A. B. P. Lever, J. Molec. Spectro. 26, 189 (1968).

31. Jørgensen, C. K., Prog. Inorg. Chem. 4, 73 (1962).

32. Garbuny, M., Optical Physics, Academic Press (1965).

33. Orgel, L. E., J. Chem. Phys. 23, 1824 (1955).

34. Sulzer, P., and K. Wieland, Helv. Phys. Acta 25, 653 (1952).

35. Jørgensen, C. K., Acta Chem. Scand. 8, 1495 (1954).

36. Holmes, O. G., and D. S. McClure, J. Chem. Phys. 26, 1686 (1957).

37. Stolarczyk, L., Acta Chem. Scand. 12, 1885 (1958).

38. Dunn, T. M., Modern Coordination Chemistry, ed. Lewis and Wilkins, Interscience (1960).

39. Van Vleck, J.H., J. Phys. Chem. 41, 67 (1937).

40. Sandorfy, C., Electronic spectra and quantum chemistry, Prentice-Hall, (1964).

41. Ballhausen, C.J., Prog. Inorg. Chem. 2, 251 (1960).

42. Nakamoto, K., Infra-red Spectra of Inorganic and Coordination Compounds, Wiley, (1963).

43. Liehr, A. D., Adv. Chem. Phys., 5, 241 (1963).

44. Griffith, J. S., Theory of Transition - Metal Ions, Cambridge University Press, (1961).

45. Ballhausen, C.J., and A. D. Liehr, J. Molec. Spectro. 2, 342 (1958).

46. Englman, R., Mol. Phys., 3, 48 (1960).

47. Englman, R., Mol. Phys., 4, 183 (1961).

48. Satten, R. A., and E. Y. Wong, J. Chem. Phys., 43, 3025 (1965).

49. Brynestad, J., H. L. Yakel and G. P. Smith, J. Chem. Phys. 45, 4652 (1966).

50. Moore, R.H., J. Chem. Eng. Data 9, 502 (1964).

51. Griffith, W. P., The Chemistry of the Rarer Platinum Metals, Interscience (1967).

52. Jørgensen, C. K., Acta Chem. Scand. 10, 518 (1956).

53. Jørgensen, C. K., Mol. Phys. 2, 309 (1959).

54. Cady, H. H., and R. E. Connick, J. Am. Chem. 80, 2646 (1958).

55. Olliff, R. W., and A. L. Odell, J. Chem. Soc., 2467 (1964).

56. Larson, L. L., and C. S. Garner, J. Am. Chem. Soc. 76, 2180 (1954).

57. Jørgensen, C. K., Acta Chem. Scand. 16, 793 (1962).

58. Johannesen, R. B., and G. A. Candela, Inorg. Chem. 2, 67 (1963).

59. von Blasius, E., and W. Preetz, Z. Anorg. Allgem. Chem. 335, 1, (1965).

60. Brown, D. H., D. R. Russell and D. W. A. Sharp, J. Chem. Soc. (A), 18 (1966).

61. Hendra, P. J., and P. J. D. Park, Spectrochim. Acta 23A, 1635 (1967).

62. Ito, K., D. Nakamura, K. Ito and M. Kubo, Inorg. Chem. 2, 690 (1963)

63. Figgis, B.N., J. Lewis, R. S. Nyholm and R. D. Peacock, Disc. Faraday Soc. 26, 103 (1958)

64. Earnshaw A., B. N. Figgis, J. Lewis and R. D. Peacock, J. Chem. Soc. 3132 (1961).

65. Griffith, J. S., Disc. Faraday Soc. 26, 174 (1958).

66. Stone, M. E., Unpublished Results.

67. Walker, S., and H. Straw, Spectroscopy, Chapman and Hall (1961).

68. Jørgensen, C. K., Acta Chem. Scand. 17, 1034 (1963).

69. Jørgensen, C. K., Acta Chem. Scand. 17, 1043 (1963).

70. Carlin, R.L., Transition Metal Chemistry 1, 1 (1965).

71. Figgis, B. N., and R. S. Nyholm, J. Chem. Soc. 12, (1954).

72. Ciampolini, M., and N. Nardi, Inorg. Chem. 5, 41 (1966).

73. Alderman, P. R. H., P. G. Owston, and J. M. Rowe, J. Chem. Soc. 668 (1962).

74. Cotton, F. A., D. M. L. Goodgame, M. Goodgame and A. Sacco, J. Am. Chem. Soc. 83, 4157 (1961).

75. Cotton, F. A., and M. Goodgame, J. Am. Chem. Soc. 83, 1777 (1961).

76. Ferguson, J., J. Chem. Phys. 39, 116 (1963).

77. Pappalardo, R., D. L. Wood, and R. C. Linares, J. Chem. Phys. 35, 2041 (1961).

78. Lever, A. B. P., and S. M. Nelson, J. Chem. Soc. (A) 859 (1966).

79 Phillips, C. S. G., and R. J. P. Williams, Inorganic Chemistry, Oxford University Press, (1966).

80. Koide, S., Phil. Mag. 4, 243 (1959).

81. Lever, A. B. P., and D. Ogden, J. Chem. Soc. (A) 2041 (1967).

82. Low, W., Phys. Rev. 109, 256 (1958).

83. Hatfield, W. E., J. F. Anders, and L. J. Rivela, Inorg. Chem. 4, 1088 (1965).

84. Andreev, S. N., and V. G. Khaldin, Zhurnal Obshchei Khim 32, 3845 (1962), (English translation).

85. West, C. D., Z. Krist (A) 91, 480 (1935).

86. Wilson, E. B. Jr., J. C. Decius, and P. C. Cross, Molecular Vibrations, McGraw-Hill (1955).

87. Johnson, K. E., and T. S. Piper, Disc. Fara. Soc. No. 32, 32 (1961).

88. Arris, J., and J. A. Duffy, J. Chem. Soc. 5850 (1964).

89. Duffy, J. A., F. P. Glasser, and M. D. Ingram, J. Chem. Soc. (A) 551 (1968).

90. Scaife, D. E., and K. P. Wood, Inorg. Chem. 6, 358 (1967).

91. Swift, T. J., and R. E. Connick, J. Chem. Phys. 37, 307 (1962).

92. Chatt, J., L. E. Orgel, and G. A. Gamlen, J. Chem. Soc. 486 (1958).

93. Chmelnick, A. M., and D. Fiat, J. Chem. Phys. 47, 3986 (1967).

94. Evans, D. F., J. Chem. Soc. 2003 (1959).

95. Cini, R., and N. Pernicone, Ann. Chim (Rome) 49, 441 (1959).

96. Figgis, B. N., and J. Lewis, in Modern Coordination Chemistry, ed. J. Lewis and R. G. Wilkins, Interscience (1960).

97. Huang, K. P. and W. C. Lin, J. Chinese Chem. Soc., Ser. II, 7, 1 (1960) (in English).

98. Angell, C. A., and D. M. Gruen, J. Inorg. Nucl. Chem. 29, 2243 (1967).

99. Cotton, F. A., D. M. L. Goodgame and M. Goodgame, J. Am. Chem. Soc. 83, 4690 (1961).

100. Øye, H. A., and D. M. Gruen, Inorg. Chem. 3, 836 (1964).

101. Gruen, D. M., Private communication.

102. Siegel, S., and E. Gebert, Acta Cryst. 17, 790 (1964).

103. Øye, H. A., and D. M. Gruen, Inorg. Chem. 4, 1173 (1965).

104. Ferguson, J., D. L. Wood, and K. Knox, J. Chem. Phys. 39, 881 (1963).

105. Ibers, J. A., Acta Cryst. 15, 967 (1962).

106. Stahl-Brada, R., and W. Low, Phys. Rev. 113, 775 (1959).

107. Coing-Bayat, J., and G. Bassi, Compt. Rend. 256, 1482 (1963).

108. Dunitz, J. D., and P. Pauling, Acta Cryst. 18, 737 (1965).

109. Pappalardo, R., and R. E. Dietz, Phys. Rev. 123, 1188 (1961).

110. Cotton, F. A., and T. G. Dunne, J. Am. Chem. Soc. 84, 2013 (1962).

111. Addison, C. C., and D. Sutton, J. Chem. Soc. 5553 (1964).

112. Gruen, D. M., and R. L. McBeth, J. Phys. Chem. 66, 57 (1962).

113. McClure, D. S., in Adv. Chem. Coord. Compounds ed. S. Kirschner, Macmillan (1961).

114. Khakhlova, N. V., and N. S. Dombrovskaya, Russ. J. Inorg. Chem. 4, 416 (1959).

115. Robinson, R. A., and R. H. Stokes, Electrolyte Solutions, Butterworths (1959).

116. Nakamoto, K., J. Fujita, S. Tanaka, and M. Kobayashi, J. Am. Chem. Soc. 79, 4904 (1957).

117. Barraclough, C. G., and M. C. Tobe, J. Chem. Soc. 1993 (1961).

118. Johnson, K. E., and H. A. Laitinen, J. Electrochem. Soc. 110, 314, (1963).

119. Schwarzenbach, G., Complexometric Titrations, Methuen (1957).

120. Kitson, R. E., Anal. Chem. 22, 664 (1950).

121. Jørgensen, C. K., Acta Chem. Scand. 10, 500 (1956).

122. Wolsey, W. C., C. A. Reynolds, and J. Kleinberg, Inorg. Chem. 2, 463 (1963).

123. Paulsen, I. A., and C. S. Garner, J. Am. Chem. Soc. 84, 2032 (1962).

124. Schroeder, K. A., J. Chem. Phys. 37, 2553 (1962).

125. Plambeck, J. A., J. Chem. Eng. Data 12, 77 (1967).

126. Liu, C. H., Unpublished results.

127. Schäffer, C. E., Chemistry of Coordination Compounds (Rome 1957) p 149.

128. Ayres, G.H., B.L. Tuffly and J.S. Forrester, Anal. Chem. 27, 1742 (1955).

129. MacNevin, W.M. and O. H. Kriege, Anal. Chem. 28, 16 (1956).

130. Maynes, A. D., and W. A.E. McBryde, Analyst 79, 230 (1954).

131. Ayres, G.H. and Q. Quick, Anal. Chem. 22, 1403 (1950).

132. Beevers, C.A. and C. M. Schwartz, Z. Krist. 91, 157 (1935), Chem. Abstr. 29, 7732 (7) (1935).

133. McClure, D. S., Solid State Physics, Advances in Research and Applications, 9, 399, (1959).

134. Brynestad, J., C. R. Boston, and G. P. Smith, J. Chem. Phys. 47, 3179 (1967).

135. Brynestad, J., and G. P. Smith, J. Chem. Phys. 47, 3190 (1967).

136. Charlot, G., and D. Bezier, Quant. Inorganic Analysis, Wiley (1957).

137. Gray, H. B., Transition Metal Chemistry 1, 239 (1965).

138. Cohen, A. J. and N. Davidson, J. Am. Chem. Soc. 73, 1955 (1951).

139. Harris, C. M., S. E. Livingstone, and I. H. Reece, J. Chem. Soc. 1505 (1959).

140. Miller, J. R., J. Chem. Soc. 713 (1965).

141. Day, P., A. F. Orchard, A. J. Thomson and R. J. P. Williams, J. Chem. Phys. 42, 1973 (1965).

142. Fenske, R. F., D. S. Martin, and K. Ruedenberg, Inorg. Chem. 1, 441 (1962).

143. Martin, D. S., and C. A. Lenhardt, Inorg. Chem. 3, 1368 (1964).

144. Maki, G., J. Chem. Phys. 28, 651 (1958).

145. Gray, H. B., and C. J. Ballhausen, J. Am. Chem. Soc. 85, 260 (1963).

146. Mason, W. Roy, III, and H. B. Gray, J. Am. Chem. Soc. 90, 5721 (1968).

147. Day, P., M. J. Smith, and R. J. P. Williams, J. Chem. Soc. (A) 668 (1968).

148. Martin, D. S., M. A. Tucker, and A. J. Kassman, Inorg. Chem. 4, 1682 (1965), Amended 5, 1298 (1966).

149. McCaffery, A. J., P. N. Schatz, and P. J. Stephens, J. Am. Chem. Soc. 90, 5730 (1968).

150. Cook, C. D., and G. S. Jauhal, J. Am. Chem. Soc. 89, 3066 (1967).

151. Gadberry, N. M., and E. Peterson, U. S. Patent No. 2, 639, 226 Chem. Abst. 47, 7997d (1953).

152. Lautie, R., Bull. Soc. Chim. France, 508 (1947).

153. McIntyre, J. A., Ph.D. Thesis, Rensselaer Polytechnic Institute, 1966.

154. Dickinson, R. G., J. Am. Chem. Soc. 44, 2404 (1922).

155. Griffith, W. P., J. Lewis, and G. Wilkinson, J. Chem. Soc. 775, (1961).

156. Sundaram, A. K., and E. B. Sandell, J. Am. Chem. Soc. 77, 855 (1955).

157. Livingstone, S. E., J. Chem. Soc. 5091 (1957).

158. Kawahata, M., H. Mochinguki, and T. Misaki, Bunseki Kagaku 11, 819 (1962), Chem Abst. 57, 11846h (1962).

159. Menis, O., and T. C. Rains, Anal. Chem. 27, 1932 (1955).

160. Maynes, A. D., and W. A. E. McBryde, Analyst 79, 230 (1954).

161. Cotton, F. A., and G. Wilkinson, Advanced Inorganic Chemistry 2nd Edition, Interscience (1967).

162. Van Artsdalen, E. R., in The Structure of Electrolytic Solutions ed. W. J. Hamer, Wiley (1959).

163. Inman, D., and S. H. White, Ann. Repts. Chem. Soc. 72, 106 (1965).

164. Bell, J. T., and R. E. Biggers, J. Mol. Spectro. 18, 247 (1965).

165. LaMar, G. N., J. Chem. Phys. 41, 2992 (1964).

166. Mackenzie, J. R., and K. E. Johnson, to be published.

167. Maricle, D. L., and D. N. Hume, J. Electrochem. Soc. 107, 354 (1960).

168. Janz, G. J., Molten Salts Handbook, Academic (1967).

169. Vereshchetina, J. P., and N. P. Luzhnaya, J. Appl. Chem. U. S. S. R. 24, 165 (1951) (English translation).

170. Gruen, D. M., J. Inorg. Nucl. Chem. 4, 74 (1966).

171. Gruen, D. M., Quart. Revs. Chem. Soc. 19, 349 (1965).

172. Johnson, K. E., J. R. Mackenzie and J. N. Sandoe, J. Chem. Soc. (A), 2644 (1968).